

**THIOPHENE BEARING BIS-CHALCONE
BASED MONOMERS AND POLYMERS
FOR ENVIRONMENTAL
APPLICATIONS**

*Thesis submitted
to the University of Calicut for the
award of*

DOCTOR OF PHILOSOPHY IN CHEMISTRY

SOWMYA P



**DEPARTMENT OF CHEMISTRY
UNIVERSITY OF CALICUT
KERALA- 673635
MAY 2023**

Certificate

This is to certify that the thesis entitled “**Thiophene bearing Bis-Chalcone based Monomers and Polymers for Environmental Applications**” submitted by **Sowmya P** to the University of Calicut for the award of the degree of Doctor of Philosophy in Chemistry, is a record of precise research work carried out at the Department of Chemistry, University of Calicut under my guidance and supervision. The contents of the thesis have been checked for plagiarism using the UGC-approved software ‘Ouriginal’ and the similarity index falls under the permissible limit. I further certify that the thesis or part has not previously formed the basis for the award of any degree, diploma or associateship of any other University or Institute.

I also certify that the adjudicators have not suggested any major changes or corrections in the scientific content, results and interpretations of the thesis. However, a minor suggestion recommended by one of the examiners is incorporated in the revised thesis.

Calicut University

Dr. Abraham Joseph
Senior professor

Declaration

I, **Sowmya P**, hereby declare that the thesis entitled “**Thiophene bearing Bis-Chalcone based Monomers and Polymers for Environmental Applications**” submitted to the University of Calicut is a bonafide record of the project done by me under the guidance and supervision of **Prof. Abraham Joseph**, Department of Chemistry, University of Calicut and it has not formed the basis for the award of any Degree/Diploma/Associateship/ Fellowship or other similar titles of any other University or Institution.

University of Calicut

Sowmya P

Acknowledgement

I am honoured to extend my sincere appreciation and fondness to the notable individuals who have made an immense contribution to the realization of this Ph.D. thesis. Foremost, I owe a profound debt of gratitude to my supervisor, Prof. Abraham Joseph, from the Department of Chemistry, University of Calicut. His unwavering encouragement, inspiration, and invaluable support throughout my research journey have been decisive. His guidance and steadfast assistance were indispensable in completing this dissertation. I am grateful for his kindness and the freedom he gave me to pursue this work.

I would also like to express my hearty thanks to Dr. Rajeev S Menon, the Head of the Department of Chemistry, and the former HODs of the department for their support in providing the necessary facilities during my Ph.D. programme. My gratitude extends to all other faculty members of the department. I would like to extend thanks to my research group colleagues, Dr. K. M. Shainy, Dr. Sabeel M Basheer, Dr. Anupama R Prasad, Dr. K. O. Shamsheera, Sr.Asha Thomas, Dr. A. T. Jeeja Rani, Julia Garvasis, Linda Williams, Muhammed Arshad, Anila Paul, Vismaya Joseph, A. Athira, and T. Sreelakshmi for their untiring support and valuable suggestions.

Furthermore, I am indebted to other research scholars, ex-research colleagues, M.Phil. students, and non-teaching staff of our department for fostering a pleasant working atmosphere and providing support and care. I am grateful to Dr. S Jambu, K. Kalidass, S. Chindhu, and K

Ramshad, for their invaluable support. I express my gratitude to Dr. P. P. Soufeena, Dr. C.P. Jijil, Deepak Joshy, T. Anjitha, Lijin Rajan, and Anusruthi for being my constant companions.

I would like to acknowledge the Central Sophisticated Instrument Facility (CSIF) of the University of Calicut, Sophisticated Test and Instrumentation Centre (STIC) of CUSAT, Sophisticated Analytical Instrument Facility (SAIF) of IIT Madras, Karunya University, IISER, and NIIST (Thiruvananthapuram) for their services in the characterization part. I am grateful to the University Grants Commission, Government of India, for the financial assistance that enabled me to complete this work.

My family has been a constant source of love, support, care, and encouragement, and I will always cherish their priceless contributions. I would like to pay tribute to my father, my hero and the foundation of my strength. I am grateful for the selfless efforts of my Achan and Amma, who have always understood, supported, and given me the freedom to choose my path. I am indebted to my husband, Mr. Sivakrishna Prakash, for his unwavering trust, love, care, and sacrifices that have helped me achieve my dreams. Thank you for standing by my side in the tough times, loving me even when I lost myself, and bringing a smile to my face even when I am not able to. Words are not enough to express my love and intimacy to my sweet little angel Tanu whose smile helped us to conquer all the struggles and challenges that we had faced in the meantime. I am also grateful for the support I received from all other family members, particularly from Suramama and my Chechi.

Finally, I wish to express my deepest gratitude to everybody whose assistance was important to the successful realization of this thesis. Above all, I thank the supreme power for giving me the strength and patience to overcome all the tests and trials of the preceding years.

Sowmya P

Contents	Page.No.
Preface	i-iv
Chapter 1: Introduction and literature review	1- 46
1.1. Motivation and background	1
1.2. Survey on various methods employed to detect bisulfite/sulfite anions	8
1.3. Survey on various methods and materials employed for the iodine capture process	12
1.4. Survey on various methods and materials employed for heavy metal ion removal	16
1.5. Survey on various methods and materials employed for organic dye removal	20
1.6. Present investigation	25
References	25
Chapter 2: Materials, methods, and characterization	47-92
2.1. Materials	47
2.2. Characterization techniques	47
2.2.1. Fourier transform infrared spectroscopy (FT-IR)	48
2.2.2. UV-Visible spectroscopy (UV/Vis, UV-DRS)	49
2.2.3. X-Ray diffraction studies (XRD)	49
2.2.4. Field emission scanning electron microscopy (FE-SEM)	50

2.2.5. High-resolution transmission electron microscopy (HR-TEM)	50
2.2.6. Zeta potential analysis	50
2.2.7. Elemental analysis (CHNS analysis)	51
2.2.8. Thermogravimetric analysis (TGA)	51
2.2.9. Brunauer–Emmett–Teller analysis (BET)	52
2.2.10. X-ray photoelectron spectroscopy (XPS)	52
2.2.11. Raman spectroscopy	53
2.2.12. Nuclear magnetic resonance (NMR) spectroscopy	53
2.2.13. High-resolution mass spectrometry (HR-MS)	54
2.2.14. Inductively coupled plasma mass spectrometry (ICP-MS)	54
2.3. Synthetic procedures	55
2.3.1. Synthesis of monomers MTCA and MTCM	55
2.3.2. Synthesis of polymers PTCA and PTCM	56
2.4. Methods and measurements	57
2.4.1. Sensing of SO ₂ - derivatives	57
2.4.1.1. Absorbance titration	57
2.4.1.2. pH titrations	57
2.4.1.3. Detection limit	57
2.4.1.4. Reproducibility	58
2.4.1.5. Selectivity and competition study	58

2.4.1.6. Measurement of spiked sulfite in realistic samples	58
2.4.2. Iodine capture studies	59
2.4.2.1. Iodine uptake	59
2.4.2.2. Kinetics of iodine capture	59
2.4.2.3. Iodine release	60
2.4.2.4. Recycling percentage	60
2.4.3. Removal of heavy metal ions	61
2.4.3.1. Adsorbate solutions	61
2.4.3.2. Single-heavy metal ion adsorption	61
2.4.3.3. Mixed-heavy metal ion adsorption	62
2.4.3.4. Adsorption isotherms	62
2.4.3.5. Adsorption kinetics	63
2.4.3.6. Desorption and reusability study	64
2.4.3.7. Computational study	65
2.4.4. Adsorption of cationic dyes	65
2.4.4.1. Adsorbate solutions	65
2.4.4.2. Adsorption studies	65
2.4.4.3. pH-dependent studies	66
2.4.4.4. Adsorption isotherms	66
2.4.4.5. Adsorption kinetics	67
2.4.4.6. Selectivity studies	68
2.4.4.7. Desorption and reusability studies	68
2.5. Characterization of monomers MTCA and MTCM	69

2.6. Characterization of synthesized polymers PTCA and PTCM	70
References	89
Chapter 3: Thiophene bearing bis-chalcone-based colorimetric probe for the selective detection of bisulfite/sulfite anions	93-118
3.1. Introduction	93
3.2. Results and discussion	93
3.2.1. Effect of pH on the absorbance of the probe towards SO ₂ -derivatives	106
3.2.2. Effect of various surfactants on the absorbance of the probe towards SO ₂ -derivatives	109
3.2.3. Selectivity and competition of the probe toward SO ₂ - derivatives	112
3.2.4. Detection of SO ₂ derivatives in real samples	115
3.3. Conclusions	116
References	116
Chapter 4: Thiophene bearing bis-chalcone-based mesoporous polymers for volatile iodine capture	119-133
4.1. Introduction	119
4.2. Results and discussion	120
4.2.1. Iodine capture	120
4.2.2. Kinetics of iodine capture	121

4.2.3. Mechanism of Iodine capture	124
4.2.4. Iodine release and recyclability	129
4.3. Conclusions	131
References	132
Chapter 5: Thiophene bearing bis-chalcone-based mesoporous polymers for heavy metal ion removal	135-172
5.1. Introduction	135
5.2. Results and discussion	135
5.2.1. Adsorption of heavy metal ions	135
5.2.2. Adsorption mechanism	139
5.2.3. Adsorption isotherm	145
5.2.4. Kinetics of metal ion adsorption	150
5.2.5. Desorption and reusability study	153
5.2.6. Computational study	159
5.3. Conclusions	169
References	170
Chapter 6: Thiophene bearing bis-chalcone-based mesoporous polymers for the selective removal of cationic dyes	173-196
6.1. Introduction	173
6.2. Results and discussion	174
6.2.1. Adsorption performance test	174
6.2.2. Effect of adsorbent dosage	177

6.2.3. Effect of pH	177
6.2.4. Effect of initial concentration and adsorption isotherms	179
6.2.5. Effect of contact time and adsorption kinetics	182
6.2.6. Adsorption mechanism	185
6.2.7. Selective adsorption experiments	190
6.2.8. Desorption and reusability studies	192
6.3. Conclusions	193
References	195
Summary and future outlook	197-198
Publications and presentations	199-201

To,

Achan and Amma

Preface

Global pollution presents a grave danger to the environment, its ecosystems, and the flora and fauna that rely on it. Urgent attention must be given to the three primary forms of pollution, namely water, air, and soil. It is of paramount importance that we take measures to minimize the impact of these pollutants and safeguard the essential components of our ecosystem, as well as the health of living creatures. Proper waste management is particularly critical, as the careless or illegal disposal of waste is the primary source of pollution. Nonetheless, there are also hidden threats to human well-being that demand our attention. Numerous everyday items, such as personal care products, medicines, food and beverages, contain harmful substances that can affect our health. Among these, food and beverages have garnered greater scrutiny due to the presence of additives used to improve their appearance, taste, and shelf life. While we cannot avoid these additives completely, we must ensure that their use adheres to legal limits. Various detection methods can be employed to identify harmful additives, including bisulfite and sulfite, and many reports prompted the development of a colorimetric probe capable of detecting $\text{HSO}_3^-/\text{SO}_3^{2-}$ ions in aqueous solutions under mild conditions. By harnessing the sensing potential of chalcones, two bis chalcones, MTCA and MTCM, were synthesized using the Claisen-Schmidt condensation reaction of thiophene-2-carbaldehyde with acetone and 3-pentanone, respectively. MTCA was found to be an excellent chemosensor for the detection of both bisulfite and sulfite anions. The presence of heteroatoms and terminal thiophene units in the bis chalcones prompted a FeCl_3 -mediated oxidative coupling

polymerization reaction, resulting in the synthesis of PTCA and PTCM, which are effective for capturing iodine, removing heavy metal ions, and organic dyes. These polymers contribute to a small role towards environmental remediation.

The thesis is comprised of six chapters, which cover the synthesis, characterization, and applications of monomers, as well as polymers.

Chapter 1 provides an introduction to the study's motivation and background, and includes a literature review of the methods and materials used for bisulfite/sulfite anion sensing, iodine capture, heavy metal ion removal, and organic dye removal.

In **Chapter 2**, the materials, methods, and characterization techniques used in the synthesis, characterization, and application of the monomers and polymers are discussed. The monomers were synthesized by Claisen–Schmidt reaction and characterized using FT-IR, ¹H NMR, ¹³C NMR, and Mass spectrometric techniques, while the polymers were synthesized by anhydrous FeCl₃-promoted oxidative coupling reactions and were characterized using FT-IR, PXRD, UV-DRS, TGA, SEM, TEM, BET, XPS, and CHNS analysis. The sensing property of the monomer MTCA and the organic dye removal efficiency of the polymers were studied using UV-Vis spectroscopy. Furthermore, gravimetric measurements were utilized to assess the iodine capture properties, and inductively coupled plasma mass spectroscopy (ICP-MS) was utilized to analyze the heavy metal ion removal efficiency of the polymers.

In **Chapter 3**, the sensing capabilities of the monomer MTCA towards bisulfite/sulfite anions are presented. This colorimetric probe, based on 1,4-Michael addition, exhibits a rapid, remarkably selective, and sensitive response to HSO_3^- and SO_3^{2-} ions in both aqueous solutions and real food samples. Moreover, this probe displays superior selectivity and sensitivity towards bisulfite and sulfite over other interfering anions, with a detection limit of 0.43 μM and 0.23 μM , respectively. Additionally, this chapter delves into the impact of pH, various surfactants, and selective and competitive studies.

Moving onto **Chapter 4**, the focus shifts to the performance of synthesized polymers PTCA and PTCM in capturing volatile iodine. The maximum iodine capture capacity attained for PTCA and PTCM was 242 and 221 wt.%, respectively. The kinetic study reveals that adsorption adheres to pseudo-second-order kinetics and chemisorption is the principal process involved. This chapter further explores the mechanism of iodine capture, as well as the polymers' iodine release and recyclability in intricate detail.

Chapter 5 discusses the efficacy of the polymers in removing heavy metal ions, the mechanism and kinetics of adsorption, adsorption isotherms, and reusability of the polymers. The results indicate that the polymers hold great potential in effectively removing Zn^{2+} and Pb^{2+} ions. Specifically, the maximum adsorption capacity of the polymer PTCA for Zn^{2+} and Pb^{2+} was calculated as 729.4 mg/g and 569.1 mg/g respectively, and the maximum adsorption capacity of the polymer PTCM for Zn^{2+} and Pb^{2+} was calculated as 652.7 mg/g and 545.1 mg/g respectively. These values rank among the highest reported thus far.

Chapter 6 explores the polymers' efficacy in removing various organic dyes, demonstrating high effectiveness in removing cationic dyes, in contrast to anionic dyes. As both polymers exhibited the highest removal efficiency towards crystal violet dye, it was chosen as the model cationic dye to investigate various factors that affect the adsorption process. The maximum adsorption capacity of crystal violet obtained was 151.49 mg/g for PTCA and 142.28 mg/g for PTCM. A complex interplay of chemical interaction, n- π interactions, and π - π stacking interactions is responsible for the outstanding adsorption ability of the adsorbents. In conclusion, this thesis highlights the monomer's outstanding potential for sensing bisulfite/sulfite anions, and the polymers' remarkable suitability for environmental applications. Finally, the thesis also provides insights into potential future directions.

Chapter 1

Introduction and literature review



The introduction section deals with two major threats faced by mankind – pollution and food additives. This section also deals with the need for constant checks on the sources of pollution, the amount of added additives and measures taken to control pollution and detect the food additives. The literature review section deals with various studies reported so far in the field of bisulfite/sulfite sensing, iodine capture, heavy metal ion removal and dye adsorption.

1.1. Motivation and background

1.2. Methods employed to detect bisulfite/sulfite anions.

1.3 Methods and materials employed for iodine capture process.

1.4 Methods and materials employed for heavy metal ion removal

1.5 Methods and materials employed for organic dye removal

1.6 Present investigation

1.1 Motivation and Background

Global pollution poses a serious threat to the environment, the ecology, and the lives of flora and fauna. Water pollution, air pollution, and soil pollution are the three main forms of pollution that must be addressed immediately and with utmost care [1]. The main sources of water pollution are industrial discharge, agricultural waste, radioactive waste, marine dumping, accidental spills, microorganisms, parasites, pesticides, fertilizers, heavy metals, volatile organic compounds (VOCs), plastics, oil spills, and medications [2]. Water pollution has various detrimental effects on human health, including gastrointestinal infections, typhoid, skin irritation, cardiovascular and respiratory problems, reproductive difficulties, and cancer [3].

There are numerous sources of air pollution, which include waste incineration, fossil fuel combustion, power plants, forest fires and industries. Particulate matter and gases such as sulphur dioxide, nitrous oxide, carbon monoxide, carbon dioxide, and chlorofluorocarbons are the major pollutants that cause air pollution [4]. These pollutants are extremely hazardous to live beings, materials, and the environment. Air pollution creates health issues in humans such as lung cancer, acute and chronic respiratory diseases, heart disease and strokes [5, 6].

Industrial wastes, agricultural wastes, radioactive wastes, household wastes, inefficient waste management, and mining activities are the leading causes of soil pollution worldwide. The major pollutants associated with these sources are fungicides, pesticides, fertilizers, radioactive materials, toxic organic and inorganic compounds, plastics, and other solid debris. Soil pollution harms the biodiversity, texture,

Introduction and Literature Review

composition, and fertility of the soil [7-9]. Contact with polluted soil for an extended time can alter the genetic makeup of the human body, resulting in difficult-to-treat congenital disorders and chronic health issues [10, 11].

Furthermore, these pollutions are deeply interconnected. Pollution of even one environmental factor eventually leads to pollution of all other environmental factors. As a result, it is critical to make efforts to minimize water pollution, air pollution, and soil pollution to protect the quality of the basic components of the environment and the lives of living beings. To do this, we need to focus on policy development and implementation, proper waste treatment, reducing harmful chemicals, and reusing or recycling contaminants wherever possible. Of these, proper waste treatment is particularly crucial, as careless and illegal dumping of waste is the primary source of pollution.

Despite the ongoing battle against pollution, it's important to recognize that there are additional, less visible threats to human well-being. Countless indispensable items that we use on a daily basis carry harmful consequences on our health. This includes commonly-used beauty and personal care products [12, 13], medications [14], and food and beverages that we consume [15, 16]. Among these, food and beverages acquired greater attention due to the presence of various additives added to enhance their colour, taste and shelf life. Table 1 lists some of the food additives, as well as their uses which cause adverse effects.

Table 1. Food additives, their uses and proven health risks

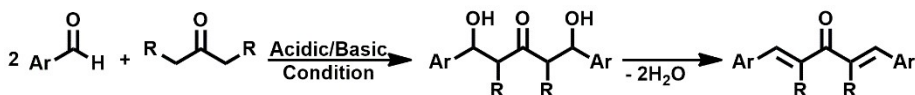
Additives	Examples	Uses	Health risk
Preservatives	Sodium nitrate	-to prevent bacterial growth in meat products	-causes cancer
	Sulfur dioxide	-to increase the shelf life and vitamin C of beverages	-gastric irritation and allergy
Antioxidants	Ascorbic acid	-stop the reaction of food with oxygen that causes fouling	- excess dose cause diarrhoea, gas, or stomach upset
Coloring agents	Sunset yellow	-impart orange-yellow color to food	-allergic reactions
	Red 3	-impart a pink color to food	-hyperactivity in children -increase the risk of thyroid tumours
Flavouring agents	Monosodium glutamate	-enhance the taste of food	-impaired growth and development
Texturing agents	Lecithin	-uses as an emulsifier to prevent the spoiling of milk	- diarrhoea, nausea, stomach pain
	Guar gum	-uses as a thickening agent	-obstruction of the oesophagus or small intestine
Artificial Sweeteners	Sucralose Aspartame	-suited for cooking, baking -used for cooking and baking	-increase your risk of cancer -harmful to gut health

Introduction and Literature Review

Even though we cannot sidestep these additives, we must ensure that the added amount does not exceed the legal limit. There are various detection methods available depending on the nature of the additives. For example, monosodium glutamate can be detected using high-performance liquid chromatography coupled with mass spectrometry (HPLC-MS) or HPLC with an evaporative light scattering detector (ELSD)[17, 18]. Sodium nitrate can be detected using the spectrophotometric method [19], and sulphur dioxide (SO₂) can be detected using the methods such as chromatography, electrochemistry, titration, and spectroscopy. However, the majority of these methods require miscellaneous sample pre-treatment and the use of relatively multiple reagents. Spectroscopy, on the other hand, has been widely employed for detecting analytes due to its ease, high selectivity, sensitivity, and suitability for real-time monitoring.

Since bisulfite/sulfite is one of the notable additives which fall in the category of harmful additives [20], many reports prompted us to develop a colorimetric probe capable of detecting HSO₃⁻/SO₃²⁻ ions in an aqueous solution under mild conditions. We selected a thiophene-containing bis chalcone-based probe to sense bisulfite/sulfite ions.

Bis-chalcones and chalcones are small organic molecules containing α , β -unsaturated ketones. They are commonly synthesised by Claisen-Schmidt condensation reaction employing the condensation between an aromatic aldehyde and an acetone derivative catalysed by either acidic or basic conditions to form β -hydroxycarbonyl compounds followed by dehydration [21-23]. The general reaction is depicted in scheme 1.



Scheme 1: Claisen-Schmidt condensation reaction

Chalcones are considered an open-chain flavonoid compound and hence they belong to the flavonoid family. They are continuing to attract attention from the scientific community because of their potential to use in medicine as a precursor for many biologically active compounds [21]. They exhibit a range of pharmacological activities such as anti-inflammatory, anti-cancer, anti-microbial, anti-diabetic, and anti-oxidant effects [24]. They also have found utility as dye sensitizers, optical limiting materials, sensing probes, and non-linear optics (NLO) materials. They are effective as dye sensitizers due to their high molar extinction coefficients [25, 26]. Chalcones have also been used as sensing materials for various applications such as fluorescent probes for the detection of metal ions such as copper and iron, and chemosensors for the detection of amino acids and other biomolecules [27, 28]. Chalcones exhibit second-order non-linear optical properties, which make them potential materials for non-linear optics [29-31]. Moreover, they have been utilized as optical limiting materials, rendering them suitable for use in optical limiting devices[32, 33].

By considering the potentiality of chalcones for sensing biomolecules, we have designed two bis chalcones (1E,4E)-1,5-Di-2-thienylpenta-1,4-dien-3-one (MTCA) and (1E,4E)-2,4-dimethyl-1,5-di(thiophen-2-yl)penta-1,4-dien-3-one (MTCM). They are synthesised by Claisen-Schmidt condensation reaction of thiophene-2- carbaldehyde with

Introduction and Literature Review

acetone, and 3-pentanone respectively. The chalcone MTCA was found as an excellent chemosensor for the detection of both bisulfite and sulfite anions. The probe based on the surfactant-promoted Michael addition mechanism detects both SO₂ derivatives (HSO₃⁻ and SO₃²⁻) rather than a single SO₂ derivative (either HSO₃⁻ or SO₃²⁻), allowing the accurate determination of SO₂ toxicity. The advantage of our work lies here. The terminal thiophene units and the presence of heteroatoms in the synthesized bis chalcones prompted us to carry out a polymerisation reaction expecting a polythiophene-type polymer with donor-π-acceptor-π-donor type repeating units [34-37]. Here we employed FeCl₃-mediated oxidative coupling reaction to synthesize the polymers. The synthesized polymers were found to be porous and highly insoluble in common organic solvents and are expected to have NLO properties and potential environmental applications similar to other reported porous polymers.

While considering inorganic polymers and materials, organic polymers especially porous organic polymers (POPs) have been proven to be one of the promising candidates for various environmental applications. Among the most primary uses of porous polymers is groundwater remediation, where they can immobilize or adsorb contaminants, such as heavy metals or organic pollutants, from the groundwater [38-40]. In wastewater treatment, they are used to remove suspended solids, oils, and other contaminants, and to coagulate or flocculate suspended solids to facilitate their removal [41-43]. For oil spill cleanup, porous polymers are used to encapsulate the oil and prevent it from spreading. They can also be used to increase the viscosity of the oil, making it easier to skim

Introduction and Literature Review

or collect [44-46]. Finally, these polymers are used in air pollution control to capture and remove pollutants, such as iodine [47-49], and volatile organic compounds [50, 51] emitted from industrial processes.

Overall, POPs have generated greater interest in the field of environmental remediation due to their superiority including tunable porosity and functionality, higher loading capacity, lower overall cost, tremendous specific surface area, multiple preparation methods, robust thermal and chemical stability, and so on. So far, several porous organic polymers such as hyper-cross-linked polymers (HCPs), conjugated microporous polymers (CMPs), covalent triazine-based frameworks (CTFs), porous aromatic frameworks (PAFs), covalent organic frameworks (COFs) have been developed. Along with POPs, several other organic polymers with mesoporous and macroporous properties have been extensively used for the above-mentioned applications. Scientists and researchers continue to develop and refine new polymers to increase their effectiveness and efficiency in a variety of environmental remediation scenarios. Here we mainly focus on two novel polymers; poly [(1E,4E)-1,5-Di-2-thienylpenta-1,4-dien-3-one] (PTCA) and poly[(1E,4E)-2,4-dimethyl-1,5-di(thiophen-2-yl)penta-1,4-dien-3-one] (PTCM) which are effective towards iodine capture, adsorption of heavy metal ions and organic dyes, thereby contributing their role towards the wellbeing of the environment.

Now, let's have a look into various studies reported in the field of sensing SO₂ derivatives, the capture of volatile iodine, the adsorption of heavy metal ions, and the removal of organic dyes.

1.2 Survey on various methods employed to detect bisulfite/sulfite anions.

To date, the existing conventional methods to detect bisulfite/sulfites include ion chromatography [52, 53], spectroscopy [54-57], electrochemistry [58, 59], and iodometric titration [60]. The main disadvantage of these methods is that the majority of them require various sample pre-treatment and the use of a relatively large number of reagents. Among these conventional approaches, spectroscopy has been widely applied in analyte detection because of its high selectivity, simplicity, low detection limit, and suitability for real-time monitoring. Therefore, calorimetric and fluorescent probes have been regarded as versatile tools for monitoring ions and biomolecules [61-64]. Till now, several colorimetric and fluorescent probes for the detection of the SO₂ derivatives (HSO₃⁻/SO₃²⁻) have been designed and developed based on different sensing mechanisms such as the selective deprotection of levulinate group [65-67], complexation with amines [68, 69], the selective reaction with aldehyde [70, 71], coordination to metal ions [72], and Michael-type additions [73, 74].

The first fluorescent probe for the detection of SO₃²⁻ was reported by Chang et al [66]. The detection is based on the reaction of SO₃²⁻ with the keto group of the probe (levulinate of resorufin dye) which eventually leads to the release of a fluorophore. The limit of detection of the probe was determined to be 49 μM in HEPES buffer (pH 7.0, 10 mM) containing 2% acetonitrile. Based on this report, several other reports have been published on the detection of SO₂ derivatives by employing the mechanism of selective deprotection of the levulinate group [75-80].

Introduction and Literature Review

Fewer reported probes function by the complexation with the amines mechanism are known. The fluorescent chemosensor in which a guanidiniocarbonyl pyrrole moiety is covalently attached to 9-(aminomethyl)anthracene was reported by Fu et al, which selectively detect SO_3^{2-} in 90% water/DMSO solution medium. The change in the fluorescence was caused by SO_3^{2-} complex generated photochemical reaction combined with fluorescence resonance energy transfer (FRET). The detection limit of the probe was 0.78 mM [69]. A polymer vesicle sensor that was disclosed in 2017 demonstrated great selectivity towards HSO_3^- with a very good detection limit of 25 nM. The polymer vesicle was created by grafting tertiary amine alcohol (TAA) groups to an amphiphilic hyperbranched polymer, which will subsequently engage in proton exchange with cresol red (CR) to create CR-immobilized vesicles (CR@vesicles). These CR@vesicles are involved in the naked eye sensing of HSO_3^- ions [81].

As an optical probe for bisulfite detection, 4-(1H-Phenanthro[9,10-d]imidazol-2-yl)benzaldehyde was made, and the detection limit was found to be as low as 2 μM . The addition of HSO_3^- to the probe's aldehyde group causes an intramolecular charge transfer (ICT), which underlies how the probe functions. Later several groups reported numerous probes that operate using the same addition mechanism [82-86].

A zinc ion-assisted fluorescence probe for the detection of bisulfite was disclosed by Chen et al. The interaction of bisulfite with zinc ions results in a change in the coordination of zinc ions within the probe and it leads to improved fluorescence intensity [87]. Later, a variety of sensors based

Introduction and Literature Review

on the Michael addition of SO₂ derivatives to the C=C bonds of the probe have been described. Coumarin-based [88-90], pyrene-based [91-93], benzothiazole based [94-97], indolium moiety-bearing [98-101] probes are some among them.

Among these different approaches 1,4 - Michael addition of nucleophiles to α , β unsaturated systems that contain ester, ketone, nitrile, and nitro groups is one of the most versatile methods [102, 103] for the development of chemosensors for the detection of SO₂ derivatives because this method allows the reaction to proceed under mild conditions [101, 104-107].

Interestingly, Zhang et al. [106] reported promising studies in this area, using a cationic cetyltrimethylammonium bromide (CTAB) micelle, to create a hydrophobic and basic microenvironment that promotes the addition reaction of sulfite to an activated olefin in aqueous solutions. Based on this study, many groups have reported new probes that can detect SO₂ derivatives in aqueous solutions via micelle-mediated Michael-type addition reaction [108, 109], and the studies are summarised in Table 2. The findings indicate that the probe reported by our group is competitive with other surfactant-based sensing probes in terms of detection limit and response time.

Table 2. Probes that employ micelle-mediated Michael-type addition reaction as a sensing mechanism towards SO₂ derivatives

Probe	Detection medium	Detection limit	Response time	Reference
TSP-1	PBS buffer (20 mM, pH 7.4) containing 1mM CTAB	2×10^{-7} M	60 min	[106]
BICO	PBS buffer (20 mM, pH 7.4) containing 1mM CTAB	5.3×10^{-8} M	60 min	[74]
CY-SO ₂	PBS buffer (10 mM, pH 7.4) containing 25 μ M CTAB	2.67×10^{-9} M	90 sec	[110]
Probe-1	Britton-Robinson (BR) buffer (20 mM, pH 7) with 1.2 mM CPB	2×10^{-6} M	30 min	[108]
ChC16	Britton–Robinson (BR) buffer (20 mM, pH 7, 1% DMSO) containing 1mM CTAB	2.4×10^{-7} M	15 min	[109]
QNP	PBS buffer (DMSO: PBS = 2:98, 20 mM, pH = 7.4) containing 1 mM CTAB	2×10^{-6} M	90 sec	[111]
MTCA	HEPES buffer (20 mM, pH 7.4) containing 1mM CTAB	2.3×10^{-7} M	10 min	present work

1.3 Survey on various methods and materials employed for iodine capture.

Among various radioactive wastes, ^{129}I generates strong interest and concern, mainly because of its very long radioactive half-life and radiological effects on human health and the environment. The major approaches for iodine vapor removal are wet scrubbing and physical adsorption. The wet scrubbing process shows the disadvantages of poor stability, complex operation procedures, and low capture performance, which is evident from the metal–organic framework ZIF-8 [zeolitic imidazolate framework-8] [112] reported by Sava et.al (efficiency 100 wt%) and Cu-BTC metal–organic framework [113] reported by the same group (efficiency of 175wt%). While, adsorption using porous materials was considered one of the efficient methods for the effective capture and reliable storage of radioactive iodine due to its remarkable advantages, such as simplicity, low operating cost, and speedy operation conditions. Compared to those porous adsorbents such as zeolites [112, 114-116], and metal-organic framework (MOFs) [113, 117-121], POPs have been proven to be promising candidates for the efficient capture and storage of volatile iodine [122, 123] due to the advantages explained before. It is worth noting that the porosity of the polymers is not the sole determinant of iodine capture performance, but rather various functional groups, heteroatoms, and chemical and electronic structures also play a significant role. Table 3 provides a comprehensive summary of different porous polymers used for iodine capture, demonstrating that the efficiency of polymers reported by our group is comparable to that of polymers reported by other groups.

Table 3. Salient features and iodine capture performance of various porous polymers reported in the literature

Material	Category	BET surface area (m ² /g)	Structural features	Iodine uptake (wt %)	Reference
HCPs-B/N	HCPs	582	Microporous, B and N doped	217	[124]
HCPs-N/S	HCPs	481	Microporous, N and S doped	216	[124]
HCPs-B/N/S	HCPs	414	Microporous, B, N and S doped	176	[124]
N-HCP	HCPs	222.8	Microporous, π -conjugated, N-rich	257	[125]
HCP 5	HCPs	34.8	Meso/macroporous, N-rich	254	[126]
SHCMP-1	CMPs	75	S-rich, alkyne bonds, π -conjugated	590	[127]
CMP-LS7	CMPs	507	π -conjugated, N-doped	277	[128]
CMP-LS4	CMPs	462	Meso/macroporous, N-rich	332	[129]
CMP-LS6	CMPs	679	Meso/macroporous, N-rich, alkyne bonds	244	[129]
SNCMP-1	CMPs	16.1	S, N-rich, electron-rich aromatic network	570	[130]
SCMP-I	CMPs	2.72	S-rich, electron-rich aromatic network	100	[131]

Introduction and Literature Review

SCMP-II	CMPs	119.76	S-rich, electron-rich aromatic network	345	[131]
NiP-CMP	CMPs	2600	N- rich, Nickel-containing	202	[132]
HCMP-3	CMPs	82	N-rich, electron-rich aromatic network	316	[133]
SCMP-1	CMPs	413	Meso/macroporous, S-rich, alkyne bonds	188	[134]
SCMP-2	CMPs	855	Meso/macroporous, S-rich, alkyne bonds	222	[134]
CTF-CI-1	CTFs	516	Cationic, Cl ⁻ counter ions	268	[135]
CTF-CI-2	CTFs	599	Cationic, Cl ⁻ counter ions	289	[135]
CTF-PF-3	CTFs	590	Cationic, PF ₆ ⁻ counter ions	285	[135]
FCTF@350	CTFs	6.88	N, F- rich, π-conjugated	285	[136]
NCTF@350	CTFs	1.51	N- rich, π-conjugated	232	[136]
CICTF@350	CTFs	2.23	N, Cl- rich, π-conjugated	231	[136]
CTF-CSU43	CTFs	638	N, F- rich, π-conjugated	250	[137]
CTF-CSU44	CTFs	500	N, F- rich, π-conjugated	278	[137]
PAF-23	PAFs	82	Charged, B and Li bearing, alkyne bonds	271	[123]
PAF-24	PAFs	136	Charged, B and Li bearing, alkyne bonds	276	[123]
PAF-25	PAFs	262	Charged, B and Li bearing, alkyne bonds	260	[123]

Introduction and Literature Review

P-DPDA	PAFs	24.2	Mesoporous, N- rich, π -conjugated	408	[138]
P-TC	PAFs	560.4	N-rich, electron-rich aromatic network	268	[138]
JUC-561	COFs	2359	3D framework, interconnected channels, tetrathiafulvalene group	819	[139]
Hz-COF	COFs	145	-C=N linkages, rigid functionalities	205	[140]
NH-COF	COFs	78	-NH- functionalities, flexible linkages	260	[140]
Cu _{0.5} Pc-COF	COFs	37.32	N-coordinated Cu atoms	240	[141]
Cu _{0.125} Pc-COF	COFs	9.31	N-coordinated Cu atoms	266	[141]
TpPa-1	COFs	765	N, O-rich, electron-rich aromatic network	245	[142]
CMPH	Mesoporous	222.4	N-rich, alkyne bonds	125	[143]
TBHCP-OH	Mesoporous	234.9	N, O-rich, triptycene-based	260	[144]
PSIF-4a	Aerogel	209.6	Si, N, O-rich, micro/meso/macroporous	244	[145]
PTCA	Mesoporous	34.31	S, O-rich, electron-rich aromatic network	242	present work
PTCM	Mesoporous	22.13	S, O-rich, electron-rich aromatic network	222	present work

1.4 Survey on various methods and materials employed for heavy metal ion removal.

There are several conventional methods such as solvent extraction [146], membrane separation [147], ion exchange [148], reverse osmosis [149], precipitation [150], and electrolysis [151], etc have been applied for the removal of heavy metal ions from wastewater. However, adsorption by porous solid adsorbents is considered one of the most cost-effective, simple, and competent methods among all of the aforesaid methods. Layered double hydroxides (LDHs) [152, 153] and metal oxides (TiO_2 , Fe_xO_y , Al_2O_3 , etc) [154-156] are noticeable candidates among solid adsorbents. Even though they are cost-effective, low surface area and lack of porosity limit their adsorption capacities. At the same time, many adsorbents, such as porous resins [157, 158], silicas [159, 160], carbon materials (activated carbon, nanotubes, and their composites)[161-163], and metal-organic frameworks offer high surface area and high removal efficiency, but they are generally expensive. So, materials with improved properties are more attractive. Porous organic polymers (POPs) and several other mesoporous and macroporous organic polymers meet these needs and have been widely used for the elimination of heavy metal ions [164-167]. Table 4 summarises various porous organic polymers used for heavy metal ion removal. Polymers synthesised by our group show the highest adsorption capacity towards Zn^{2+} ions on comparison with previously reported works. While the polymers show excellent adsorption capacity towards Pb^{2+} ions compared to majority of other reported works.

Table 4. Salient features of various porous organic polymers used for heavy metal ion removal

Adsorbent	Surface area (m ² /g)	Structural/functional properties	Target ions	Q _{max} (mg/g)	Reference
HCP	823.89	Polystyrene-based, micro/meso/macroporous	Ni, Pb	146.6, 137.3	[168]
2-HTA-HCP	167.98	2-hydroxyterephthalic acid modified styrene based hyper crosslinked polymer	Ni, Cu, Cd, Pb	33.5, 50.3, 69.7, 178.3	[169]
HCP	853.89	Polystyrene-based, micro/meso/macroporous	Cd	950	[170]
HCMP-1	432	Microporous, triazine and dibenzofuran units	Hg	604	[171]
PFCPP-0	901	Fluorinated CMP, acetylene groups	Pb	808.2	[172]
PTIA	139	Indole-based, meso/macroporous	Ni, Cu, Zn	290, 323, 203.8	[173]

Introduction and Literature Review

CMP-2a	118	cyano and pyridyl groups, heterogeneous pores	Pb	62.7	[174]
CMP-3a	168	cyano and pyridyl groups, heterogeneous pores	Pb	93.2	[174]
Por-CMP-3	382.38	porphyrin-based conjugated microporous polymers	Zn, Cu, Pb	640, 334, 334	[175]
COF-TP	-	Amide-based COFs	Pb	384	[176]
COF-TE	-	Amide-based COFs	Pb	480	[176]
COF-Tz-OH	1897	COF with triazine and -OH bifunctional groups	Pb	476	[177]
SiNPz-Th	310.1	silica surface grafted with β -ketoenol-pyrazole-thiophene, mesoporous	Pb, Cu, Zn, Cd	102.2, 76.4, 68.9, 32.7	[178]
PAF-10c	244	pyridine ring and carboxyl group bounded hierarchically porous material	Pb	62.79	[179]

Introduction and Literature Review

PAF-10d	146	pyridine ring and carboxyl group bounded hierarchically porous material	Pb	90.36	[179]
PAF-10d	87	pyridine ring and carboxyl group bounded hierarchically porous material	Pb	75.59	[179]
S ₃	218	chitosan/poly (ethylene oxide) nanofibers, mesoporous	Cu, Zn, Pb	96, 91, 83	[180]
FC-POP-CH ₂ TETA-E	413	porous organic polymer (POP) with an extended triethylenetetramine (TETA) chain	Pb	1134	[166]
FC-POP-CH ₂ TETA-H	599	porous organic polymer (POP) with hooped triethylenetetramine (TETA) chain	Pb	561	[166]
PTCA	34.31	Thiophene containing bis-chalcone-based mesoporous polymer	Zn, Pb	729.4, 569.1	present work
PTCM	22.13	Thiophene containing bis-chalcone-based mesoporous polymer	Zn, Pb	652.7, 545.1	present work

1.5 Survey on various methods and materials employed for organic dye removal.

Wastewater treatment is a challenging process, particularly when it comes to eliminating synthetic dyes such as methylene blue (MB), rhodamine B (RB), malachite green (MG), crystal violet (CV), methyl orange (MO), congo red (CR) etc. Many different techniques have been developed to address this issue, such as chemical coagulation, irradiation, membrane processes, electrocatalytic degradation, ultrafiltration, chlorine oxidation, and adsorption etc [181-187]. Although many of these methods offer several benefits, they also have several drawbacks, including poor removal efficiency, high costs, and the generation of sludge waste. Among the various technologies applied, adsorption has received the most attention due to its high efficiency, practicability, and cost-effectiveness. However, the success of the adsorption process largely depends on the choice of adsorbent employed. Several adsorbents have been used in the past, such as carbon nanotubes [188, 189], gypsum [190], zeolite-based porous material [191, 192], chitosan composites [193, 194], and hydrogels [195, 196] etc. However, their use is often limited by factors such as high costs, poor removal efficiency, and limited availability. In recent years, researchers have turned their attention to porous organic polymers [197, 198] due to their aforesaid desirable properties. Table 5 summarises different reported works in the field of porous organic polymer-based dye adsorption, and Table 6 focuses on the studies related to the removal of crystal violet dye, which is our primary focus in this study.

Table 5. Salient features of different organic polymers used for the removal of various dyes

Adsorbent	Surface area ((m ² /g)	Structural/functional properties	Dye adsorbed	Qmax (mg/g)	Reference
NH ₂ -HCP	77.3	electrostatic interactions between the amino groups and anionic dyes	MO	1754	[199]
AHCP-1	939	anionic hypercrosslinked polymer bearing boron atoms	RB	229.89	[200]
DPT-HPP	1230	Triphenylamine based	RB	256.40	[201]
TPP-PP	698.14	tritycene-based porous polymer	MO, MB	220.82, 159.80	[202]
CPTP	391.3	sulfonate-conjugated, microporous	MB	957.9	[203]
CMP-Im	533	cationic framework of imidazolium unit	MO, CR	588, 2600	[204]
CMP-PM	416	pyrimidine-based conjugated microporous polymer	CR	344.8	[205]

CMP-PM-Me	241	Post-synthetic modification of pyrimidine-based polymer by MeI	CR	400	[205]
TzDBd	162.3	carboxyl-functionalized triazine-based covalent organic framework	CV	307.7	[206]
PAF-111	857	Electron-rich aromatic networks	RB	1462	[207]
PAF-112A	526	Electron-rich aromatic networks	RB	658	[207]
PAF-112B	725	Electron-rich aromatic networks	RB	898	[207]
PAF-113	598	Electron-rich aromatic networks	RB	574	[207]
POP-8F	192.42	calixarene-based porous organic polymers	RB, MB, CV, MO	2433, 862.07, 1181.02, 93.7	[208]
POP-10F	167.6	calixarene-based porous organic polymers	RB, MB, CV, MO	1729.9, 793.6, 925.9, 89.6	[208]
PHCP	1074	pentipycene-based hyper-cross-linked polymer, hierarchical porous structure	CV, MB	877,289	[209]
Cz-pyr-P	1065	Carbazole-tagged pyridinic microporous polymer	MB	175.44	[210]

Table 6. Salient features of various adsorbents reported for the removal of crystal violet dye

Adsorbent	Surface area ((m ² /g))	Structural/functional properties	Q _{max} (mg/g)	Reference
NMRH	-	NaOH-modified rice husk, chemisorption	41.483	[211]
fMWNT	-	-OH and -COOH functionalized multi-walled carbon nanotubes	90.52	[212]
XG-HNC	24.87	xanthan gum-based GO crosslinked hydrogel nanocomposites, mesoporous	1566.97	[213]
PAAC	328.2	Phosphoric acid-activated carbon	60.42	[214]
SAAC	556.3	Sulphuric acid-activated carbon	85.84	[214]
MCM-41	1059	Mesoporous silicate	114.2	[215]
sulfated MCM-41	938	Sulphated mesoporous silicate	138.7	[215]
kaolin	13.72	natural clay adsorbent	45	[216]

Introduction and Literature Review

GA-cl-poly(AAm) NHG	-	arabic-cl-poly(acrylamide) nanohydrogel, amide linkage, - OH functional groups.	90.90	[217]
OLP	-	Olive leaf powder	181.1	[218]
CHP	-	Coconut husk powder	454.54	[219]
TLGL-CA	-	lemongrass leaf fibers incorporated with cellulose acetate	33.47	[220]
SCB–Ben/SA	12.44	sugarcane bagasse–bentonite/sodium alginate composite aerogel	839.9	[221]
TSCB	1.01	treated sugarcane bagasse, mesoporous	107.5	[222]
PUF	0.9473	Composite of tire rubber and polyurethane foam polymer wastes	20.92	[223]
PTCA	34.31	Thiophene containing bis-chalcone-based mesoporous polymer	151.49	present work
2PTCM	22.13	Thiophene containing bis-chalcone-based mesoporous polymer	142.28	present work

1.6 Present investigation

Water, air, and soil resources are fundamental to human existence, but their contamination poses a significant threat to our health and well-being. Thus, we must take proper measures to identify, monitor, and reduce the various pollutants that cause pollution. In this groundbreaking study, we take a small yet significant step towards reducing the pollution caused by radioactive iodine, heavy metal ions, and organic dyes, by utilizing two novel thiophene-containing bis-chalcone-based polymers. Our approach primarily focuses on the adsorption mechanism to effectively remove iodine, heavy metal ions, and organic dyes from the environment.

It is important to note that in addition to environmental pollution, the food we consume daily can also impact our health. Although food additives are sometimes unavoidable, it is critical to carefully monitor whether the added additives are legally allowed and also whether they are under safe limits. In this study, we mainly focus on the detection of bisulfite/sulfite anions, which are commonly added to food items to increase their shelf life. Our research also proposes a colorimetric probe for the detection of bisulfite/sulfite anions in the aqueous solution as well as in real-life samples, paving the way for enhanced monitoring and regulation of food additives to ensure the well-being of individuals.

References

[1] A. Siddiqua, J.N. Hahladakis, W.A.K. Al-Attiya, An overview of the environmental pollution and health effects associated with waste landfilling

Introduction and Literature Review

and open dumping, *Environmental Science and Pollution Research*, 29(2022) 58514-36.

[2] N. Morin-Crini, E. Lichtfouse, G. Liu, V. Balaram, A.R.L. Ribeiro, Z. Lu, et al., Worldwide cases of water pollution by emerging contaminants: a review, *Environmental Chemistry Letters*, 20(2022) 2311-38.

[3] A.A. Mitiku, A review on water pollution: causes, effects and treatment methods, *Int J Pharm Sci Rev Res*, 60(2020) 94-101.

[4] A.A. Almetwally, M. Bin-Jumah, A.A. Allam, Ambient air pollution and its influence on human health and welfare: an overview, *Environmental Science and Pollution Research*, 27(2020) 24815-30.

[5] I. Manisalidis, E. Stavropoulou, A. Stavropoulos, E. Bezirtzoglou, Environmental and health impacts of air pollution: a review, *Frontiers in public health*, (2020) 14.

[6] M. Kampa, E. Castanas, Human health effects of air pollution, *Environmental pollution*, 151(2008) 362-7.

[7] F.B. Elehinafe, O. Olomukoro, A. Ayeni, O. Okedere, A Short Review on Land/Soil Pollution: The Pollutants and the Treatment Techniques, *Advanced Manufacturing in Biological, Petroleum, and Nanotechnology Processing: Application Tools for Design, Operation, Cost Management, and Environmental Remediation*, (2022) 267-75.

[8] A. Ghaly, V. Ramakrishnan, Nitrogen sources and cycling in the ecosystem and its role in air, water and soil pollution: A critical review, *Journal of Pollution Effects & Control*, (2015) 1-26.

[9] A. Zwolak, M. Sarzyńska, E. Szyrka, K. Stawarczyk, Sources of soil pollution by heavy metals and their accumulation in vegetables: A review, *Water, air, & soil pollution*, 230(2019) 1-9.

[10] S. Khan, M. Naushad, E.C. Lima, S. Zhang, S.M. Shaheen, J. Rinklebe, Global soil pollution by toxic elements: Current status and future perspectives on the risk assessment and remediation strategies—A review, *Journal of Hazardous Materials*, 417(2021) 126039.

[11] A. Di Nisio, C. Foresta, Water and soil pollution as determinant of water and food quality/contamination and its impact on male fertility, *Reproductive biology and endocrinology*, 17(2019) 1-13.

[12] G.J. Nohynek, E. Antignac, T. Re, H. Toutain, Safety assessment of personal care products/cosmetics and their ingredients, *Toxicology and applied pharmacology*, 243(2010) 239-59.

[13] M. Khalid, M. Abdollahi, Environmental distribution of personal care products and their effects on human health, *Iranian Journal of Pharmaceutical*

Research: IJPR, 20(2021) 216.

[14] O. Akinyemi, S. Oyewole, K. Jimoh, Medicinal plants and sustainable human health: a review, Horticulture International Journal, 2(2018) 194-5.

[15] A. Christ-Ribeiro, J.V. Maciel, E.M. Bier, J.S. Pinto, D. Dias, Application of Electrochemical Sensors in the Determination of Synthetic Dyes in Foods or Beverages and Their Toxicological Effects on Human Health: a Review, Food Analytical Methods, 15(2022) 2394-413.

[16] S. Dey, B.H. Nagababu, Applications of food colour and bio-preservatives in the food and its effect on the human health, Food Chemistry Advances, (2022) 100019.

[17] M. Soyseven, H.Y. Aboul-Enein, G. Arli, Development of a HPLC method combined with ultraviolet/diode array detection for determination of monosodium glutamate in various food samples, International Journal of Food Science & Technology, 56(2021) 461-7.

[18] M. Soyseven, G. Arli, Method validation and rapid determination of monosodium glutamate in various food products by HPLC–fluorescence detection and method optimization of HPLC–Evaporative light scattering detection approach without derivatization, Journal of Chromatographic Science, 60(2022) 760-9.

[19] P. Singh, M.K. Singh, Y.R. Beg, G.R. Nishad, A review on spectroscopic methods for determination of nitrite and nitrate in environmental samples, Talanta, 191(2019) 364-81.

[20] M.R. Lester, Sulfite sensitivity: significance in human health, Journal of the American College of Nutrition, 14(1995) 229-32.

[21] A. Rammohan, J.S. Reddy, G. Sravya, C.N. Rao, G.V. Zyryanov, Chalcone synthesis, properties and medicinal applications: a review, Environmental Chemistry Letters, 18(2020) 433-58.

[22] M. Xu, P. Wu, F. Shen, J. Ji, K. Rakesh, Chalcone derivatives and their antibacterial activities: Current development, Bioorganic Chemistry, 91(2019) 103133.

[23] A.M. Asiri, S.A. Khan, Synthesis, characterization and optical properties of mono-and bis-chalcone, Materials Letters, 65(2011) 1749-52.

[24] S.L. Gaonkar, U. Vignesh, Synthesis and pharmacological properties of chalcones: a review, Research on chemical intermediates, 43(2017) 6043-77.

[25] R. Chauhan, R. Yadav, A.K. Singh, M. Trivedi, G. Kociok-Köhn, A. Kumar, et al., Ferrocenyl chalcones with phenolic and pyridyl anchors as

Introduction and Literature Review

potential sensitizers in dye-sensitized solar cells, RSC advances, 6(2016) 97664-75.

[26] S.N.A.M. Nizar, M.M. Rosli, S.A.M. Samsuri, I.A. Razak, S. Arshad, Involvement of Halogen and Polyaromatic Substituents in Chalcone Derivatives as Dye-Sensitizer in Solar Cell Application, New Journal of Chemistry, (2023).

[27] P. Mahesha, N.S. Shetty, S.D. Kulkarni, A Review on Metal Ion Sensors Derived from Chalcone Precursor, Journal of Fluorescence, 32(2022) 835-62.

[28] A. Gupta, S. Garg, H. Singh, Development of chalcone-based derivatives for sensing applications, Analytical Methods, 12(2020) 5022-45.

[29] N. Sudha, R. Surendran, S. Jeyaram, Synthesis, characterization, linear and nonlinear optical features of novel organic compound Pyridylcarboxamide chalcone for nonlinear optical applications, Optical Materials, 131(2022) 112668.

[30] L.R. Almeida, M.M. Anjos, G.C. Ribeiro, C. Valverde, D.F. Machado, G.R. Oliveira, et al., Synthesis, structural characterization and computational study of a novel amino chalcone: a potential nonlinear optical material, New Journal of Chemistry, 41(2017) 1744-54.

[31] P.R. Kumar, V. Ravindrachary, K. Janardhana, H. Manjunath, P. Karegouda, V. Crasta, et al., Optical and structural properties of chalcone NLO single crystals, Journal of Molecular Structure, 1005(2011) 1-7.

[32] J.C. Jebapriya, J.C. Prasana, U.M. Sumaya, P.S. Patil, Molecular structure and third-order non-linear optical properties of two novel tetralone-based chalcone derivatives: Promising materials for optical limiting applications, Journal of Physics and Chemistry of Solids, 173(2023) 111091.

[33] P. Vinaya, A. Prabhu, K.S. Bhat, V. Upadhyaya, Synthesis, growth and characterization of a long-chain π -conjugation based methoxy chalcone derivative single crystal; a third order nonlinear optical material for optical limiting applications, Optical Materials, 89(2019) 419-29.

[34] L. Yang, R. Dorsinville, Q. Wang, W. Zou, P.P. Ho, N. Yang, et al., Third-order optical nonlinearity in polycondensed thiophene-based polymers and polysilane polymers, JOSA B, 6(1989) 753-6.

[35] J. Pei, W.-L. Yu, W. Huang, A.J. Heeger, A novel series of efficient thiophene-based light-emitting conjugated polymers and application in polymer light-emitting diodes, Macromolecules, 33(2000) 2462-71.

[36] C.-Y. Yu, C.-P. Chen, S.-H. Chan, G.-W. Hwang, C. Ting, Thiophene/phenylene/thiophene-based low-bandgap conjugated polymers for

efficient near-infrared photovoltaic applications, *Chemistry of Materials*, 21(2009) 3262-9.

[37] G. Barbarella, M. Melucci, G. Sotgiu, The versatile thiophene: an overview of recent research on thiophene-based materials, *Advanced Materials*, 17(2005) 1581-93.

[38] M.G. Mohamed, A.F.M. El-Mahdy, M.G. Kotp, S.-W. Kuo, Advances in porous organic polymers: syntheses, structures, and diverse applications, *Materials Advances*, 3(2022) 707-33.

[39] M. Verma, I. Lee, Y. Hong, V. Kumar, H. Kim, Multifunctional β -Cyclodextrin-EDTA-Chitosan polymer adsorbent synthesis for simultaneous removal of heavy metals and organic dyes from wastewater, *Environmental Pollution*, 292(2022) 118447.

[40] X.-Q. Huang, X. Hong, H. Lin, X.-M. Cao, Q. Dang, S.-B. Tang, et al., Hypercrosslinked triazine-phloroglucinol hierarchical porous polymers for the effective removal of organic micropollutants, *Chemical Engineering Journal*, 435(2022) 134990.

[41] S. Sun, B. Gao, Q. Yue, R. Li, W. Song, F. Bu, et al., Comparison of epichlorohydrin–dimethylamine with other cationic organic polymers as coagulation aids of polyferric chloride in coagulation–ultrafiltration process, *Journal of Hazardous Materials*, 307(2016) 108-18.

[42] J. Wei, B. Gao, Q. Yue, Y. Wang, Effect of dosing method on color removal performance and flocculation dynamics of polyferric-organic polymer dual-coagulant in synthetic dyeing solution, *Chemical Engineering Journal*, 151(2009) 176-82.

[43] H. Rong, B. Gao, R. Li, Y. Wang, Q. Yue, Q. Li, Effect of dose methods of a synthetic organic polymer and PFC on floc properties in dyeing wastewater coagulation process, *Chemical Engineering Journal*, 243(2014) 169-75.

[44] Q. Sun, B. Aguila, Y. Song, S. Ma, Tailored porous organic polymers for task-specific water purification, *Accounts of chemical research*, 53(2020) 812-21.

[45] X. Yu, P. Yang, M.G. Moloney, L. Wang, J. Xu, Y. Wang, et al., Electrospun Gelatin Membrane Cross-Linked by a Bis(diarylcarbene) for Oil/Water Separation: A New Strategy To Prepare Porous Organic Polymers, *ACS Omega*, 3(2018) 3928-35.

[46] X.-S. Wang, J. Liu, J.M. Bonfont, D.-Q. Yuan, P.K. Thallapally, S. Ma, A porous covalent porphyrin framework with exceptional uptake capacity of

saturated hydrocarbons for oil spill cleanup, *Chemical Communications*, 49(2013) 1533-5.

[47] T. Geng, C. Zhang, M. Liu, C. Hu, G. Chen, Preparation of biimidazole-based porous organic polymers for ultrahigh iodine capture and formation of liquid complexes with iodide/polyiodide ions, *Journal of Materials Chemistry A*, 8(2020) 2820-6.

[48] Z. Li, H. Li, D. Wang, A. Suwansoontorn, G. Du, Z. Liu, et al., A simple and cost-effective synthesis of ionic porous organic polymers with excellent porosity for high iodine capture, *Polymer*, 204(2020) 122796.

[49] S. Xiong, X. Tang, C. Pan, L. Li, J. Tang, G. Yu, Carbazole-bearing porous organic polymers with a mulberry-like morphology for efficient iodine capture, *ACS applied materials & interfaces*, 11(2019) 27335-42.

[50] J. Jia, Z. Chen, H. Jiang, Y. Belmabkhout, G. Mouchaham, H. Aggarwal, et al., Extremely Hydrophobic POPs to Access Highly Porous Storage Media and Capturing Agent for Organic Vapors, *Chem*, 5(2019) 180-91.

[51] S. Lu, Q. Liu, R. Han, M. Guo, J. Shi, C. Song, et al., Potential applications of porous organic polymers as adsorbent for the adsorption of volatile organic compounds, *Journal of Environmental Sciences*, 105(2021) 184-203.

[52] Z. Zhong, G. Li, B. Zhu, Z. Luo, L. Huang, X. Wu, A rapid distillation method coupled with ion chromatography for the determination of total sulphur dioxide in foods, *Food chemistry*, 131(2012) 1044-50.

[53] D. Urupina, V. Gaudion, M.N. Romanias, M. Verrielle, F. Thevenet, Method development and validation for the determination of sulfites and sulfates on the surface of mineral atmospheric samples using reverse-phase liquid chromatography, *Talanta*, 219(2020) 121318.

[54] K. Xiang, S. Chang, J. Feng, C. Li, W. Ming, Z. Liu, et al., A colorimetric and ratiometric fluorescence probe for rapid detection of SO₂ derivatives bisulfite and sulfite, *Dyes and Pigments*, 134(2016) 190-7.

[55] G. Asaithambi, V. Periasamy, Ratiometric sensing of sulfite/bisulfite ions and its applications in food samples and living cells, *Journal of Photochemistry and Photobiology A: Chemistry*, 389(2020) 112214.

[56] C. Nandhini, P.S. Kumar, R. Shanmugapriya, K. Vennila, A.G. Al-Sehemi, M. Pannipara, et al., A combination of experimental and TD-DFT investigations on the fluorescent detection of sulfite and bisulfite ions in aqueous solution via nucleophilic addition reaction, *Journal of Photochemistry and Photobiology A: Chemistry*, 425(2022) 113668.

[57] Y. Zhou, J. Gou, Y.-X. Zhou, C. Liu, X. Xiao, H.-J. Liu, Tunable energy level induced fluorescence enhancement in copper functionalized silicon

- quantum dots for highly selective detection of bisulfite, *Sensors and Actuators B: Chemical*, 370(2022) 132444.
- [58] A. Isaac, A.J. Wain, R.G. Compton, C. Livingstone, J. Davis, A novel electroreduction strategy for the determination of sulfite, *Analyst*, 130(2005) 1343-4.
- [59] P. Begum, T. Morozumi, T. Kawaguchi, T. Sone, Development of an Electrochemical Sensing System for Wine Component Analysis, *ACS Food Science & Technology*, 1(2021) 2030-40.
- [60] J.M. Vahl, J.E. Converse, Ripper procedure for determining sulfur dioxide in wine: collaborative study, *Journal of the Association of Official Analytical Chemists*, 63(1980) 194-9.
- [61] L. Zhang, L. Wang, X. Zhang, Z.-J. Zhu, A colorimetric and fluorescent probe for sulfite/bisulfite based on conjugated benzothiazole derivative and imaging application in living cells, *Journal of Photochemistry and Photobiology A: Chemistry*, 395(2020) 112498.
- [62] J.H. Han, W.Y. Gao, L.H. Feng, Y. Wang, S.M. Shuang, An AIE-active probe for selective fluorometric–colorimetric detection of HSO_3^- in aqueous solution and real samples, *Journal of Photochemistry and Photobiology A: Chemistry*, 421(2021) 113515.
- [63] S. Roy, A. Maity, N. Mudi, M. Shyamal, A. Misra, Rhodamine scaffolds as real time chemosensors for selective detection of bisulfite in aqueous medium, *Photochemical & Photobiological Sciences*, 18(2019) 1342-9.
- [64] D. Don, K. Velmurugan, J. Prabhu, N. Bhuvanesh, A. Thamilselvan, R. Nandhakumar, A dual analyte fluorescent chemosensor based on a furan-pyrene conjugate for Al^{3+} & HSO_3^- , *Spectrochimica Acta Part A: Molecular and Biomolecular Spectroscopy*, 174(2017) 62-9.
- [65] P. Hou, S. Chen, K. Voitchovsky, X. Song, A colorimetric and ratiometric fluorescent probe for sulfite based on an intramolecular cleavage mechanism, *Luminescence*, 29(2014) 749-53.
- [66] M.G. Choi, J. Hwang, S. Eor, S.-K. Chang, Chromogenic and fluorogenic signaling of sulfite by selective deprotection of resorufin levulinate, *Organic letters*, 12(2010) 5624-7.
- [67] K. Wang, W. Wang, S.-Y. Chen, J.-C. Guo, J.-H. Li, Y.-S. Yang, et al., A novel Near-Infrared rhodamine-derived turn-on fluorescence probe for sensing SO_3^{2-} detection and their bio-imaging in vitro and in vivo, *Dyes and Pigments*, 188(2021) 109229.

Introduction and Literature Review

- [68] A.V. Leontiev, D.M. Rudkevich, Revisiting noncovalent SO₂-amine chemistry: an indicator-displacement assay for colorimetric detection of SO₂, *Journal of the American Chemical Society*, 127(2005) 14126-7.
- [69] Y. Sun, C. Zhong, R. Gong, H. Mu, E. Fu, A Ratiometric Fluorescent Chemodosimeter with Selective Recognition for Sulfite in Aqueous Solution, *The Journal of Organic Chemistry*, 74(2009) 7943-6.
- [70] Y. Yang, F. Huo, J. Zhang, Z. Xie, J. Chao, C. Yin, et al., A novel coumarin-based fluorescent probe for selective detection of bisulfite anions in water and sugar samples, *Sensors and Actuators B: Chemical*, 166(2012) 665-70.
- [71] X.-F. Yang, M. Zhao, G. Wang, A rhodamine-based fluorescent probe selective for bisulfite anion in aqueous ethanol media, *Sensors and Actuators B: Chemical*, 152(2011) 8-13.
- [72] M. Albrecht, R.A. Gossage, M. Lutz, A.L. Spek, G. van Koten, Diagnostic organometallic and metallodendritic materials for SO₂ gas detection: reversible binding of sulfur dioxide to arylplatinum (II) complexes, *Chemistry—A European Journal*, 6(2000) 1431-45.
- [73] J. Chao, X. Wang, Y. Liu, Y. Zhang, F. Huo, C. Yin, et al., A pyrene-thiophene based fluorescent probe for ratiometric sensing of bisulfite and its application in vivo imaging, *Sensors and Actuators B: Chemical*, 272(2018) 195-202.
- [74] X. Dai, T. Zhang, Z.-F. Du, X.-J. Cao, M.-Y. Chen, S.-W. Hu, et al., An effective colorimetric and ratiometric fluorescent probe for bisulfite in aqueous solution, *Analytica Chimica Acta*, 888(2015) 138-45.
- [75] B. Rui, Y. Feng, Y. Wang, J. Deng, M. Wang, Y. Lyu, et al., A novel isophorone-derived fluorescent probe for detecting sulfite and the application in monitoring the state of hybridoma cells, *Analytica Chimica Acta*, 1205(2022) 339723.
- [76] C. Liu, H. Wu, W. Yang, X. Zhang, A Simple Levulinate-based Ratiometric Fluorescent Probe for Sulfite with a Large Emission Shift, *Analytical Sciences*, 30(2014) 589-93.
- [77] X. Gu, C. Liu, Y.-C. Zhu, Y.-Z. Zhu, A Boron-dipyrromethene-Based Fluorescent Probe for Colorimetric and Ratiometric Detection of Sulfite, *Journal of Agricultural and Food Chemistry*, 59(2011) 11935-9.
- [78] L. Wang, W. Li, W. Zhi, D. Ye, Y. Wang, L. Ni, et al., A rapid-responsive fluorescent probe based on coumarin for selective sensing of sulfite in aqueous solution and its bioimaging by turn-on fluorescence signal, *Dyes and Pigments*, 147(2017) 357-63.

- [79] K. Wang, T. Li, X. Yang, K.-L. Zhang, Y.-Q. Jiang, L.-H. Zou, et al., Imaging fluctuation of sulfite in mouse tumor and inflammation models with a novel quinoxaline-based fluorescent probe, *Sensors and Actuators B: Chemical*, 365(2022) 131878.
- [80] K. Li, L.-L. Li, Q. Zhou, K.-K. Yu, J.S. Kim, X.-Q. Yu, Reaction-based fluorescent probes for SO₂ derivatives and their biological applications, *Coordination Chemistry Reviews*, 388(2019) 310-33.
- [81] T. Huang, Z. Hou, Q. Xu, L. Huang, C. Li, Y. Zhou, Polymer Vesicle Sensor for Visual and Sensitive Detection of SO₂ in Water, *Langmuir*, 33(2017) 340-6.
- [82] X. Cheng, H. Jia, J. Feng, J. Qin, Z. Li, “Reactive” probe for hydrogen sulfite: Good ratiometric response and bioimaging application, *Sensors and Actuators B: Chemical*, 184(2013) 274-80.
- [83] C. Yu, M. Luo, F. Zeng, S. Wu, A fast-responding fluorescent turn-on sensor for sensitive and selective detection of sulfite anions, *Analytical Methods*, 4(2012) 2638-40.
- [84] X. Cheng, H. Jia, J. Feng, J. Qin, Z. Li, “Reactive” probe for hydrogen sulfite: “turn-on” fluorescent sensing and bioimaging application, *Journal of Materials Chemistry B*, 1(2013) 4110-4.
- [85] H.-X. Yu, J. Zhi, J.-L. Wang, Regioisomeric AIE-active luminogens with a substituent aldehyde group for controllable and reversible photochromic behavior and sensitive fluorescence detection of hydrogen sulfite, *Journal of Materials Chemistry C*, 9(2021) 3882-91.
- [86] C. Ma, L. Zhang, L. Hou, F. Chen, A. Liu, R. Ji, et al., A fluorescent probe with a large Stokes shift for sensing sulfite in dry white wine based on pyrazolo[1,5-a]pyridine fluorophore, *Tetrahedron Letters*, 76(2021) 153210.
- [87] T. Wei, F. Wang, Y. Chen, J. Qiang, Z. Zhang, T. Chen, et al., A fluorescence probe for bisulfite sensing based on the bisulfite-induced binding site transfer between Zn²⁺ and an aminoquinoline derivate, *Dyes and Pigments*, 159(2018) 322-30.
- [88] Q. Wang, Y. Sun, J. Ge, L. Li, J. Lu, D. Zhang, et al., Ratiometric fluorescent nanoprobe based on coumarin dye-functionalized carbon dots for bisulfite detection in living cells and food samples, *Microchemical Journal*, 189(2023) 108561.
- [89] Y. Chen, X. Wang, X.-F. Yang, Y. Zhong, Z. Li, H. Li, Development of a ratiometric fluorescent probe for sulfite based on a coumarin–benzopyrylium platform, *Sensors and Actuators B: Chemical*, 206(2015) 268-75.

- [90] M. Li, W. Feng, H. Zhang, G. Feng, An aza-coumarin-hemicyanine based near-infrared fluorescent probe for rapid, colorimetric and ratiometric detection of bisulfite in food and living cells, *Sensors and Actuators B: Chemical*, 243(2017) 51-8.
- [91] J.-S. Lan, R.-F. Zeng, Y. Ding, Y. Zhang, T. Zhang, T. Wu, A simple pyrene-hemicyanine fluorescent probe for colorimetric and ratiometric detection of SO₂ derivatives in the mitochondria of living cells and zebrafish in vivo, *Sensors and Actuators B: Chemical*, 268(2018) 328-37.
- [92] G. Xu, H. Wu, X. Liu, R. Feng, Z. Liu, A simple pyrene-pyridinium-based fluorescent probe for colorimetric and ratiometric sensing of sulfite, *Dyes and Pigments*, 120(2015) 322-7.
- [93] X. Wang, H. Tang, X. Huang, Water-soluble fluorescent probes for bisulfite and viscosity imaging in living cells: Pyrene vs. anthracene, *Spectrochimica Acta Part A: Molecular and Biomolecular Spectroscopy*, 260(2021) 119902.
- [94] Y. Zhang, L. Guan, H. Yu, Y. Yan, L. Du, Y. Liu, et al., Reversible Fluorescent Probe for Selective Detection and Cell Imaging of Oxidative Stress Indicator Bisulfite, *Analytical Chemistry*, 88(2016) 4426-31.
- [95] H. Zhang, Z. Huang, G. Feng, Colorimetric and ratiometric fluorescent detection of bisulfite by a new HBT-hemicyanine hybrid, *Analytica Chimica Acta*, 920(2016) 72-9.
- [96] C.-J. Sun, X.-Q. Zhao, P.-F. Wang, H. Wang, B.-H. Han, Thiophene-based conjugated microporous polymers: synthesis, characterization and efficient gas storage, *Science China Chemistry*, 60(2017) 1067-74.
- [97] F. Qi, F. Zhang, L. Mo, X. Ren, Y. Wang, X. Li, et al., A HBT-based bifunctional fluorescent probe for the ratiometric detection of fluoride and sulphite in real samples, *Spectrochimica Acta Part A: Molecular and Biomolecular Spectroscopy*, 219(2019) 547-51.
- [98] L. Zhu, J. Nie, Q. Li, J. Du, X. Fan, F. Bai, et al., Reaction-based fluorescent probe for differential detection of cyanide and bisulfite in the aqueous media, *Journal of Luminescence*, 215(2019) 116620.
- [99] J. Qin, F. Kong, Y. Guo, D. Wang, C. Zhang, Y. Li, Rational construction of a two-photon NIR ratiometric fluorescent probe for the detection of bisulfite in live cells, tissues, and foods, *Journal of Agricultural and Food Chemistry*, 70(2022) 7314-20.
- [100] B. Yang, J. Xu, H.-L. Zhu, Recent progress in the small-molecule fluorescent probes for the detection of sulfur dioxide derivatives (HSO₃⁻/SO₃²⁻), *Free Radical Biology and Medicine*, 145(2019) 42-60.

Introduction and Literature Review

- [101] Y. Sun, S. Fan, S. Zhang, D. Zhao, L. Duan, R. Li, A fluorescent turn-on probe based on benzo [e] indolium for bisulfite through 1, 4-addition reaction, *Sensors and Actuators B: Chemical*, 193(2014) 173-7.
- [102] H. Feng, J. Liu, A. Qaitoon, Q. Meng, Y. Sultanbawa, Z. Zhang, et al., Responsive small-molecule luminescence probes for sulfite/bisulfite detection in food samples, *TrAC Trends in Analytical Chemistry*, 136(2021) 116199.
- [103] T. Li, X. Chen, K. Wang, Z. Hu, Small-Molecule Fluorescent Probe for Detection of Sulfite, *Pharmaceuticals*, 15(2022) 1326.
- [104] Y. Sun, D. Zhao, S. Fan, L. Duan, R. Li, Ratiometric fluorescent probe for rapid detection of bisulfite through 1, 4-addition reaction in aqueous solution, *Journal of agricultural and food chemistry*, 62(2014) 3405-9.
- [105] M.-Y. Wu, K. Li, C.-Y. Li, J.-T. Hou, X.-Q. Yu, A water-soluble near-infrared probe for colorimetric and ratiometric sensing of SO₂ derivatives in living cells, *Chemical Communications*, 50(2014) 183-5.
- [106] H. Tian, J. Qian, Q. Sun, H. Bai, W. Zhang, Colorimetric and ratiometric fluorescent detection of sulfite in water via cationic surfactant-promoted addition of sulfite to α , β -unsaturated ketone, *Analytica chimica acta*, 788(2013) 165-70.
- [107] H.-W. Chen, H.-C. Xia, O. Hakeim, Q.-H. Song, Phenothiazine and semi-cyanine based colorimetric and fluorescent probes for detection of sulfites in solutions and in living cells, *RSC advances*, 11(2021) 34643-51.
- [108] M. Gómez, E.G. Perez, V. Arancibia, C. Iribarren, C. Bravo-Díaz, O. García-Beltrán, et al., New fluorescent turn-off probes for highly sensitive and selective detection of SO₂ derivatives in a micellar media, *Sensors and Actuators B: Chemical*, 238(2017) 578-87.
- [109] M. Gómez, M.E. Aliaga, V. Arancibia, A. Moya, C. Segura, M.T. Nunez, et al., Detection of SO₂ derivatives using a new chalcone-coumarin derivative in cationic micellar media: application to real samples, *RSC advances*, 8(2018) 31261-6.
- [110] H. Li, Q. Yao, J. Fan, C. Hu, F. Xu, J. Du, et al., A Fluorescent Probe for Ratiometric Imaging of SO₂ Derivatives in Mitochondria of Living Cells, *Industrial & Engineering Chemistry Research*, 55(2016) 1477-83.
- [111] Z. Shang, J. Liu, Z. Hu, Q. Meng, Y. Wang, R. Zhang, et al., A near-infrared fluorescence probe for the detection of bisulfite in vivo and food samples, *Dyes and Pigments*, 200(2022) 110119.
- [112] D.F. Sava, M.A. Rodriguez, K.W. Chapman, P.J. Chupas, J.A. Greathouse, P.S. Crozier, et al., Capture of volatile iodine, a gaseous fission

product, by zeolitic imidazolate framework-8, *Journal of the American Chemical Society*, 133(2011) 12398-401.

[113] D.F. Sava, K.W. Chapman, M.A. Rodriguez, J.A. Greathouse, P.S. Crozier, H. Zhao, et al., Competitive I₂ Sorption by Cu-BTC from Humid Gas Streams, *Chemistry of Materials*, 25(2013) 2591-6.

[114] H. Li, X. Ding, B.H. Han, Porous azo-bridged porphyrin–phthalocyanine network with high iodine capture capability, *Chemistry–A European Journal*, 22(2016) 11863-8.

[115] K.W. Chapman, P.J. Chupas, T.M. Nenoff, Radioactive iodine capture in silver-containing mordenites through nanoscale silver iodide formation, *Journal of the American Chemical Society*, 132(2010) 8897-9.

[116] K.S. Subrahmanyam, D. Sarma, C.D. Malliakas, K. Polychronopoulou, B.J. Riley, D.A. Pierce, et al., Chalcogenide aerogels as sorbents for radioactive iodine, *Chemistry of Materials*, 27(2015) 2619-26.

[117] H. Kitagawa, H. Ohtsu, M. Kawano, Kinetic assembly of a thermally stable porous coordination network based on labile CuI units and the visualization of I₂ sorption, *Angewandte Chemie*, 125(2013) 12621-5.

[118] M.-H. Zeng, Q.-X. Wang, Y.-X. Tan, S. Hu, H.-X. Zhao, L.-S. Long, et al., Rigid pillars and double walls in a porous metal-organic framework: single-crystal to single-crystal, controlled uptake and release of iodine and electrical conductivity, *Journal of the American chemical society*, 132(2010) 2561-3.

[119] C. Falaise, C. Volkringer, J. Facqueur, T. Bousquet, L. Gasnot, T. Loiseau, Capture of iodine in highly stable metal–organic frameworks: a systematic study, *Chemical Communications*, 49(2013) 10320-2.

[120] X. Zhang, I. Da Silva, H.G. Godfrey, S.K. Callear, S.A. Sapchenko, Y. Cheng, et al., Confinement of iodine molecules into triple-helical chains within robust metal–organic frameworks, *Journal of the American Chemical Society*, 139(2017) 16289-96.

[121] B. Li, X. Dong, H. Wang, D. Ma, K. Tan, S. Jensen, et al., Capture of organic iodides from nuclear waste by metal-organic framework-based molecular traps, *Nature communications*, 8(2017) 1-9.

[122] A. Sigen, Y. Zhang, Z. Li, H. Xia, M. Xue, X. Liu, et al., Highly efficient and reversible iodine capture using a metalloporphyrin-based conjugated microporous polymer, *Chemical Communications*, 50(2014) 8495-8.

[123] Z. Yan, Y. Yuan, Y. Tian, D. Zhang, G. Zhu, Highly efficient enrichment of volatile iodine by charged porous aromatic frameworks with three sorption sites, *Angewandte Chemie*, 127(2015) 12924-8.

Introduction and Literature Review

- [124] X. Suo, F. Zhang, Z. Yang, H. Chen, T. Wang, Z. Wang, et al., Highly Perfluorinated Covalent Triazine Frameworks Derived from a Low-Temperature Ionothermal Approach Towards Enhanced CO₂ Electroreduction, *Angewandte Chemie International Edition*, 60(2021) 25688-94.
- [125] X. Li, Y. Peng, Q. Jia, Construction of hypercrosslinked polymers with dual nitrogen-enriched building blocks for efficient iodine capture, *Separation and Purification Technology*, 236(2020) 116260.
- [126] L. Shao, Y. Sang, N. Liu, Q. Wei, F. Wang, P. Zhan, et al., One-step synthesis of N-containing hyper-cross-linked polymers by two crosslinking strategies and their CO₂ adsorption and iodine vapor capture, *Separation and Purification Technology*, 262(2021) 118352.
- [127] J. Xu, W. Xie, C. Yao, G. Xu, S. Zhang, Y. Xu, Preparation of sulfur-containing conjugated microporous polymer for adsorbing iodine and Fe³⁺ sensing, *Journal of Environmental Chemical Engineering*, 9(2021) 106399.
- [128] S. Wang, Q. Hu, Y. Liu, X. Meng, Y. Ye, X. Liu, et al., Multifunctional conjugated microporous polymers with pyridine unit for efficient iodine sequestration, exceptional tetracycline sensing and removal, *Journal of Hazardous Materials*, 387(2020) 121949.
- [129] S. Wang, Y. Liu, Y. Ye, X. Meng, J. Du, X. Song, et al., Ultrahigh volatile iodine capture by conjugated microporous polymer based on N, N, N', N'-tetraphenyl-1, 4-phenylenediamine, *Polymer Chemistry*, 10(2019) 2608-15.
- [130] L. Wang, C. Yao, W. Xie, G. Xu, S. Zhang, Y. Xu, A series of thiophene- and nitrogen-rich conjugated microporous polymers for efficient iodine and carbon dioxide capture, *New Journal of Chemistry*, 45(2021) 19636-40.
- [131] F. Ren, Z. Zhu, X. Qian, W. Liang, P. Mu, H. Sun, et al., Novel thiophene-bearing conjugated microporous polymer honeycomb-like porous spheres with ultrahigh iodine uptake, *Chemical Communications*, 52(2016) 9797-800.
- [132] S. A, Y. Zhang, Z. Li, H. Xia, M. Xue, X. Liu, et al., Highly efficient and reversible iodine capture using a metalloporphyrin-based conjugated microporous polymer, *Chemical Communications*, 50(2014) 8495-8.
- [133] Y. Liao, J. Weber, B.M. Mills, Z. Ren, C.F.J. Faul, Highly Efficient and Reversible Iodine Capture in Hexaphenylbenzene-Based Conjugated Microporous Polymers, *Macromolecules*, 49(2016) 6322-33.
- [134] X. Qian, Z.-Q. Zhu, H.-X. Sun, F. Ren, P. Mu, W. Liang, et al., Capture and reversible storage of volatile iodine by novel conjugated microporous

polymers containing thiophene units, *ACS Applied Materials & Interfaces*, 8(2016) 21063-9.

[135] G. Xu, Y. Zhu, W. Xie, S. Zhang, C. Yao, Y. Xu, Porous cationic covalent triazine-based frameworks as platforms for efficient CO₂ and iodine capture, *Chemistry—An Asian Journal*, 14(2019) 3259-63.

[136] S. Chang, W. Xie, C. Yao, G. Xu, S. Zhang, Y. Xu, Preparation of covalent triazine frameworks with multiactive sites for efficient and reversible iodine capture, *European Polymer Journal*, 159(2021) 110753.

[137] P. Tu, X. He, R. Abu-Reziq, C. Pan, J. Tang, G. Yu, Fluorinated covalent triazine frameworks for effective CH₄ separation and iodine vapor uptake, *Separation and Purification Technology*, 290(2022) 120857.

[138] J. Wang, C. Wang, H. Wang, B. Jin, P. Zhang, L. Li, et al., Synthesis of N-containing porous aromatic frameworks via Scholl reaction for reversible iodine capture, *Microporous and Mesoporous Materials*, 310(2021) 110596.

[139] J. Chang, H. Li, J. Zhao, X. Guan, C. Li, G. Yu, et al., Tetrathiafulvalene-based covalent organic frameworks for ultrahigh iodine capture, *Chemical Science*, 12(2021) 8452-7.

[140] N. Mokhtari, M. Dinari, Developing novel amine-linked covalent organic frameworks towards reversible iodine capture, *Separation and Purification Technology*, 301(2022) 121948.

[141] X. Liu, A. Zhang, R. Ma, B. Wu, T. Wen, Y. Ai, et al., Experimental and theoretical insights into copper phthalocyanine-based covalent organic frameworks for highly efficient radioactive iodine capture, *Chinese Chemical Letters*, 33(2022) 3549-55.

[142] Y. Yang, X. Xiong, Y. Fan, Z. Lai, Z. Xu, F. Luo, Insight into volatile iodine uptake properties of covalent organic frameworks with different conjugated structures, *Journal of Solid State Chemistry*, 279(2019) 120979.

[143] M. Xu, T. Wang, L. Zhou, D. Hua, Fluorescent conjugated mesoporous polymers with N,N-diethylpropylamine for the efficient capture and real-time detection of volatile iodine, *Journal of Materials Chemistry A*, 8(2020) 1966-74.

[144] M. Ansari, A. Hassan, A. Alam, N. Das, A mesoporous polymer bearing 3D-Triptycene, -OH and azo- functionalities: Reversible and efficient capture of carbon dioxide and iodine vapor, *Microporous and Mesoporous Materials*, 323(2021) 111242.

[145] M. Janeta, W. Bury, S. Szafert, Porous Silsesquioxane-Imine Frameworks as Highly Efficient Adsorbents for Cooperative Iodine Capture, *ACS Applied Materials & Interfaces*, 10(2018) 19964-73.

Introduction and Literature Review

- [146] N.T. Hung, M. Watanabe, T. Kimura, Solvent extraction of palladium (II) with various ketones from nitric acid medium, *Solvent Extraction and Ion Exchange*, 25(2007) 407-16.
- [147] C. Blöcher, J. Dorda, V. Mavrov, H. Chmiel, N. Lazaridis, K. Matis, Hybrid flotation—membrane filtration process for the removal of heavy metal ions from wastewater, *Water Research*, 37(2003) 4018-26.
- [148] A. Bashir, L.A. Malik, S. Ahad, T. Manzoor, M.A. Bhat, G. Dar, et al., Removal of heavy metal ions from aqueous system by ion-exchange and biosorption methods, *Environmental Chemistry Letters*, 17(2019) 729-54.
- [149] U. Ipek, Removal of Ni (II) and Zn (II) from an aqueous solution by reverse osmosis, *Desalination*, 174(2005) 161-9.
- [150] A. Pohl, Removal of heavy metal ions from water and wastewaters by sulfur-containing precipitation agents, *Water, Air, & Soil Pollution*, 231(2020) 1-17.
- [151] H.-C. Tao, T. Lei, G. Shi, X.-N. Sun, X.-Y. Wei, L.-J. Zhang, et al., Removal of heavy metals from fly ash leachate using combined bioelectrochemical systems and electrolysis, *Journal of Hazardous materials*, 264(2014) 1-7.
- [152] H. Chen, Z. Gong, Z. Zhuo, X. Zhong, M. Zhou, X. Xiang, et al., Tuning the defects in lignin-derived-carbon and trimetallic layered double hydroxides composites (LDH@ LDC) for efficient removal of U (VI) and Cr (VI) in aquatic environment, *Chemical Engineering Journal*, 428(2022) 132113.
- [153] X. Guan, X. Yuan, Y. Zhao, H. Wang, H. Wang, J. Bai, et al., Application of functionalized layered double hydroxides for heavy metal removal: A review, *Science of The Total Environment*, (2022) 155693.
- [154] P. Sherugar, N.S. Naik, M. Padaki, V. Nayak, A. Gangadharan, A.R. Nadig, et al., Fabrication of zinc doped aluminium oxide/polysulfone mixed matrix membranes for enhanced antifouling property and heavy metal removal, *Chemosphere*, 275(2021) 130024.
- [155] P. Wang, D. Sun, M. Deng, S. Zhang, Q. Bi, W. Zhao, et al., Amorphous phosphated titanium oxide with amino and hydroxyl bifunctional groups for highly efficient heavy metal removal, *Environmental Science: Nano*, 7(2020) 1266-74.
- [156] Y. Gong, Y. Wang, N. Lin, R. Wang, M. Wang, X. Zhang, Iron-based materials for simultaneous removal of heavy metal (loid) s and emerging organic contaminants from the aquatic environment: Recent advances and perspectives, *Environmental Pollution*, (2022) 118871.

- [157] C.-Y. Chen, C.-L. Chiang, C.-R. Chen, Removal of heavy metal ions by a chelating resin containing glycine as chelating groups, *Separation and Purification Technology*, 54(2007) 396-403.
- [158] M. Cegłowski, G. Schroeder, Preparation of porous resin with Schiff base chelating groups for removal of heavy metal ions from aqueous solutions, *Chemical Engineering Journal*, 263(2015) 402-11.
- [159] G. Li, Z. Zhao, J. Liu, G. Jiang, Effective heavy metal removal from aqueous systems by thiol functionalized magnetic mesoporous silica, *Journal of hazardous materials*, 192(2011) 277-83.
- [160] M. Anbia, K. Kargosha, S. Khoshbooei, Heavy metal ions removal from aqueous media by modified magnetic mesoporous silica MCM-48, *Chemical Engineering Research and Design*, 93(2015) 779-88.
- [161] E.A. Deliyanni, G.Z. Kyzas, K.S. Triantafyllidis, K.A. Matis, Activated carbons for the removal of heavy metal ions: A systematic review of recent literature focused on lead and arsenic ions, *Open Chemistry*, 13(2015).
- [162] R.B. Onyancha, U.O. Aigbe, K.E. Ukhurebor, P.W. Muchiri, Facile synthesis and applications of carbon nanotubes in heavy-metal remediation and biomedical fields: a comprehensive review, *Journal of Molecular Structure*, 1238(2021) 130462.
- [163] A.T. Hoang, S. Nižetić, C.K. Cheng, R. Luque, S. Thomas, T.L. Banh, et al., Heavy metal removal by biomass-derived carbon nanotubes as a greener environmental remediation: A comprehensive review, *Chemosphere*, 287(2022) 131959.
- [164] N. Rajesh, A.K. Kumar, S. Kalidhasan, V. Rajesh, Trialkylamine impregnated macroporous polymeric sorbent for the effective removal of chromium from industrial wastewater, *Journal of Chemical & Engineering Data*, 56(2011) 2295-304.
- [165] M.X. Tan, Y.N. Sum, J.Y. Ying, Y. Zhang, A mesoporous poly-melamine-formaldehyde polymer as a solid sorbent for toxic metal removal, *Energy & Environmental Science*, 6(2013) 3254-9.
- [166] K. Zhao, L. Kong, W. Yang, Y. Huang, H. Li, S. Ma, et al., Hooped amino-group chains in porous organic polymers for enhancing heavy metal ion removal, *ACS applied materials & interfaces*, 11(2019) 44751-7.
- [167] Y. He, Q. Liu, J. Hu, C. Zhao, C. Peng, Q. Yang, et al., Efficient removal of Pb (II) by amine functionalized porous organic polymer through post-synthetic modification, *Separation and Purification Technology*, 180(2017) 142-8.

Introduction and Literature Review

- [168] H. Masoumi, A. Ghaemi, H. Ghanadzadeh Gilani, Exploiting the performance of hyper-cross-linked polystyrene for removal of multi-component heavy metal ions from wastewaters, *Journal of Environmental Chemical Engineering*, 9(2021) 105724.
- [169] Z. Yang, G. Wu, Q. Li, H. Ai, X. Yao, H. Ji, Removal of various pollutants from wastewaters using an efficient and degradable hypercrosslinked polymer, *Separation Science and Technology*, 56(2021) 860-9.
- [170] H. Masoumi, A. Ghaemi, H. Gannadzadeh Gilani, Synthesis of polystyrene-based hyper-cross-linked polymers for Cd(II) ions removal from aqueous solutions: Experimental and RSM modeling, *Journal of Hazardous Materials*, 416(2021) 125923.
- [171] L. Xiang, Y. Zhu, S. Gu, D. Chen, X. Fu, Y. Zhang, et al., A luminescent hypercrosslinked conjugated microporous polymer for efficient removal and detection of mercury ions, *Macromolecular Rapid Communications*, 36(2015) 1566-71.
- [172] R.-X. Yang, T.-T. Wang, W.-Q. Deng, Extraordinary capability for water treatment achieved by a perfluorous conjugated microporous polymer, *Scientific Reports*, 5(2015) 10155.
- [173] Q. Wang, R. Li, X. Ouyang, G. Wang, A novel indole-based conjugated microporous polymer for highly effective removal of heavy metals from aqueous solution via double cation- π interactions, *RSC advances*, 9(2019) 40531-5.
- [174] X.-X. Qiao, G.-F. Liu, J.-T. Wang, Y.-Q. Zhang, J. Lü, Highly Efficient and Selective Removal of Lead Ions from Aqueous Solutions by Conjugated Microporous Polymers with Functionalized Heterogeneous Pores, *Crystal Growth & Design*, 20(2020) 337-44.
- [175] Q.-M. Hasi, Z.-C. Han, Y.-P. Guo, J.-L. Yu, C.-H. Xiao, Y.-H. Zhang, et al., Porphyrin-Based Conjugated Microporous Polymers for Highly Efficient Adsorption of Metal Ions, *Langmuir*, 38(2022) 9507-17.
- [176] G. Li, J. Ye, Q. Fang, F. Liu, Amide-based covalent organic frameworks materials for efficient and recyclable removal of heavy metal lead (II), *Chemical Engineering Journal*, 370(2019) 822-30.
- [177] T. Xu, L. Zhou, Y. He, S. An, C. Peng, J. Hu, et al., Covalent Organic Framework with Triazine and Hydroxyl Bifunctional Groups for Efficient Removal of Lead(II) Ions, *Industrial & Engineering Chemistry Research*, 58(2019) 19642-8.

- [178] S. Tighadouini, S. Radi, M. El Massaoudi, Z. Lakbaibi, M. Ferbinteanu, Y. Garcia, Efficient and Environmentally Friendly Adsorbent Based on β -Ketoenol-Pyrazole-Thiophene for Heavy-Metal Ion Removal from Aquatic Medium: A Combined Experimental and Theoretical Study, *ACS Omega*, 5(2020) 17324-36.
- [179] Y. Yang, Z. Yan, L. Wang, Q. Meng, Y. Yuan, G. Zhu, Constructing synergistic groups in porous aromatic frameworks for the selective removal and recovery of lead(ii) ions, *Journal of Materials Chemistry A*, 6(2018) 5202-7.
- [180] M.I. Shariful, S.B. Sharif, J.J.L. Lee, U. Habiba, B.C. Ang, M.A. Amalina, Adsorption of divalent heavy metal ion by mesoporous-high surface area chitosan/poly (ethylene oxide) nanofibrous membrane, *Carbohydrate Polymers*, 157(2017) 57-64.
- [181] G. Derouich, S.A. Younssi, J. Bennazha, J.A. Cody, M. Ouammou, M. El Rhazi, Development of low-cost polypyrrole/sintered pozzolan ultrafiltration membrane and its highly efficient performance for congo red dye removal, *Journal of Environmental Chemical Engineering*, 8(2020) 103809.
- [182] A. Singh, D.B. Pal, A. Mohammad, A. Alhazmi, S. Haque, T. Yoon, et al., Biological remediation technologies for dyes and heavy metals in wastewater treatment: New insight, *Bioresource Technology*, 343(2022) 126154.
- [183] L. Suhadolnik, A. Pohar, U. Novak, B. Likozar, A. Mihelič, M. Čeh, Continuous photocatalytic, electrocatalytic and photo-electrocatalytic degradation of a reactive textile dye for wastewater-treatment processes: Batch, microreactor and scaled-up operation, *Journal of industrial and engineering chemistry*, 72(2019) 178-88.
- [184] S. Ihaddaden, D. Aberkane, A. Boukerroui, D. Robert, Removal of methylene blue (basic dye) by coagulation-flocculation with biomaterials (bentonite and *Opuntia ficus indica*), *Journal of Water Process Engineering*, 49(2022) 102952.
- [185] G. Bal, A. Thakur, Distinct approaches of removal of dyes from wastewater: A review, *Materials Today: Proceedings*, 50(2022) 1575-9.
- [186] H. Mittal, M. Khanuja, Hydrothermal in-situ synthesis of MoSe₂-polypyrrole nanocomposite for efficient photocatalytic degradation of dyes under dark and visible light irradiation, *Separation and Purification Technology*, 254(2021) 117508.
- [187] A. Fetimi, S. Merouani, M.S. Khan, M.N. Asghar, K.K. Yadav, B.-H. Jeon, et al., Modeling of Textile Dye Removal from Wastewater Using

Introduction and Literature Review

Innovative Oxidation Technologies (Fe (II)/Chlorine and H₂O₂/Periodate Processes): Artificial Neural Network-Particle Swarm Optimization Hybrid Model, *ACS omega*, 7(2022) 13818-25.

[188] F. Mashkoor, A. Nasar, Carbon nanotube-based adsorbents for the removal of dyes from waters: a review, *Environmental Chemistry Letters*, 18(2020) 605-29.

[189] F.S.A. Khan, N.M. Mubarak, Y.H. Tan, M. Khalid, R.R. Karri, R. Walvekar, et al., A comprehensive review on magnetic carbon nanotubes and carbon nanotube-based buckypaper for removal of heavy metals and dyes, *Journal of Hazardous Materials*, 413(2021) 125375.

[190] M.J. Hassan, M.F. Islam, N. Akter, M.N. Uddin, A.Y. Abir, S.B. Aoun, et al., Applicability of gypsum in selective removal of anionic dye molecules from aqueous medium, *Applied Water Science*, 11(2021) 1-11.

[191] M. Tony, Zeolite-based adsorbent from alum sludge residue for textile wastewater treatment, *International Journal of Environmental Science and Technology*, 17(2020) 2485-98.

[192] C. Wang, J. Yu, K. Feng, L. Wang, J. Huang, Synthesis of porous magnetic zeolite-based material and its performance on removal of Cd²⁺ ion and methylene blue from aqueous solution, *Microporous and Mesoporous Materials*, 345(2022) 112256.

[193] T. Saeed, A. Naeem, I.U. Din, M. Farooq, I.W. Khan, M. Hamayun, et al., Synthesis of chitosan composite of metal-organic framework for the adsorption of dyes; kinetic and thermodynamic approach, *Journal of Hazardous Materials*, 427(2022) 127902.

[194] J.-L. Miao, J.-Q. Ren, H.-J. Li, D.-G. Wu, Y.-C. Wu, Mesoporous crosslinked chitosan-activated clinoptilolite biocomposite for the removal of anionic and cationic dyes, *Colloids and Surfaces B: Biointerfaces*, 216(2022) 112579.

[195] A.G. Pereira, F.H. Rodrigues, A.T. Paulino, A.F. Martins, A.R. Fajardo, Recent advances on composite hydrogels designed for the remediation of dye-contaminated water and wastewater: A review, *Journal of Cleaner Production*, 284(2021) 124703.

[196] S. Huang, L. Wu, T. Li, D. Xu, X. Lin, C. Wu, Facile preparation of biomass lignin-based hydroxyethyl cellulose super-absorbent hydrogel for dye pollutant removal, *International journal of biological macromolecules*, 137(2019) 939-47.

Introduction and Literature Review

- [197] S.-W. Lv, J.-M. Liu, Z.-H. Wang, H. Ma, C.-Y. Li, N. Zhao, et al., Recent advances on porous organic frameworks for the adsorptive removal of hazardous materials, *Journal of Environmental Sciences*, 80(2019) 169-85.
- [198] G. Xiong, B.-B. Wang, L.-X. You, B.-Y. Ren, Y.-K. He, F. Ding, et al., Hypervalent silicon-based, anionic porous organic polymers with solid microsphere or hollow nanotube morphologies and exceptional capacity for selective adsorption of cationic dyes, *Journal of Materials Chemistry A*, 7(2019) 393-404.
- [199] P. Su, X. Zhang, Z. Xu, G. Zhang, C. Shen, Q. Meng, Amino-functionalized hypercrosslinked polymers for highly selective anionic dye removal and CO₂/N₂ separation, *New Journal of Chemistry*, 43(2019) 17267-74.
- [200] R. Shen, X. Yan, Y.-J. Guan, W. Zhu, T. Li, X.-G. Liu, et al., One-pot synthesis of a highly porous anionic hypercrosslinked polymer for ultrafast adsorption of organic pollutants, *Polymer Chemistry*, 9(2018) 4724-32.
- [201] M.G. Mohamed, A.F. El-Mahdy, T.-S. Meng, M.M. Samy, S.-W. Kuo, Multifunctional hypercrosslinked porous organic polymers based on tetraphenylethene and triphenylamine derivatives for high-performance dye adsorption and supercapacitor, *Polymers*, 12(2020) 2426.
- [202] Y. He, W. Bao, Y. Hua, Z. Guo, X. Fu, B. Na, et al., Efficient adsorption of methyl orange and methyl blue dyes by a novel triptycene-based hypercrosslinked porous polymer, *RSC advances*, 12(2022) 5587-94.
- [203] W. Zhao, Y. Jiao, R. Gao, L. Wu, S. Cheng, Q. Zhuang, et al., Sulfonate-grafted conjugated microporous polymers for fast removal of cationic dyes from water, *Chemical Engineering Journal*, 391(2020) 123591.
- [204] S. Wang, X. Meng, H. Luo, L. Yao, X. Song, Z. Liang, Post-synthetic modification of conjugated microporous polymer with imidazolium for highly efficient anionic dyes removal from water, *Separation and Purification Technology*, 284(2022) 120245.
- [205] Y. Liu, Y. Cui, C. Zhang, J. Du, S. Wang, Y. Bai, et al., Post-cationic modification of a pyrimidine-based conjugated microporous polymer for enhancing the removal performance of anionic dyes in water, *Chemistry–A European Journal*, 24(2018) 7480-8.
- [206] Y. Li, C.-X. Yang, H.-L. Qian, X. Zhao, X.-P. Yan, Carboxyl-Functionalized Covalent Organic Frameworks for the Adsorption and Removal of Triphenylmethane Dyes, *ACS Applied Nano Materials*, 2(2019) 7290-8.

Introduction and Literature Review

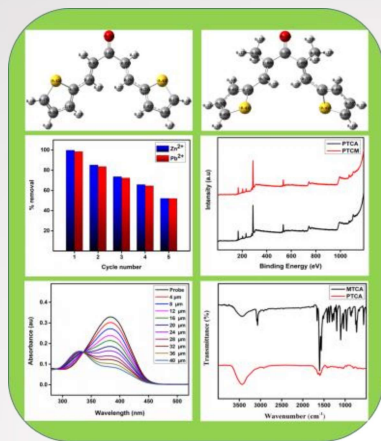
- [207] L. Zhang, J.S. Sun, F. Sun, P. Chen, J. Liu, G. Zhu, Facile synthesis of ultrastable porous aromatic frameworks by Suzuki–Miyaura coupling reaction for adsorption removal of organic dyes, *Chemistry–A European Journal*, 25(2019) 3903-8.
- [208] S. Zhou, L. Jin, P. Gu, L. Tian, N. Li, D. Chen, et al., Novel calixarene-based porous organic polymers with superfast removal rate and ultrahigh adsorption capacity for selective separation of cationic dyes, *Chemical Engineering Journal*, 433(2022) 134442.
- [209] Q. Ou, Q.-M. Zhang, P.-C. Zhu, Q.-P. Zhang, Z. Cheng, C. Zhang, Pentiptycene-based microporous polymer for removal of organic dyes from water, *European Polymer Journal*, 120(2019) 109216.
- [210] N. Rajendran, J. Samuel, M.O. Amin, E. Al-Hetlani, S. Makhseed, Carbazole-tagged pyridinic microporous network polymer for CO₂ storage and organic dye removal from aqueous solution, *Environmental Research*, 182(2020) 109001.
- [211] S. Chakraborty, S. Chowdhury, P. Das Saha, Adsorption of Crystal Violet from aqueous solution onto NaOH-modified rice husk, *Carbohydrate Polymers*, 86(2011) 1533-41.
- [212] V. Sabna, S.G. Thampi, S. Chandrakaran, Adsorption of crystal violet onto functionalised multi-walled carbon nanotubes: Equilibrium and kinetic studies, *Ecotoxicology and Environmental Safety*, 134(2016) 390-7.
- [213] H. Mittal, A. Al Alili, P.P. Morajkar, S.M. Alhassan, Graphene oxide crosslinked hydrogel nanocomposites of xanthan gum for the adsorption of crystal violet dye, *Journal of Molecular Liquids*, 323(2021) 115034.
- [214] S. Senthilkumar, P. Kalaamani, C.V. Subburaam, Liquid phase adsorption of Crystal violet onto activated carbons derived from male flowers of coconut tree, *Journal of Hazardous Materials*, 136(2006) 800-8.
- [215] P. Monash, G. Pugazhenthii, Adsorption of crystal violet dye from aqueous solution using mesoporous materials synthesized at room temperature, *Adsorption*, 15(2009) 390-405.
- [216] B.K. Nandi, A. Goswami, A.K. Das, B. Mondal, M.K. Purkait, Kinetic and Equilibrium Studies on the Adsorption of Crystal Violet Dye using Kaolin as an Adsorbent, *Separation Science and Technology*, 43(2008) 1382-403.
- [217] G. Sharma, A. Kumar, M. Naushad, A. García-Peñas, A.a.H. Al-Muhtaseb, A.A. Ghfar, et al., Fabrication and characterization of Gum arabic-cl-poly(acrylamide) nanohydrogel for effective adsorption of crystal violet dye, *Carbohydrate Polymers*, 202(2018) 444-53.

Introduction and Literature Review

- [218] K. Elsherif, A. El-Dali, A. Alkarewi, A. Ewlad-Ahmed, A. Treban, Adsorption of crystal violet dye onto olive leaves powder: Equilibrium and kinetic studies, KM Elsherif, A El-Dali, AA Alkarewi, AM Ewlad-Ahmed and A Treban Adsorption of crystal violet dye onto olive leaves powder: Equilibrium and kinetic studies Chemistry International, 7(2021) 79-89.
- [219] S. Sultana, K. Islam, M.A. Hasan, H.M.J. Khan, M.A.R. Khan, A. Deb, et al., Adsorption of crystal violet dye by coconut husk powder: Isotherm, kinetics and thermodynamics perspectives, Environmental Nanotechnology, Monitoring & Management, 17(2022) 100651.
- [220] K.N.A. Putri, A. Keereerak, W. Chinpa, Novel cellulose-based biosorbent from lemongrass leaf combined with cellulose acetate for adsorption of crystal violet, International Journal of Biological Macromolecules, 156(2020) 762-72.
- [221] X.-L. Gong, H.-Q. Lu, K. Li, W. Li, Effective adsorption of crystal violet dye on sugarcane bagasse–bentonite/sodium alginate composite aerogel: Characterisation, experiments, and advanced modelling, Separation and Purification Technology, 286(2022) 120478.
- [222] A. salah omer, G. A.El Naeem, A.I. Abd-Elhamid, O. O.M. Farahat, A. A. El-Bardan, H. M.A. Soliman, et al., Adsorption of crystal violet and methylene blue dyes using a cellulose-based adsorbent from sugercane bagasse: characterization, kinetic and isotherm studies, Journal of Materials Research and Technology, 19(2022) 3241-54.
- [223] M. Sulyman, J. Kucinska-Lipka, M. Sienkiewicz, A. Gierak, Development, characterization and evaluation of composite adsorbent for the adsorption of crystal violet from aqueous solution: Isotherm, kinetics, and thermodynamic studies, Arabian Journal of Chemistry, 14(2021) 103115.

Chapter 2

Materials, methods, and characterization



This chapter deals with various materials and methods used to carry out the synthesis and studies that have been done throughout this research work. This chapter also explains different characterisation techniques employed to characterize the monomers and polymers.

2.1. Materials

2.2. Characterization techniques

2.3. Synthetic procedures

2.3.1. Synthesis of monomers

2.3.2. Synthesis of polymers

2.4. Methods and measurements

2.4.1. Sensing of SO₂ - derivatives

2.4.2. Iodine capture studies

2.4.3. Removal of heavy metal ions

2.4.4. Adsorption of cationic dyes

2.5. Characterization of synthesized monomers

2.6. Characterization of synthesized polymers

2.1. Materials

All chemicals and solvents used for synthesis and study were purchased from commercial suppliers and used without further purification. Anhydrous ferric chloride (FeCl_3), thiophene-2-carbaldehyde, acetone, and 3-pentanone were the chemicals used for the synthesis of monomers and polymers. Sodium sulfite (Na_2SO_3) and sodium bisulfite (NaHSO_3) were employed as chemical analytes, while crystal sugar and brown sugar were employed as real food samples to conduct the sensing studies. Cetyl trimethyl ammonium bromide (CTAB), cocamidopropyl betaine (CAPB), and sodium dodecyl benzene sulfonate (SDBS) were various surfactants, and 4-(2-hydroxyethyl)-1-piperazineethanesulfonic acid (HEPES) was the buffer used for the aforesaid investigation. Iodine granules were used to conduct an iodine capture experiment. Nitrate salts of cobalt, copper, nickel, cadmium, zinc, and lead were used to prepare metal ion solutions for conducting adsorption studies. Methylene blue (MB), rhodamine B (RB), malachite green (MG), and crystal violet (CV) are the cationic dyes and methyl orange (MO), methyl red (MR), and congo red (CR) are the anionic dyes selected for the dye adsorption studies. Ethanol, methanol, acetone, dichloromethane, chloroform, distilled water, and de-ionized water are the solvents used throughout this study.

2.2. Characterization techniques

This section outlines the various analytical techniques employed in this study. Fourier transform infrared (FT-IR) spectra was recorded using a Jasco-FT/IR-4100 spectrometer in the range of $4000 - 400 \text{ cm}^{-1}$. UV-Visible (UV-Vis) spectra and UV diffuse reflectance spectra (UV-DRS)

Materials, Methods, and Characterization

were obtained by using a Jasco V-770 UV-Vis-NIR spectrophotometer. Powder X-ray diffraction (PXRD) patterns were recorded on an X'pert3 powder diffractometer, and the CHNS elemental analyses were done using a Thermo Scientific FLASH 2000 HT analyzer. Thermogravimetric analysis (TGA) was conducted on an STA 8000 thermogravimeter, and the nitrogen adsorption-desorption isotherms were recorded with a BELCAT-M analyzer at 77 K. Scanning electron microscopic (SEM) images were acquired on a ZEISS GeminiSEM 300 electron microscope, and Transmission electron microscopic (TEM) images were obtained on a Jeol/JEM 2100 electron microscope. ^1H NMR (400 MHz) and ^{13}C NMR (400 MHz) spectra were recorded on a Bruker AVANCE III - 400 MHz NMR spectrometer, and HR-MS data were obtained with a Q-TOF MS spectrometer. Solid-state (SS) NMR has recorded on a BRUKER AVANCE NEO (500 MHz) NMR spectrometer, and the pH measurements were done on a Mettler Toledo pH meter. The X-ray photoelectron spectroscopy (XPS) was performed with a PHI Versa Probe II X-ray photoelectron spectrometer and Raman spectra were recorded on Bruker's MultiRAM Raman system. Zeta potential analysis was performed with a Malvern Zetasizer, and metal ion concentration was determined by using Agilent 7800 inductively coupled plasma mass spectrometer (ICP-MS).

2.2.1. Fourier transform infrared spectroscopy (FT-IR)

This analytical method makes use of how matter and IR radiation interact with each other. The sample absorbs the radiation of different wavelengths corresponding to the characteristic vibrational frequencies of the functional groups present in the sample. A molecular fingerprint

Materials, Methods, and Characterization

of the sample can be derived from its FT-IR spectra. Here we have used FT-IR spectroscopy to elucidate the structure of monomers and polymers, to explain the mechanism of sensing, iodine capture, dye adsorption, and heavy metal ion removal.

2.2.2. UV-Visible spectroscopy (UV/Vis, UV-DRS)

UV-Vis spectroscopy is an analytical technique that measures the amount of particular wavelengths of UV or visible light that are absorbed by or transmitted through a sample in contrast to a reference sample. The amount of absorbed or transmitted light depends on the sample composition, hence providing qualitative and quantitative information on the composition of the sample. UV- diffused reflectance spectroscopy measures the absorbance or reflectance of the sample in its solid form. This technique was mostly used in this investigation to estimate bisulfite/sulfite concentrations and to verify the synthesis of polymers.

2.2.3. X-Ray diffraction studies (XRD)

It is a non-destructive method that offers thorough details about the crystallographic structure, chemical composition, and physical characteristics of the sample. Bragg's peaks of XRD patterns, which are created by the constructive interference of monochromatic X-rays reflected from the sample, give information about the crystalline or amorphous nature of the sample. Sharp peaks represent the crystalline nature, while broad peaks represent the amorphous nature. From the XRD patterns obtained, we deduced the amorphous nature of polymers.

2.2.4. Field emission scanning electron microscopy (FE-SEM)

It is a cutting-edge technology used to photograph sample surfaces. An electron beam is used to scan the sample, and as the electrons interact with the atoms of the sample, signals such as backscattered electrons, secondary electrons, X-rays, or light are produced. The most favoured FE-SEM method, which produces high-resolution images, is secondary electron detection. This analysis is widely used to examine the topography, morphology, and composition of the sample. Using FE-SEM examination, the morphology of the synthesized polymers was determined.

2.2.5. High-resolution transmission electron microscopy (HR-TEM)

The atomic structure of samples can be directly imaged using an analytical method called HR-TEM. It is a prevailing method to investigate the properties of materials on the atomic scale. It accounts for how electron beams interact with the sample, and images of the sample are produced by sensing the transmitted electrons. When TEM transmits electrons through the sample, it can reveal details about the internal structure of the material, including pore volume, pore size, and pore shape. The uniform distribution of nanoscale pores in the polymers was identified from the TEM analysis.

2.2.6. Zeta potential analysis

Zeta potential value merely provides an indirect evaluation of the samples' surface charges. It is a measurement of the electric potential at the boundary between a suspended solid particle and a liquid. If the sample is charged, the oppositely charged ions in the liquid will

Materials, Methods, and Characterization

surround it, creating a thin charged layer known as the Stern layer. A second outer layer, referred to as the diffusive layer, is present in addition to the Stern layer and is created by weakly bound ions with the opposite charge. A barrier between the ions in the diffusive layer and the ions still present in the bulk is created when this double layer travels in liquid under the influence of an electric field or gravity. Zeta potential is the measure of the electrostatic potential at this boundary. Surface charges of polymers and iodine-loaded polymers were measured using this method.

2.2.7. Elemental analysis (CHNS analysis)

The process in which a sample is examined for its elemental and occasionally isotopic composition is known as elemental analysis. It gives qualitative as well as quantitative information about the elements present in the sample. In the field of organic chemistry, elemental analysis mainly focuses on the detection of the mass fractions of carbon, nitrogen, hydrogen, and a heteroatom usually halogen or sulfur, hence elemental analysis in organic chemistry is largely known as CHNS analysis. The elemental analysis data is significant to determine the structure and purity of samples. Here we used CHNS analysis to find out the elemental composition of the synthesized polymers.

2.2.8. Thermogravimetric analysis (TGA)

Thermal analysis (TGA) is a method that determines the weight loss of the sample as a function of temperature or time. This measurement reveals details regarding both chemical and physical processes, such as phase transitions, thermal decomposition, chemisorption, physisorption,

adsorption, desorption, etc. TGA of the polymers was conducted to record the thermal stability of the polymers.

2.2.9. Brunauer–Emmett–Teller analysis (BET)

BET analysis is used to evaluate the surface areas and pore size distributions of the sample. The process relies on the physical adsorption of inert gas, like nitrogen, onto the sample surface. The whole microscopic surface area of the sample may be recorded since the gas molecules can travel through all pores and fissures, as well as between particles, in the sample. The Barrett, Joyner, and Halenda (BJH) approach is used to determine pore size distributions using experimental nitrogen adsorption-desorption isotherms. The surface area and mesoporous nature of the polymers were concluded from the BET analysis.

2.2.10. X-ray photoelectron spectroscopy (XPS)

X-ray photoelectron spectroscopy (XPS), commonly referred to as electron spectroscopy for chemical analysis (ESCA), is a method for examining the surface chemistry of a material. By using XPS, it is possible to determine the elemental composition of the sample surface along with its chemical and electronic states. The photoelectric effect is used in XPS as its working principle. According to the characteristic energy values, the electrons that are emitted from each atom produce corresponding characteristic peaks on the XPS spectrum. Hence, by analyzing the intensity and energy values of the peaks in the XPS spectra of the samples, we can determine the composition and chemical state of all the elements present in the sample (other than

hydrogen and helium). With the help of XPS, we elucidated the mechanism of iodine capture and heavy metal ion removal.

2.2.11. Raman spectroscopy

Detailed information regarding chemical structure, crystallinity, and molecular interactions can be obtained using the non-destructive chemical analysis method known as Raman spectroscopy. Raman scattering, a type of inelastic photon scattering, is the basis for this technique. It makes use of a monochromatic light source, often a laser operating in the visible, near-infrared range. The interaction of this laser light with the sample results in an upward or downward shift in the energy of the laser photons. The energy shift provides details on the vibrational modes in the sample. In this work, we have used Raman spectroscopy to elucidate the mechanism of iodine capture.

2.2.12. Nuclear magnetic resonance (NMR) spectroscopy

The molecular structure of a sample is ascertained at the atomic level using NMR spectroscopy. NMR spectroscopy can also be used to identify reaction states, phase changes, conformational and configurational changes, etc. This method of analysis utilizes the interaction of atomic nuclei and externally applied radiowaves. The nuclear spin state changes as a result of the net energy exchange that occurs during this interaction. The ^1H NMR and ^{13}C NMR techniques are the two most often utilized NMR kinds. To differentiate between a CH_3 group, a CH_2 group, and a CH group, an NMR technique called distortionless enhancement by polarisation transfer (DEPT) is utilized. Structural characterization of monomers was done using ^1H NMR, ^{13}C

Materials, Methods, and Characterization

NMR, and DEPT analysis. Solid-state NMR (SS-NMR) with the ^{13}C cross-polarization magic angle spinning NMR (^{13}C CP/MAS NMR) was used for the structural elucidation of polymers.

2.2.13. High-resolution mass spectrometry (HR-MS)

It is an analytical method for figuring out the exact molecular mass of the components present in the sample. These tools can be used to discriminate distinct compounds with the same nominal mass, identify unknowns, and ascertain elemental compositions. During the analysis, the sample is ionized by bombarding it with a beam of electrons. As a result, some of the molecules in the sample get fragmented into positively charged parts or some become positively charged as a whole. These ions or fragments are separated based on their mass-to-charge ratio, and finally, detected using a suitable detector. The results are displayed as a mass spectrum, which is a plot of intensity Vs ion mass-to-charge ratio. Here we used HR-MS for the characterization of sensing products and monomers.

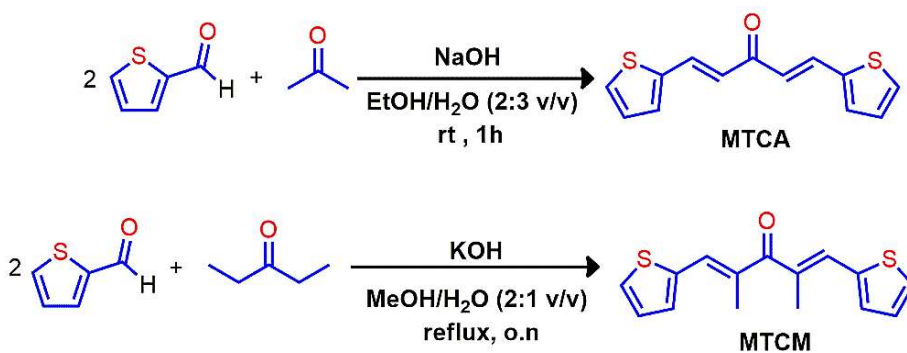
2.2.14. Inductively coupled plasma mass spectrometry (ICP-MS)

ICP-MS is a kind of mass spectrometry that uses an inductively coupled plasma to ionize the sample. The material is atomized to produce atomic and polyatomic ions, which are later identified. It is utilized to detect trace amounts of metals and several non-metals in liquid samples. Even various isotopes of the same element can be detected. ICP-MS was used to calculate the concentration of heavy metal ions during the metal adsorption studies.

2.3. Synthetic procedures

2.3.1. Synthesis of monomers MTCA and MTCM

The monomers (1E,4E)-1,5-Di-2-thienylpenta-1,4-dien-3-one (MTCA) and (1E,4E)-2,4-dimethyl-1,5-di(thiophen-2-yl)penta-1,4-dien-3-one (MTCM) were synthesized by Claisen–Schmidt reaction (Scheme 1) as per the reported procedures [1-4].



Scheme 1. Synthesis of monomers MTCA and MTCM.

To a mixture of 1.87 mL (0.02 mol) of thiophene-2-carboxaldehyde, 2g (0.05 mol) NaOH in water (0.1g/mL ratio), 40 mL of EtOH and 60 mL of water, 0.74 mL (0.01 mol) of acetone was added dropwise. The reaction was carried out at room temperature for 1 h and the reaction mixture was poured into crushed ice. The yellow crystalline solid was collected by filtration, dried in the oven at 75°C, and recrystallized from MeOH to afford pure MTCA.

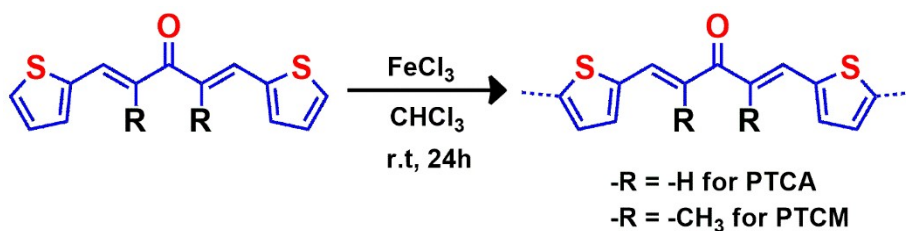
A mixture of 1.87 mL (0.02 mol) thiophene-2-carboxaldehyde and 1.06 ml (0.01 mol) 3-pentanone was added to a flask already containing 0.0014 g KOH (0.025 mmol) in 2:1 MeOH/H₂O mixture (1.0 M towards 3-pentanone). The mixture was refluxed overnight, cooled to room

Materials, Methods, and Characterization

temperature, and neutralized with a 2M HCl solution. Organic compounds were extracted three times with DCM, rinsed with brine, dried with MgSO₄, and evaporated in the vacuum oven. The crude product was recrystallized with MeOH to afford pure MTCM.

2.3.2. Synthesis of polymers PTCA and PTCM

The polymers poly [(1E,4E)-1,5-Di-2-thienylpenta-1,4-dien-3-one] (PTCA) and poly[(1E,4E)-2,4-dimethyl-1,5-di(thiophen-2-yl)penta-1,4-dien-3-one] (PTCM) were synthesized via straight forward anhydrous ferric chloride oxidative coupling polymerization at room temperature (300K) as shown in the Scheme 2 [5, 6].



Scheme 2. Synthesis of polymers PTCA and PTCM.

Monomers (0.001 mol) dissolved in chloroform medium were polymerized by using anhydrous FeCl₃ (0.006 mol for MTCA and 0.008 mol for MTCM respectively) at room temperature. After 24 h of stirring, the crude products obtained were filtered and washed with acetone and methanol. The products were dried in a vacuum at 75°C overnight. The polymer PTCA was obtained as black powder and the polymer PTCM was obtained as a blackish-brown powder with a yield of 97% and 85% respectively.

2.4. Methods and measurements

2.4.1. Sensing of SO₂ - derivatives

2.4.1.1. Absorbance titration

An accurately weighed amount of buffering agent was added to ultra-pure water to make a HEPES buffer solution (20 mM, pH 7.4) and an accurately weighed amount of the probe was dissolved in DMF to obtain a 1×10^{-3} M probe stock solution. All other solutions employed in this study were prepared in the HEPES buffer. Stock solutions of surfactant CTAB (10^{-1} M) and probe were added to 3 mL of the HEPES buffer solution taken in the cuvette to make $[\text{CTAB}] = 1 \text{ mM}$ and $[\text{probe}] = 1 \times 10^{-5}$ M. 0–12 μL of 10 mM of analyte ($\text{NaHSO}_3/\text{Na}_2\text{SO}_3$)-buffer stock solution was added into the cuvette containing probe-surfactant buffer solution. Absorption spectra were measured with a Jasco V-750 UV-Visible spectrophotometer [7].

2.4.1.2. pH titrations

The pH of probe-surfactant solutions was adjusted with HCl or NaOH aqueous solution and absorption spectra were recorded after the addition of a fixed amount (20 eq.) of analyte solution.

2.4.1.3. Detection limit

The absorption intensity of the probe with NaHSO_3 and Na_2SO_3 has measured three times and the standard deviation of the calibration curve was determined. The detection limit (LOD) was obtained by $3\sigma/k$, where σ is the standard deviation of the calibration curve, and k is the slope of the plot of absorption intensity versus sample concentration [8].

2.4.1.4. Reproducibility

The stability of the method was investigated by calculating the relative standard deviation (RSD) of three absorbance measurements in the presence of the analyte after 10 minutes.

2.4.1.5. Selectivity and competition study

All the testing anions (F^- , Cl^- , Br^- , I^- , AcO^- , HCO_3^- , CO_3^{2-} , HPO_4^{2-} , SO_4^{2-} , NO_3^- , $S_2O_3^{2-}$, CN^- , SCN^-) were prepared from their sodium salts. The solutions of cysteine (Cys.) were prepared in deionised water. A selectivity study was conducted by adding 20 eq. of interfering ions to a 10 μ M probe solution and a competition study was conducted by adding 10 eq. of HSO_3^-/SO_3^{2-} to a 10 μ M probe solution in the presence of 20 eq. of interfering ions [7, 9].

2.4.1.6. Measurement of spiked sulfite in realistic samples

Crystal sugar and brown sugar were purchased from a supermarket and were used without further pre-treatment. Sugar sample solutions were prepared by dissolving 25 g of sugar in deionized water and diluting it to 100 mL. Stock solutions of CTAB, probe, and a known volume of sugar sample solution were added to 3 mL of the buffer solution to make $[CTAB] = 1 \text{ mM}$ and $[probe] = 1 \times 10^{-5} \text{ M}$, and after 10 min, the absorption intensities were recorded. Sugar samples were then spiked with different concentrations of $NaHSO_3$ (5,10 μ M) and Na_2SO_3 (5,10 μ M) that had been accurately prepared. The resulting samples were then treated with the probe for 10 min and the absorption intensities were recorded. The concentration of the sample was determined using a calibration plot [7].

2.4.2. Iodine capture studies

2.4.2.1. Iodine uptake

Iodine uptake studies based on gravimetric measurements were performed using the following procedure. Polymeric samples (10 mg) were taken in an open glass vial which is placed already in a sealed vessel with an excess of iodine at 350 K and under ambient pressure. These conditions are typical fuel reprocessing requirements according to previous studies [10]. After definite time intervals, the vial was taken out, cooled down to room temperature, weighed, and then loaded back into the vapor of iodine to continue the iodine adsorption. The iodine uptake capacity was calculated as

$$\text{Iodine uptake} = \frac{(m_2 - m_1)}{m_1} \times 100 \text{ wt\%} \quad (\text{Equation 2.1})$$

where m_1 and m_2 are the mass of the polymeric sample before and after the iodine uptake.

2.4.2.2. Kinetics of iodine capture

To analyze the adsorption kinetics of iodine onto the polymers, we adopt three models that are pseudo-first-order kinetics, pseudo-second-order kinetics, and the intraparticle diffusion model [11, 12]. The linear forms of aforesaid models can be expressed by equations 2.2-2.4.

$$\ln(q_e - q_t) = \ln q_e - k_1 t \quad (\text{Equation 2.2})$$

$$\frac{t}{q_t} = \frac{1}{k_2 q_e^2} + \frac{t}{q_e} \quad (\text{Equation 2.3})$$

$$q_t = k_{\text{int}} t^{1/2} + C \quad (\text{Equation 2.4})$$

Materials, Methods, and Characterization

In these equations, q_t is the amount of I_2 adsorbed ($g\ g^{-1}$) at any time t , k_1 (h^{-1}) and k_2 ($g\ g^{-1}\ h^{-1}$) are the pseudo-first-order and the pseudo-second-order rate constants, respectively. k_{int} ($g\ g^{-1}\ h^{-1/2}$) is the intraparticle diffusion rate constant, and C ($g\ g^{-1}$) is the constant proportional to the extent of boundary layer thickness [13].

2.4.2.3. Iodine release

Iodine release efficiency was calculated by heating 10 mg of iodine-loaded polymers containing m_0 mg of iodine in the air under ambient pressure and at 398 K for 360 minutes. The iodine release efficiency was calculated as

$$\text{Iodine release efficiency} = \frac{(10 - m_t)}{m_0} \times 100\ \text{wt\%} \quad (\text{Equation 2.5})$$

where m_t is the mass of the polymers after heating.

2.4.2.4. Recycling percentage

Cyclic experiments were performed by taking 10 mg of iodine-loaded polymeric samples (after exposure of as-synthesized polymers to iodine for 24 h at 350 K) and heating them in an open vial at 398 K for 6 h. These recovered samples were then reused for iodine uptake at 350 K for 24 h. The recycling percentage of the adsorbents was calculated as

$$\text{Recycling percentage} = \frac{I}{I_0} \times 100\ \text{wt\%} \quad (\text{Equation 2.6})$$

where, I_0 is the initial uptake of I_2 , and I is the iodine uptake capacity of polymers after heat recovery. The same polymeric samples were recycled five times.

2.4.3. Removal of heavy metal ions

2.4.3.1. Adsorbate solutions

The stock solutions (1000 ppm) of metal ions (Co^{2+} , Cu^{2+} , Ni^{2+} , Cd^{2+} , Zn^{2+} , and Pb^{2+}) were prepared by dissolving the corresponding nitrate salts in de-ionized water, and working solutions were prepared by diluting stock solutions into the required concentration [14].

2.4.3.2. Single-heavy metal ion adsorption

To investigate the adsorption capacities of the polymers for heavy metal ions, 10 mg of the polymer was added into a glass bottle containing 10 mL of 10 ppm metal ion solution. The mixture was shaken at a speed of 200 rpm at room temperature for 24 h, and the supernatant was collected to determine the metal ion concentration by ICP-MS [15].

The % removal of metal ions was calculated with equation 2.7 and the removal capacity (Q_e) is given by equation 2.8. The distribution coefficient (K_d) is defined by equation 2.9.

$$\% \text{ Removal of metal ions} = \frac{c_0 - c_e}{c_0} \times 100\% \quad (\text{Equation 2.7})$$

$$Q_e = ((c_0 - c_e) \times 10^{-3}) \times \frac{V}{m} \quad (\text{Equation 2.8})$$

$$K_d = \frac{(c_0 - c_e)}{c_e} \times \frac{V}{m} \quad (\text{Equation 2.9})$$

where C_0 and C_e are the initial and equilibrium concentrations of metal ions (ppm), V is the solution volume (mL), and m is the amount of solid sorbent (g).

2.4.3.3. Mixed-heavy metal ion adsorption

To decide the selectivity of polymers toward various metal ions, a 10 ml solution of 10 ppm for each ion (Co^{2+} , Cu^{2+} , Ni^{2+} , Cd^{2+} , Zn^{2+} , and Pb^{2+}) was shaken with polymeric samples at a speed of 200 rpm at room temperature for 24 h. The supernatant solution was analyzed by ICP-MS [15]. Percentage removal, removal capacity, and distribution coefficient were calculated as mentioned above.

2.4.3.4. Adsorption isotherms

Polymer (10 mg) was mixed with a 10 mL solution of heavy metal ions at various concentrations (20, 50, 100, 250, 500, 750, and 1000 ppm). The mixture was shaken at a speed of 200 rpm at room temperature for 24 h to ensure complete adsorption. The metal ion concentration in the supernatant solutions was determined by ICP-MS.

Two typical models including Freundlich and Langmuir models were applied to the obtained experimental results to interpret the adsorption isotherms. The linear forms of Langmuir and Freundlich isotherms are given as equations 2.10 and 2.11 respectively [16].

$$\frac{C_e}{Q_e} = \frac{1}{Q_m K_L} + \frac{C_e}{Q_m} \quad (\text{Equation 2.10})$$

$$\ln Q_e = \ln K_F + \left(\frac{1}{n}\right) \ln C_e \quad (\text{Equation 2.11})$$

where C_e (mg/L) is the equilibrium concentration of metal ions, Q_e (mg/g) is the adsorption capacity of metal ions at equilibrium, and Q_m (mg/g) is the maximum adsorption capacity of the metal ions (mg/g). K_L (L/mg) and K_F (L/mg) are Langmuir and Freundlich equilibrium

Materials, Methods, and Characterization

constants, respectively and $1/n$ (0-1) is the Freundlich equilibrium exponent.

2.4.3.5. Adsorption kinetics

The effect of contact time on the adsorption of metal ions onto the polymers was determined by adding 10 mg of the adsorbent into 10 mL of 20ppm solution of heavy metal ions. These samples were shaken at 200 rpm at room temperature, and the supernatant was taken out at the time intervals of 1, 3, 6, 12, and 24 h, and then analyzed by ICP-MS to determine metal ion concentration.

To study the adsorption kinetics of metal ions onto the polymers, we adopted three representative models, pseudo-first-order kinetic, pseudo-second-order kinetic, and intraparticle diffusion models. The linear forms of the pseudo-first-order, pseudo-second-order, and intraparticle diffusion model equations are given as equations 2.12-2.14.

$$\ln(Q_e - Q_t) = \ln Q_e - k_1 t \quad (\text{Equation 2.12})$$

$$\frac{t}{Q_t} = \frac{1}{k_2 Q_e^2} + \frac{t}{Q_e} \quad (\text{Equation 2.13})$$

$$Q_t = k_{\text{int}} t^{1/2} + C \quad (\text{Equation 2.14})$$

where Q_e (mg/g) is the equilibrium adsorption capacity of heavy metal ions, Q_t (mg/g) is the amount of the heavy metal ions adsorbed at time t (h), and k_1 (h^{-1}) and k_2 (g/mg h) are the rate constants of the pseudo-first-order and the pseudo-second-order, respectively [16]. k_{int} ($\text{mg g}^{-1} \text{h}^{-1/2}$) is the intraparticle diffusion rate constant, and C (mg g^{-1}) is the constant proportional to the extent of boundary layer thickness.

2.4.3.6. Desorption and reusability study

10 mg of polymers obtained from the formerly described adsorption test was put into 200 mL of desorbent solution (2 M of HCl) taken in an Erlenmeyer flask. These samples were shaken at 200 rpm for 24 h at room temperature, and the supernatant was analyzed by ICP-MS to determine the desorption equilibrium concentration of metal ions.

The desorption efficiency of metal ions was determined by the following equation

$$\text{Desorption efficiency} = \frac{Q_{de}}{Q_{ad}} \times 100 \% \quad (\text{Equation 2.15})$$

where Q_{de} is the amount of metal ions desorbed per unit mass of the desorbent (mg/g), and Q_{ad} is the amount of metal ions adsorbed onto the polymer per unit mass of the adsorbent (mg/g) at equilibrium.

The amount of metal ion desorbed from the polymer into the solution per unit mass of adsorbent, Q_{de} (mg/g) at equilibrium is calculated by equation 2.16 [17].

$$Q_{de} = \frac{C_{de}}{m} \times V \quad (\text{Equation 2.16})$$

where C_{de} (mg/L) is the liquid phase metal concentration detected in the desorbing solution at equilibrium conditions, m is the mass of adsorbent (g) and V (L) is the volume of the desorbing solution.

To validate the reusability of the used polymers, the adsorption-desorption cycle was repeated five times with 100 ml of 10 ppm solution of metal ions. The percentage removal of metal ions was calculated during each cycle with an adsorbent dosage of 0.10g.

2.4.3.7. Computational study

Geometry optimizations of the monomers and monomer–metal ion complexes were carried out using the Gaussian09 program with the Becke-3-Parameter-Lee-Yang-Parr (B3LYP) level of theory. The 6-311G basis set was used for C, H, S, and O atoms, while the LANL2DZ basis set was employed for Zn²⁺ and Pb²⁺ ions. Also, the Los Alamos National Laboratory with double zeta (LANL2DZ) core pseudopotentials was employed for metal ions. The energy of the highest occupied molecular orbital (HOMO), the energy of the lowest unoccupied molecular orbital (LUMO), the band gap, and the stabilization energy of both monomers and metal ion complexes were obtained by computational quantum chemical calculations using density functional theory (DFT).

2.4.4. Adsorption of cationic dyes

2.4.4.1. Adsorbate solutions

The dye stock solutions (1000 ppm) were prepared by dissolving the corresponding dyes (MB, MG, RB, CV, MO, MR, and CR) in de-ionized water, which were then diluted and mixed to achieve the necessary concentrations and compositions for the working solutions [18].

2.4.4.2. Adsorption studies

To examine the dye removal efficiency of the polymers, 1.6 mg of the polymer was added into a 50 mL of 4 ppm dye solution. The mixture was shaken at a speed of 600 rpm at room temperature, a fixed volume

Materials, Methods, and Characterization

solution was withdrawn at different time intervals, and changes in the concentrations of the dyes were analyzed using UV- Vis spectroscopy [18].

Equation 2.17 was used to compute the percentage removal of the dye, and equation 2.18 was used to determine the equilibrium adsorption capacity Q_e (mg/g).

$$\% \text{ Removal} = \frac{c_0 - c_i}{c_0} \times 100 \quad (\text{Equation 2.17})$$

$$Q_e = (c_0 - c_e) \times \frac{V}{m} \quad (\text{Equation 2.18})$$

where C_0 , C_i , and C_e are the initial, final, and equilibrium concentrations of the dye solution (ppm), V is the volume of the dye solution (L), and m is the amount of solid sorbent (g).

2.4.4.3. pH-dependent studies

Experiments were carried out at initial pH values ranging from 2 to 12. The initial pH of the solution was adjusted to the desired value by adding either HCl solution or NaOH solution [18].

2.4.4.4. Adsorption isotherms

Polymer (1.6 mg) was mixed with 50 mL dye solutions of various concentrations (1, 2, 3, 4, 5, 6, and 7 ppm). The mixture was shaken at a speed of 600 rpm at room temperature for 24 h to ensure complete adsorption. The equilibrium concentration of the dye solutions was determined by using UV- Vis spectroscopy.

To understand the adsorption isotherms, two common models, the Freundlich and Langmuir models, were applied to the obtained

Materials, Methods, and Characterization

experimental results. Equations 2.19 and 2.20 are the linear forms of the Langmuir and Freundlich isotherms, respectively [19].

$$\frac{C_e}{Q_e} = \frac{1}{Q_m K_L} + \frac{C_e}{Q_m} \quad (\text{Equation 2.19})$$

$$\ln Q_e = \ln K_F + \left(\frac{1}{n}\right) \ln C_e \quad (\text{Equation 2.20})$$

where C_e (mg/L) is the equilibrium concentration of metal ions, Q_e (mg/g) is the adsorption capacity of metal ions at equilibrium, and Q_m (mg/g) is the maximum adsorption capacity of the metal ions (mg/g). K_L (L/mg) and K_F (L/mg) are Langmuir and Freundlich equilibrium constants, respectively and $1/n$ (0-1) is the Freundlich equilibrium exponent.

2.4.4.5. Adsorption kinetics

The effect of contact time on the dye removal efficiency of the polymers was determined by adding 1.6 mg of the adsorbent into 50 mL of 4 ppm dye solution. These samples were shaken at 600 rpm at room temperature, a fixed volume solution was withdrawn at different time intervals, and changes in the concentrations of the dyes were analyzed using UV- Vis spectroscopy.

We used the pseudo-first-order kinetic, pseudo-second-order kinetic, and intraparticle diffusion models as three representative models to evaluate the adsorption kinetics of dye removal. Equations 2.21-2.23 represent the linear form of the pseudo-first-order, pseudo-second-order, and intraparticle diffusion model equations [20, 21].

$$\ln(Q_e - Q_t) = \ln Q_e - k_1 t \quad (\text{Equation 2.21})$$

Materials, Methods, and Characterization

$$\frac{t}{Q_t} = \frac{1}{k_2 Q_e^2} + \frac{t}{Q_e} \quad (\text{Equation 2.22})$$

$$Q_t = k_{\text{int}} t^{1/2} + C \quad (\text{Equation 2.23})$$

where Q_e (mg/g) is the adsorption capacity at equilibrium, Q_t (mg/g) is the mass of dye adsorbed at time t (h), and k_1 (h^{-1}) and k_2 ($\text{g}/\text{mg h}$) are the rate constants of the pseudo-first-order and the pseudo-second-order, respectively [16]. k_{int} ($\text{mg g}^{-1} \text{h}^{-1/2}$) is the intraparticle diffusion rate constant, and C (mg g^{-1}) is the constant proportional to the extent of boundary layer thickness.

2.4.4.6. Selectivity studies

To decide the selectivity of polymers toward cationic dyes, a selectivity study was conducted using a mixture of anionic (MO) and cationic dyes (CV). At room temperature, the polymer was shaken with 50 mL of a mixture of CV and MO solution (4 ppm each) at a speed of 600 rpm. A fixed-volume solution was withdrawn at different time intervals, and changes in the concentrations of the dyes were analyzed using UV-Vis spectroscopy. As previously noted, percentage removal and adsorption capacity were computed [20].

2.4.4.7. Desorption and reusability studies

Regeneration of the dye-saturated polymer was done using the solvent desorption technique. Polymers obtained from the formerly described adsorption test were added to 50 mL of ethanol. These samples were agitated for six hours at room temperature at 600 rpm, filtered, and the concentration of desorbed dye was examined using UV-Vis

Materials, Methods, and Characterization

spectroscopy. The percentage desorption of the dyes from the polymers was determined by equation 2.24

$$\% \text{ desorption} = \frac{C_d \times V}{Q_a \times m} \quad (\text{Equation 2.24})$$

Q_a (mg/g) is the adsorption capacity of the polymer, C_d (mg/L) is the concentration of dye desorbed from the adsorbent by absolute ethanol, V (L) is the volume of desorption fluid used, and m (g) is the mass of polymer used. The adsorption-desorption cycle was done five times to confirm the applicability of these polymers. The percentage removal and percentage desorption of dyes was calculated during each cycle [22].

2.5. Characterization of monomers MTCA and MTCM

The monomers (MTCA and MTCM) were synthesized by Claisen–Schmidt reaction as per the reported procedures and characterized using FT-IR, ^1H NMR, ^{13}C NMR, and Mass spectroscopic techniques [1, 4]. Fig. 1, Fig. 2, Fig. 3, and Fig. 4 respectively show the FT-IR, ^1H NMR, ^{13}C NMR, and HR-MS analysis results of the monomer MTCA, and the results are summarised below.

Yellow crystalline solid; 89% yield; mp 114-116 °C; ^1H NMR (400 MHz, CDCl_3 , TMS): δ (ppm) 7.83 (d, 2 H, $J = 15$ Hz), 7.40 (d, 2 H, $J = 5.0$ Hz), 7.33 (d, 2 H, $J = 3.6$ Hz), 7.08 (dd, 2H, $J = 3.6, 5.0$ Hz), 6.82 (d, 2 H, $J = 15$ Hz); ^{13}C NMR (400 MHz, CDCl_3): δ 187.8, 140.3, 135.6, 131.9, 128.8, 128.3, 124.4; MS (EI, 70 eV): m/z (%) 247 ($\text{M}+\text{H}$) $^+$; IR (KBr) 3087, 1661, 1604, 1565, 1105, 749, 729 cm^{-1} .

Fig. 5, Fig. 6, Fig. 7, and Fig. 8 respectively show the FT-IR, ^1H NMR, ^{13}C NMR, and HR-MS analysis results of the monomer MTCM, and the

Materials, Methods, and Characterization

sum of the results is given below.

Yellow crystalline solid; 69 % yield; mp: 80-81 °C; ^1H NMR (400 MHz, CDCl_3 , TMS): δ (ppm) 7.52 (d, 2H, $J=5.0$ Hz), 7.36 (s, 2H), 7.25 (d, 2H, $J=3.7$ Hz), 7.13 (dd, 2H, $J = 5.1, 3.6$ Hz), 2.28 (s, 6H, $J=1.3$ Hz); ^{13}C NMR (400 MHz, CDCl_3): δ 200.8, 139.4, 133.6, 131.9, 131.3, 129.0, 127.4, 15.5; MS (EI, 70 eV): m/z (%) 274 ($\text{M}+\text{H}$) $^+$; IR (KBr): 3107, 2926, 1714, 1607, 1450, 1075, 698 cm^{-1} .

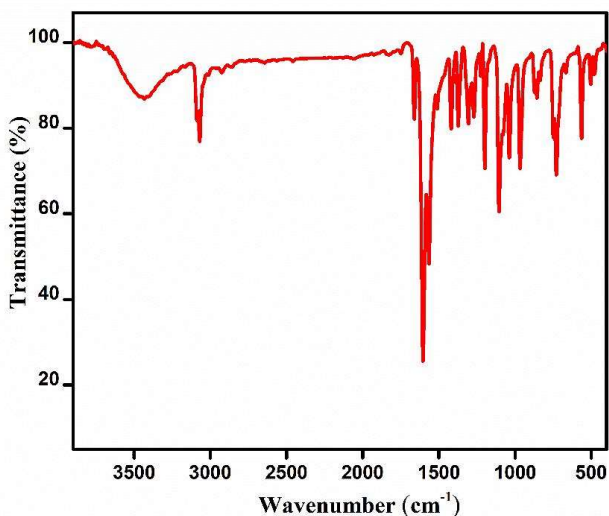


Fig. 1. FT-IR spectra of monomer MTCA.

2.6. Characterization of synthesized polymers PTCA and PTCM

The polymers (PTCA and PTCM) were synthesized by anhydrous FeCl_3 -promoted oxidative coupling reactions and were characterized using FT-IR, PXRD, UV-DRS, TGA, SEM, TEM, BET, XPS, and CHNS analysis techniques.



Fig. 2. ¹H NMR spectra of monomer MTCA in CDCl₃

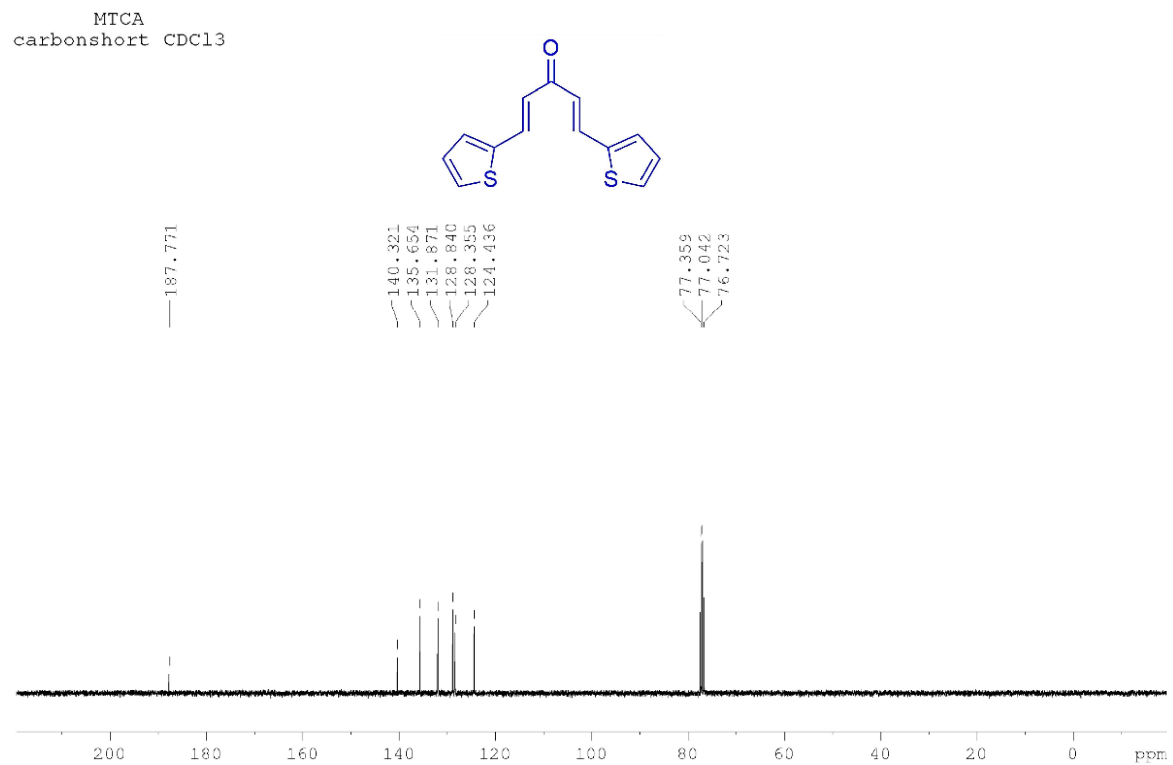
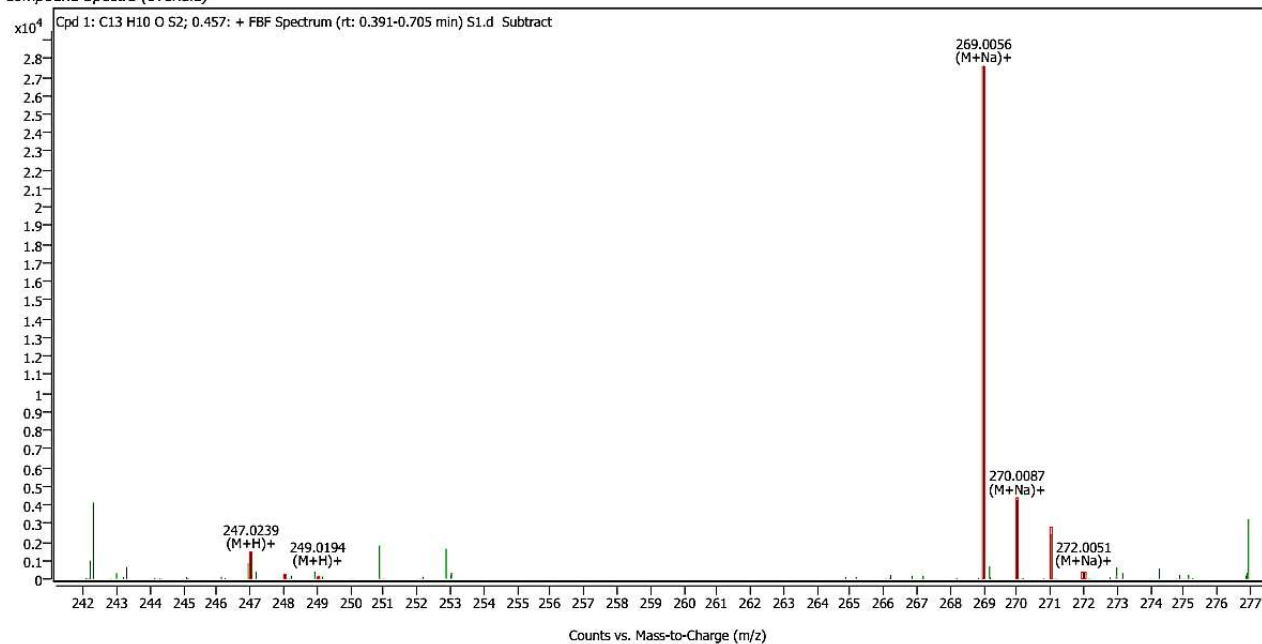


Fig. 3. ¹³C NMR spectra of monomer MTCA in CDCl₃.

Compound Spectra (overlaid)



Compound ID Table

Cpd	Formula	Mass (Tgt)	Calc. Mass	Mass	Species	Diff(Tgt.ppm)	mDa
1	C13 H10 O S2	246.0173	246.0164	247.0239 269.0056	(M+H) ⁺ (M+Na) ⁺	-3.88	-0.95

Fig. 4. HR-MS spectra of monomer MTCA.

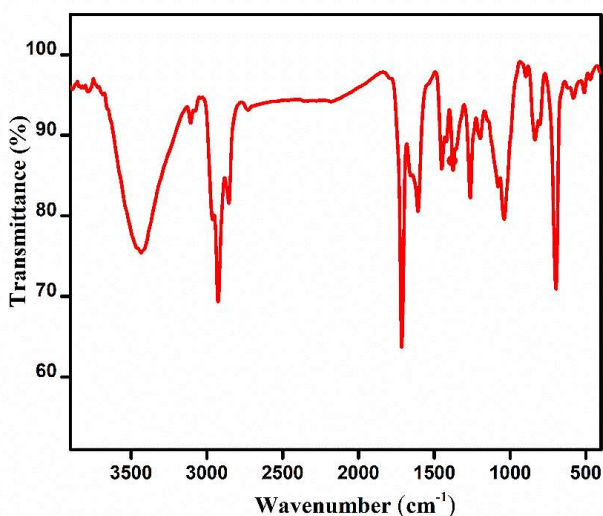


Fig. 5. FT-IR spectra of monomer MTCM.

The formation of polymers from the monomers can be deduced from the peak broadening observed in the polymers compared to the sharp peaks observed in the monomers (Fig. 9) [1, 23]. The peaks correspond to C=O stretching, C=C stretching of α,β -unsaturated ketone, and C-S deformation in the monomer MTCM appeared to be shifted from 1661 to 1637 cm^{-1} , 1604 to 1597 cm^{-1} , and 729 to 705 cm^{-1} respectively in PTCA. Also, the peaks at 1565/1510, and 1105 cm^{-1} representing C=C stretching of the thiophene ring, and C-S-C stretching vibration of the monomer MTCM was found to be nearly disappeared in the polymer PTCA. Peak broadening as well as the intensity reduction point to the restricted vibrations that arise due to the formation of polymers from the monomers. Likewise, as shown in Fig. 10, the formation of the second polymer PTCM was concluded from the near disappearance of the peaks at 1607, 1450, and 1075 cm^{-1} which was assigned to C=C stretching

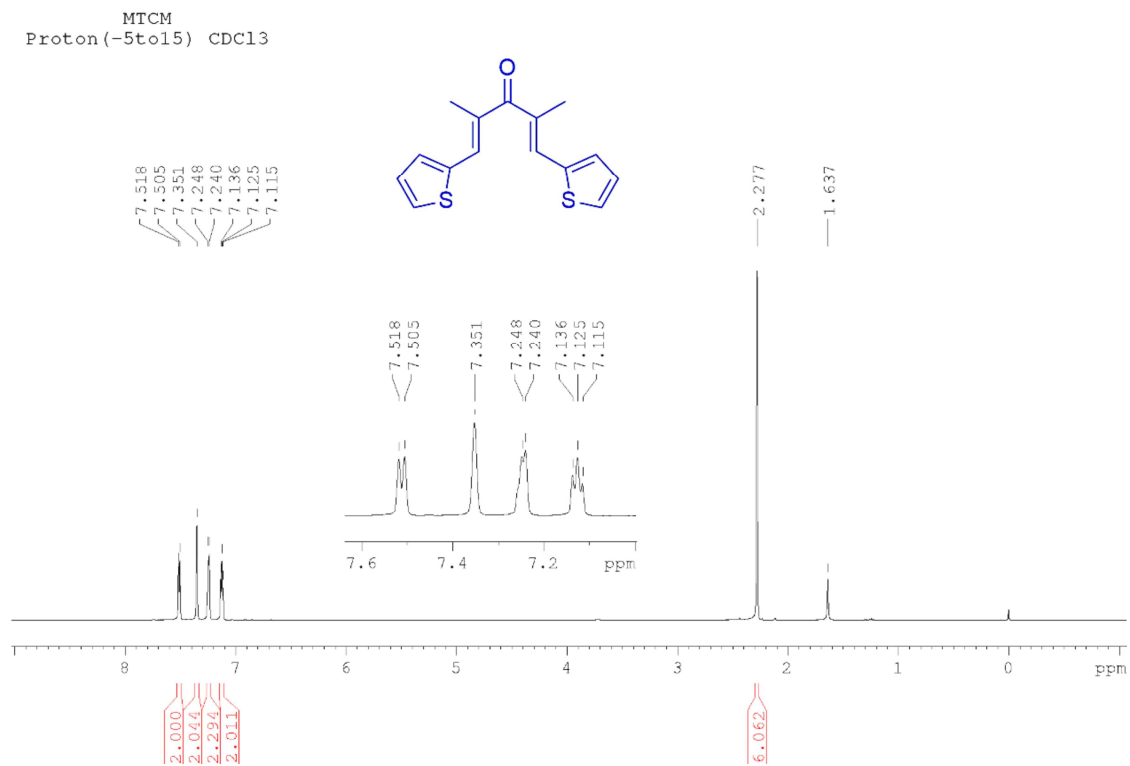


Fig. 6. ¹H NMR spectra of monomer MTCM in CDCl₃.

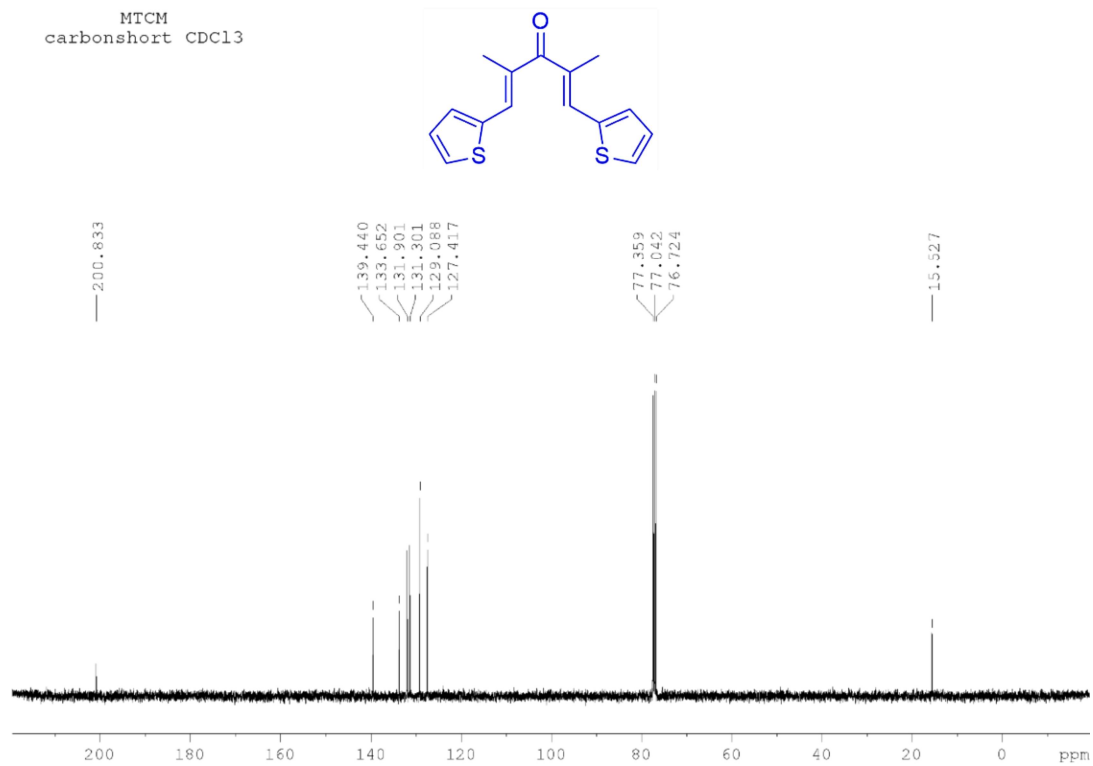
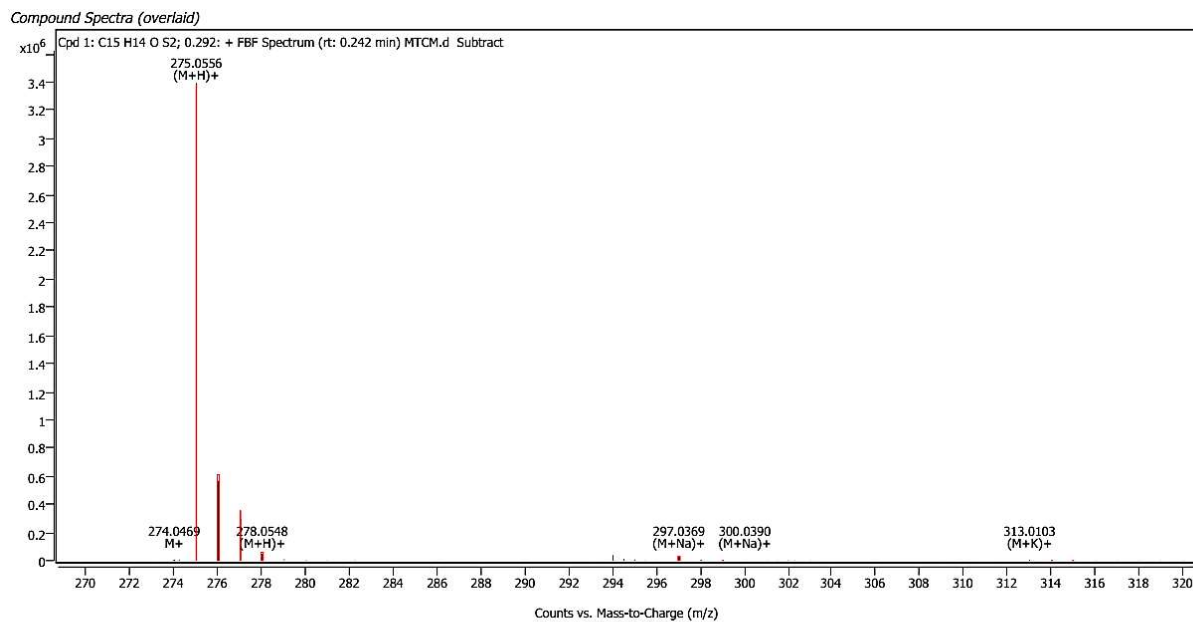


Fig. 7. ¹³C NMR spectra of monomer MTCM in CDCl₃.



Compound ID Table

Cpd	Formula	Mass (Tgt)	Calc. Mass	Mass	Species	Diff(Tgt.ppm)	mDa
1	C ₁₅ H ₁₄ O S ₂	274.0486	274.0483	274.0469	M+ (M+H) ⁺	-1.21	-0.33
				275.0556	(M+Na) ⁺		
				297.0369	(M+K) ⁺		
				313.0103			

Fig. 8. HR-MS spectra of monomer MTCM.

Materials, Methods, and Characterization

vibration of α , β – unsaturated ketone, C=C stretching vibration of the thiophene ring, and C-S-C stretching vibration respectively in the monomer MTCA. Also, the shift of C=O stretching frequency to lower wavenumbers from 1714 to 1657 cm^{-1} confirms the formation of polymer PTCA. In both of the polymers, a new peak appeared around 800 cm^{-1} which represents the characteristic absorption band of 2,5-disubstituted thiophenes. The aforesaid shreds of evidence confirm the homocoupling of the terminal thiophene units [10] to form polymeric PTCA and PTCA.

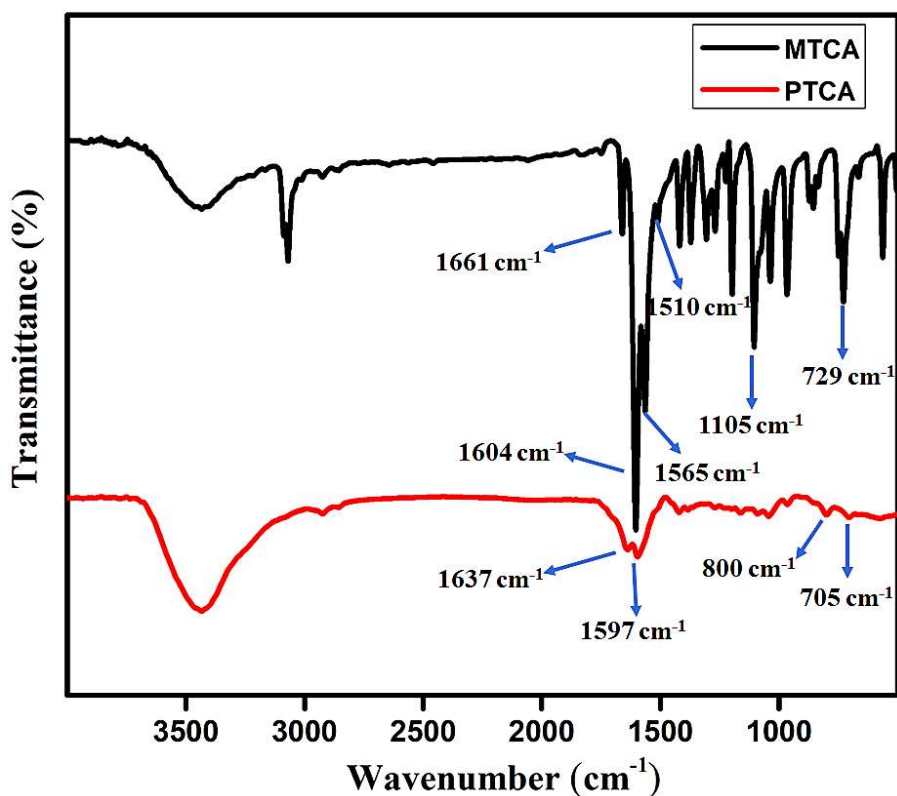


Fig. 9. FT-IR spectra of monomer MTCA and polymer PTCA.

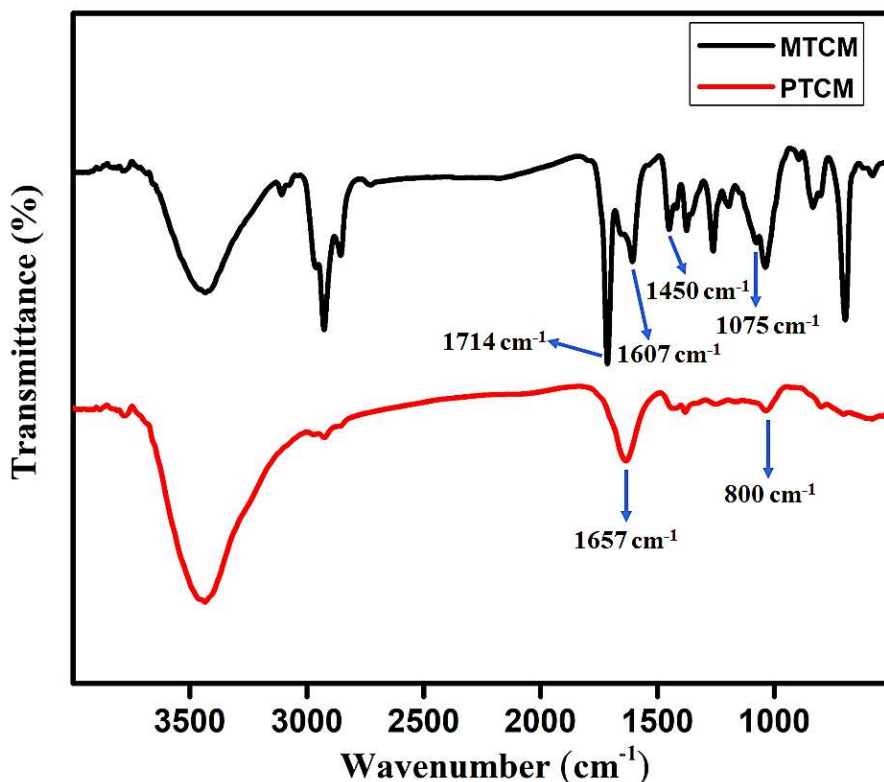


Fig. 10. FT-IR spectra of monomer MTCM and polymer PTCM.

UV-DRS spectra of the monomers and polymers were shown in Fig. 11 and Fig. 12. Two peaks present at 314 and 431 nm in MTCM appeared as a single broad peak at around 500 nm in PTCM, and peaks present at 265 and 385 nm in MTCM were appeared as a single broad peak at around 475 nm in PTCM (red shift). The observed red shift in the absorbance of the polymers related to the monomers proposes the extended π -conjugation resulting from the polymerization reaction [23]. Additionally, the aforesaid evidence also shows the effective synthesis of the expected polymers PTCM and PTCM.

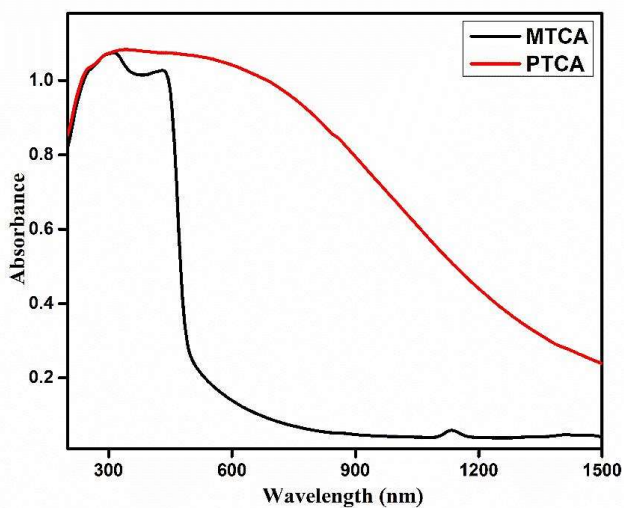


Fig. 11. UV-DRS spectra of monomer MTCA and polymer PTCA.

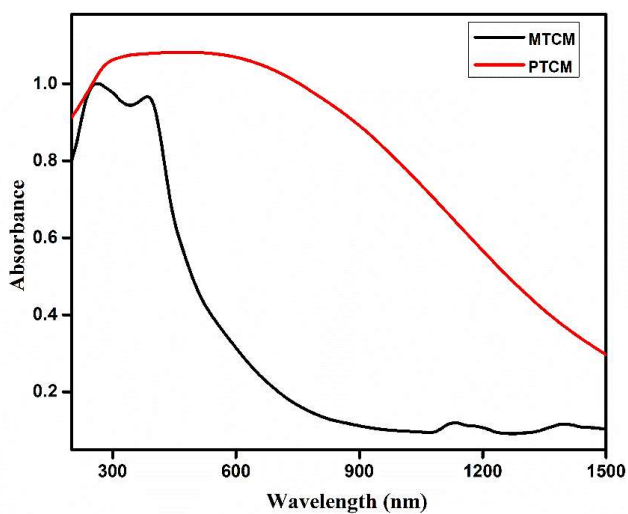


Fig. 12. UV-DRS spectra of monomer MTCM and polymer PTCM.

Materials, Methods, and Characterization

To further confirm the structure of synthesized polymers at the molecular level, the solid-state ^{13}C cross-polarization magic angle spinning (CP/MAS) NMR was recorded [24]. As shown in Fig. 13, the resonance peak at around 250 ppm represents carbonyl carbon and peaks in the range of 120-190 ppm represent carbon atoms of the thiophene ring and C=C group of the polymer PTCA. Similarly, as shown in Fig. 14, the resonance peak at around 210 ppm represents carbonyl carbon and peaks in the range of 120-160 ppm represent carbon atoms of the thiophene ring and C=C group of the polymer PTCM. Solid-state NMR spectra of PTCM also exhibit a peak at around 10 ppm which is ascribed to the carbon atom of the methyl group. Signals marked with asterisks denote the spinning side peaks.

The amorphous nature of PTCA and PTCM was exposed by a characteristic broad peak observed in the PXRD patterns of the polymers (Fig. 15) [25], and high sulfur content of 21.8% and 19.3% respectively in PTCA and PTCM was revealed by the CHNS elemental analysis. CHNS analysis results are given in Table 1.

The thermal stability of polymeric samples was studied by TGA analysis (Fig. 16), and no noticeable mass loss was observed upon heating up to 210 °C. Also, more than 42 wt% and 68 wt% of PTCA and PTCM remained even heating up to 700 °C [26]. Hence the synthesized polymers display exceptional thermal stability. The insolubility of synthesized polymers in water and common organic solvents, and inertness in the dilute solutions of acids and bases point to the good chemical stability of these polymers [27].

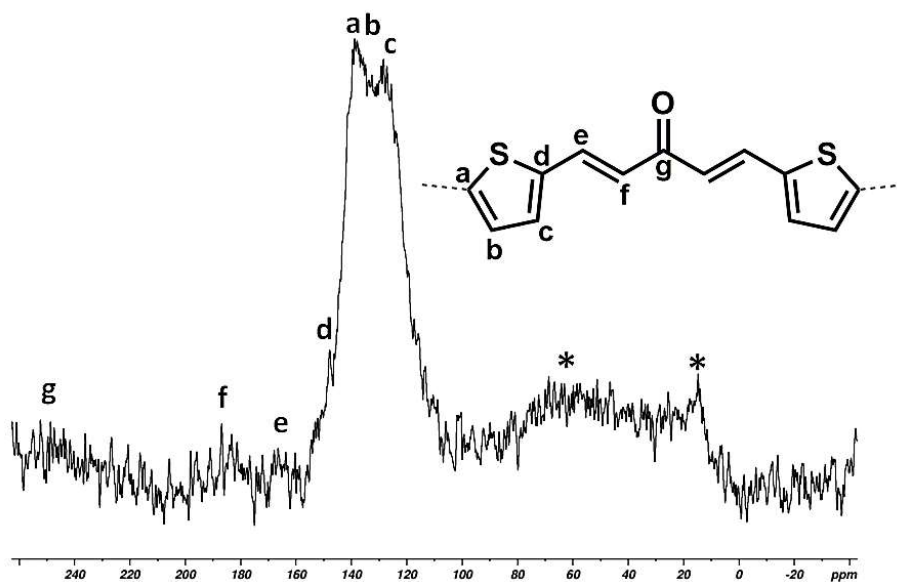


Fig. 13. ^{13}C solid-state NMR spectrum of polymer PTCA.

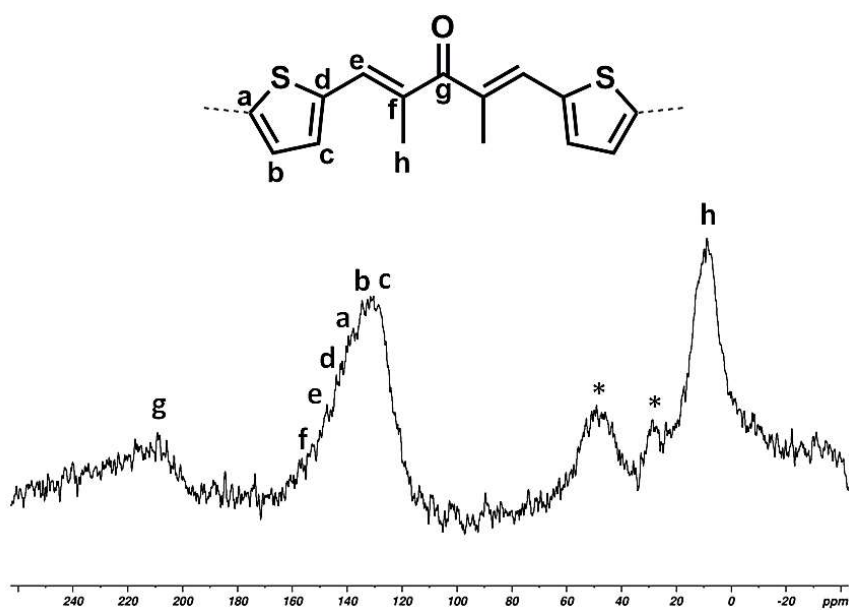


Fig. 14. ^{13}C solid-state NMR spectrum of polymer PTCM.

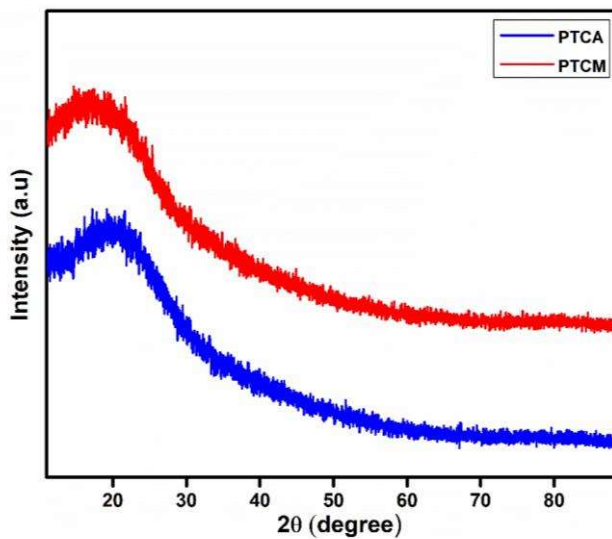


Fig. 15. XRD Patterns of the polymer PTCA and PTCM.

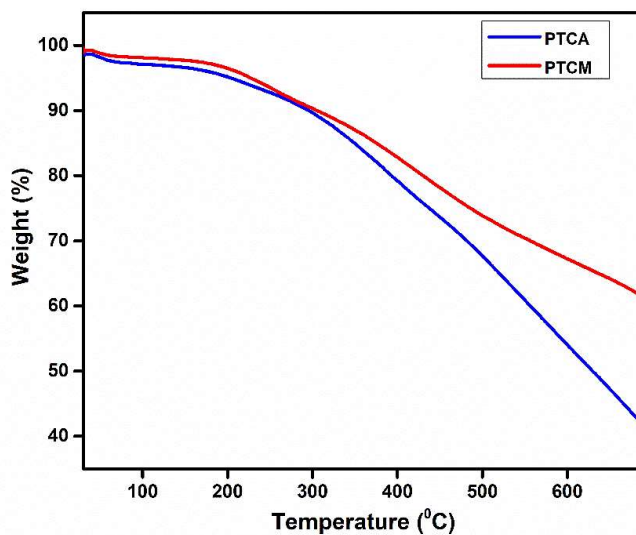


Fig. 16. TGA curves of the polymers PTCA and PTCM.

Table 1. CHNS analysis results for the polymers PTCA and PTCM.

Element	Weight %	
	PTCA	PTCM
Carbon	55.9	56.0
Hydrogen	2.9	3.6
Sulphur	21.8	19.3

Scanning electron microscopy (SEM) image of PTCA (Fig. 17a, 17b) looks like a fused polymer mass and that of PTCM (Fig. 17c, 17d) looks like an irregularly connected flake-like structure. While the transmission electron microscopy (TEM) images of both PTCA (Fig. 18a, 18b) and PTCM (Fig. 18c, 18d) show the amorphous texture and uniform distribution of nanometer-scale pores throughout the structure.

The porous nature of the polymers was characterized by measuring the N₂ sorption isotherms at 77.3 K [28, 29]. As shown in Fig. 19, the polymers PTCA and PTCM display mixed type-II/IV nitrogen sorption isotherm characteristics which signify the co-existence of micropores and mesopores [30, 31]. A rapid rise of nitrogen gas uptake at low relative pressures ($P/P_0 < 0.1$) also suggests the microporous and mesoporous nature of synthesized polymers [32, 33]. Strong nitrogen gas adsorption exists in the relative pressure range greater than 0.8 revealing the coexistence of mesopores and macropores as well [34]. PTCA and PTCM possess a surface area of 34.31 m² g⁻¹ and 22.13 m² g⁻¹ respectively as calculated from the BET model. The average pore diameters were centered around 4.14 nm and 4.96 nm for

PTCA and PTCM respectively, as calculated by the Barrett-Joyner-Halenda (BJH) method (Fig. 20) [33].

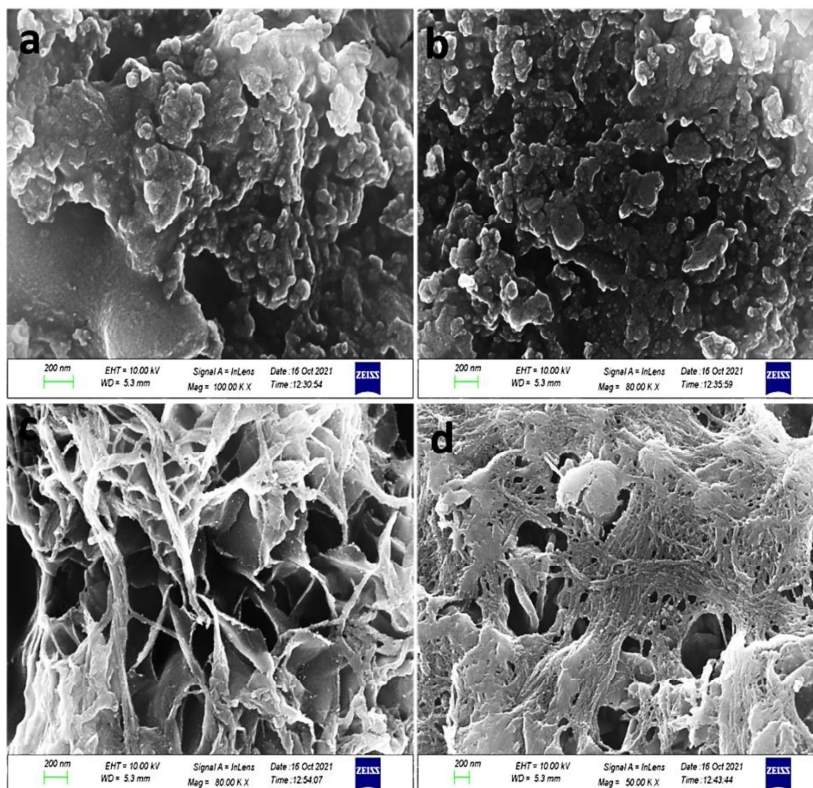


Fig. 17. (a,b) SEM images of the polymer PTCA; (c,d) SEM images of the polymer PTCM.

The surface element composition and the binding atmospheres of the polymers were studied by using XPS [35]. The XPS survey spectra of polymers PTCA and PTCM (Fig. 21a and Fig. 22a) show peaks corresponding to C 1s, O 1s, and S 2p as common peaks. The deconvoluted XPS spectra (Fig. 21b) of C 1s electrons of PTCA exhibit four peaks at the binding energies of 284.5, 285.3, 286.4, and 288.5 eV corresponding to C=C, C-C, C-S, C=O respectively. The O 1s spectrum

Materials, Methods, and Characterization

(Fig. 21c) of PTCA shows a peak at the binding energy of 531.6 eV corresponding to the carbonyl oxygen [36]. Two characteristic peaks at 164.0 and 165.2 eV are assigned to S 2p_{3/2} and S 2p_{1/2} respectively in the S 2p spectrum (Fig. 21d) of PTCA [37]. Similarly, the deconvoluted XPS spectra of C 1s electrons (Fig. 22b) of PTCM exhibit four peaks at the binding energies of 284.5, 285.0, 285.4, and 287.0 eV corresponding to C=C, C-C, C-S, C=O respectively. The O1s spectrum (Fig. 22c) of PTCM shows a peak at the binding energy of 531.7 eV corresponding to the carbonyl oxygen. Two characteristic peaks at 164.2 and 165.4 eV

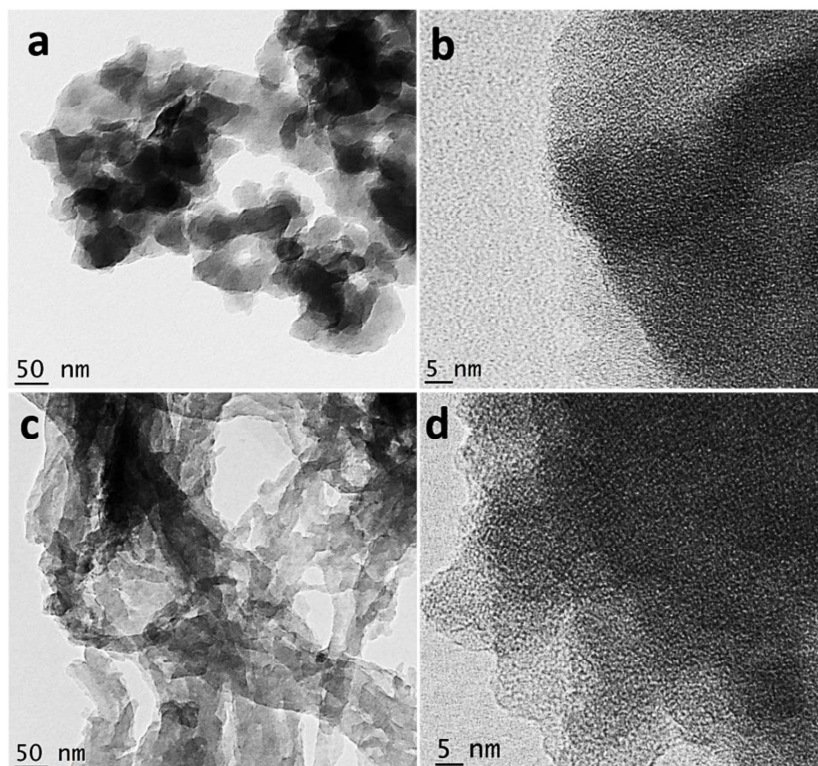


Fig. 18. (a,b) TEM images of the polymer PTCA; (c,d) TEM images of the polymer PTCM.

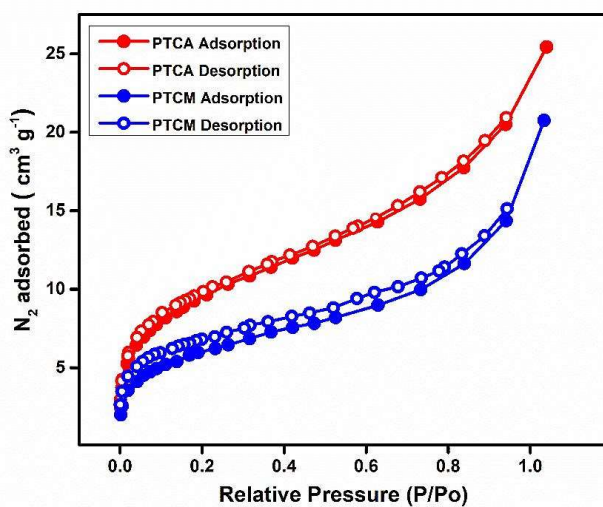


Fig. 19. Nitrogen adsorption/desorption isotherms of the polymers PTCA and PTCM.

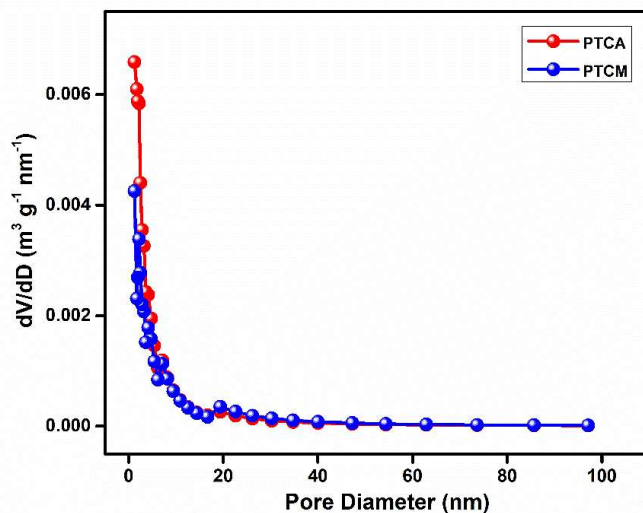


Fig. 20. Pore size distribution of the polymers PTCA and PTCM.

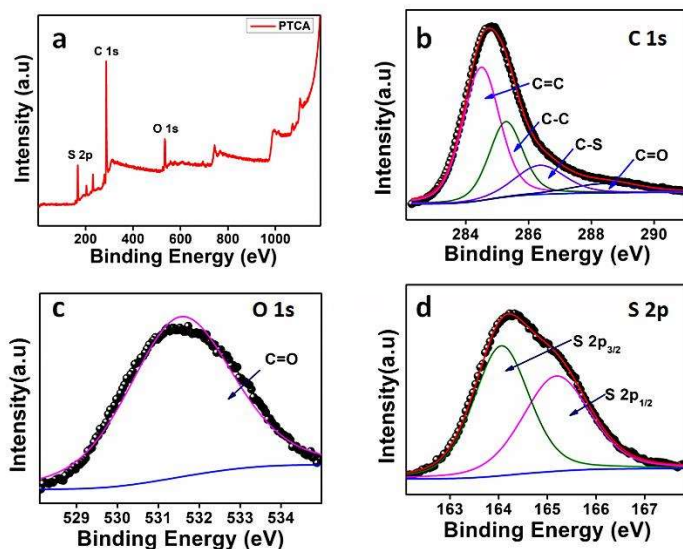


Fig. 21. XPS spectra of the polymer PTCA (a) survey, (b) C 1s, (c) O 1s, and (d) S 2p

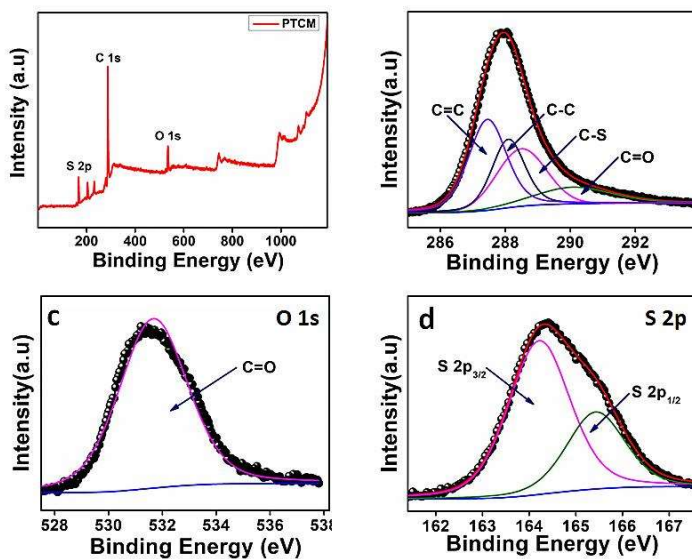


Fig. 22. XPS spectra of the polymer PTCM (a) survey, (b) C 1s, (c) O 1s, and (d) S 2p s

Materials, Methods, and Characterization

are assigned to S 2p_{3/2} and S 2p_{1/2} respectively in the S 2p spectrum (Fig. 22d) of PTCM.

Overall, in this chapter, we verified the synthesis of monomers and polymers and investigated several structural and chemical properties of the produced polymers using the characterization techniques outlined above.

References

- [1] B. Rajashekar, P. Sowmendran, S.S.S. Sai, G.N. Rao, Synthesis, characterization and two-photon absorption based broadband optical limiting in diarylideneacetone derivative, *Journal of Photochemistry and Photobiology A: Chemistry*, 238(2012) 20-3.
- [2] L. Yu, M. Han, J. Luan, L. Xu, Y. Ding, Q. Xu, Ca (OH) 2-catalyzed condensation of aldehydes with methyl ketones in dilute aqueous ethanol: a comprehensive access to α , β -unsaturated ketones, *Scientific reports*, 6(2016) 1-11.
- [3] Z. Daneshfar, A. Rostami, Cellulose sulfonic acid as a green, efficient, and reusable catalyst for Nazarov cyclization of unactivated dienones and pyrazoline synthesis, *RSC advances*, 5(2015) 104695-707.
- [4] C. Prandi, S. Nejrotti, M. Iannicelli, S.S. Jamil, D. Arnodo, M. Blangetti, Natural Deep Eutectic Solvents as an Efficient and Reusable Catalytic System for the Nazarov Cyclization, (2019).
- [5] L. Pan, Q. Chen, J.-H. Zhu, J.-G. Yu, Y.-J. He, B.-H. Han, Hypercrosslinked porous polycarbazoles via one-step oxidative coupling reaction and Friedel–Crafts alkylation, *Polymer Chemistry*, 6(2015) 2478-87.
- [6] A. Palma-Cando, G. Brunklaus, U. Scherf, Thiophene-based microporous polymer networks via chemical or electrochemical oxidative coupling, *Macromolecules*, 48(2015) 6816-24.
- [7] H. Tian, J. Qian, Q. Sun, H. Bai, W. Zhang, Colorimetric and ratiometric fluorescent detection of sulfite in water via cationic surfactant-promoted addition of sulfite to α , β -unsaturated ketone, *Analytica chimica acta*, 788(2013) 165-70.

Materials, Methods, and Characterization

- [8] X. Dai, T. Zhang, Z.-F. Du, X.-J. Cao, M.-Y. Chen, S.-W. Hu, et al., An effective colorimetric and ratiometric fluorescent probe for bisulfite in aqueous solution, *Analytica Chimica Acta*, 888(2015) 138-45.
- [9] S. Roy, A. Maity, N. Mudi, M. Shyamal, A. Misra, Rhodamine scaffolds as real time chemosensors for selective detection of bisulfite in aqueous medium, *Photochemical & Photobiological Sciences*, 18(2019) 1342-9.
- [10] T. Geng, L. Ma, G. Chen, C. Zhang, W. Zhang, H. Xia, et al., Poly [1, 3, 6, 8-tetra (2-thiophenyl) pyrene] and poly [1, 3, 6, 8-tetra (3-thiophenyl) pyrene] conjugated microporous polymers for reversible adsorbing and fluorescent sensing iodine, *Journal of Polymer Research*, 26(2019) 1-10.
- [11] E. Mirzaee, M. Sartaj, Activated carbon-based magnetic composite as an adsorbent for removal of polycyclic aromatic hydrocarbons from aqueous phase: Characterization, adsorption kinetics and isotherm studies, *Journal of Hazardous Materials Advances*, 6(2022) 100083.
- [12] A. Shekhawat, S. Kahu, D. Saravanan, S. Pandey, R. Jugade, Rational modification of chitosan biopolymer for remediation of Cr(VI) from water, *Journal of Hazardous Materials Advances*, 7(2022) 100123.
- [13] K. Su, W. Wang, B. Li, D. Yuan, Azo-bridged calix [4] resorcinarene-based porous organic frameworks with highly efficient enrichment of volatile iodine, *ACS Sustainable Chemistry & Engineering*, 6(2018) 17402-9.
- [14] J. Bayuo, M.A. Abukari, K.B. Pelig-Ba, Desorption of chromium (VI) and lead (II) ions and regeneration of the exhausted adsorbent, *Applied Water Science*, 10(2020) 1-6.
- [15] L. Feng, W.-M. Chen, J.-L. Li, G. Day, H. Drake, E. Joseph, et al., Biological antagonism inspired detoxification: removal of toxic elements by porous polymer networks, *ACS applied materials & interfaces*, 11(2019) 14383-90.
- [16] T.N. Dharmapriya, D. Li, Y.-C. Chung, P.-J. Huang, Green Synthesis of Reusable Adsorbents for the Removal of Heavy Metal Ions, *ACS omega*, 6(2021) 30478-87.
- [17] E. Katsou, S. Malamis, M. Tzanoudaki, K.J. Haralambous, M. Loizidou, Regeneration of natural zeolite polluted by lead and zinc in wastewater treatment systems, *Journal of hazardous materials*, 189(2011) 773-86.
- [18] X. Liu, Y. Wang, H. Ju, F. Yang, L. Zhang, X. Luo, Micro-mesoporous divinyl benzene-based polymer for ultrafast, effective and selective removal of cationic dyes, *Materials Chemistry and Physics*, 255(2020) 123564.
- [19] J. Zhang, F. Li, Q. Sun, Rapid and selective adsorption of cationic dyes by a unique metal-organic framework with decorated pore surface, *Applied*

Materials, Methods, and Characterization

Surface Science, 440(2018) 1219-26.

[20] Y. Gao, S.-Q. Deng, X. Jin, S.-L. Cai, S.-R. Zheng, W.-G. Zhang, The construction of amorphous metal-organic cage-based solid for rapid dye adsorption and time-dependent dye separation from water, Chemical Engineering Journal, 357(2019) 129-39.

[21] A. salah omer, G. A.El Naeem, A.I. Abd-Elhamid, O. O.M. Farahat, A. A. El-Bardan, H. M.A. Soliman, et al., Adsorption of crystal violet and methylene blue dyes using a cellulose-based adsorbent from sugarcane bagasse: characterization, kinetic and isotherm studies, Journal of Materials Research and Technology, 19(2022) 3241-54.

[22] Y. Yi, G. Tu, G. Ying, Z. Fang, E.P. Tsang, Magnetic biochar derived from rice straw and stainless steel pickling waste liquor for highly efficient adsorption of crystal violet, Bioresource Technology, 341(2021) 125743.

[23] R. Venkatesan, L. Cindrella, Semiconducting composite of chalcone-bridged polythiophene and titania, its ammonia vapor sensing property, Materials Science in Semiconductor Processing, 34(2015) 126-37.

[24] T. Narasimhaswamy, D. Lee, N. Somanathan, A. Ramamoorthy, Solid-state NMR characterization of a novel thiophene-based three phenyl ring mesogen, Chemistry of materials, 17(2005) 4567-9.

[25] S. Ravi, P. Puthiaraj, K.H. Row, D.-W. Park, W.-S. Ahn, Aminoethanethiol-grafted porous organic polymer for Hg²⁺ removal in aqueous solution, Industrial & Engineering Chemistry Research, 56(2017) 10174-82.

[26] Z. Yang, G. Wu, Q. Li, H. Ai, X. Yao, H. Ji, Removal of various pollutants from wastewaters using an efficient and degradable hypercrosslinked polymer, Separation Science and Technology, 56(2021) 860-9.

[27] Y. Zhang, A. Sigen, Y. Zou, X. Luo, Z. Li, H. Xia, et al., Gas uptake, molecular sensing and organocatalytic performances of a multifunctional carbazole-based conjugated microporous polymer, Journal of Materials Chemistry A, 2(2014) 13422-30.

[28] S. Zawar, G. Ali, G.M. Mustafa, S.A. Patil, S.M. Ramay, S. Atiq, Mn_{0.06}Co_{2.94}O₄ nano-architectures anchored on reduced graphene oxide as highly efficient hybrid electrodes for supercapacitors, Journal of Energy Storage, 50(2022) 104298.

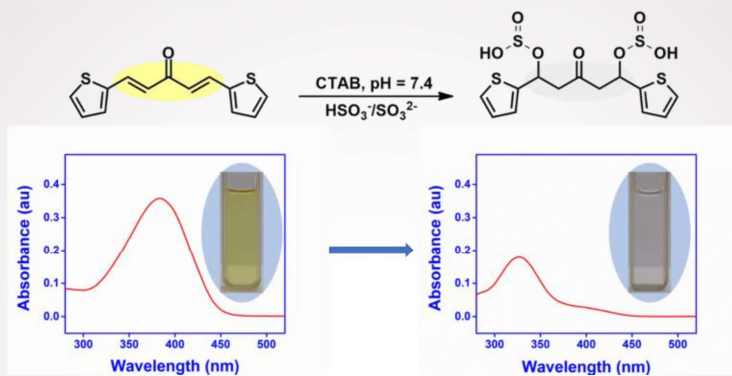
[29] S. Zawar, M. Akbar, G.M. Mustafa, G. Ali, S. Riaz, S. Atiq, et al., CNTs embedded in layered Zn-doped Co₃O₄ nano-architectures as an efficient hybrid anode material for SIBs, Journal of Alloys and Compounds, 867(2021) 158730.

Materials, Methods, and Characterization

- [30] L.Y. Molefe, N.M. Musyoka, J. Ren, H.W. Langmi, P.G. Ndungu, R. Dawson, et al., Synthesis of porous polymer-based metal–organic frameworks monolithic hybrid composite for hydrogen storage application, *Journal of Materials Science*, 54(2019) 7078-86.
- [31] Y. Zhang, J. Wu, J. Gao, X. Chen, Q. Wang, X. Yu, et al., Oxygen ether chain containing covalent organic frameworks as efficient fluorescence-enhanced probe for water detection, *Journal of Solid State Chemistry*, (2022) 123727.
- [32] X. Yang, H. Liu, Ferrocene-Functionalized Silsesquioxane-Based Porous Polymer for Efficient Removal of Dyes and Heavy Metal Ions, *Chemistry–A European Journal*, 24(2018) 13504-11.
- [33] M. Xu, T. Wang, L. Zhou, D. Hua, Fluorescent conjugated mesoporous polymers with N, N-diethylpropylamine for the efficient capture and real-time detection of volatile iodine, *Journal of Materials Chemistry A*, 8(2020) 1966-74.
- [34] C. Zhang, Y. He, P. Mu, X. Wang, Q. He, Y. Chen, et al., Toward high performance thiophene-containing conjugated microporous polymer anodes for lithium-ion batteries through structure design, *Advanced Functional Materials*, 28(2018) 1705432.
- [35] X. Yu, L. Jiajun, Y. Xianglin, Z. Feng, L. Yongjun, L. Junbo, Preparation of graphdiyne-doped TiO₂/SiO₂ composite for enhanced photocatalytic activity, *Journal of Nanoparticle Research*, 22(2020) 1-10.
- [36] R. Peng, G. Chen, F. Zhou, R. Man, J. Huang, Catalyst-free synthesis of triazine-based porous organic polymers for Hg²⁺ adsorptive removal from aqueous solution, *Chemical Engineering Journal*, 371(2019) 260-6.
- [37] Q. Lian, Z.U. Ahmad, D.D. Gang, M.E. Zappi, D.L.B. Fortela, R. Hernandez, The effects of carbon disulfide driven functionalization on graphene oxide for enhanced Pb (II) adsorption: Investigation of adsorption mechanism, *Chemosphere*, 248(2020) 126078.

Chapter 3

Bis-chalcone based colorimetric probe for the selective detection of bisulfite/sulfite anions



A probe based on surfactant mediated Michael addition reaction was developed for rapid, colorimetric, and selective detection of bisulfite/ sulfite anions in aqueous solutions as well as in real samples. The probe showed high selectivity and sensitivity towards bisulfite and sulfite over other interfering anions, with a detection limit of $0.43 \mu\text{M}$ and $0.23 \mu\text{M}$ respectively.

3.1. Introduction

3.2. Results and discussion

3.2.1. Effect of pH

3.2.2. Effect of various surfactants

3.2.3. Selectivity and competition study

3.2.4. Detection of SO_2 derivatives in real samples

3.3. Conclusions

3.1. Introduction

Sulfur dioxide (SO₂) is a well-known air pollutant released in many industrial processes and it exhibits significant impacts on human health and the environment [1, 2]. Studies have shown that frequent exposure to SO₂ induces many health issues such as lung and brain cancer, cardiovascular diseases, respiratory problems, and neurological disorders [3-6]. The toxicity of SO₂ is determined mainly by bisulfite (HSO₃⁻) and sulfite (SO₃²⁻) ions which are its main form in aqueous media [7]. These sulfite and bisulfite anions have been widely used as preservatives and additives in many food items, beverages, and pharmaceutical products to preserve freshness and increase their shelf life [8]. However, the excessive intake of bisulfites/sulfites would induce adverse effects on human health [9]. Hence, the sulfite intake by the human body must be limited. This demands the development of rapid, selective, and sensitive methods for the detection and quantification of SO₂ derivatives. In this study, we have employed the spectroscopic technique [10-13] for the detection of HSO₃⁻/SO₃²⁻ ions because of the great advantages of the aforesaid method such as high selectivity, simplicity, high sensitivity, and suitability for real-time monitoring. The developed 1,4 - Michael addition-based colorimetric probe (MTCA) shows a rapid, highly selective, and sensitive sensing of HSO₃⁻ and SO₃²⁻ ions in an aqueous solution as well as in real food samples [14-16].

3.2. Results and discussion

Fig. 1 shows the time-dependent absorbance of the probe in the presence of bisulfite/sulfite in HEPES buffer (20 mM, pH 7.4) containing 1 mM

CTAB. As the reaction progressed, the absorption peak centered at 383 nm decreased, along with the simultaneous emergence of a new absorption at 328 nm; after that, the absorption at 328 nm gradually increased first and then decreased accompanied by the solution color changing from yellow to colorless (inset of Fig. 1). The isosbestic point (337 nm) indicates a clear formation of a new compound and decrease in the peak intensity at 328 nm may be due to the decomposition or aggregation of product molecules. The probe was transformed to the addition product within 10 minutes after the addition of HSO_3^- and SO_3^{2-} [16]. Therefore, the assay time of 10 min was used in the evaluation of the selectivity and sensitivity of the probe toward the analytes.

To investigate the spectral changes of the probe toward HSO_3^- and SO_3^{2-} , the absorption titration was performed at optimal experimental conditions. Fig. 2 shows the spectral behavior upon the addition of HSO_3^- and SO_3^{2-} to the probe solution, which indicates a behavior similar to that of a time-dependent study. A notable color change with increasing the concentration of the analyte was observed, suggesting that the present probe could serve as a colorimetric probe for the detection of SO_2 derivatives.

The marked blue shifts in the absorbance spectra could be attributed to the Michael addition of bisulfite/sulfite to the electrophilic $\text{C}=\text{C}$ double bond in the probe, leading to a non-conjugated structure of the reaction product [16]. To confirm the formation of the addition product probe- SO_3H , the probe was treated with Na_2SO_3 , and the reaction product was isolated.

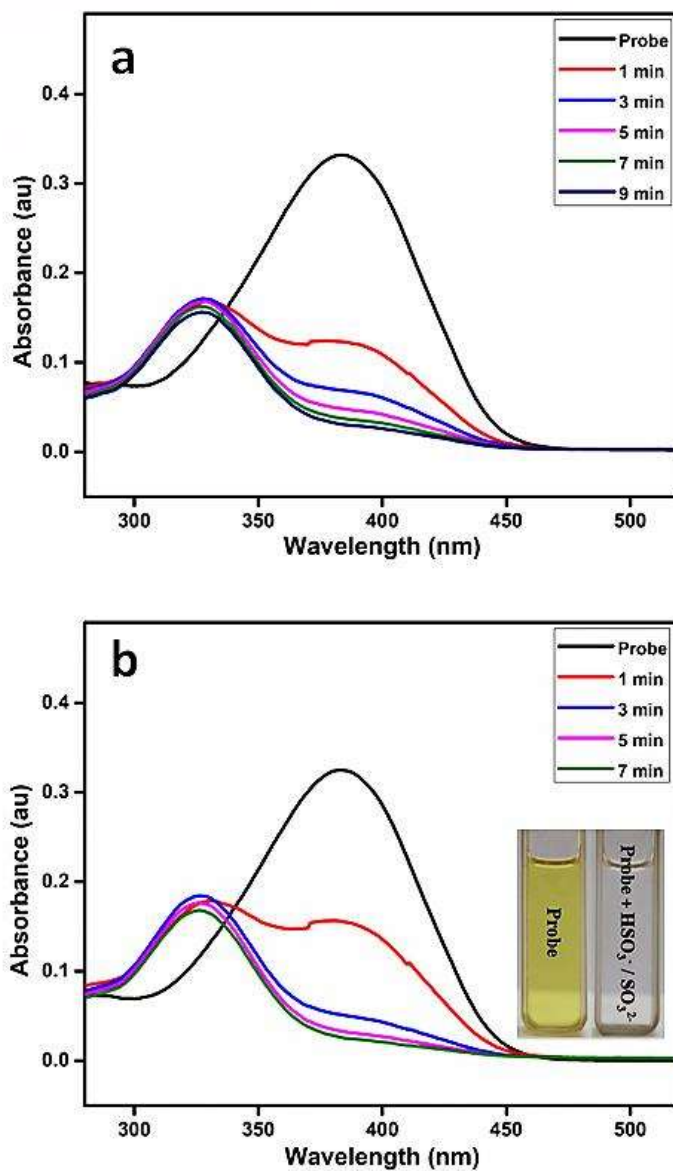


Fig. 1. (a) Time-dependent absorption of the probe (10 μM) in the presence of 20 eq. of bisulfite and (b) sulfite respectively in CTAB-HEPES (1 mM) system. The inset shows the visible color change of the probe with 20 eq. of bisulfite/sulfite for 10 minutes in CTAB-HEPES system (20 mM HEPES, pH 7.4) at 25 $^{\circ}\text{C}$.

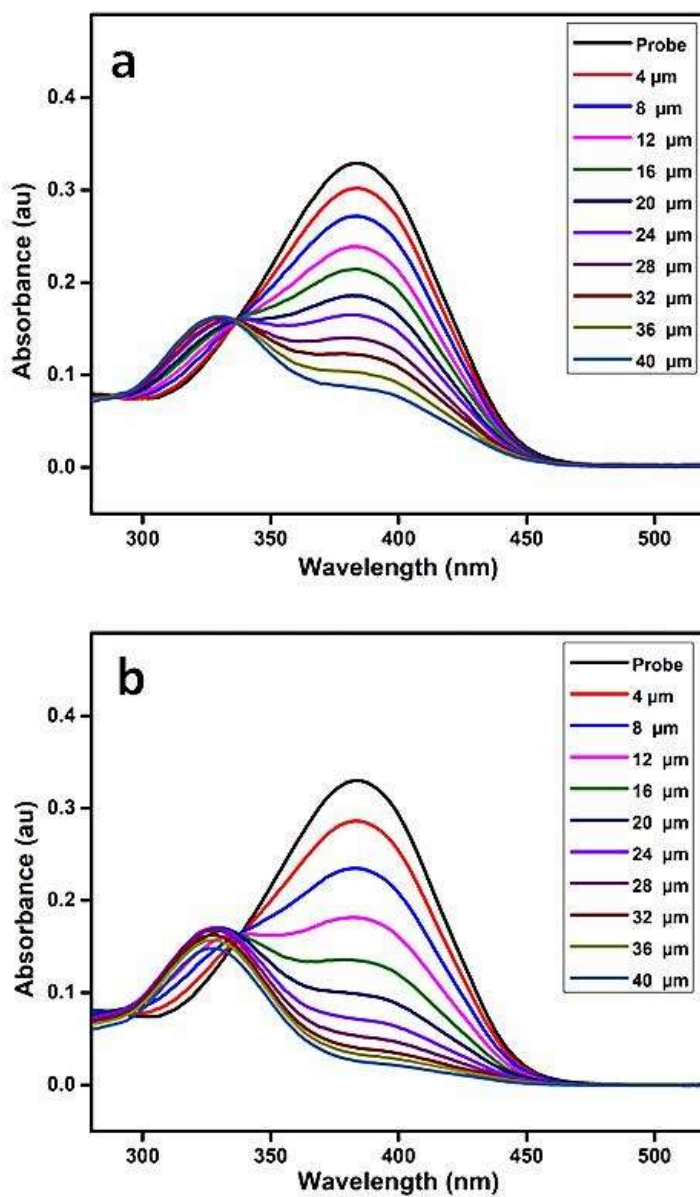
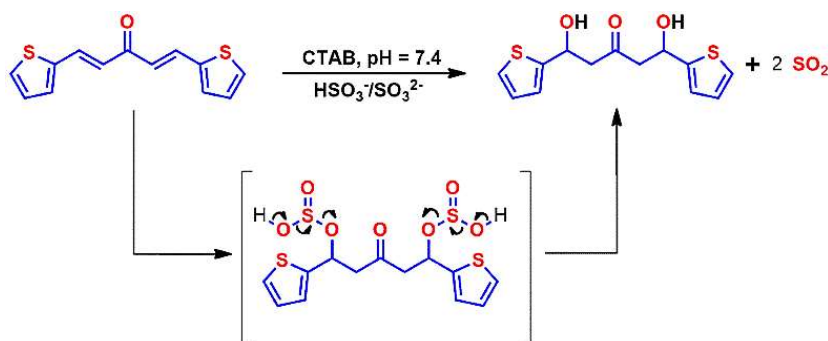


Fig. 2. (a) Absorption spectra of probe (10 μM) upon the addition of increasing concentration of NaHSO₃ and (b) Na₂SO₃ respectively from 0 to 40 μM in HEPES buffer solution (20 mM, pH 7.4) at 25°C.

To provide evidence for the sensing mechanism, ^1H NMR, ^{13}C NMR, HR-MS, and IR analysis of the probe and its reaction product with $\text{HSO}_3^-/\text{SO}_3^{2-}$ (probe- SO_3H) were performed. Surprisingly, the result from the HRMS-ESI (Fig. 3) shows a major ion peak at $m/z = 359.2409$ which is identical to the theoretical molecular mass of the probe-OH adduct ($[\text{probe-2OH } 2\text{K}]^{2+}$ calculated molecular mass = 359.97) rather than probe- SO_3H adduct.

The proposed mechanism of formation of the probe-OH adduct is shown in Scheme 1. These data strongly support the 1: 2 adduct (probe- SO_3H adduct) formation of the probe with $\text{HSO}_3^-/\text{SO}_3^{2-}$ which undergoes an elimination reaction to form probe-OH adduct as the final product.



Scheme 1. The proposed mechanism of the probe for SO_2 derivatives $\text{HSO}_3^- / \text{SO}_3^{2-}$

Furthermore, the formation of the adduct was also confirmed by ^{13}C NMR (Fig. 4), DEPT (Fig. 5), and ^1H NMR (Fig. 6) analysis. As shown in Fig. 7, the resonance signal corresponding to the alkene proton H_β at 7.8 ppm (d) of the probe disappeared, and a new peak at 4.71 ppm (dd)

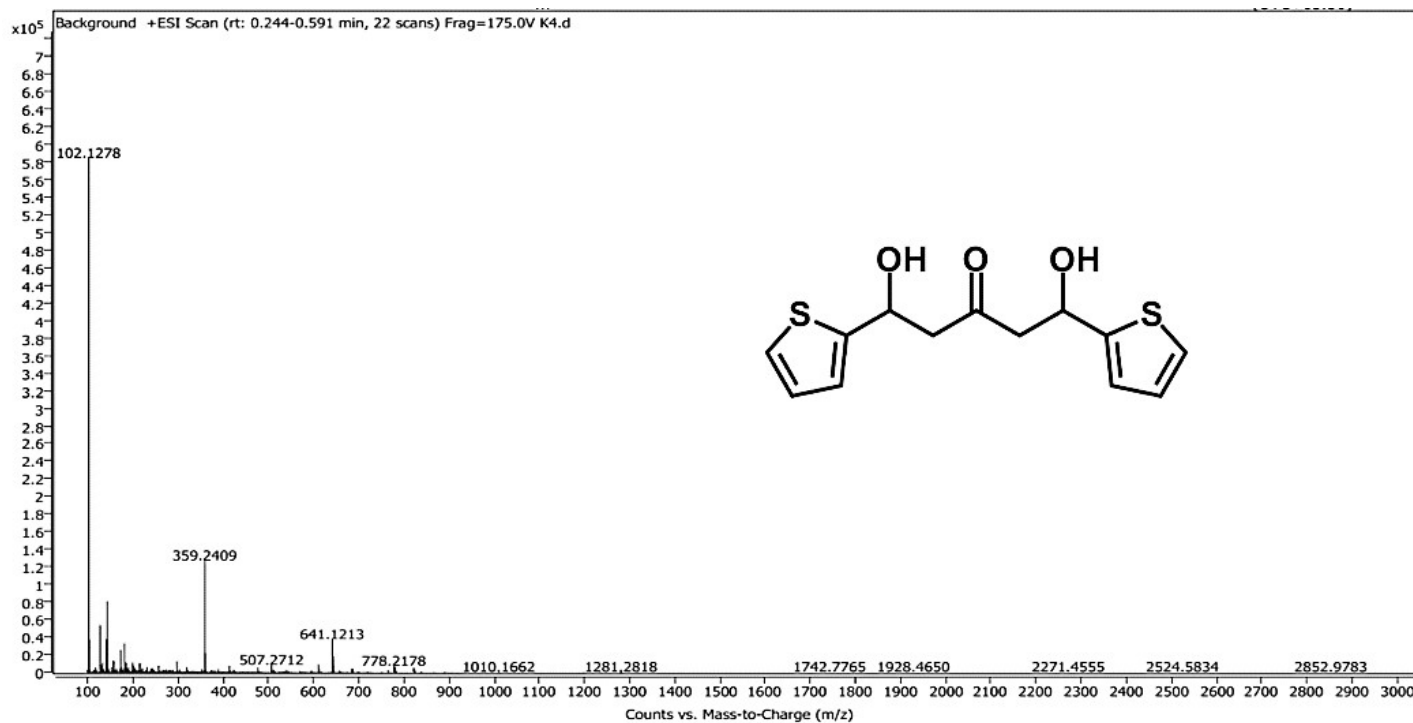


Fig. 3. HRMS-ESI of the adduct (probe-OH) formed by the reaction between the probe and $\text{HSO}_3^- / \text{SO}_3^{2-}$.

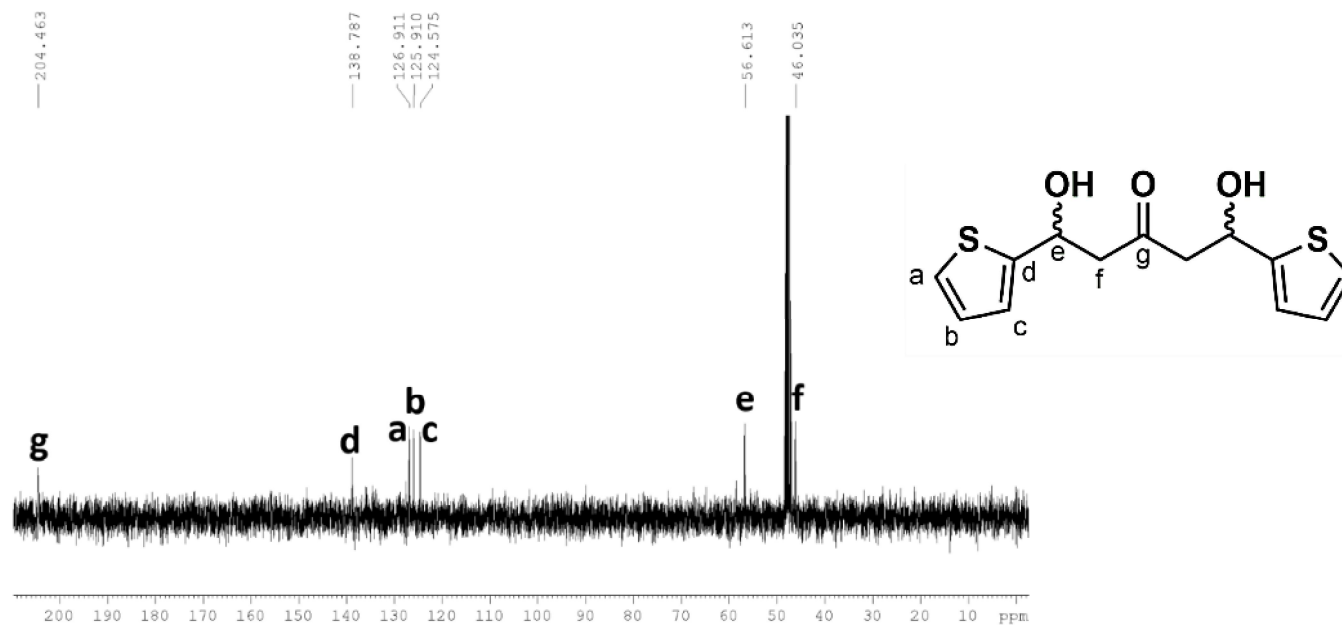


Fig. 4. ^{13}C NMR spectra of the probe-OH adduct in CD_3OD .

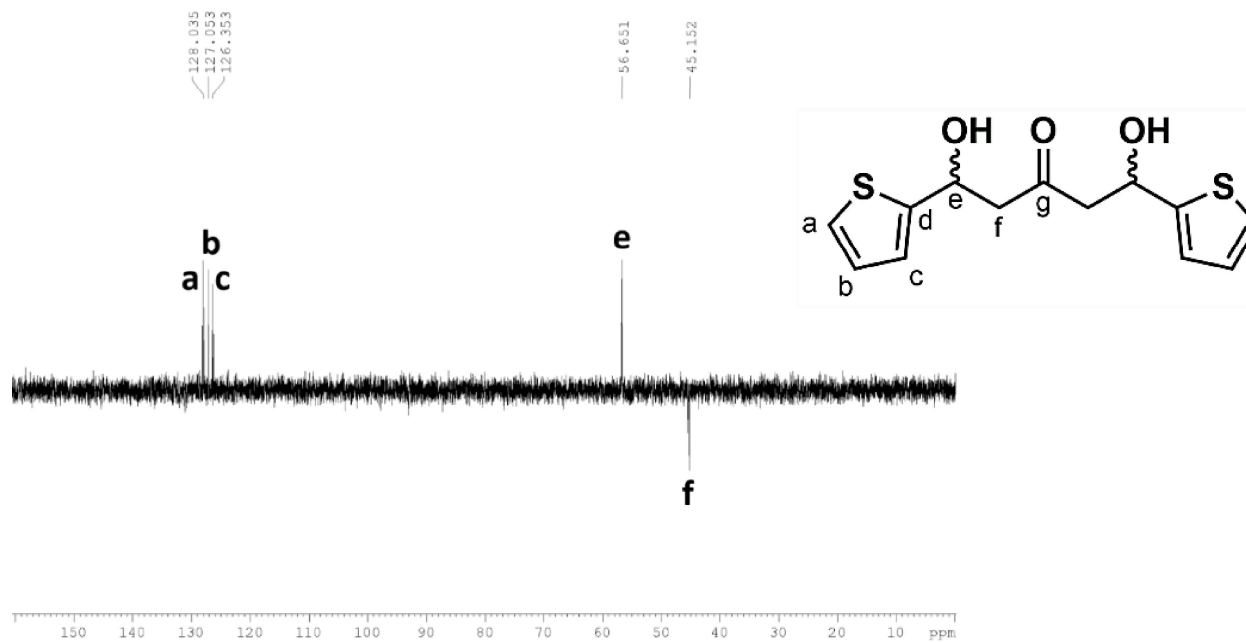


Fig. 5. DEPT analysis spectra of the probe-OH adduct in CD₃OD.

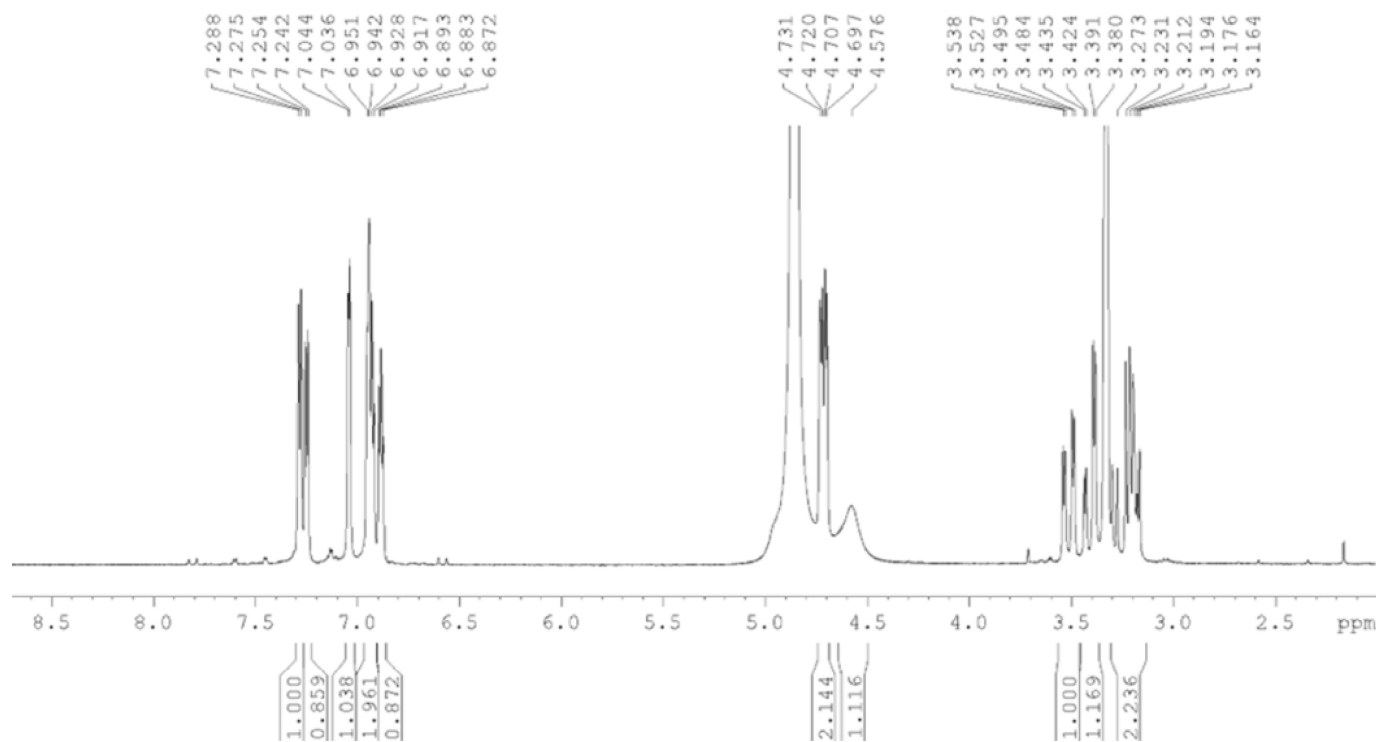


Fig. 6. ^1H NMR spectra of the probe-OH adduct in CD_3OD .

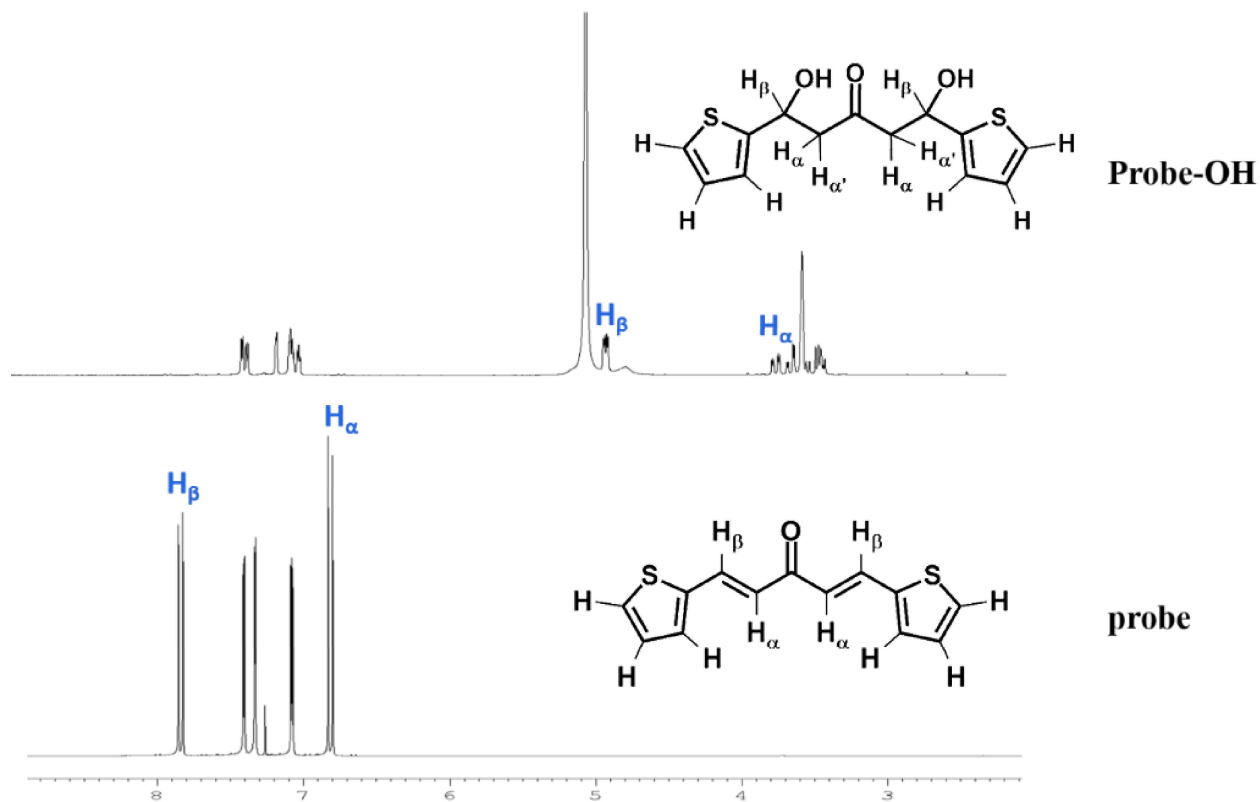


Fig. 7. ¹H NMR spectra of the probe and probe-OH in CDCl₃ and CD₃OD respectively.

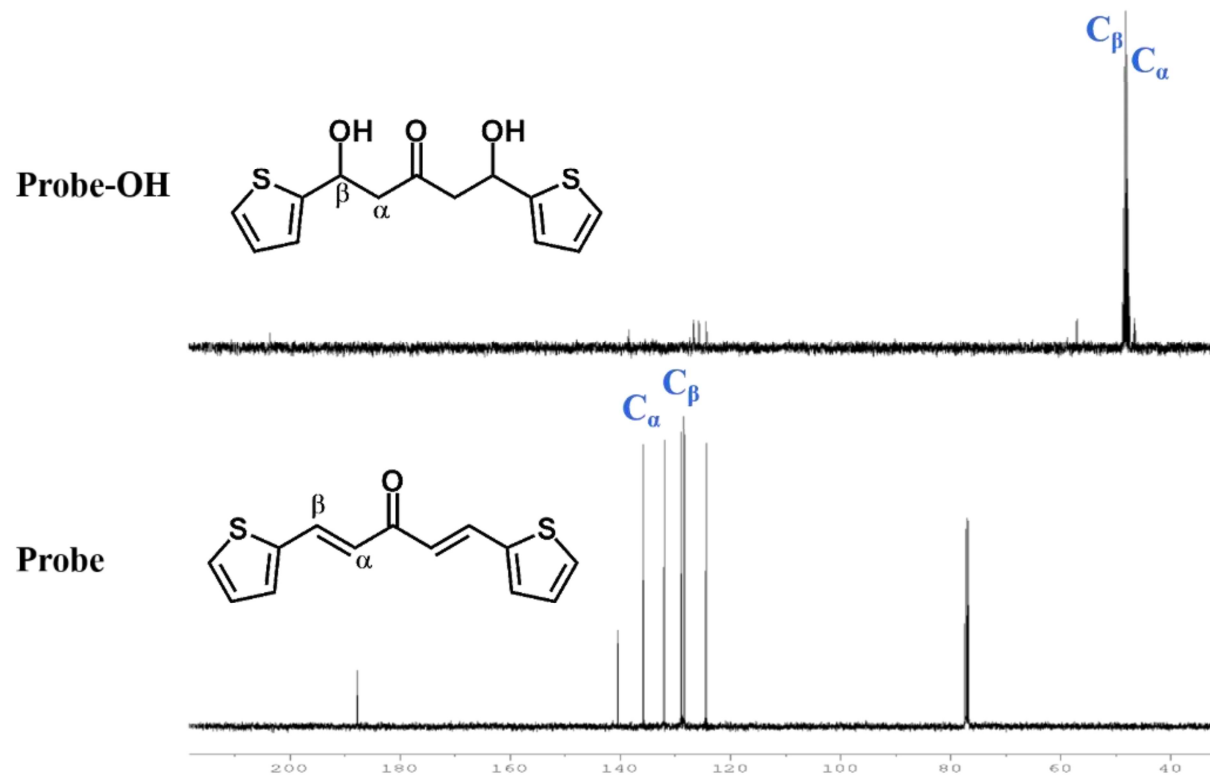


Fig. 8. ^{13}C NMR spectra of the probe and probe-OH in CDCl_3 and CD_3OD respectively.

emerged from the protons at C_β carbon of the probe-OH adduct, which confirms the addition of bisulfite/sulfite to the C=C group. Also, the addition of bisulfite/sulfite to C=C resulted in the formation of a chiral center at C_β of the probe-OH adduct, and as a result, the two protons of the methylene group at C_α of the probe-OH adduct were found to be non-equivalent. Therefore, the signal for H_α of the probe at 6.8 ppm (d) shifted to a higher field in the probe-OH adduct and appeared as two doublets of a doublet in the range of 3.15-3.51 ppm. ^{13}C resonance peaks of C_α and C_β (Fig. 8) show a shift from 135.6 and 128.8 ppm to 46 and 56.6 ppm respectively on moving from the probe to probe-OH adduct, which also confirms the addition of bisulfite/sulfite to the double bond to form a Michael adduct.

IR spectra of the probe (Fig. 9) show two characteristic peaks at 1604 cm^{-1} and 1661 cm^{-1} which correspond to the C=C group and C=O group respectively. In the case of probe-OH, the peak at 1604 cm^{-1} disappeared and a new peak appeared at 2972 cm^{-1} (C-H stretching of alkane) due to the addition of $\text{HSO}_3^-/\text{SO}_3^{2-}$ to the C=C group during the step leading to the formation of final product probe-OH adduct. On the other hand, the carbonyl peak at 1661 cm^{-1} was shifted to 1650 cm^{-1} may be due to the formation of a hydrogen bond with the -OH group of the probe-OH adduct. IR spectra of the probe-OH show two more new peaks around 3394 (broad) and 1402 cm^{-1} which corresponds to O-H stretching and O-H bending of alcohol respectively. This result is consistent with the addition of $\text{HSO}_3^-/\text{SO}_3^{2-}$ to the C=C group and the formation of the probe-OH adduct from the probe- SO_3H adduct.

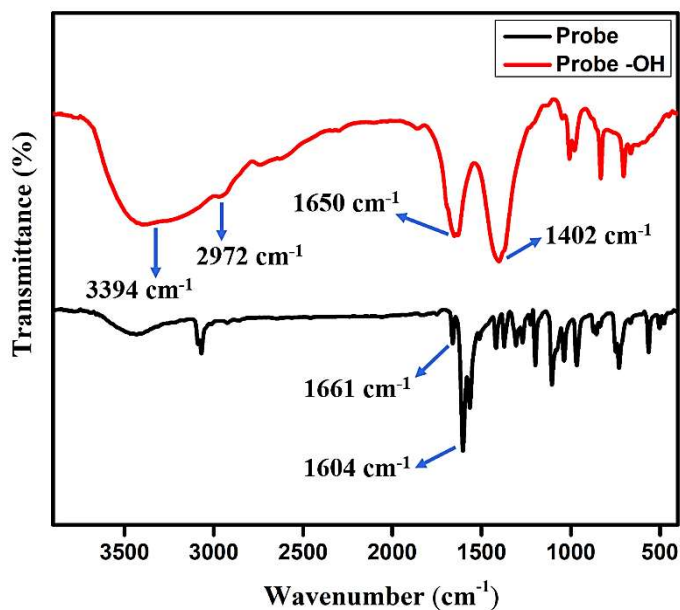


Fig. 9. FT-IR spectrum of the probe and probe-OH.

To confirm the proposed sensing mechanism of $\text{HSO}_3^-/\text{SO}_3^{2-}$ by the probe, the density functional theory (DFT) was carried out at the B3LYP/6-311+G(d,p) level by the Gaussian 09 program [17]. The optimized structures in the ground states of the probe and possible products of the reaction between the probe and SO_2 derivatives were shown in Fig. 10, in which A represents the product formed by the 1,2 addition of SO_2 derivatives to the probe, and B represents the product formed by the 1,4 addition of SO_2 derivatives to the probe at only one olefinic site. The stabilization energy of A and B differ slightly but are almost the same as -5.2×10^6 KJ/mol. C represents the product formed by the 1,4 addition of SO_2 derivatives to the probe at both olefinic sites.

We found that the stabilization energy of C (-6.9×10^6 KJ/mol) is higher than that of A (-5.2×10^6 KJ/mol), B (-5.2×10^6 KJ/mol), and that of the probe (-3.6×10^6 KJ/mol). Since C is the more stable product, these results confirm that the Michael addition of $\text{HSO}_3^-/\text{SO}_3^{2-}$ to the probe takes place at both olefinic sites of the probe. This result was consistent with the experimental data.

Normally, the addition of bisulfite/sulfite to olefin takes place in organic solvents at elevated temperatures or in the presence of catalysts. Here we report the addition of sulfite to olefin under aqueous conditions. To further investigate the reaction mechanism, we also studied the spectral response of the probe toward bisulfite/sulfite in HEPES buffer solution (20 mM, pH 7.4) in the presence and absence of CTAB. No new absorption peak was found even after 1h in the absence of CTAB (Fig. 11), which implies that the addition reaction between bisulfite/sulfite and probe cannot occur without CTAB. The slight decrease in the absorbance at 383 nm might be caused by the aggregation or precipitation of probe molecules.

3.2.1. Effect of pH on the absorbance of the probe towards SO_2 -derivatives

To investigate the effect of pH on the absorbance of the probe, the reaction was executed at different pH by adjusting the pH by HCl and NaOH. As shown in Fig. 12 and Fig. 13, the absorbance of the probe was almost pH insensitive, whereas, upon the interaction with NaHSO_3 and Na_2SO_3 , important changes were observed depending on the pH values. The reaction proceeds slowly when the solution's pH was less

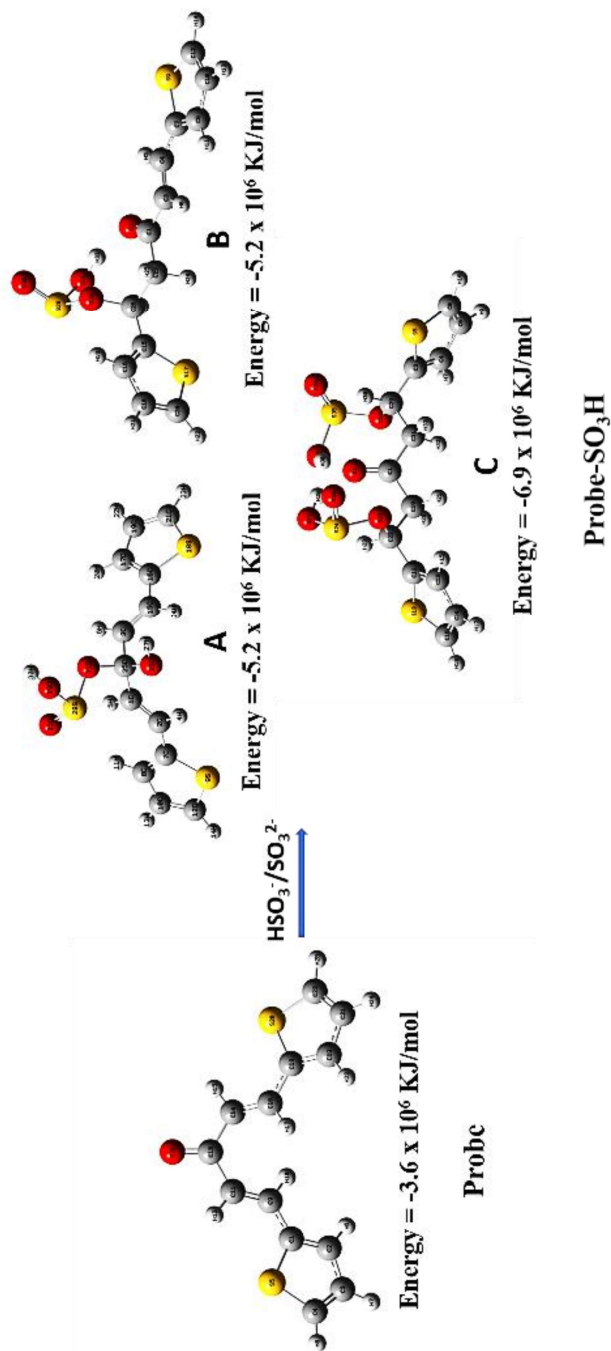


Fig. 10. The optimized structures of the probe and its expected reaction products (probe-SO₃H) of reaction with HSO₃⁻ / SO₃²⁻.

than 6, but it was greatly speeded up when the pH was near and above 7, which shows that a basic environment is essential for this reaction [18]. This behavior allows the detection of bisulfite/sulfite in physiological conditions; hence we choose a pH of 7.4 for our study.

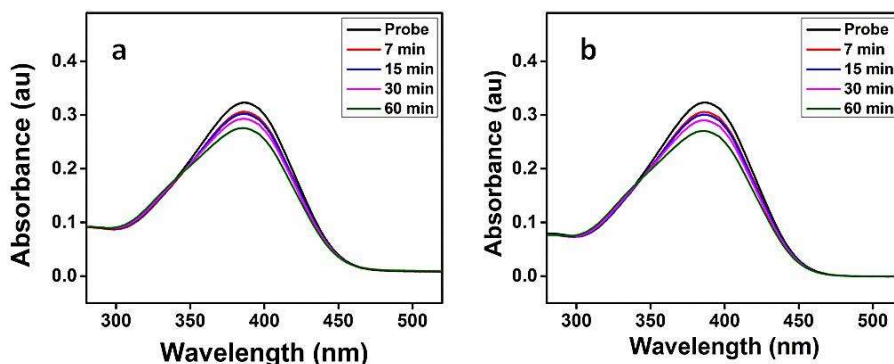


Fig. 11. (a) Absorption spectra of probe (10 μM) upon the addition of NaHSO_3 (200 μM) and (b) Na_2SO_3 (200 μM) respectively in HEPES buffer solution (20 mM, pH 7.4) in the absence of CTAB.

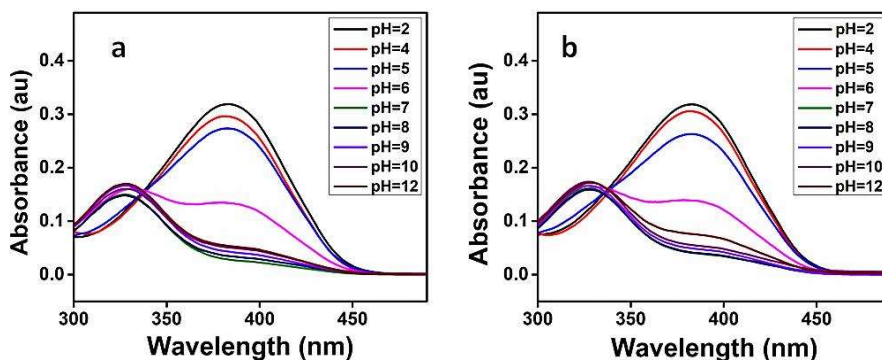


Fig. 12. (a) Spectra for the reaction between probe (10 μM) and NaHSO_3 (200 μM) and (b) Na_2SO_3 (200 μM) respectively at different pH values.

3.2.2. Effect of various surfactants on the absorbance of the probe towards SO₂-derivatives

To investigate the effect of various surfactants on the absorbance of the probe, the study was conducted using cationic, anionic, and zwitterionic surfactants. Surfactants affect the chemical reaction in the following ways: changing the local concentrations of the reactants, altering the local pH value, and providing a nonpolar microenvironment [19, 20]. Cationic surfactant CTAB can adsorb counter ions such as OH⁻, HSO₃⁻, SO₃²⁻ etc, so the pH value, as well as bisulfite/sulfite concentration, should be much higher on the CTAB micelle surface than in the bulk solution. Therefore, the reaction was accelerated greatly in CTAB–HEPES because the CTAB micelle offered a basic and nonpolar microenvironment. The anionic surfactant sodium dodecylbenzene sulfonate

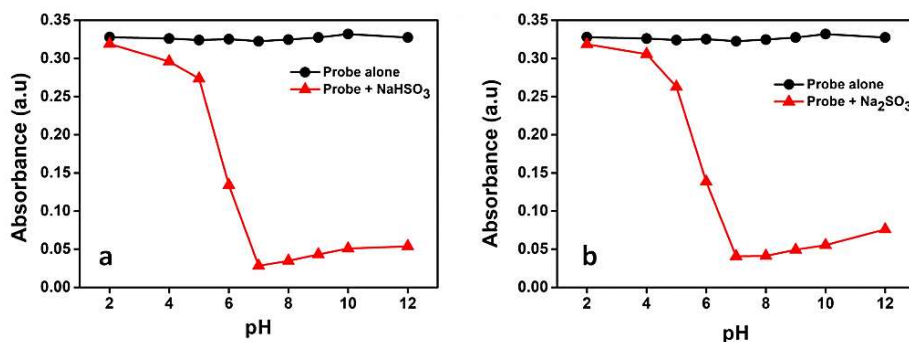


Fig. 13. Effect of pH on the absorbance of the probe (10 μM) alone and after its reaction with (a) NaHSO₃ (200 μM) and (b) Na₂SO₃ (200 μM) respectively at 25 °C after 10 minutes of reaction. Absorbance at 383 nm is recorded.

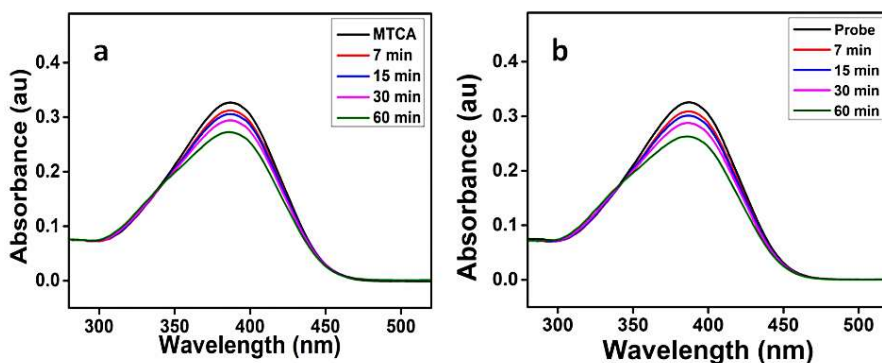


Fig. 14. (a) Absorption spectra of probe ($10\ \mu\text{M}$) upon the addition of NaHSO_3 ($200\ \mu\text{M}$) and (b) Na_2SO_3 ($200\ \mu\text{M}$) respectively in HEPES buffer solution ($20\ \text{mM}$, $\text{pH}\ 7.4$) in the presence of anionic surfactant SDBS.

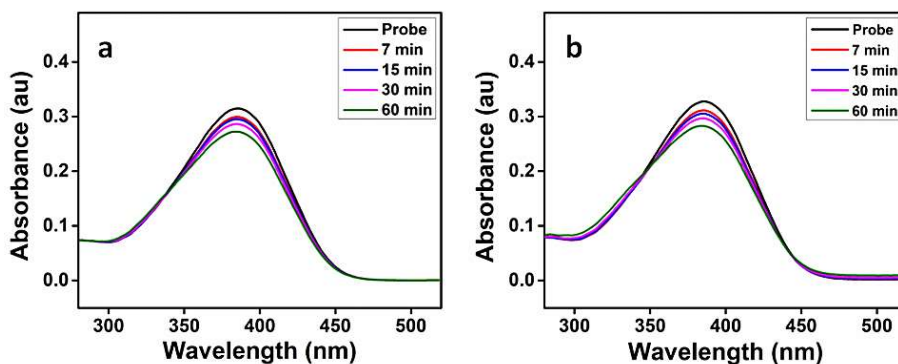


Fig. 15. (a) Absorption spectra of probe ($10\ \mu\text{M}$) upon the addition of NaHSO_3 ($200\ \mu\text{M}$) and (b) Na_2SO_3 ($200\ \mu\text{M}$) respectively in HEPES buffer solution ($20\ \text{mM}$, $\text{pH}\ 7.4$) in the presence of zwitter ionic surfactant CAPB.

(SDBS) also can provide a nonpolar microenvironment, but it adsorbs positively charged ions, as a result, the H^+ concentration around the SDBS micelle is higher than that of the bulk solution, this is why the

reaction conducted in SDBS-HEPES shows no significant change in the absorption even after 1h (Fig. 14). The presence of zwitter ionic surfactant cocamidopropyl betaine (CAPB) also didn't bring any change in absorption spectra after 1h (Fig. 15), which suggests that the zwitter ionic micelle (CAPB) is less effective than the cationic micelle (CTAB) in binding hydrophilic ions such as SO_2 derivatives [21]. This behavior of the probe verifies that the charge characteristic of the surfactant plays an essential role in this reaction.

The detection limit (LOD) of the probe for bisulfite/sulfite detection was determined from a plot of absorption intensity as a function of $\text{NaHSO}_3/\text{Na}_2\text{SO}_3$ concentration, as previously mentioned in Chapter 2 [22]. A good linear relationship is observed for the probe with a correlation coefficient as large as 0.9955 and 0.9901, and LOD of 0.43 μM and 0.23 μM for the detection of bisulfite (Fig. 16a) and sulfite (Fig. 16b) respectively.

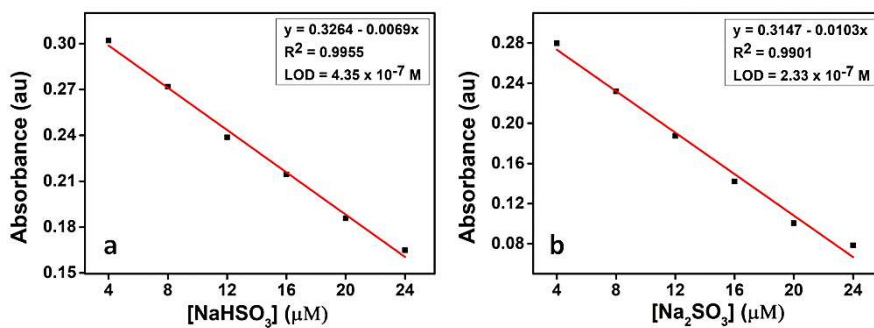


Fig. 16. (a) Changes in absorbance at 383 nm upon the gradual addition of NaHSO_3 and (b) Na_2SO_3 respectively in CTAB - HEPES buffer solution (20 mM, pH 7.4) from 4 to 24 μM .

The stability of the method was assessed as mentioned in Chapter 2. The relative standard deviation (RSD) associated with the probe was found to be 2.6% and 3.6% for the detection of bisulfite and sulfite respectively, which is <5% showing an acceptable performance and good stability of the method [23].

3.2.3. Selectivity and competition of the probe toward SO₂-derivatives

The selectivity of the probe toward SO₂ derivatives over some interfering anions including F⁻, Cl⁻, Br⁻, I⁻, AcO⁻, HCO₃⁻, CO₃²⁻, HPO₄²⁻, SO₄²⁻, NO₃⁻, S₂O₃²⁻, CN⁻, SCN⁻, and biothiol (cysteine) in CTAB-HEPES system was evaluated [24]. As illustrated in Fig. 17, there is no obvious spectral change associated with the probe even in the presence of 20 eq. of most of the interfering anions, which verifies that the probe is highly selective toward bisulfite/sulfite.

Furthermore, competitive analysis of the different interfering anions with HSO₃⁻/SO₃²⁻ was conducted, where the interfering anions were first introduced into the probe solution and followed by the addition of 10 eq. of HSO₃⁻ or SO₃²⁻. Fig. 18 shows that there is not much change in the absorbance of the probe at 383 nm upon the addition of 20 eq. of different interfering anions, while there is a considerable change in the absorbance during the addition of bisulfite/sulfite to this test solution. This shows that all the tested anions have no interference with the absorbance response of the probe toward HSO₃⁻/SO₃²⁻, thereby indicating its high level of selectivity.

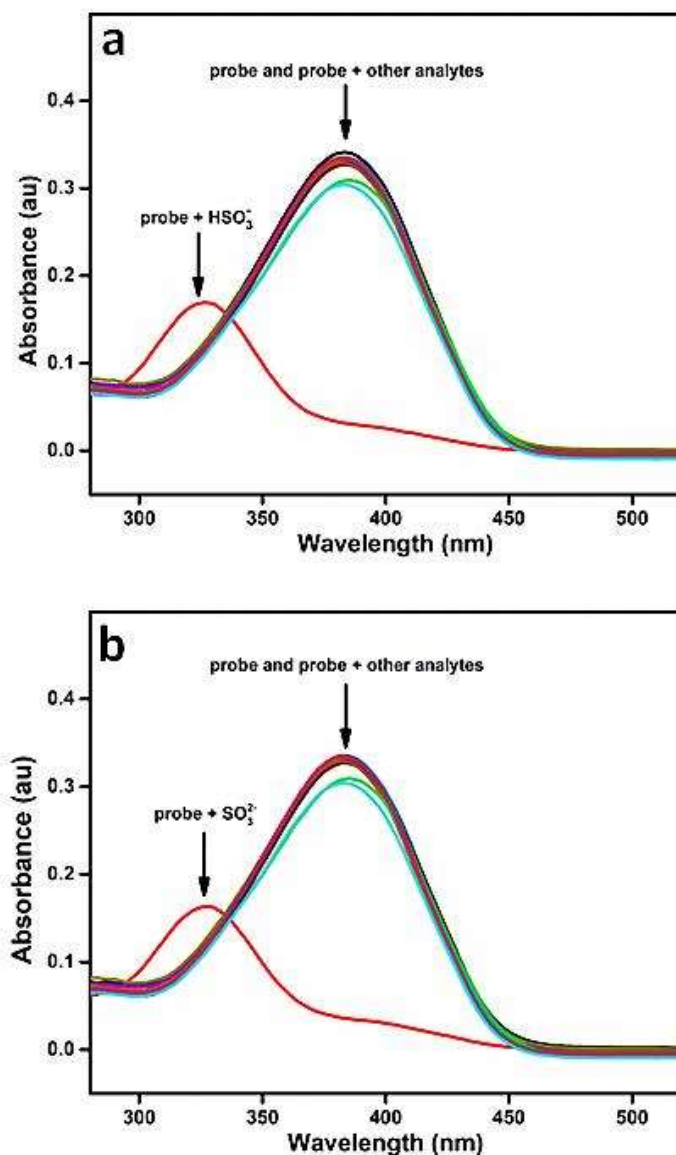


Fig. 17. (a) Absorption changes of probe (10 μM) in the presence of HSO₃⁻ (100 μM), (b) SO₃²⁻ (100 μM), and various other analytes (200 μM). Other analytes are F⁻, Cl⁻, Br⁻, I⁻, AcO⁻, HCO₃⁻, CO₃²⁻, HPO₄²⁻, SO₄²⁻, NO₃⁻, S₂O₃²⁻, CN⁻, SCN⁻, and biothiol (cysteine) respectively. All experiments were performed in HEPES buffer (20 mM, pH 7.4) at 25°C and each spectrum was obtained 10 min after the addition of the analyte.

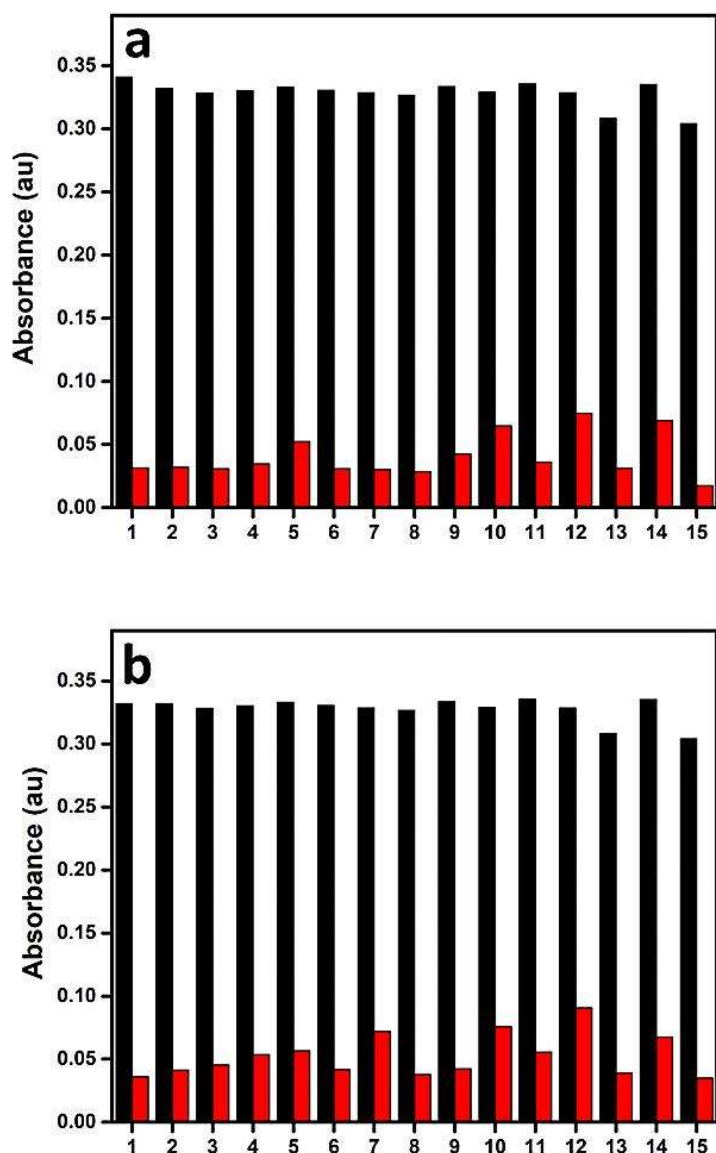


Fig. 18. (a) Absorbance of the probe (10 μM) in the presence of 20 eq. of various additives with (red) or without (black) HSO_3^- (100 μM) and (b) SO_3^{2-} (100 μM) in CTAB–HEPES for 10 minutes: (1) blank; (2) F^- ; (3) Cl^- ; (4) Br^- ; (5) I^- ; (6) AcO^- ; (7) HCO_3^- ; (8) CO_3^{2-} ; (9) HPO_4^{2-} ; (10) SO_4^{2-} ; (11) NO_3^- ; (12) $\text{S}_2\text{O}_3^{2-}$; (13) CN^- ; (14) SCN^- ; and (15) cysteine.

3.2.4. Detection of SO₂ derivatives in real samples

To demonstrate the applicability of the tested probe, the compound was assessed to detect bisulfite/sulfite in realistic samples [25]. The crystal sugar and brown sugar were purchased from a supermarket and were dissolved and diluted in water as the real food sample for analysis. As shown in Table 1, we can see that probe was able to determine the concentration of spiked HSO₃⁻ and SO₃²⁻ in these real food samples with

Table 1. Determination of bisulfite/sulfite in realistic samples.

Sample	Present concentration of SO ₂ derivatives (μM)	Added HSO ₃ ⁻ (μM)	Found HSO ₃ ⁻ (μM)	Recovery (%)	RSD (%)
Crystal sugar	2.19	5	7.38	102.6	1.7
		10	11.95	98.0	5.0
Brown Sugar	3.41	5	8.49	100.9	2.2
		10	13.07	97.5	1.3
Sample	Present concentration of SO ₂ derivatives (μM)	Added SO ₃ ²⁻ (μM)	Found SO ₃ ²⁻ (μM)	Recovery (%)	RSD (%)
Crystal sugar	2.13	5	7.07	99.2	2.4
		10	11.81	97.4	1.7
Brown Sugar	3.39	5	8.63	102.9	2.3
		10	13.93	104.0	1.3

- *In the sample solution, the concentration of sugar was 25g/100 mL.*
- *Sulfite was spiked to the samples directly and calculated as SO₂.*
- *Relative standard deviations were calculated based on three measurements.*

good recovery ranging from 97.5% to 102.6% and 97.4% to 104.0% respectively, indicating that this probe could potentially be used for quantitatively detecting bisulfite/sulfite in real food samples.

3.3. Conclusions

In summary, we have synthesized a colorimetric probe for the detection of bisulfite/sulfite anions, that works based on the Michael addition of anions to α , β -unsaturated ketones. The basic and nonpolar microenvironment provided by cationic surfactant CTAB enables the easy occurrence of the reaction in an aqueous solution, which allows the detection of both of the analytes (HSO_3^- and SO_3^{2-}). The obtained results indicate that the probe could potentially be used in the selective recognition of bisulfite/sulfite in real food samples.

References

- [1] A. Hansell, C. Oppenheimer, Health hazards from volcanic gases: a systematic literature review, *Archives of Environmental Health: An International Journal*, 59(2004) 628-39.
- [2] J.S. Pandey, R. Kumar, S. Devotta, Health risks of NO₂, SPM and SO₂ in Delhi (India), *Atmos Environ*, 39(2005) 6868-74.
- [3] N. Sang, Y. Yun, H. Li, L. Hou, M. Han, G. Li, SO₂ inhalation contributes to the development and progression of ischemic stroke in the brain, *Toxicol Sci*, 114(2010) 226-36.
- [4] D. Liu, H. Jin, C. Tang, J. Du, Sulfur dioxide: a novel gaseous signal in the regulation of cardiovascular functions, *Mini Rev Med Chem*, 10(2010) 1039-45.
- [5] Y. Yun, R. Gao, H. Yue, G. Li, N. Zhu, N. Sang, Synergistic effects of particulate matter (PM₁₀) and SO₂ on human non-small cell lung cancer A549 via ROS-mediated NF- κ B activation, *Journal of Environmental Sciences*, 31(2015) 146-53.

- [6] W. Zhang, F. Huo, F. Cheng, C. Yin, Employing an ICT-FRET integration platform for the real-time tracking of SO₂ metabolism in cancer cells and tumor models, *Journal of the American Chemical Society*, 142(2020) 6324-31.
- [7] Z. Meng, G. Qin, B. Zhang, J. Bai, DNA damaging effects of sulfur dioxide derivatives in cells from various organs of mice, *Mutagenesis*, 19(2004) 465-8.
- [8] T. Fazio, C.R. Warner, A review of sulphites in foods: Analytical methodology and reported findings, *Food Additives & Contaminants*, 7(1990) 433-54.
- [9] S.L. Bahna, J.G. Burkhardt, The dilemma of allergy to food additives, *Allergy & Asthma Proceedings* 2018.
- [10] K. Xiang, S. Chang, J. Feng, C. Li, W. Ming, Z. Liu, et al., A colorimetric and ratiometric fluorescence probe for rapid detection of SO₂ derivatives bisulfite and sulfite, *Dyes and Pigments*, 134(2016) 190-7.
- [11] G. Asaithambi, V. Periasamy, Ratiometric sensing of sulfite/bisulfite ions and its applications in food samples and living cells, *Journal of Photochemistry and Photobiology A: Chemistry*, 389(2020) 112214.
- [12] C. Nandhini, P.S. Kumar, R. Shanmugapriya, K. Vennila, A.G. Al-Sehemi, M. Pannipara, et al., A combination of experimental and TD-DFT investigations on the fluorescent detection of sulfite and bisulfite ions in aqueous solution via nucleophilic addition reaction, *Journal of Photochemistry and Photobiology A: Chemistry*, 425(2022) 113668.
- [13] Y. Zhou, J. Gou, Y.-X. Zhou, C. Liu, X. Xiao, H.-J. Liu, Tunable energy level induced fluorescence enhancement in copper functionalized silicon quantum dots for highly selective detection of bisulfite, *Sensors and Actuators B: Chemical*, 370(2022) 132444.
- [14] H. Feng, J. Liu, A. Qaitoon, Q. Meng, Y. Sultanbawa, Z. Zhang, et al., Responsive small-molecule luminescence probes for sulfite/bisulfite detection in food samples, *TrAC Trends in Analytical Chemistry*, 136(2021) 116199.
- [15] T. Li, X. Chen, K. Wang, Z. Hu, Small-Molecule Fluorescent Probe for Detection of Sulfite, *Pharmaceuticals*, 15(2022) 1326.
- [16] H. Tian, J. Qian, Q. Sun, H. Bai, W. Zhang, Colorimetric and ratiometric fluorescent detection of sulfite in water via cationic surfactant-promoted addition of sulfite to α , β -unsaturated ketone, *Analytica chimica acta*, 788(2013) 165-70.
- [17] J. Chao, X. Wang, Y. Liu, Y. Zhang, F. Huo, C. Yin, et al., A pyrene-thiophene based fluorescent probe for ratiometric sensing of bisulfite and its

application in vivo imaging, *Sensors and Actuators B: Chemical*, 272(2018) 195-202.

[18] D. Don, K. Velmurugan, J. Prabhu, N. Bhuvanesh, A. Thamilselvan, R. Nandhakumar, A dual analyte fluorescent chemosensor based on a furan-pyrene conjugate for Al^{3+} & HSO_3^- , *Spectrochimica Acta Part A: Molecular and Biomolecular Spectroscopy*, 174(2017) 62-9.

[19] R. Badugu, J.R. Lakowicz, C.D. Geddes, Enhanced fluorescence cyanide detection at physiologically lethal levels: reduced ICT-based signal transduction, *Journal of the American Chemical Society*, 127(2005) 3635-41.

[20] M.L. Satnami, S. Dhritlahre, R. Nagwanshi, I. Karbhal, K.K. Ghosh, F. Nome, Nucleophilic Attack of Salicylhydroxamate Ion at C=O and P=O Centers in Cationic Micellar Media, *The Journal of Physical Chemistry B*, 114(2010) 16759-65.

[21] C.A. Bunton, M.M. Mhala, J.R. Moffatt, Nucleophilic reactions in zwitterionic micelles of amine oxide or betaine sulfonate surfactants, *The Journal of Physical Chemistry*, 93(1989) 854-8.

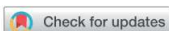
[22] M. Gómez, E.G. Perez, V. Arancibia, C. Iribarren, C. Bravo-Díaz, O. García-Beltrán, et al., New fluorescent turn-off probes for highly sensitive and selective detection of SO_2 derivatives in a micellar media, *Sensors and Actuators B: Chemical*, 238(2017) 578-87.

[23] M. Gómez, M.E. Aliaga, V. Arancibia, A. Moya, C. Segura, M.T. Nunez, et al., Detection of SO_2 derivatives using a new chalcone-coumarin derivative in cationic micellar media: application to real samples, *RSC advances*, 8(2018) 31261-6.

[24] L. Zhang, L. Wang, X. Zhang, Z.-J. Zhu, A colorimetric and fluorescent probe for sulfite/bisulfite based on conjugated benzothiazole derivative and imaging application in living cells, *Journal of Photochemistry and Photobiology A: Chemistry*, 395(2020) 112498.

[25] X. Dai, T. Zhang, Z.-F. Du, X.-J. Cao, M.-Y. Chen, S.-W. Hu, et al., An effective colorimetric and ratiometric fluorescent probe for bisulfite in aqueous solution, *Analytica Chimica Acta*, 888(2015) 138-45.

PAPER

Cite this: *RSC Adv.*, 2023, 13, 2552

A bis-chalcone based colorimetric probe for the selective detection of bisulfite/sulfite anions: exploring surfactant promoted Michael addition of anions to α , β -unsaturated ketones†

Sowmya P, Sivakrishna Prakash and Abraham Joseph *

A probe, (E,E)-1,5-di(thiophen-2-yl)penta-1,4-dien-3-one, was developed for rapid, colorimetric, and selective detection of bisulfite/sulfite anions in aqueous solutions. This probe is based on the Michael addition reaction which is favoured in the presence of cationic micellar medium CTAB. CTAB promoted Michael addition is an effective tool to determine SO_2 toxicity, which is mainly expressed in terms of collective concentration of bisulfite and sulfite anions. The probe showed high selectivity and sensitivity toward bisulfite and sulfite over other interfering anions, with a detection limit of $0.43 \mu\text{M}$ and $0.23 \mu\text{M}$, respectively. The possible recognition mechanism of the probe and the analyte was illustrated by NMR, HR-MS, IR, and computational analysis. Moreover, this probe showed great potential for the detection of bisulfite/sulfite in real samples, such as crystal sugar and brown sugar.

Received 29th October 2022
Accepted 1st January 2023

DOI: 10.1039/d2ra06832j

rsc.li/rsc-advances

1. Introduction

Sulfur dioxide (SO_2) is a well-known air pollutant released in many industrial processes and it exhibits significant impacts on human health and the environment.^{1,2} Studies have shown that frequent exposure to SO_2 induces many health issues such as lung and brain cancer, cardiovascular diseases, respiratory problems, and neurological disorders.³⁻⁶ Since SO_2 can be easily hydrated to sulfurous acid once inhaled and subsequently forms an equilibrium state between its derivatives bisulfite (HSO_3^-) and sulfite (SO_3^{2-}) as its main forms in aqueous media, so the toxicity of SO_2 is determined mainly by these two anions.⁷

Sulfur dioxide (SO_2) derivatives such as sulfite and bisulfite anions have been widely used as preservatives and additives in many food items, beverages, and pharmaceutical products to preserve freshness and increase their shelf life.⁸ However, excessive intake of bisulfites/sulfites would induce adverse effects on human health.⁹ Hence, the sulfite intake by the human body must be limited. This demands the development of rapid, selective, and sensitive methods for the detection and quantification of SO_2 derivatives.

To date, the existing conventional methods to detect bisulfite/sulfites include ion chromatography,^{10,11} spectroscopy,¹²⁻¹⁵ electrochemistry,^{16,17} and iodometric titration.¹⁸ However, the main disadvantage of these methods is that

the majority of them require miscellaneous sample pre-treatment and the use of relatively multiple reagents. Among these conventional approaches, spectroscopy has been widely applied in analyte detection because of its high selectivity, simplicity, low detection limit, and suitability for real-time monitoring. Therefore, calorimetric and fluorescent probes have been regarded as versatile tools for monitoring ions and biomolecules.¹⁹⁻²²

Till now, several colorimetric and fluorescent probes for the detection of the SO_2 derivatives ($\text{HSO}_3^-/\text{SO}_3^{2-}$) have been designed and developed based on different sensing mechanisms such as the selective deprotection of levulinic group,²³⁻²⁵ complexation with amines,^{26,27} the selective reaction with aldehyde,^{28,29} coordination to metal ions,³⁰ and Michael-type additions.^{31,32} Among these different approaches 1,4-Michael addition of nucleophiles to α , β unsaturated systems that contain ester, ketone, nitrile, and nitro groups is one of the most versatile methods^{33,34} for the development of chemosensors for the detection of SO_2 derivatives because this method allows the reaction to proceed under mild conditions.³⁵⁻³⁹

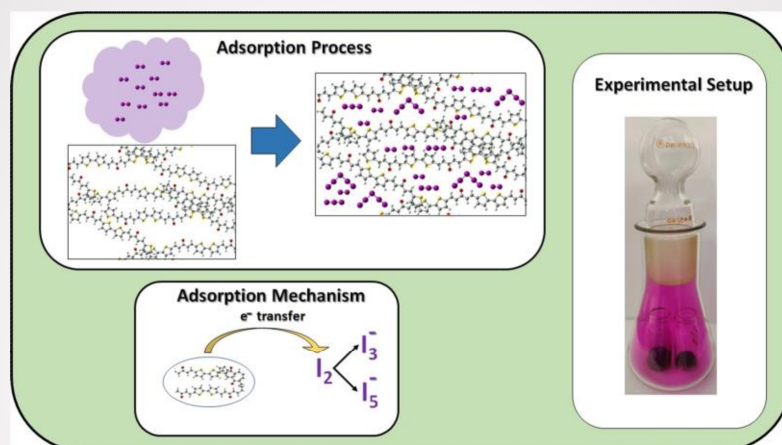
Interestingly, Zhang *et al.* (2013)³⁸ reported promising studies in this area, using a cationic cetyltrimethylammonium bromide (CTAB) micelle, to create a hydrophobic and basic microenvironment that promotes the addition reaction of sulfite to an activated olefin in aqueous solutions. The limit of detection of the probe was $0.2 \mu\text{M}$. Based on this study, many groups have reported new probes that can detect SO_2 derivatives in aqueous solutions via micelle-mediated Michael-type addition reaction. In 2017, Gómez *et al.* reported two fluorescent turn-off probes for the detection of SO_2 derivatives in a micellar

Department of Chemistry, University of Calicut, Calicut University, 673 635, Kerala, India. E-mail: abrahamjoseph@uoc.ac.in

† Electronic supplementary information (ESI) available. See DOI: <https://doi.org/10.1039/d2ra06832j>

Chapter 4

Thiophene containing bis-chalcone-based mesoporous polymers for volatile iodine capture



Two novel thiophene-containing bis-chalcone-based polymers PTCA and PTCM were tested for their iodine capture performance. The maximum iodine capture capacity obtained for PTCA and PTCM were 242 and 221 wt.% respectively. The adsorption follows pseudo-second-order kinetics, and chemisorption is the major process involved in the process of adsorption.

4.1. Introduction

4.2. Results and discussion

4.2.1. Iodine capture

4.2.2. Kinetics of iodine capture

4.2.3. Mechanism of iodine capture

4.2.4. Iodine release and recyclability

4.3. Conclusions

4.1. Introduction

Since fossil fuels are non-renewable, there is a great demand for developing an alternative source to meet the necessary energy requirements for the future without the emission of greenhouse gases. Although nuclear energy is considered an efficient alternative source, the main safety concern related to nuclear energy is the appropriate management of nuclear wastes (^{129}I , ^{127}Xe , ^{85}Kr , etc) generated from nuclear reactions [1-4]. Among them, ^{129}I generates strong interest and concern, mainly because of its very long radioactive half-life (1.57×10^7 years) and radiological effects on human health and the environment. The major approaches for iodine vapour removal are wet scrubbing and physical adsorption. While considering different adsorbents, adsorption by using porous polymers is considered one of the efficient methods for the effective capture and reliable storage of radioactive iodine due to its remarkable advantages, such as simplicity, low operating cost, and speedy operation conditions. In this context, we attempted to use thiophene-containing monomers to develop a new class of porous sorbents with very good iodine capture properties. In light of previous studies, we expect that the electron-rich heteroatoms on the polymer network boost different types of interactions between the adsorbent and adsorbates which may lead to enhanced iodine capture irrespective of their low surface area [5]. Moreover, FeCl_3 -promoted oxidative coupling polymerization offers an advantage of facile, low-cost, and large-scale syntheses.

4.2. Results and discussion

4.2.1. Iodine capture

The porous character, remarkable stability, and electron-rich sites of as-synthesized polymeric samples prompted us to examine its adsorption properties for iodine. The adsorption capacity of iodine was calculated based on the sorption curves of the samples where iodine uptake (wt.%) was plotted as a function of time (Fig. 1).

During the iodine uptake, gravimetric measurements were performed at different time intervals, and the results showed that the mass of polymeric samples increased significantly with prolonged exposure time. The curve shows a steep increase of iodine uptake in the initial 3 h, while no significant weight gain of the sample was observed after 24 h, indicating that the system is saturated. The saturated iodine loading is 242 and 221 wt.% for PTCA and PTCM respectively, which are comparable to most of the reported porous adsorbents such as NiP-CMP (202 wt%) [6], PAF-23 (271 wt%), PAF-24 (276 wt%), and PAF-25 (260 wt%) [7], SCMPs (222 wt%) [8], SCMP-600@3 (204 wt%) [9], and so on. We also compared our adopted adsorption method and material with the existing wet scrubbing method. The wet scrubbing process shows the disadvantages of poor stability, complex operation procedures, and low capture performance, which is evident from the zeolitic imidazolate framework-8 [10] reported by Sava et.al (efficiency of 100 wt%) and Cu-BTC metal–organic framework [11] reported by the same group (efficiency of 175wt%). Hence adsorption is considered an effective method and porous polymers are considered competent materials for efficient volatile iodine capture. The considerable iodine

uptake may be due to the porous nature as well as due to the collective effect of electron-rich heteroatoms and π conjugated structures [12-14].

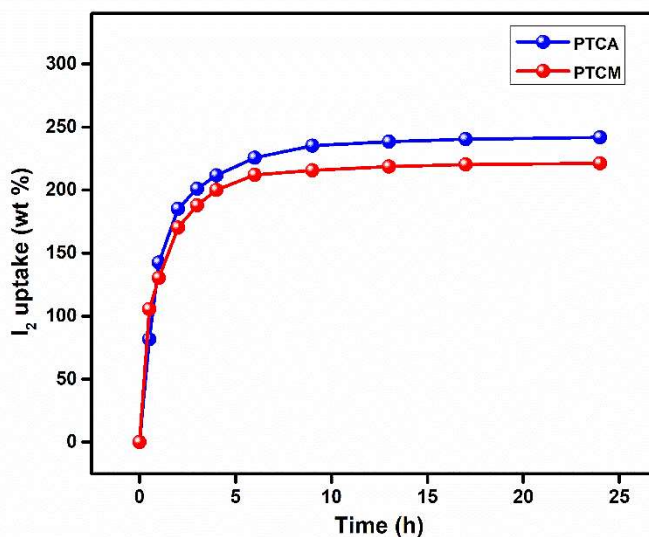


Fig. 1. Gravimetric uptake of iodine as a function of time at 77°C and ambient pressure.

4.2.2. Kinetics of iodine capture

The results obtained from the kinetic study (Fig. 2 and Table 1) suggest that the adsorption process of iodine onto the polymers fit well in the pseudo-second-order kinetic model, and a good linear correlation coefficient $R^2 > 0.99$ was achieved for both of the polymers. Further concluded that the pseudo-second-order kinetic model supports the assumption of the strong interaction, indicating that chemical adsorption may be the main process in these adsorbents [15]. Furthermore, the

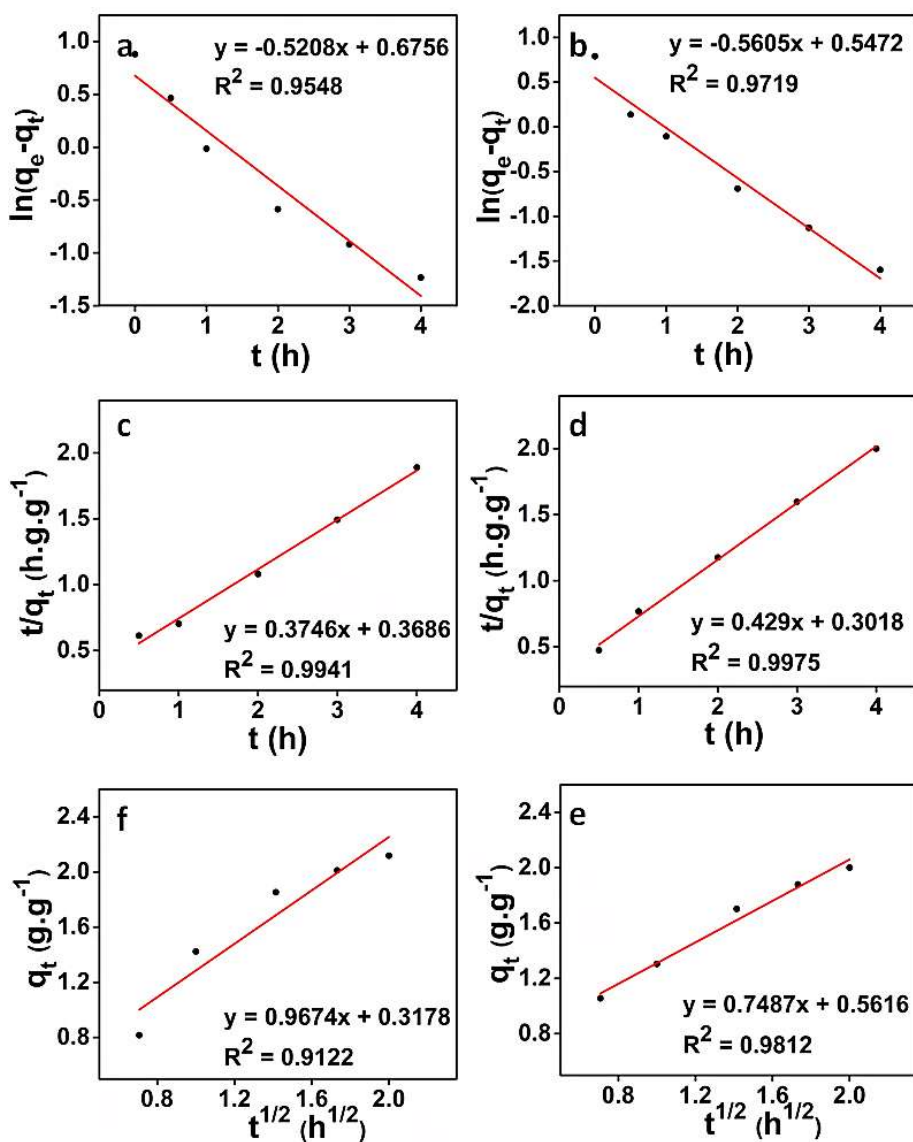


Fig. 2. (a,b) Pseudo-first-order, (c,d) pseudo-second-order, and (e,f) intraparticle diffusion model plots for the iodine uptake by the polymer PTCA and PTCM respectively.

Table 1. Kinetic parameters for iodine vapour uptake into the polymers PTCA and PTCM.

PTCA									
q_e (exp)	Pseudo-first order			Pseudo-second order			Intraparticle diffusion		
	q_e	k_1	R^2	q_e	k_2	R^2	k_{int}	C	R^2
	(g g ⁻¹)	(h ⁻¹)		(g g ⁻¹)	(g g ⁻¹ h ⁻¹)		(gg ⁻¹ h ^{-1/2})	(g g ⁻¹)	
2.418 (g g ⁻¹)	1.965	0.5208	0.9548	2.669	0.3813	0.9941	0.9674	0.3178	0.9122
PTCM									
q_e (exp)	Pseudo-first order			Pseudo-second order			Intraparticle diffusion		
	q_e	k_1	R^2	q_e	k_2	R^2	k_{int}	C	R^2
	(g g ⁻¹)	(h ⁻¹)		(g g ⁻¹)	(g g ⁻¹ h ⁻¹)		(gg ⁻¹ h ^{-1/2})	(g g ⁻¹)	
2.222 (g g ⁻¹)	1.728	0.5605	0.9719	2.331	0.610	0.9975	0.7487	0.5616	0.9812

maximum iodine uptake (2.669 g g^{-1} for PTCA and 2.331 g g^{-1} for PTCM) obtained from the pseudo-second-order kinetic model is in good agreement with the maximum iodine uptake (2.418 g g^{-1} for PTCA and 2.222 g g^{-1} for PTCM) obtained from the experimental data.

4.2.3. Mechanism of Iodine capture

The interactions expected to exist between the iodine and the synthesized polymers could be studied by employing, XRD, TGA, UV - Vis, FT-IR, XPS, and Raman spectroscopy. FT-IR spectrum (Fig. 3) shows that compared with polymers, the peak corresponds to C-S-C stretching vibration, and C-S deformation was almost absent in iodine-loaded polymers which indicates the involvement of thiophene ring in the iodine capture process [15]. A shift in C=O stretching vibration frequency observed in the iodine-loaded polymers PTCAI and PTCMI (1637 to 1634 cm^{-1} for PTCAI and 1657 to 1631 cm^{-1} for PTCMI) compared to that of the pure polymers indicates the possibility of strong interaction between the C=O group and iodine molecules during the capture process.

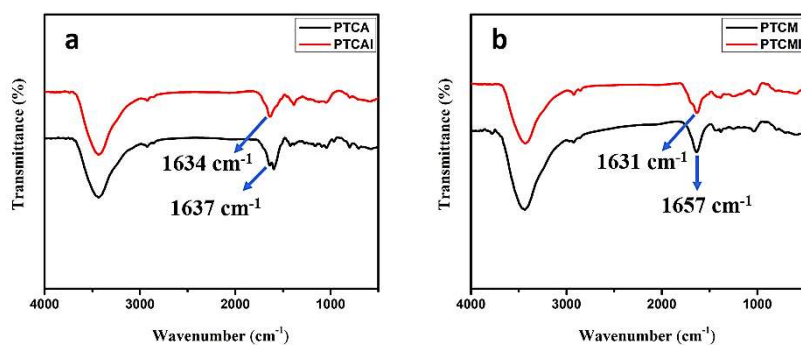


Fig. 3. FT-IR spectra of (a) PTCA and PTCAI (b) PTCM and PTCMI.

UV-DRS spectra (Fig. 4) indicate that the iodine-loaded polymers show a band broadening around 760 nm, indicating that the adsorbed iodine may exist as iodine molecules [16]. For the I₂-loaded polymeric samples, the TGA curve (Fig. 5a) shows an obvious mass loss from 90 to 400°C (I₂ subl. = 184°C), where the mass loss associated with surface desorption occurs at 90–170°C, and a further loss range at 170–400°C

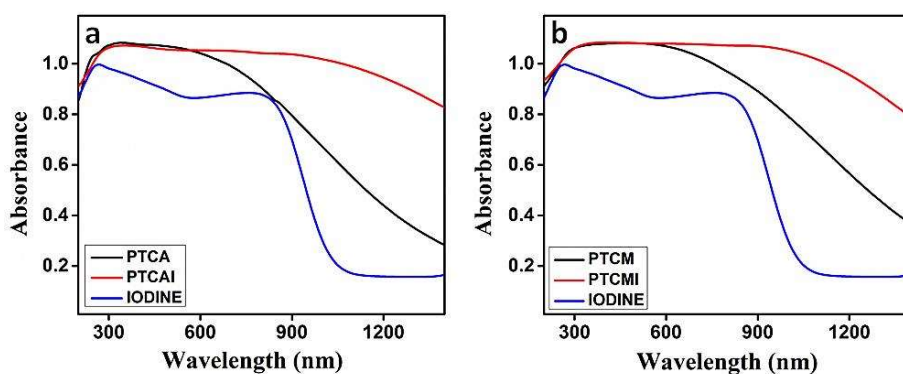


Fig. 4. UV-DRS spectra of (a) iodine, PTCA, and PTCAI and (b) iodine, PTCM, and PTCMI.

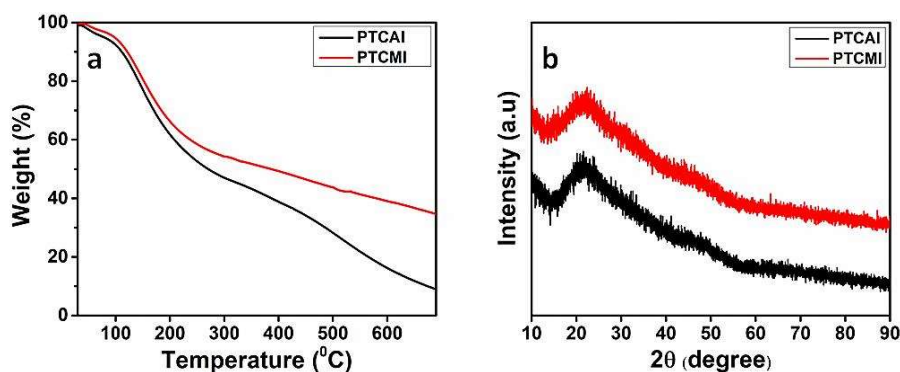


Fig. 5. (a) TGA curves and (b) XRD Patterns of the iodine-loaded polymers PTCAI and PTCMI.

was associated with the release of iodine being adsorbed inside the pores [7]. Weight loss after 400°C is due to the decomposition of polymers. Powder XRD measurements (Fig. 5b) show no obvious crystal diffraction peaks, so the iodine-loaded PTCA and PTCM are essentially amorphous.

The existence and form of the iodine captured by the polymers were also revealed by XPS and Raman spectroscopic analyses [17]. The XPS survey spectra (Fig. 6) of the iodine-loaded polymers show an extra peak near 617 and 629 eV corresponding to I 3d electrons, which indicates the adsorption of iodine onto the polymers.

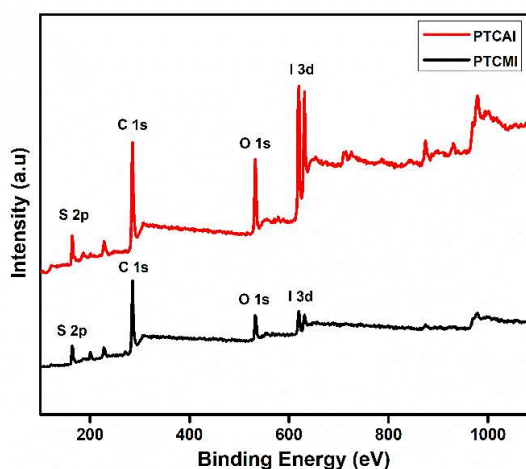


Fig. 6. XPS survey spectra of iodine-loaded polymers PTCAI and PTCMI.

Furthermore, the weight percentage of elements obtained from the XPS analysis of iodine-loaded polymers (Table 2) again confirms the successful adsorption of iodine. The deconvoluted I 3d XPS spectra indicate that iodine adsorbed on the surface of the polymers PTCA

coexists as neutral I_2 (632.2 and 620.4 eV), I_3^- (627.7 and 616.1 eV), and I_5^- (629.3 and 617.7 eV) respectively (Fig. 7a). Similarly the iodine adsorbed on the polymer PTCM also coexist as neutral I_2 (631.4 and 618.3 eV), I_3^- (627.3 and 615.7 eV) and I_5^- (629.0 and 617.3 eV) respectively (Fig. 7b) [18]. These results reveal that physisorption along with chemisorption plays a major role in the iodine adsorption process. The thiophene unit is expected to be involved in the physisorption process and the carbonyl group is expected to be involved in the chemisorption process.

Table 2. The weight percentage of elements obtained from the XPS analysis.

Iodine-loaded polymers	Weight %				
	C	O	S	Fe	I
PTCAI	35.08	13.49	13.85	0.66	36.93
PTCMI	56.38	12.62	15.38	-	15.63

The structure of the trapped iodine inside the polymeric pores was further confirmed by Raman spectroscopy. Raman spectrum of PTCA (Fig. 8a) shows three new peaks after iodine adsorption. The peaks at 181 cm^{-1} , 174 cm^{-1} and 142 cm^{-1} are attributed to the characteristic stretching vibration of I_2 , I_5^- and I_3^- respectively. The Raman spectra of PTCM (Fig. 8b) showed three new peaks at about 180, 168.6, and 139 cm^{-1} , also indicating the existence of I_2 , I_5^- and I_3^- respectively. The above studies demonstrate that iodine exists both as molecular iodine and polyiodide ions. Polyiodide anions are expected to be formed due to the charge transfer interaction between iodine guest molecules and

electron-rich polymeric heteroatoms [15], which is in agreement with the previous findings [17, 19, 20].

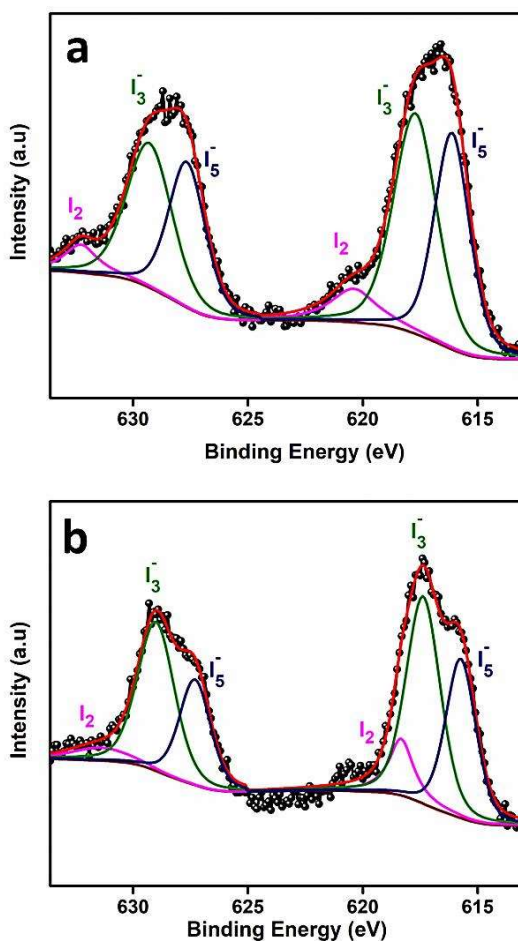


Fig. 7. Deconvoluted XPS spectra corresponding to the I 3d electrons of iodine-loaded polymer (a) PTCAI, and (b) PTCMI.

The Zeta potential values for the pure polymers were found to be 2.9 mV and 20.5 mV for PTCA and PTCM respectively. This positive value may be due to the acid doping taking place during the synthetic

procedure, where HCl is formed as a byproduct of the polymerization reaction. While the Zeta potential values for the iodine-loaded polymers are -2.04 mV and -12.4 mV for PTCAI and PTCMI respectively. Following the formation of negatively charged polyiodide anions by the charge transfer interaction, the positively charged polymeric structure may engage in electrostatic interaction to keep the polyiodide anions

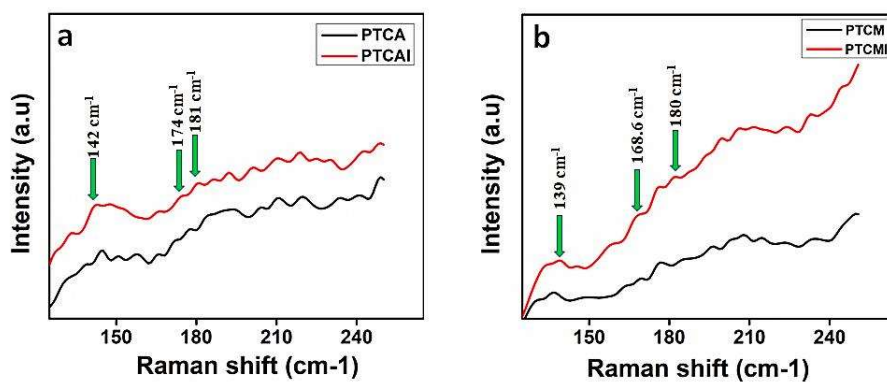


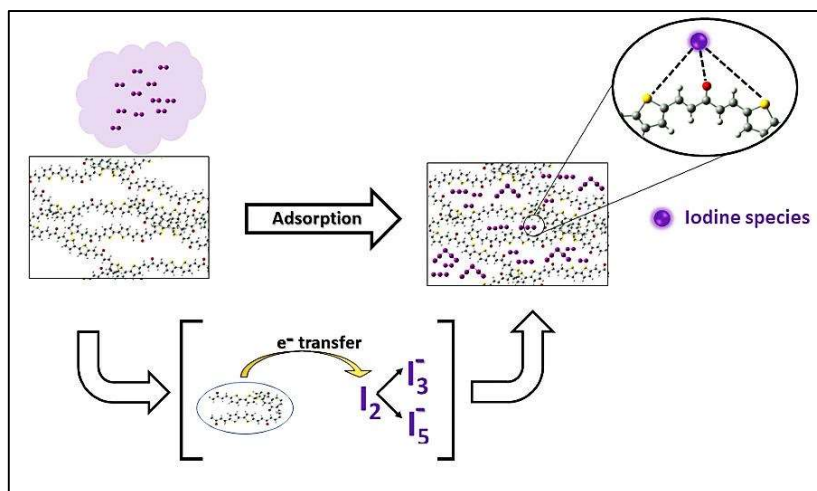
Fig. 8. Raman spectra of (a) PTCA and PTCAI (b) PTCM and PTCMI.

attached to the polymeric structure. These polyiodide anions adsorbed on the surface of the polymers are responsible for the negative zeta potential values of polymers after iodine capture. A pictorial representation of the iodine capture mechanism is given in Scheme 1.

4.2.4. Iodine release and recyclability

When the iodine-loaded polymers were heated in the air under ambient pressure and at 398 K for 360 min, iodine release efficiency was as high as 89% and 93% for PTCA and PTCM respectively (Fig. 9a). Cyclic experiments were performed as per the procedure reported in chapter 2.

As shown in Fig. 9b, the I_2 uptake capacity of recovered PTCA and PTCM was found to be 89.2% and 86.5% upon completion of the five



Scheme 1. Mechanism of iodine capture by the polymers.

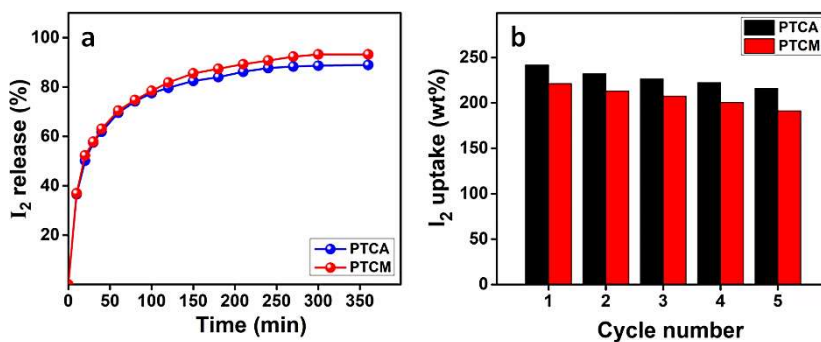


Fig. 9. (a) Release of iodine from the iodine-loaded polymers PTCAI and PTCMI at 398 K. (b) Reusability of the polymers PTCA and PTCM for iodine adsorption.

cycles. The polymers can be competently recycled and reused for five cycles without significant loss of iodine uptake [6, 19]. The iodine

released at 125°C was the iodine adsorbed on the surface or in the mesopores of the material, and the iodine captured deeply in the micropores could only be released when the framework collapsed at over 300°C. Based on the release studies, only about 11% and 7% of the adsorbed iodine was trapped in the micropores of PTCA and PTCM respectively [20].

4.3. Conclusions

In summary, we have designed and synthesized two novel mesoporous polymers PTCA and PTCM via FeCl₃-promoted oxidative coupling polymerization of thiophene-based bis-chalcone type monomers MTCA and MTCM. The designed polymers are highly promising in the field of iodine capture owing to their high thermal and chemical stability, and the presence of mesopores and electron-rich heteroatoms. PTCA exhibited a maximum iodine capture capacity of 242 wt% and PTCM exhibited a maximum iodine capture capacity of 221 wt%, and the experimental maximum capture capacity is in good agreement with the theoretical value (2.669 g g⁻¹ for PTCA and 2.331 g g⁻¹ for PTCM) calculated from the pseudo-second-order kinetic model. The XPS and Raman studies demonstrated that the iodine exists both as molecular iodine and polyiodide ions in the polymeric samples. The recyclability test shows that both the polymers are suitable for reuse even after five cycles with a retention of iodine uptake efficiency of 89.2% and 86.5% for PTCA and PTCM respectively. Also, we suggest that these polymers may also open up opportunities for the template-free design of the same kind of novel porous polymers with desired porosity and

functionalities by modifying the structures and composition of monomers.

References

- [1] R.C. Ewing, F.N. von Hippel, Nuclear waste management in the United States—Starting over, *Science*, 325(2009) 151-2.
- [2] E. Kintisch, Congress tells DOE to take fresh look at recycling spent reactor fuel, *Science*, 310(2005) 1406-.
- [3] N.R. Soelberg, T.G. Garn, M.R. Greenhalgh, J.D. Law, R. Jubin, D.M. Strachan, et al., Radioactive iodine and krypton control for nuclear fuel reprocessing facilities, *Science and Technology of Nuclear Installations*, 2013(2013).
- [4] J.D. Vienna, Nuclear waste vitrification in the United States: recent developments and future options, *International Journal of Applied Glass Science*, 1(2010) 309-21.
- [5] Y. He, Q. Liu, F. Liu, C. Huang, C. Peng, Q. Yang, et al., Porous organic polymer bifunctionalized with triazine and thiophene groups as a novel adsorbent for removing Cu (II), *Microporous and Mesoporous Materials*, 233(2016) 10-5.
- [6] A. Sigen, Y. Zhang, Z. Li, H. Xia, M. Xue, X. Liu, et al., Highly efficient and reversible iodine capture using a metalloporphyrin-based conjugated microporous polymer, *Chemical Communications*, 50(2014) 8495-8.
- [7] Z. Yan, Y. Yuan, Y. Tian, D. Zhang, G. Zhu, Highly efficient enrichment of volatile iodine by charged porous aromatic frameworks with three sorption sites, *Angewandte Chemie*, 127(2015) 12924-8.
- [8] X. Qian, Z.-Q. Zhu, H.-X. Sun, F. Ren, P. Mu, W. Liang, et al., Capture and reversible storage of volatile iodine by novel conjugated microporous polymers containing thiophene units, *ACS Applied Materials & Interfaces*, 8(2016) 21063-9.
- [9] M. Liu, C. Yao, C. Liu, Y. Xu, Thiophene-based porous organic networks for volatile iodine capture and effectively detection of mercury ion, *Scientific reports*, 8(2018) 1-8.
- [10] D.F. Sava, M.A. Rodriguez, K.W. Chapman, P.J. Chupas, J.A. Greathouse, P.S. Crozier, et al., Capture of Volatile Iodine, a Gaseous Fission

Product, by Zeolitic Imidazolate Framework-8, *Journal of the American Chemical Society*, 133(2011) 12398-401.

[11] D.F. Sava, K.W. Chapman, M.A. Rodriguez, J.A. Greathouse, P.S. Crozier, H. Zhao, et al., Competitive I₂ Sorption by Cu-BTC from Humid Gas Streams, *Chemistry of Materials*, 25(2013) 2591-6.

[12] S. Chang, K. Wang, Y. Li, J. Wang, X. Song, Z. Zhang, et al., A novel three-dimensionally ordered macroporous aerogel for capturing radioactive gaseous iodine, *Ceramics International*, 48(2022) 35310-6.

[13] B.J. Riley, J.D. Vienna, D.M. Strachan, J.S. McCloy, J.L. Jerden, Materials and processes for the effective capture and immobilization of radioiodine: A review, *Journal of Nuclear Materials*, 470(2016) 307-26.

[14] L. Puppe, J. Wilhelm, Process for removal of iodine and iodine compounds from gases and vapours with silver containing zeolite X, Patent Number EP332964 A, 3(1989) 1989.

[15] K. Su, W. Wang, B. Li, D. Yuan, Azo-bridged calix [4] resorcinarene-based porous organic frameworks with highly efficient enrichment of volatile iodine, *ACS Sustainable Chemistry & Engineering*, 6(2018) 17402-9.

[16] T. Geng, L. Ma, G. Chen, C. Zhang, W. Zhang, H. Xia, et al., Poly [1, 3, 6, 8-tetra (2-thiophenyl) pyrene] and poly [1, 3, 6, 8-tetra (3-thiophenyl) pyrene] conjugated microporous polymers for reversible adsorbing and fluorescent sensing iodine, *Journal of Polymer Research*, 26(2019) 1-10.

[17] X. Li, G. Chen, H. Xu, Q. Jia, Task-specific synthesis of cost-effective electron-rich thiophene-based hypercrosslinked polymer with perylene for efficient iodine capture, *Separation and Purification Technology*, 228(2019) 115739.

[18] D. Shetty, J. Raya, D.S. Han, Z. Asfari, J.-C. Olsen, A. Trabolsi, Lithiated polycalix [4] arenes for efficient adsorption of iodine from solution and vapor phases, *Chemistry of Materials*, 29(2017) 8968-72.

[19] Y. Wang, J. Tao, S. Xiong, P. Lu, J. Tang, J. He, et al., Ferrocene-based porous organic polymers for high-affinity iodine capture, *Chemical Engineering Journal*, 380(2020) 122420.

[20] M. Xu, T. Wang, L. Zhou, D. Hua, Fluorescent conjugated mesoporous polymers with N, N-diethylpropylamine for the efficient capture and real-time detection of volatile iodine, *Journal of Materials Chemistry A*, 8(2020) 1966-74.



Contents lists available at ScienceDirect

Journal of Hazardous Materials Advances

journal homepage: www.elsevier.com/locate/hazadv

Design and synthesis of thiophene containing bis-chalcone-based mesoporous polymers for volatile iodine capture

P. Sowmya, Linda Williams, Sivakrishna Prakash, Abraham Joseph*

Department of Chemistry, University of Calicut, Calicut University P O, 673 635, Kerala, India



ARTICLE INFO

Keywords:
Mesoporous polymers
Oxidative coupling
Iodine capture
Bis-chalcone-based polymers

ABSTRACT

Two novel thiophene-containing bis-chalcone-based polymers poly [(1E,4E)-1,5-Di-2-thienylpenta-1,4-dien-3-one] (PTCA) and poly[(1E,4E)-2,4-dimethyl-1,5-di(thiophen-2-yl)penta-1,4-dien-3-one] (PTCM) were designed and synthesized by FeCl₃ mediated oxidative coupling polymerization reaction. The formation of polymers was confirmed by FT-IR and UV-DRS analysis, and the structural and morphological characterizations were done by PXRD, SEM, TEM, TGA, CHNS, and BET analysis techniques. Owing to their mesoporous nature, and excellent thermal and chemical stability, they found significant applications in the field of environmental remediation. Regardless of their low surface area, they emerged as strong candidates for the iodine capture process due to the presence of electron-rich heteroatoms. The maximum iodine capture capacity obtained for PTCA and PTCM were 242 and 221 wt.% respectively. The kinetic study revealed that the adsorption of iodine onto the polymers fit well in the pseudo-second-order kinetic model with a correlation coefficient $R^2 > 0.99$, pointing to the chemisorptive nature of adsorption. The polymers can be competently recycled and reused even after five cycles without a significant loss of iodine uptake. After the first cycle, the iodine release efficiency was as high as 89% and 93% for PTCA and PTCM respectively. The iodine uptake capacity of the reused polymers PTCA and PTCM was found to be 89.2% and 86.5% respectively after five successive cycles. And these materials offer the benefits of facile, low-cost, large-scale, and template-free synthesis of mesoporous polymers. This study also provides an opportunity for the design same kind of polymers with different heteroatoms and functional groups.

1. Introduction

Since fossil fuels are non-renewable, there is a great demand for developing an alternative source to meet the necessary energy requirements for the future without the emission of greenhouse gases. Although nuclear energy is considered an efficient alternative source, the main safety concern related to nuclear energy is the appropriate management of nuclear wastes (¹²⁹I, ¹²⁷Xe, ⁸⁵Kr, etc) generated from nuclear reactions (Ewing and von Hippel, 2009, Kintisch, 2005, Soelberg et al., 2013, Vienna, 2010). Among them, ¹²⁹I generates strong interest and concern, mainly because of its very long radioactive half-life (1.57×10^7 years) and radiological effects on human health and the environment. The major approaches for iodine vapor removal are wet scrubbing and physical adsorption. Among them, adsorption by using porous materials was considered as one of the efficient methods for the effective capture and reliable storage of radioactive iodine due to its remarkable advantages, such as simplicity, low operating cost, and speedy operation conditions. Compared to those porous adsorbents such as natural or synthetic metal-exchanged zeolites (Sava et al., 2011, Li et al., 2016, Chapman et al., 2010, Subrahmanyam et al., 2015), and metal-organic

frameworks (MOFs) (Sava et al., 2013, Kitagawa et al., 2013, Zeng et al., 2010, Falaise et al., 2013, Zhang et al., 2017, Li et al., 2017), porous organic polymers (POPs) have been proven to be one of the promising candidates for efficient capture and storage of volatile iodine (Sigen et al., 2014, Yan et al., 2015).

In particular, POPs have generated greater interest due to their superiority including tunable porosity and functionality, higher loading capacity, lower overall cost, tremendous specific surface area, multiple preparation methods, robust thermal and chemical stability, and so on. Owing to their excellent physicochemical properties, they are highly promising in the field of gas storage (Cousins and Zhang, 2019, Song et al., 2013, Li et al., 2017, Bhanja et al., 2019), catalysis (Wang et al., 2020, Xu et al., 2018, Zhang and Riduan, 2012, Kramer et al., 2018, Tao et al., 2020), energy storage (Liu et al., 2020, Bandyopadhyay et al., 2018, Kang and Son, 2021), supercapacitors (Liu et al., 2013, Liu et al., 2022, Mohamed et al., 2020, Li et al., 2018), water treatment (Aguila et al., 2017, Ravi et al., 2020, Zhang et al., 2021, Shen et al., 2018), iodine capture (Xie et al., 2019, Pan et al., 2020, Xiong et al., 2019, Li et al., 2020), etc. Along with POPs, several organic polymers with mesoporous and macroporous proper-

* Corresponding author.

E-mail address: abrahamjoseph@uoc.ac.in (A. Joseph).

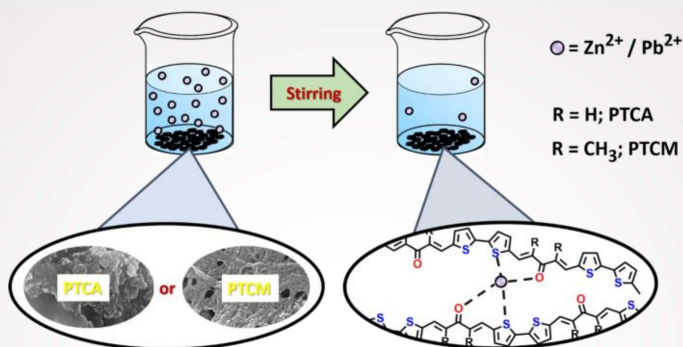
<https://doi.org/10.1016/j.hazadv.2023.100272>

Received 12 January 2023; Received in revised form 16 February 2023; Accepted 2 March 2023

2772-4166/© 2023 The Author(s). Published by Elsevier B.V. This is an open access article under the CC BY-NC-ND license (<http://creativecommons.org/licenses/by-nc-nd/4.0/>)

Chapter 5

Thiophene containing bis-chalcone-based mesoporous polymers for heavy metal ion removal



The polymers PTCA and PTCM were tested for the adsorption of heavy metal ions from aqueous solutions and found to be promising in the effective removal of Zn²⁺ and Pb²⁺ ions. The maximum adsorption capacity of the polymer PTCA for Zn²⁺ and Pb²⁺ was calculated as 729.4 mg/g and 569.1 mg/g respectively, and the maximum adsorption capacity of the polymer PTCM for Zn²⁺ and Pb²⁺ was calculated as 652.7 mg/g and 545.1 mg/g respectively.

- 5.1. Introduction
- 5.2. Results and discussion
 - 5.2.1. Adsorption of heavy metal ions
 - 5.2.2. Adsorption mechanism
 - 5.2.3. Adsorption isotherm
 - 5.2.4. Kinetics of metal ion adsorption
 - 5.2.5. Desorption and reusability study
 - 5.2.6. Computational study
- 5.3. Conclusions

5.1. Introduction

The removal of toxic metal ions from industrial run-offs has acquired great interest due to their long-standing harmful effects on human health and the environment [1, 2]. Thus, it is necessary to develop new methods and materials for removing such contaminants by effective means. Several conventional methods such as solvent extraction [3], membrane separation [4], ion exchange [5], reverse osmosis [6], precipitation [7], and electrolysis [8], etc have been applied for the removal of metal ions from wastewater. However, adsorption by porous solid adsorbents is considered one of the most cost-effective, simple, and competent methods among all of the aforesaid methods. Here in this chapter, we mainly test the potentiality of two porous polymeric sorbents (PTCA and PTCM) in the field of heavy metal ion adsorption. Based on previous reports, we assume that the synthesized polymers may show excellent metal adsorption properties due to the presence of electron-rich heteroatoms such as O and S [9, 10].

5.2. Results and discussion

5.2.1. Adsorption of heavy metal ions

Considering the porous nature and high content of heteroatoms, we investigated the adsorption efficiency of synthesized polymers towards the heavy metal ions. Co^{2+} , Cu^{2+} , Ni^{2+} , Cd^{2+} , Zn^{2+} , and Pb^{2+} were selected to examine the adsorption behaviors in this study. As shown in Fig. 1a, Fig. 1b, and Table 1, the single-heavy metal ion adsorption experiment reveals that both the polymers PTCA and PTCM show high removal efficiency towards Zn^{2+} (greater than 99%), and Pb^{2+} (greater

than 97%) ions with a distribution coefficient (K_d) value $> 10^4$. Since the distribution coefficient signifies the affinity of polymers towards the metal ions and also the sorbents with K_d value $> 10^4$ are regarded as exceptional sorbents [11], the polymers synthesized by us can be considered as exceptional sorbents for the removal of Zn^{2+} and Pb^{2+} ions.

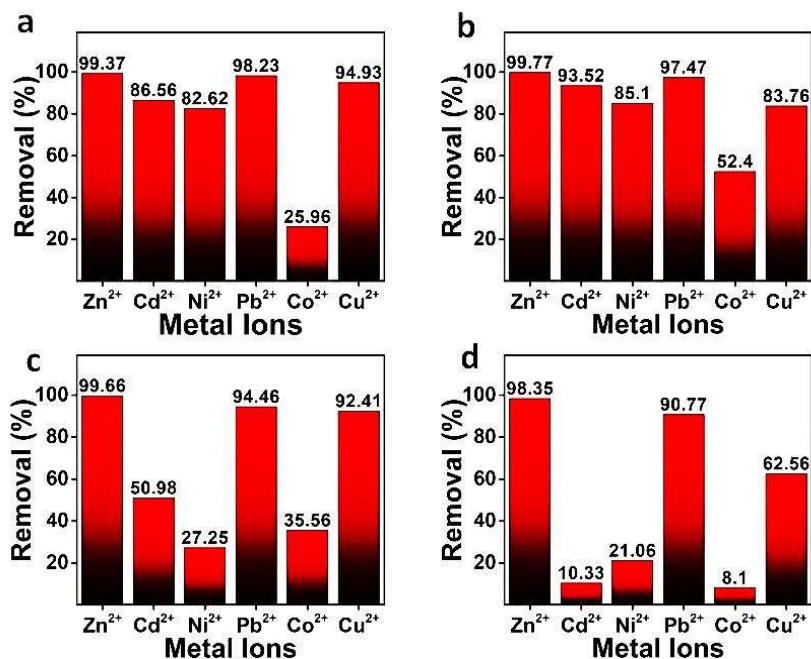


Fig. 1. (a,b) Removal efficiency of six individual metal ions (Co^{2+} , Cu^{2+} , Ni^{2+} , Cd^{2+} , Zn^{2+} , and Pb^{2+}) by PTCA and PTCM respectively. (c,d) The removal efficiency of six mixed metal ion systems (Co^{2+} , Cu^{2+} , Ni^{2+} , Cd^{2+} , Zn^{2+} , and Pb^{2+}) by PTCA and PTCM respectively.

Next, all of the six ions were mixed to conduct a mixed-heavy metal ion adsorption experiment and the results are summarized in Fig. 1c, Fig. 1d, and Table 2. The results show that the synthesized polymers show

greater affinity towards Zn^{2+} (greater than 98%), and Pb^{2+} (greater than 90%) than other metal ions [11].

Table 1. Adsorption results of PTCA and PTCM toward six individual metal ions (10 ppm).

M_{n+}	C_0 (ppm)	C_e (ppm)	Removal (%)	K_d (mL/g)
PTCA				
Zn^{2+}	10	0.063	99.4	1.5×10^5
Cd^{2+}	10	1.345	86.6	6437.7
Ni^{2+}	10	1.738	82.6	4752.3
Pb^{2+}	10	0.177	98.2	5.5×10^4
Co^{2+}	10	7.404	26.0	350.6
Cu^{2+}	10	0.507	94.9	1.8×10^4
PTCM				
Zn^{2+}	10	0.024	99.8	4.2×10^5
Cd^{2+}	10	0.648	93.5	1.4×10^4
Ni^{2+}	10	1.491	85.1	5709.2
Pb^{2+}	10	0.253	97.5	3.8×10^4
Co^{2+}	10	4.760	52.4	1100.7
Cu^{2+}	10	1.626	83.7	5152.0

$m = 0.010$ g, $V = 10$ mL, $V:m = 1000$ mL/g, 24 h contact time.

Table 2. Adsorption results of PTCA and PTCM toward six mixed ion systems (10 ppm).

M_{n+}	C_0 (ppm)	C_e (ppm)	Removal (%)	K_d (mL/g)
PTCA				
Zn^{2+}	10	0.034	99.7	3.0×10^5
Cd^{2+}	10	4.902	51.0	1039.8
Ni^{2+}	10	7.276	27.2	374.5
Pb^{2+}	10	0.554	94.5	1.7×10^4
Co^{2+}	10	6.447	35.5	551.2
Cu^{2+}	10	0.759	92.4	1.2×10^4
PTCM				
Zn^{2+}	10	0.165	98.3	6.0×10^4
Cd^{2+}	10	8.967	10.3	115.2
Ni^{2+}	10	7.894	21.1	266.8
Pb^{2+}	10	0.923	90.8	9831.9
Co^{2+}	10	9.190	8.1	88.1
Cu^{2+}	10	3.745	62.6	1670.5

$m = 0.010$ g, $V = 10$ mL, $V:m = 1000$ mL/g, 24 h contact time.

The greater affinity of the polymers toward Zn^{2+} , and Pb^{2+} are mainly due to the following reasons. Firstly, the mesoporous structure of polymers ensures the easy diffusion of metal ions into the polymeric pores, and secondly, the high content of electron-rich heteroatoms (O

and S) helps the polymers to bind with metal ions through coordination or electrostatic interaction [12].

5.2.2. Adsorption mechanism

To understand the possible mechanism of adsorption of metal ions onto the polymers, FTIR spectra of the polymers before and after the adsorption were recorded. For PTCA, as shown in Fig. 2, the peak at 1637 cm^{-1} , ascribed to the C=O bond stretching was found to be shifted to 1635 cm^{-1} after the adsorption of heavy metal ions. The small shift of 2 cm^{-1} could be due to the combined effect of two factors- first, the coordination of the carbonyl group to the metal ion which reduces the C=O stretching frequencies, and second, the electron density shift to the carbonyl group via an enhanced mesomeric effect by the coordination between the oxygen atom and metal center which increases the C=O stretching frequencies. These two effects nearly nullify the change in C=O stretching frequencies. The peak at 1597 cm^{-1} attributed to C=C stretching of α , β - unsaturated ketone was found to be shifted to 1594 cm^{-1} , and the peak at 1423 cm^{-1} which corresponds to C=C stretching of thiophene was shifted to around 1418 cm^{-1} after the adsorption of heavy metal ions. The shift to a lower wavenumber value arises due to the partial single-bond character acquired by the electron delocalization during the interaction. The peak at 1118 cm^{-1} ascribed to the C-S-C stretching vibration of the thiophene unit was shifted to around 1124 cm^{-1} , which attributes to the partial double bond character of the C-S bond arises by the enhanced delocalization of the lone pair of electrons on the S atom of the thiophene moiety during the adsorption of metal ions. All of the above shreds of evidence point to the possibility of

electron delocalization and coordination interaction between the carbonyl group and metal ions [13, 14].

For PTCM, as shown in Fig. 3, the peak at 1657 cm^{-1} , which is ascribed to stretching of the C=O bond found to be shifted to 1651 cm^{-1} after the adsorption of heavy metal ions. Again, the shift of 6 cm^{-1} could be due to the combined effect of two factors- first, the coordination of the carbonyl group to the metal ion which reduces the C=O stretching frequencies, and second, the electron density shift to the carbonyl group via an enhanced mesomeric effect by the coordination between the oxygen atom and metal center which increases C=O stretching frequencies. But this mesomeric effect is not predominant as in PTCA due to the steric hindrance of methyl substituents. A peak that appeared around 1617 cm^{-1} attributed to C=C stretching of α , β - unsaturated ketone was shifted to around 1614 cm^{-1} and the peak at 1439 cm^{-1} which corresponds to C=C stretching of thiophene was shifted to 1434 cm^{-1} after the adsorption of heavy metal ions. The peak at 1049 cm^{-1} attributed to the stretching frequency of the skeleton of the thiophene ring also shows a shift to a lower wavenumber around 1037 cm^{-1} after adsorption. The peak at 1116 cm^{-1} ascribed to the C-S-C stretching vibration of the thiophene moiety appeared around 1120 cm^{-1} after interaction between PTCM and metal ions. The reasons for the shift to lower wavenumbers and higher wavenumbers are the same as explained above. The pieces of evidence indicate the involvement of the carbonyl group in the metal adsorption process [15]. The bands appear at a lower frequency range of around $420\text{--}670\text{ cm}^{-1}$ for both the polymers and are assigned to M(II)-O stretching frequencies [16].

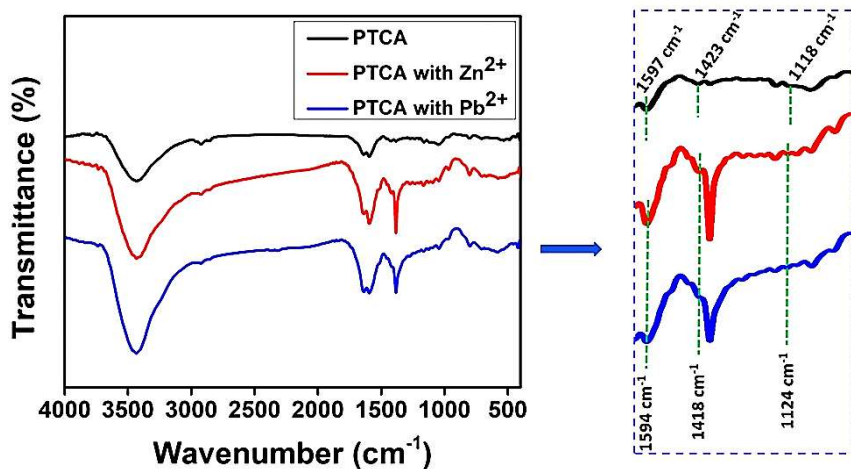


Fig. 2. FTIR spectra of PTCA (black) and PTCA loaded with Zn²⁺ (red), and Pb²⁺ (blue) ions.

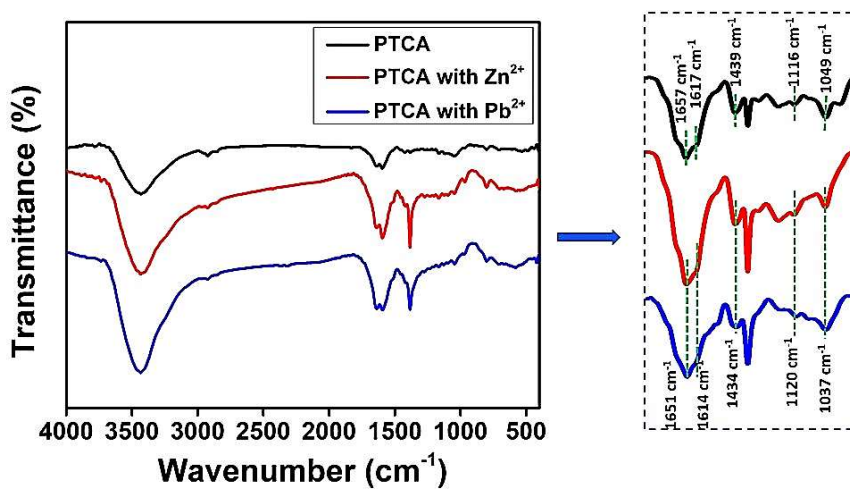


Fig. 3. FTIR spectra of PTCM (black) and PTCM loaded with Zn²⁺ (red), and Pb²⁺ (blue) ions.

From FTIR analysis we found that the adsorption of both metal ions on PTCA results in almost the same shift to the characteristic IR

frequencies associated with the polymer before the adsorption of metal ions. So, we concluded that the adsorption of both metal ions on polymer PTCA follows the same mechanism. The same is true for the polymer PTCM also. So, to understand the mechanism in detail we performed XPS analysis on polymer PTCA before and after the adsorption of Zn^{2+} ions, and on PTCM before and after the adsorption of Pb^{2+} ions.

The XPS survey spectrum of PTCA after the adsorption of Zn^{2+} exhibits a strong signal peak of Zn 2p which confirms the successful adsorption of Zn^{2+} onto the polymer PTCA (Fig. 4a). After the adsorption of Zn^{2+} , the deconvoluted C 1s peaks of PTCA appeared at 284.5, 285.3, 286.5, and 288.4 eV corresponding to C=C, C-C, C-S, C=O respectively (Fig. 5a). A peak shift corresponding to C-S, and C=O was observed after adsorption, which indicates the possible interaction of thiophene moiety and the carbonyl group of PTCA with Zn^{2+} ions. The O 1s peak of PTCA (Fig. 5b) exhibited a shift to 531.5 eV from 531.6 eV after the adsorption of Zn^{2+} , illustrating the coordination of oxygen to Zn^{2+} ions [17]. After the adsorption of Zn^{2+} , the lone pair of oxygen coordinates with the metal resulting in increased electron density and decreased binding energy which is also evident from the theoretical calculations discussed in the coming section [18]. A new peak at 533.4 eV generated after Zn^{2+} adsorption could be related to the oxygen atom involved in the formation of new Zn-O bonds. Furthermore, the two characteristic peaks at 164.0 and 165.2 eV corresponding to S 2p_{3/2} and S 2p_{1/2} in the S 2p spectrum of PTCA (Fig. 5c) show an increase in the binding energy of 164.1 and 165.3 eV after the adsorption, which also

indicates the involvement of the thiophene in the adsorption process [13].

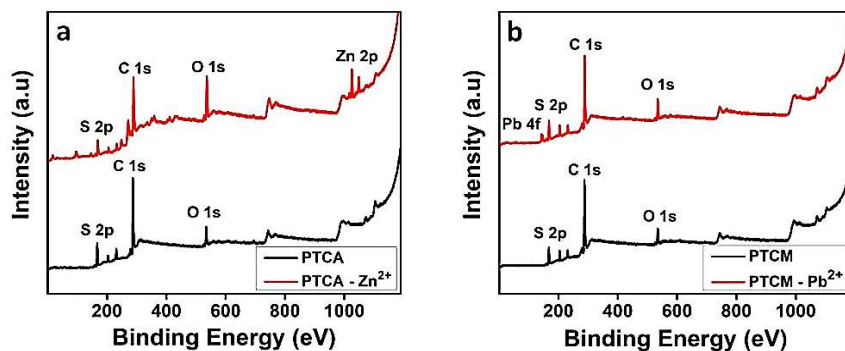


Fig. 4. XPS survey spectra of the polymer (a) PTCA before and after the adsorption of Zn²⁺ ions and (b) PTCM before and after the adsorption of Pb²⁺ ions.

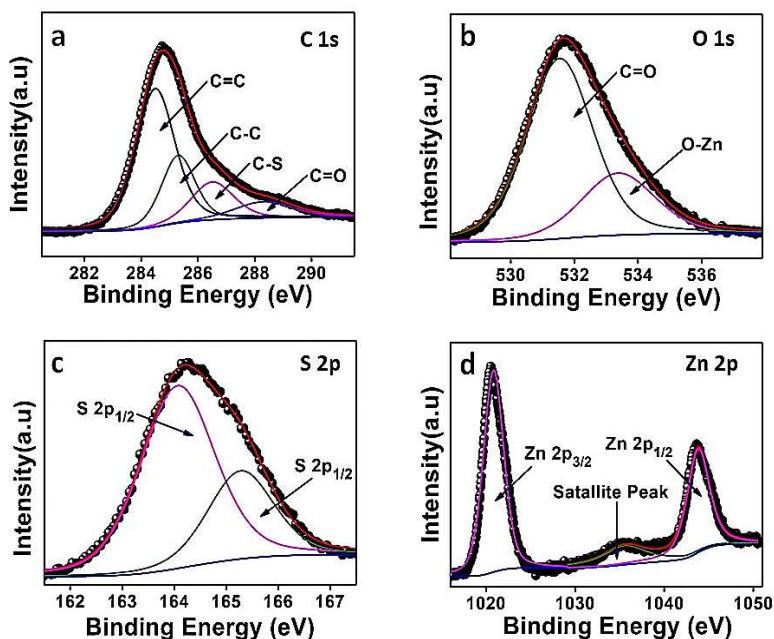


Fig. 5. (a) C 1s, (b) O 1s, and (c) S 2p XPS spectra of the polymer PTCA after the adsorption of Zn²⁺ ions. (d) XPS spectra of Zn 2p in the polymer.

As shown in Fig. 5d, the Zn 2p spectra of PTCA after the adsorption shows two main peaks at 1020.9 and 1043.9 eV corresponding to Zn 2p_{3/2} and Zn 2p_{1/2}, respectively, which are different from the Zn 2p peaks centered at 1022.2 and 1045.2 eV in the spectra of Zn(NO₃)₂. In addition, a satellite peak at 1035.8 eV was also found which may represent the change in the electron density of zinc ions after the adsorption.

Similarly, the survey spectrum of PTCM after the adsorption of Pb²⁺ ions exhibits a strong signal peak of Pb 4f which confirms the successful adsorption of Pb²⁺ onto the polymer PTCM (Fig. 4b). After the adsorption of Pb²⁺, the deconvoluted C 1s peaks of PTCM (Fig. 6a) appeared at 284.5, 285.0, 285.8, and 286.8 eV corresponding to C=C, C-C, C-S, C=O respectively. The shift of peak corresponds to C-S, and C=O indicates the possible interaction of thiophene moiety and the carbonyl group with Pb²⁺ ions. The O 1s peak of PTCM (Fig. 6b) exhibited a shift to 530.9 eV from 531.7 eV after the adsorption of Pb²⁺ illustrating the coordination of oxygen to Pb²⁺. After the adsorption of Pb²⁺, the lone pair of oxygen coordinates with the metal resulting in increased electron density and decreased binding energy. A new peak at 532.3 eV generated after Pb²⁺ adsorption could be related to the oxygen atom involved in the formation of new Pb-O bonds. Furthermore, the two characteristic peaks at 164.2 and 165.4 eV corresponding to S 2p_{3/2} and S 2p_{1/2} in the spectrum of S 2p of PTCM (Fig. 6c) show an increase in the binding energy of 164.6 and 165.8 eV after the adsorption of Pb²⁺, which also indicate the strong involvement of thiophene unit in the adsorption process. As shown in Fig. 6d, the spectra of Pb 4f in PTCM after the adsorption shows two peaks at 137.6 and 142.5 eV

corresponding to Pb 4f_{7/2} and Pb 4f_{5/2}, respectively, which are different from the Pb 4f peaks centered at 139.2 and 144.1 eV in the spectra of Pb (NO₃)₂ [19]. Therefore, we can conclude that the carbonyl and thiophene group of the polymers play a key role in the adsorption of metal ions from the aqueous solution.

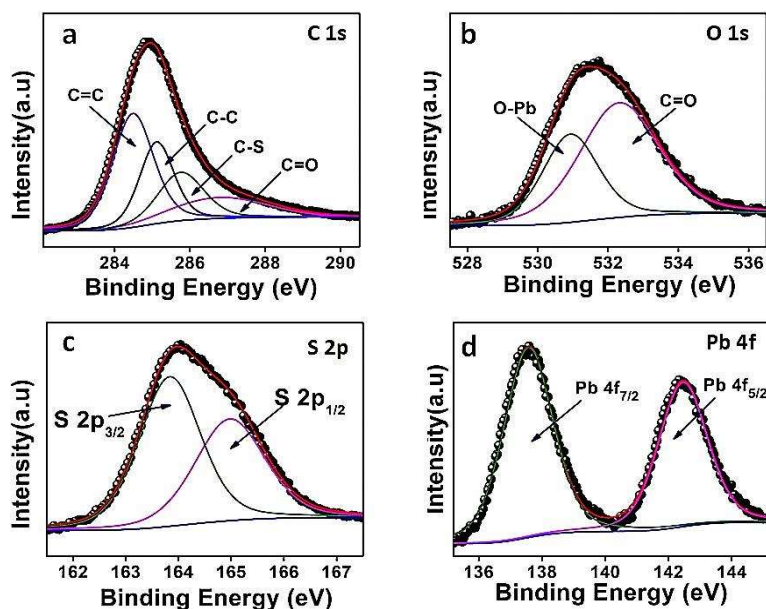


Fig. 6. (a) C 1s, (b) O 1s, and (c) S 2p XPS spectra of the polymer PTCM after the adsorption of Pb²⁺ ions. (d) XPS spectra of Pb 4f in the polymer.

5.2.3. Adsorption isotherm

The sorption study was conducted using a series of aqueous solutions of Zn²⁺ and Pb²⁺ with a concentration ranging from 20 to 1000 ppm. Fig. 7, Table 3, and Table 4 reveal that as the initial concentrations of metal ions increase, the amount of metal ions adsorbed onto the polymer increases, and becomes saturated. As indicated by the sorption isotherms, the maximum capacity of the polymer PTCA for Zn²⁺ and

Pb^{2+} was calculated as 729.4 mg/g and 569.1 mg/g respectively, and the maximum capacity of the polymer PTCM for Zn^{2+} and Pb^{2+} was calculated as 652.7 mg/g and 545.1 mg/g respectively.

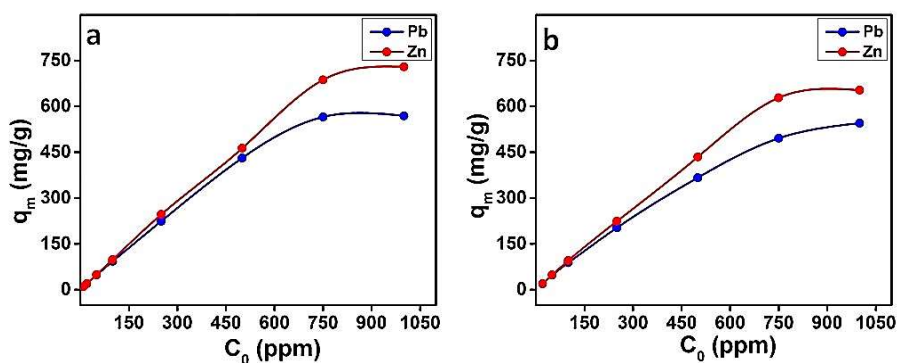


Fig. 7. Sorption isotherms for Zn^{2+} and Pb^{2+} for (a) PTCA and (b) PTCM.

As shown in Fig. 8, Fig. 9, and Table 5, the Langmuir and Freundlich models were used to analyze the experimental adsorption data. The fitting results exposed that the adsorption nature of Zn^{2+} and Pb^{2+} on PTCA fits well with the Langmuir isotherm model with a correlation coefficient $R^2 = 0.9957$ and $R^2 = 0.9939$ respectively. $R^2 = 0.9475$ and $R^2 = 0.9755$ are the correlation coefficient obtained from the Freundlich models for the adsorption of Zn^{2+} and Pb^{2+} respectively on PTCA. Since, the experimental data fits better with the Langmuir model, which indicates that the adsorption of metal ions on polymer PTCA mainly occurs through a monolayer adsorption process which may be due to the availability of a large number of adsorption sites on the surface of the polymer PTCA, and this homogenous adsorption points to negligible interaction between the adsorbed molecules [20]. Furthermore, the theoretical maximum adsorption capacities (Q_e) of the polymer PTCA

Table 3. Sorption isotherm data of PTCA towards Zn²⁺ and Pb²⁺ ions.

PTCA								
	Zn ²⁺				Pb ²⁺			
C ₀ (ppm)	C _e (ppm)	Removal (%)	K _d (mL/g)	Q _e (mg/g)	C _e (ppm)	Removal (%)	K _d (mL/g)	Q _e (mg/g)
20	0.110	99.5	1.8 x 10 ⁵	19.9	0.342	98.3	5.7 x 10 ⁴	19.7
50	0.359	99.3	1.4 x 10 ⁵	49.6	1.726	96.5	2.8 x 10 ⁴	48.3
100	1.322	98.7	7.5 x 10 ⁴	98.7	6.942	93.1	1.3 x 10 ⁴	93.1
250	3.716	98.5	6.6 x 10 ⁴	246.3	25.654	89.7	8745.2	224.3
500	37.058	92.6	1.2 x 10 ⁴	462.9	68.855	86.2	6261.6	431.1
750	63.263	91.6	1.1 x 10 ⁴	686.7	184.515	75.4	3064.7	565.5
1000	270.560	72.9	2696.0	729.4	430.875	56.9	1320.9	569.1

Table 4. Sorption isotherm data of PTCM towards Zn²⁺ and Pb²⁺ ions.

PTCM								
	Zn ²⁺				Pb ²⁺			
C ₀ (ppm)	C _e (ppm)	Removal (%)	K _d (mL/g)	Q _e (mg/g)	C _e (ppm)	Removal (%)	K _d (mL/g)	Q _e (mg/g)
20	0.199	99.0	9.9 x 10 ⁴	19.8	0.519	97.4	3.7 x 10 ⁴	19.5
50	1.242	97.5	3.9 x 10 ⁴	48.8	1.952	96.1	2.5 x 10 ⁴	48.0
100	4.696	95.3	2.0 x 10 ⁴	95.3	11.450	88.6	7734.0	88.6
250	26.126	89.5	8568.9	223.9	47.379	81.0	4276.6	202.6
500	65.498	86.9	6633.9	434.5	133.150	73.4	2755.2	366.9
750	121.760	83.8	5159.7	628.2	254.231	66.1	1950.1	495.8
1000	347.345	65.3	1879.0	652.7	454.945	54.5	1198.1	545.1

for the metal ions, Zn^{2+} and Pb^{2+} were calculated by the Langmuir adsorption model and found to be comparable with the experimental equilibrium adsorption capacities.

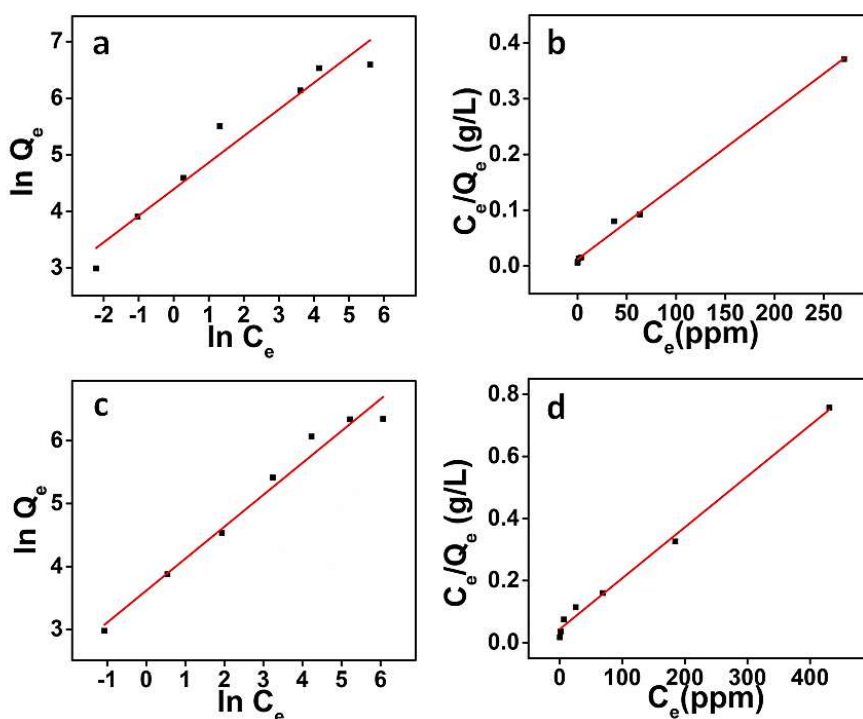


Fig. 8. (a,c) Freundlich adsorption isotherms of Zn^{2+} and Pb^{2+} respectively on PTCA. (b,d) Langmuir adsorption isotherms of Zn^{2+} and Pb^{2+} respectively on PTCA.

While the adsorption behavior of Zn^{2+} and Pb^{2+} on PTCM showed a better linear fitting with the Freundlich isotherm model with a correlation coefficient $R^2 = 0.9863$ and $R^2 = 0.9925$ respectively. $R^2 = 0.9824$ and $R^2 = 0.9721$ are the correlation coefficient obtained from the Langmuir models for the adsorption of Zn^{2+} and Pb^{2+} respectively on PTCM. A better linear fit with the Freundlich isotherm model is an

indication of multilayer adsorption occurring on the surface of the polymer PTCM, hence the occurrence of physisorption along with chemisorption. This may be due to the greater involvement of the thiophene group in the adsorption process of PTCM compared to PTCA, which is evident from XPS analysis [12].

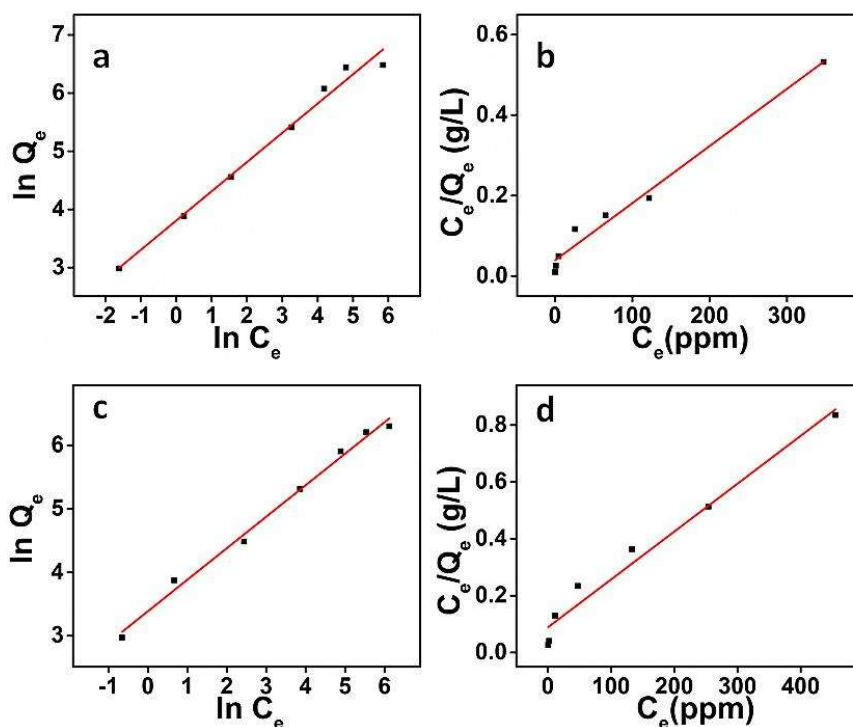


Fig. 9. (a,c) Freundlich adsorption isotherms of Zn²⁺ and Pb²⁺ respectively on PTCM. (b,d) Langmuir adsorption isotherms of Zn²⁺ and Pb²⁺ respectively on PTCM.

5.2.4. Kinetics of metal ion adsorption

The time dependence of the adsorption process was investigated by a kinetic adsorption experiment. The result (Fig. 10, Table 6, and Table 7) reveals that, as the contact time increases the adsorption increases,

reaches a maximum after a particular time, and then turns out to be almost saturated subsequently [20].

Table 5. Sorption isotherm data of PTCA and PTCM towards Zn^{2+} and Pb^{2+} ions.

PTCA						
Adsorbate	Langmuir			Freundlich		
	Q_m (mg/g)	K_L (L/mg)	R^2	K_F (L/mg)	n	R^2
Zn^{2+}	769.2	0.11	0.9957	117.82	2.12	0.9475
Pb^{2+}	625.0	0.04	0.9939	40.63	1.97	0.9755
PTCM						
Adsorbate	Langmuir			Freundlich		
	Q_m (mg/g)	K_L (L/mg)	R^2	K_F (L/mg)	n	R^2
Zn^{2+}	714.3	0.03	0.9824	45.62	1.99	0.9863
Pb^{2+}	588.2	0.02	0.9721	32.29	2.01	0.9925

The rate of adsorption of metal ions on PTCM was found to be slower than that of PTCA, especially for Pb^{2+} ions. Due to the steric hindrance offered by the methyl group of PTCM, the ions cannot easily approach the carbonyl group of PTCM as easily as approaching the carbonyl group of PTCA. So, PTCM shows a slower rate of adsorption compared to PTCA. Since the ionic radius of Zn^{2+} ions (74 pm) are less than that

of Pb^{2+} ions (119 ppm), Zn^{2+} ions can easily approach the carbonyl group compared to the Pb^{2+} ions, hence Zn^{2+} ions exhibit a faster rate of adsorption compared to Pb^{2+} ions.

Both the polymers PTCA and PTCM showed a fast removal $>95\%$, of Zn^{2+} within an initial 1h, and there is not much change in the removal efficiency afterwards. While both of the polymers exhibited a slow removing tendency towards Pb^{2+} ions, even though the percentage removal after 24h reaches 93.4% and 90.5% by PTCA and PTCM respectively. Owing to the excellent removal efficiency, these polymers can be considered a promising porous absorbent, especially for Zn^{2+} ions.

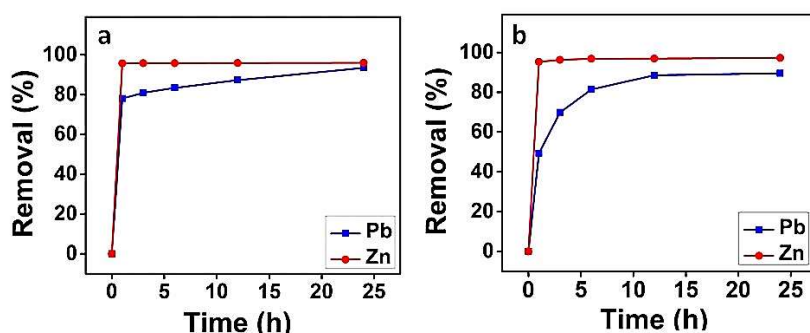


Fig. 10. Sorption kinetic curve of adsorption of metal ions on (a) PTCA (b) PTCM

To analyze the adsorption kinetics of metal ions onto the polymers, the adsorption data were fitted with three kinetic models pseudo-first-order kinetics, pseudo-second-order kinetics, and intraparticle diffusion model respectively (Fig. 11 and Fig. 12)[21]. The results (Table 8) suggest that the adsorption of metal ions to the polymers fits very well in the pseudo-second-order kinetic model with an extremely high correlation

coefficient $R^2 > 0.99$. This proposes that the rate of adsorption of metal ions on the polymers depends on the availability of adsorption sites on the polymeric adsorbents, and chemisorption may be the major process involved in the metal removal. Also, there is a good agreement exists between the experimental values of the amount of metal ions adsorbed at equilibrium and the values calculated from the pseudo-second-order kinetic model.

5.2.5. Desorption and reusability study

The desorption study was conducted as explained in Chapter 2. The study showed that the metal ions adsorbed onto the polymer PTCA could be desorbed by using 2M HCl with a maximum percentage recovery of Zn^{2+} and Pb^{2+} ions of 76.9% and 79.9% respectively. Similarly, for PTCM maximum percentage recovery of Zn^{2+} and Pb^{2+} ions was found to be 68.5% and 73.7% respectively. The elution effect of hydrochloric acid is responsible for high desorption productivity [18]. Moreover, in a strongly acidic solution, the sulfur atom and carboxyl group may lose their interaction with heavy metal ions which also makes the desorption of heavy metal ions an easy task [22].

The reusability of the polymers was tested by carrying out five consecutive adsorption-desorption cycles [23]. As the number of cycles increases both the polymers show a decrease in the removal efficiency towards Zn^{2+} and Pb^{2+} ions. As shown in Fig. 13, the % removal of PTCA and PTCM was found to be decreased to nearly 50% after five successive cycles.

Table 6. Kinetic data of PTCA towards Zn^{2+} and Pb^{2+} ions.

PTCA								
Time (h)	Zn^{2+}				Pb^{2+}			
	C_e (ppm)	Removal (%)	K_d (mL/g)	Q_e (mg/g)	C_e (ppm)	Removal (%)	K_d (mL/g)	Q_e (mg/g)
1	0.860	95.7	2.22×10^4	19.1	4.396	78.0	3549.7	15.6
3	0.855	95.7	2.24×10^4	19.1	3.826	80.9	4227.1	16.2
6	0.854	95.7	2.24×10^4	19.1	3.322	83.4	5021.2	16.7
12	0.832	95.8	2.30×10^4	19.2	2.553	87.2	6834.2	17.4
24	0.807	96.0	2.37×10^4	19.2	1.311	93.4	1.43×10^4	18.7

Table 7. Kinetic data of PTCM towards Zn^{2+} and Pb^{2+} ions.

PTCM								
	Zn^{2+}				Pb^{2+}			
Time (h)	C_e (ppm)	Removal (%)	K_d (mL/g)	Q_e (mg/g)	C_e (ppm)	Removal (%)	K_d (mL/g)	Q_e (mg/g)
1	0.940	95.3	2.03×10^4	19.1	10.148	49.3	970.8	9.9
3	0.747	96.3	2.58×10^4	19.3	6.049	69.8	2306.6	14.0
6	0.635	96.8	3.05×10^4	19.4	3.723	81.4	4372.2	16.3
12	0.616	96.9	3.15×10^4	19.4	2.306	88.5	7671.5	17.7
24	0.547	97.3	3.56×10^4	19.5	1.895	90.5	9551.9	18.1

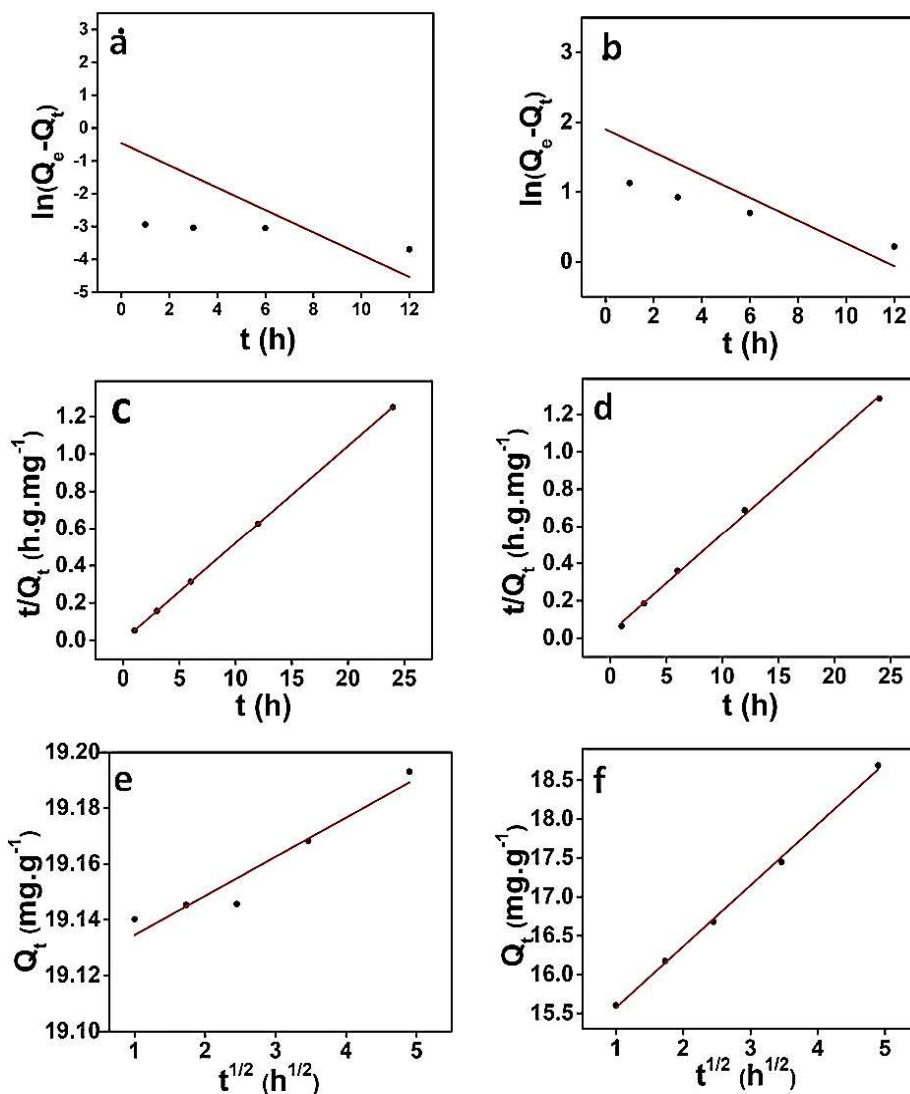


Fig. 11. (a,b) Pseudo-first-order, (c,d) pseudo-second-order, and (e,f) intraparticle diffusion model plots for the adsorption of Zn²⁺ and Pb²⁺ respectively on the polymers PTCA.

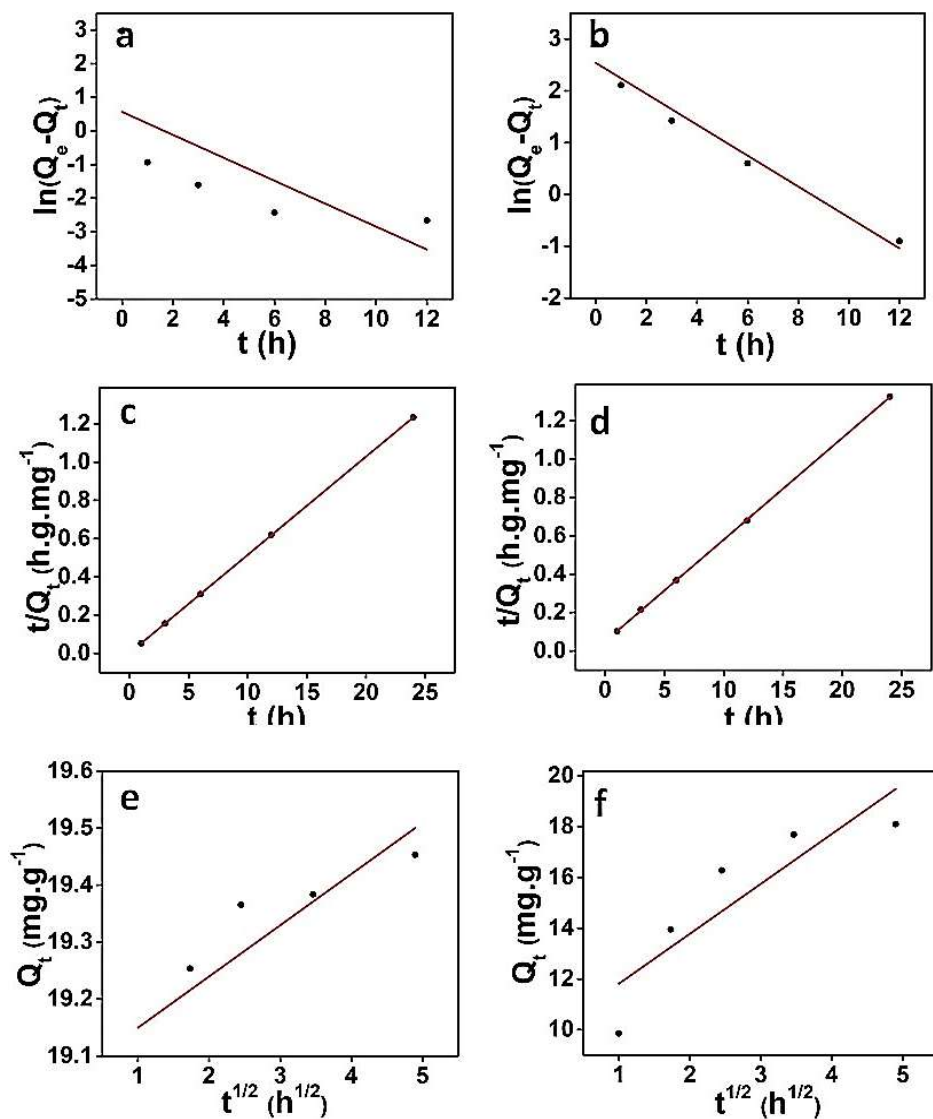


Fig. 12. (a,b) Pseudo-first-order, (c,d) pseudo-second-order, and (e,f) intraparticle diffusion model plots for the adsorption of Zn²⁺ and Pb²⁺ respectively on the polymers PTCM.

Table 8. Kinetic parameters for the adsorption of Zn^{2+} and Pb^{2+} ions on the polymers PTCA and PTCM.

PTCA									
Adsorbate	pseudo-first order			pseudo-second order			Intraparticle diffusion		
	Q_e (mg/g)	k_1 (h ⁻¹)	R^2	Q_e (mg/g)	k_2 (g/mg h)	R^2	k_{int} (mg g ⁻¹ h ^{-1/2})	C (mg/g)	R^2
Zn^{2+}	0.633	0.340	0.3537	19.194	5.429	1	0.014	19.120	0.9319
Pb^{2+}	6.670	0.164	0.5816	18.939	0.092	0.9987	0.786	14.790	0.9984
PTCM									
Adsorbate	pseudo-first order			pseudo-second order			Intraparticle diffusion		
	Q_e (mg/g)	k_1 (h ⁻¹)	R^2	Q_e (mg/g)	k_2 (g/mg h)	R^2	k_{int} (mg g ⁻¹ h ^{-1/2})	C (mg/g)	R^2
Zn^{2+}	1.760	0.341	0.5183	19.455	1.554	1	0.090	19.060	0.7975
Pb^{2+}	12.644	0.298	0.9724	18.868	0.056	0.9999	1.968	9.845	0.7842

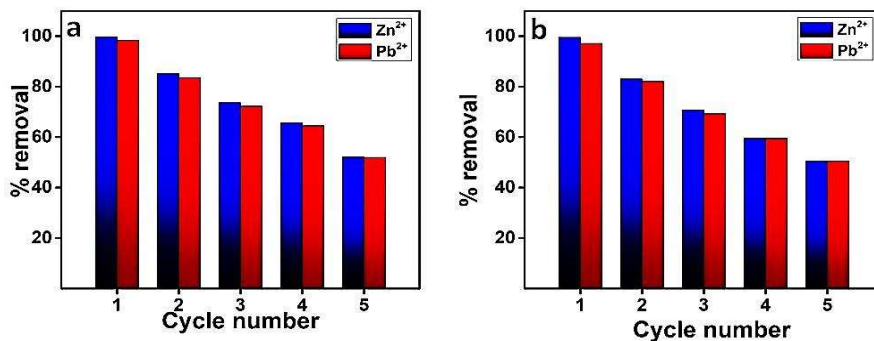


Fig. 13. Reusability of the polymer (a) PTCA and (b) PTCM during five adsorption-desorption cycles.

5.2.6. Computational study

Theoretical calculations were done on monomers and monomer metal ion complexes to support the proposed interaction between polymers and metal ions. The energy of HOMO, the energy of LUMO, the band gap, the energy of monomers, the energy of monomer-metal ion complexes, C-O bond length, metal ion-oxygen (M(II)-O) bond length, and Mulliken charges on the carbonyl carbon, oxygen atom, and metal ion were calculated, and are enlisted in Table 9.

The HOMO-LUMO orbital energies of monomers and monomer-metal ion complexes are shown in Fig. 14 and Fig. 15. The energy gap between HOMO and LUMO is known as the band gap, and it determines the reactivity of the molecule [24]. The molecule with a smaller band gap value was found to be more reactive than the one with a larger band gap [25]. Since the band gap of monomer MTCA is slightly smaller than that of monomer MTCM, the former is more reactive and the transfer of electrons from HOMO to LUMO occurs more easily in MTCA

compared to that of MTCM. This is responsible for the faster adsorption of heavy metal ions by the polymer PTCA compared to the polymer PTCM. The energy of monomer-metal complexes was found to be more negative than that of monomers, which indicates the formation of complexes during the interaction of monomer molecules and metal ions.

The stabilization energy of the MTCA-M(II) complex is less than that of the energy of the corresponding MTCM-M(II) complex which indicates less stable interaction formed between polymer PTCA and metal ions compared to the interaction between polymer PTCM and metal ions. This provides theoretical evidence for better desorption from PTCA compared to PTCM. On considering the bond length (Fig. 16 and Fig. 17), all C-C bond lengths fall in between characteristic C-C single bond length (1.54 Å) and C-C double bond length (1.34 Å) which points to complete electron delocalization existing in the polymeric structure. The Zn(II)-O bond lengths fall in the range of 1.882–1.898 Å and Pb(II)-O bond lengths fall in the range of 1.948–1.952 Å. Very short M(II)-O bond lengths obtained suggest strong covalent interaction between metal ions and monomer molecules [26]. The C-O bond length in monomer-metal complexes appeared between typical C-O single bond length (1.43 Å) and C-O double bond length (1.23 Å) which indicates the involvement of the carbonyl group in the interaction.

We can also support the results related to the reaction kinetics with the help of theoretical calculations. Due to the small size, the Zn²⁺ ions approach the carbonyl group more easily, hence they are closer to the polymer chain and experience more steric repulsion, and results in the

angular configuration of C-O-Zn bond (Fig. 16 and Fig. 17). Similarly, due to the large ionic radius of Pb^{2+} ions, it cannot approach the carbonyl group as easy as Zn^{2+} ions, thereby less close to the polymer chain, and experience less steric hindrance, hence linear C-O-Pb bond (Fig. 16 and Fig. 17). This bond angle data confirms the conclusions related to the easiness of the approach of metal ions toward the carbonyl group, and hence support the findings associated to the reaction kinetics. Mulliken charge analysis (Fig. 18 and Fig. 19) of monomers reveals the highest negative partial charge on the carbonyl carbon atoms, which may be due to the π accepting nature of carbonyl groups. During the adsorption of heavy metal cations, this charge is found to be shifted to carbonyl oxygen, and negative formal charges on carbonyl oxygen increase. This is responsible for an increase in the C=O stretching frequencies as mentioned in the adsorption mechanism section. At the same time, the formal charge of +2 on metal ions was found to be decreased nearly to 1 and 1.3 respectively for Zn^{2+} and Pb^{2+} ions upon coordination which is due to the charge transfer from the polymer molecules to the metal centers [26]. This is responsible for the decrease in the C=O stretching frequencies. ESP mapping (Fig. 20) also supports the above-mentioned findings. The charge density located on the carbonyl group of monomers was found to be shifted to metal ions, and the total electron density of the monomers was found to be decreased after the interaction with metal ions, which indicates the effective coordination between the carbonyl group and metal ions [21]. Hence the Mulliken charge analysis and ESP mapping support the IR data explaining the mechanism of adsorption of metal ions onto the polymers. Overall, the theoretical calculation outcomes are in good agreement with the experimental results.

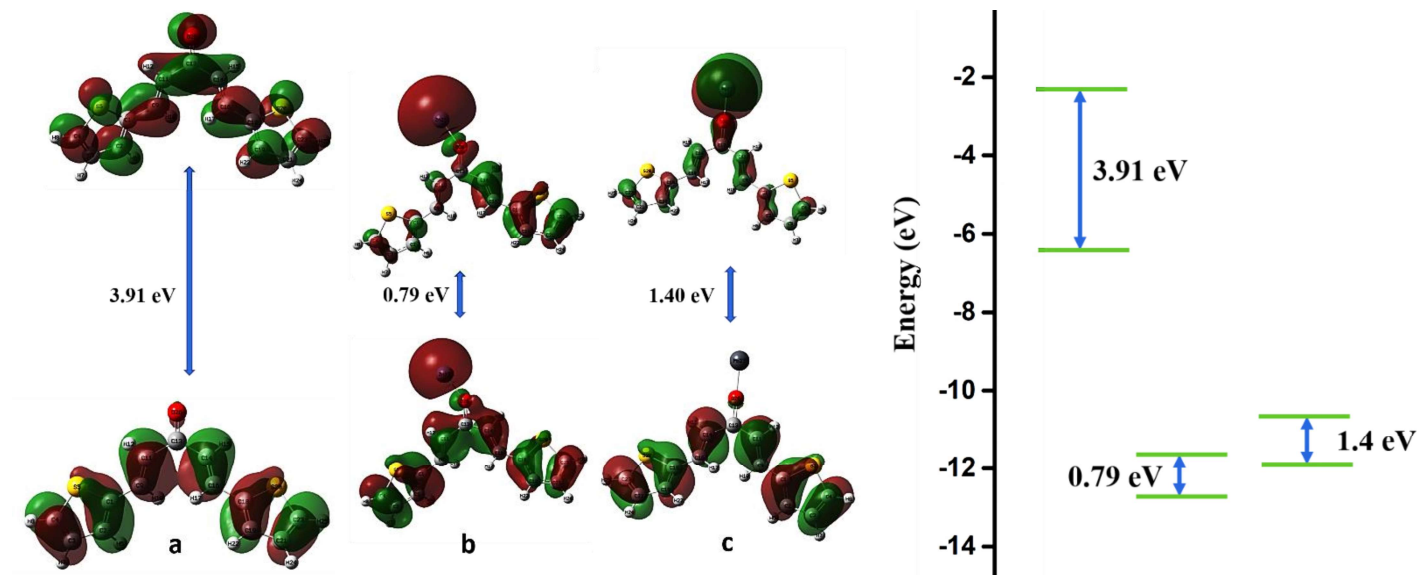


Fig. 14. The HOMO and LUMO frontier orbitals, and energies of the optimized geometric structures of (a) monomer MTCA and monomer-metal ion complexes (b) MTCA with Zn^{2+} and (c) MTCA with Pb^{2+} respectively.

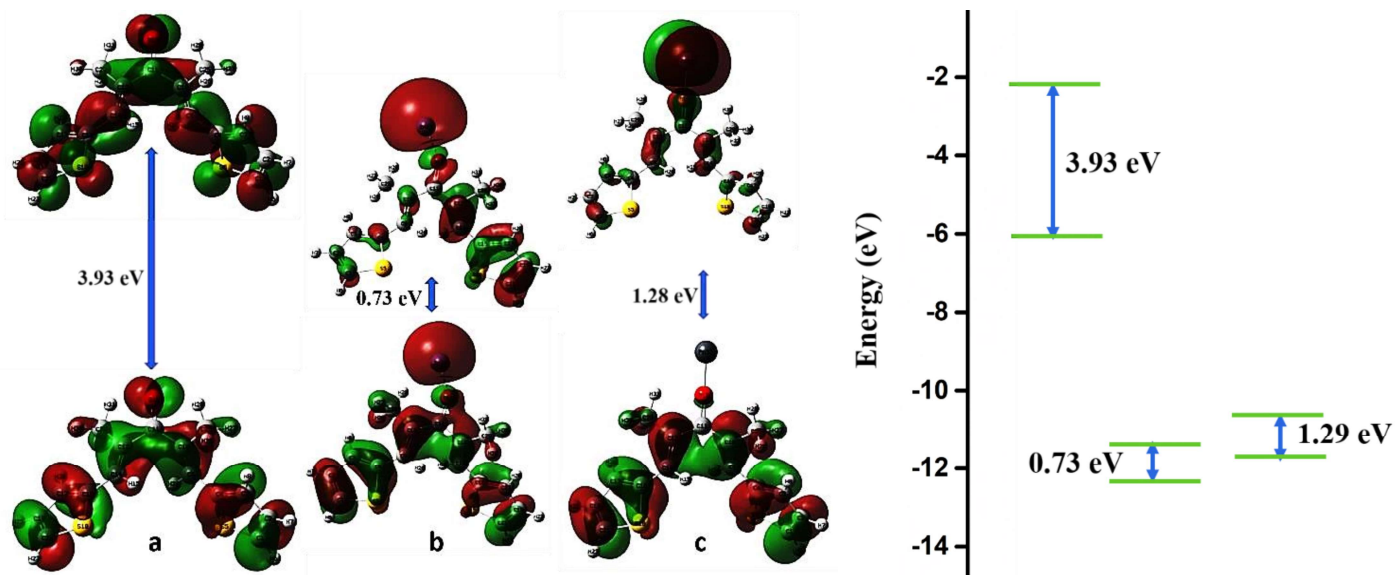


Fig. 15. The HOMO and LUMO frontier orbitals and energies of the optimized geometric structures of (a) monomer MTCM and monomer-metal ion complexes (b) MTCM with Zn²⁺ and (c) MTCM with Pb²⁺ respectively.

Table 9. Computed properties of monomers and monomer-metal ion complexes.

	MTCA	MTCA with Zn ²⁺	MTCA with Pb ²⁺	MTCM	MTCM with Zn ²⁺	MTCM with Pb ²⁺
E _{HOMO} (eV)	-6.43	-12.59	-12.03	-6.25	-12.37	-11.86
E _{LUMO} (eV)	-2.52	-11.80	-10.64	-2.32	-11.65	-10.58
Band gap ΔE (eV)	3.91	0.79	1.40	3.93	0.73	1.29
Stabilization energy (eV)	-37365.6	-39127	-37438.8	-39505.8	-41266.63	-39578.16
Bond length C=O (Å°)	1.23	1.35	1.39	1.23	1.35	1.38
Bond length M(II)-O (Å°)	-	1.882	1.948	-	1.898	1.952
Charge on carbonyl Carbon	-1.04	0.38	0.42	-1.36	0.30	0.38
Charge on Oxygen	-0.28	-0.71	-0.83	-0.25	-0.69	-0.82
Charge on metal ion	-	1.03	1.37	-	0.96	1.35

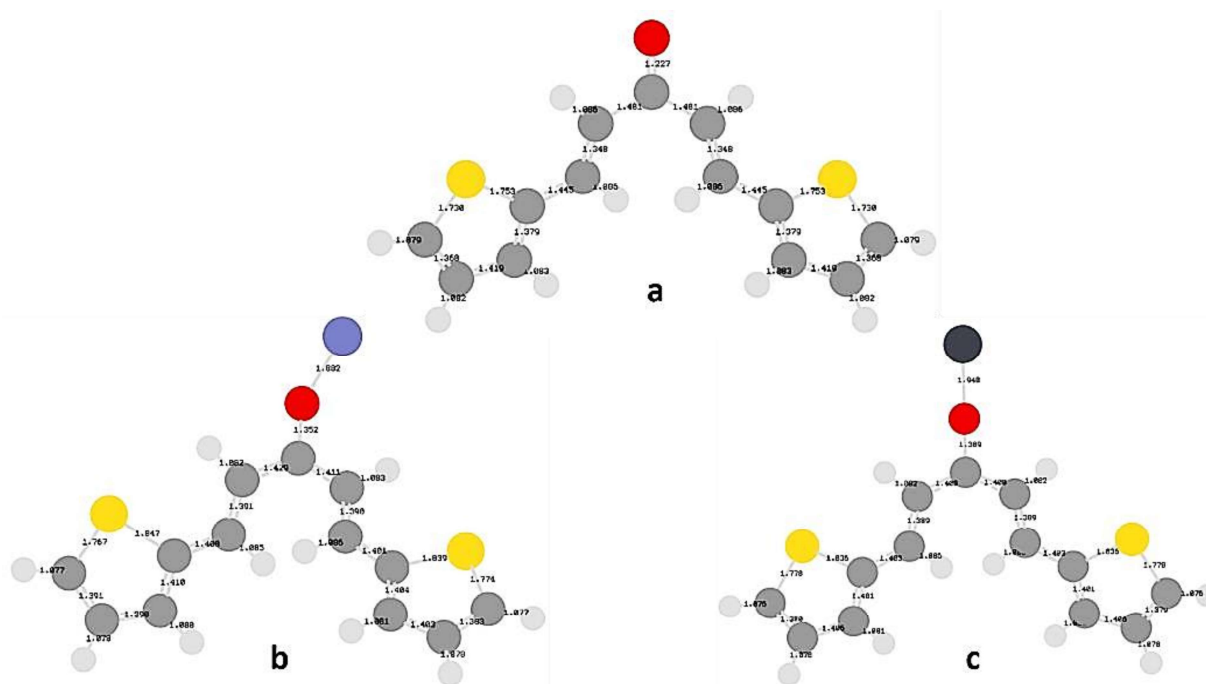


Fig. 16. The calculated bond lengths of optimized geometric structures of (a) monomer MTCA and monomer-metal ion complexes (b) MTCA with Zn²⁺ and (c) MTCA with Pb²⁺ respectively. (red - oxygen; gray - carbon; yellow - sulphur; white - hydrogen; purple-blue - zinc; dark gray - lead)

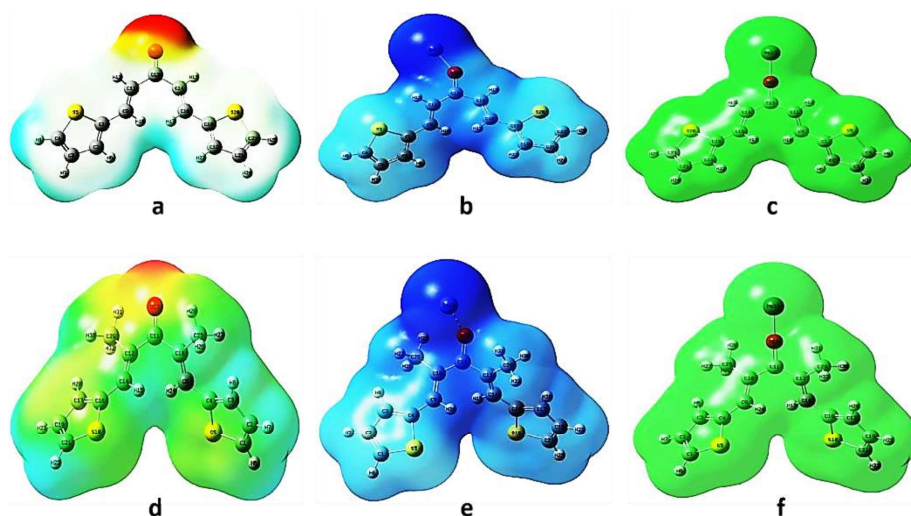


Fig. 20. The Electrostatic potential surface of optimized geometric structures of (a) monomer MTCAs and its metal ion complexes with (b) Zn^{2+} and (c) Pb^{2+} respectively; The Electrostatic potential surface of optimized geometric structures of (d) monomer MTCMs and its metal ion complexes with (e) Zn^{2+} and (f) Pb^{2+} respectively.

5.3. Conclusions

In summary, we have studied the applicability of two thiophene-based mesoporous polymers (PTCA and PTCM) as attractive adsorbents for heavy metal removal and retrieval. The mesoporous and heteroatom (O and S) comprised framework of the polymers improve the guest-host interaction and pay off for the low surface area of the polymers. The sorption study displays that the maximum adsorption capacity of the polymer PTCA for Zn^{2+} and Pb^{2+} was obtained as 729.4 mg/g and 569.1 mg/g respectively, and the maximum adsorption capacity of the polymer PTCM for Zn^{2+} and Pb^{2+} was obtained as 652.7 mg/g and 545.1 mg/g respectively. Also, there is a good agreement exists between the

experimental values of the maximum amount of metal ions adsorbed and the values calculated from the pseudo-second-order kinetic model. The desorption study proposes that the polymers are suitable to reuse in the water treatment process after acid washing. The theoretical study conducted is in good agreement with the experimental results.

References

- [1] V. Mudgal, N. Madaan, A. Mudgal, R. Singh, S. Mishra, Effect of toxic metals on human health, *The open Nutraceuticals journal*, 3(2010).
- [2] M.L. Sall, A.K.D. Diaw, D. Gningue-Sall, S. Efremova Aaron, J.-J. Aaron, Toxic heavy metals: impact on the environment and human health, and treatment with conducting organic polymers, a review, *Environmental Science and Pollution Research*, 27(2020) 29927-42.
- [3] N.T. Hung, M. Watanabe, T. Kimura, Solvent extraction of palladium (II) with various ketones from nitric acid medium, *Solvent Extraction and Ion Exchange*, 25(2007) 407-16.
- [4] C. Blöcher, J. Dorda, V. Mavrov, H. Chmiel, N. Lazaridis, K. Matis, Hybrid flotation—membrane filtration process for the removal of heavy metal ions from wastewater, *Water Research*, 37(2003) 4018-26.
- [5] A. Bashir, L.A. Malik, S. Ahad, T. Manzoor, M.A. Bhat, G. Dar, et al., Removal of heavy metal ions from aqueous system by ion-exchange and biosorption methods, *Environmental Chemistry Letters*, 17(2019) 729-54.
- [6] U. Ipek, Removal of Ni (II) and Zn (II) from an aqueous solution by reverse osmosis, *Desalination*, 174(2005) 161-9.
- [7] A. Pohl, Removal of heavy metal ions from water and wastewaters by sulfur-containing precipitation agents, *Water, Air, & Soil Pollution*, 231(2020) 1-17.
- [8] H.-C. Tao, T. Lei, G. Shi, X.-N. Sun, X.-Y. Wei, L.-J. Zhang, et al., Removal of heavy metals from fly ash leachate using combined bioelectrochemical systems and electrolysis, *Journal of Hazardous materials*, 264(2014) 1-7.
- [9] J. Chen, M. Yuan, W. Cai, J. Wei, J. Zhou, P. Liu, et al., Constructing the frustrated Lewis pairs within N, S-codoped carbon to reveal the role of

adjacent heteroatom sites for highly effective removal of heavy metal ions, *Chemical Engineering Journal*, 422(2021) 130153.

[10] S.Z.N. Ahmad, W.N.W. Salleh, A.F. Ismail, N. Yusof, M.Z.M. Yusop, F. Aziz, Adsorptive removal of heavy metal ions using graphene-based nanomaterials: Toxicity, roles of functional groups and mechanisms, *Chemosphere*, 248(2020) 126008.

[11] L. Feng, W.-M. Chen, J.-L. Li, G. Day, H. Drake, E. Joseph, et al., Biological antagonism inspired detoxification: removal of toxic elements by porous polymer networks, *ACS applied materials & interfaces*, 11(2019) 14383-90.

[12] Y. Wang, N. Yang, M. Soldatov, H. Liu, A novel phosphazene-based amine-functionalized porous polymer with high adsorption ability for I₂, dyes and heavy metal ions, *Reactive and Functional Polymers*, 173(2022) 105235.

[13] A. Modak, S. Das, D.K. Chanda, A. Samanta, S. Jana, Thiophene containing microporous and mesoporous nanoplates for separation of mercury from aqueous solution, *New Journal of Chemistry*, 43(2019) 3341-9.

[14] R. Peng, G. Chen, F. Zhou, R. Man, J. Huang, Catalyst-free synthesis of triazine-based porous organic polymers for Hg²⁺ adsorptive removal from aqueous solution, *Chemical Engineering Journal*, 371(2019) 260-6.

[15] C. Sulpizio, S.T. Müller, Q. Zhang, L. Brecker, A. Rompel, Synthesis, characterization, and antioxidant activity of Zn²⁺ and Cu²⁺ coordinated polyhydroxychalcone complexes, *Monatshefte für Chemie-Chemical Monthly*, 147(2016) 1871-81.

[16] M.J. Al-Jeboori, A.H. Al-Dujaili, A.E. Al-Janabi, Coordination of carbonyl oxygen in the complexes of polymeric N-crotonyl-2-hydroxyphenylazomethine, *Transition Metal Chemistry*, 34(2009) 109-13.

[17] Z. Chen, J. Zeng, Z.-B. Zhang, Z.-J. Zhang, S. Ma, C.-M. Tang, et al., Preparation and application of polyethyleneimine-modified corn cob magnetic gel for removal of Pb (ii) and Cu (ii) ions from aqueous solution, *RSC advances*, 12(2022) 1950-60.

[18] Q. Ge, H. Liu, Tunable amine-functionalized silsesquioxane-based hybrid networks for efficient removal of heavy metal ions and selective adsorption of anionic dyes, *Chemical Engineering Journal*, 428(2022) 131370.

[19] Q. Lian, Z.U. Ahmad, D.D. Gang, M.E. Zappi, D.L.B. Fortela, R. Hernandez, The effects of carbon disulfide driven functionalization on graphene oxide for enhanced Pb (II) adsorption: Investigation of adsorption mechanism, *Chemosphere*, 248(2020) 126078.

- [20] M. Maiti, M. Sarkar, M.A. Malik, S. Xu, Q. Li, S. Mandal, Iron oxide NPs facilitated a smart building composite for heavy-metal removal and dye degradation, *ACS omega*, 3(2018) 1081-9.
- [21] Y. He, Q. Liu, F. Liu, C. Huang, C. Peng, Q. Yang, et al., Porous organic polymer bifunctionalized with triazine and thiophene groups as a novel adsorbent for removing Cu (II), *Microporous and Mesoporous Materials*, 233(2016) 10-5.
- [22] J. Bayuo, M.A. Abukari, K.B. Pelig-Ba, Desorption of chromium (VI) and lead (II) ions and regeneration of the exhausted adsorbent, *Applied Water Science*, 10(2020) 1-6.
- [23] S. Xie, Z. Xu, C. Yu, X. Yu, Z. Zhang, J. Li, Highly Efficient Reduction of 4-Nitrophenol by Cu Nanoparticle Decorated Graphdiyne, *ChemistrySelect*, 6(2021) 13572-6.
- [24] H. Karaca, S. Kazancı, The metal sensing applications of chalcones: The synthesis, characterization and theoretical calculations, *Journal of Molecular Structure*, 1248(2022) 131454.
- [25] E.U. Mughal, R.J. Obaid, A. Sadiq, M.A. Alsharif, N. Naeem, S. Kausar, et al., Chalcone-and flavone-based novel terpyridine metal complexes: Synthesis, electrochemical, photophysical, photovoltaic and computational studies, *Dyes and Pigments*, 201(2022) 110248.
- [26] M. Malhotra, M. Puglia, A. Kalluri, D. Chowdhury, C.V. Kumar, Adsorption of metal ions on graphene sheet for applications in environmental sensing and wastewater treatment, *Sensors and Actuators Reports*, 4(2022) 100077.



Contents lists available at ScienceDirect

Journal of Solid State Chemistry

journal homepage: www.elsevier.com/locate/jssc

Adsorption of heavy metal ions by thiophene containing mesoporous polymers: An experimental and theoretical study



P. Sowmya, Sivakrishna Prakash, Abraham Joseph*

Department of Chemistry, University of Calicut, Calicut University, 673 635, Kerala, India

ARTICLE INFO

Keywords:
Thiophene
Mesoporous
Heavy metal
Adsorption

ABSTRACT

Two novel mesoporous polymers poly [(1E,4E)-1,5-Di-2-thienylpenta-1,4-dien-3-one] (PTCA) and poly[(1E,4E)-2,4-dimethyl-1,5-di(thiophen-2-yl)penta-1,4-dien-3-one] (PTCM) having electron-rich heteroatoms (O and S) have been designed and synthesized by oxidative coupling polymerization promoted by FeCl₃. Paid to their excellent physiochemical properties such as porous nature, thermal stability, chemical stability, tunable functionality, presence of electron-rich heteroatoms, etc., they are determined as a prominent candidate for heavy metal ion adsorption irrespective of their low surface area. Hence the synthesized polymers were tested for the adsorption of heavy metal ions from aqueous solutions and found to be promising in the effective removal of Zn²⁺ and Pb²⁺ ions. The maximum adsorption capacity of the polymer PTCA for Zn²⁺ and Pb²⁺ was calculated as 729.4 mg/g and 569.1 mg/g respectively, and the maximum adsorption capacity of the polymer PTCM for Zn²⁺ and Pb²⁺ was calculated as 652.7 mg/g and 545.1 mg/g respectively. The desorption study reveals that for PTCA the maximum percentage recovery of Zn²⁺ and Pb²⁺ ions was 76.9% and 79.9% respectively, and for PTCM the maximum percentage recovery of Zn²⁺ and Pb²⁺ ions was 68.5% and 73.7% respectively. The theoretical study was conducted to support the experimental results. Also, our materials generate a breakthrough in the field of simple, economic, and template-free development of the same type of novel polymers having different functionalities.

1. Introduction

The removal of toxic metal ions from industrial run-offs has acquired great interest due to their long-standing harmful effects on human health and the environment [1,2]. Thus, it is necessary to develop new methods and materials for removing such contaminants in an effective means. There are several conventional methods such as solvent extraction [3], membrane separation [4], ion exchange [5], reverse osmosis [6], precipitation [7], and electrolysis [8], etc have been applied for the removal of heavy metal ions from wastewater. However, adsorption by porous solid adsorbents is considered as one of the most cost-effective, simple, and competent methods among all of the aforesaid methods. Layered double hydroxides (LDHs) [9,10] and metal oxides (TiO₂, Fe₂O₃, Al₂O₃, etc) [11–13] are noticeable candidates among solid adsorbents. Even though they are cost-effective, low surface area and lack of porosity limit their adsorption capacities. At the same time, many adsorbents, such as porous resins [14,15], silicas [16,17], carbon materials (activated carbon, nanotubes, and their composites) [18–20], and metal-organic frameworks offer high surface area and high removal efficiency, but

they are generally expensive. So, materials with improved properties are more attractive. Along with these materials porous organic polymers (POPs) and several other organic polymers with mesoporous and macroporous nature have been widely used for the elimination of heavy metal ions [21–24] owing to their outstanding properties such as low cost, high specific surface area, modifiable porosity, and functionality, good thermal and chemical stability, etc. The efficiency of these adsorbents is not only determined by their porous nature and stability, but also by the functional sites enhancing specific host-guest interactions such as Hydrogen bonds, π - π interactions, electrostatic interactions, ion exchange interactions, coordination interactions, etc [25]. There are several reports on the incorporation of functional groups such as amine [24], carboxyl [26], and thiol [27] into porous adsorbents to enhance their adsorption capacity. Introducing heteroatoms into the adsorbents also increases the adsorption efficiency of solid sorbents [28]. For example, there are several reports on the performance of heteroatom-containing thiophene group as an efficient ligand for the removal of metal ions [29,30].

Here in this paper, we mainly test the potentiality of two novel porous

* Corresponding author.

E-mail address: abrahamjoseph@uoc.ac.in (A. Joseph).

<https://doi.org/10.1016/j.jssc.2023.123836>

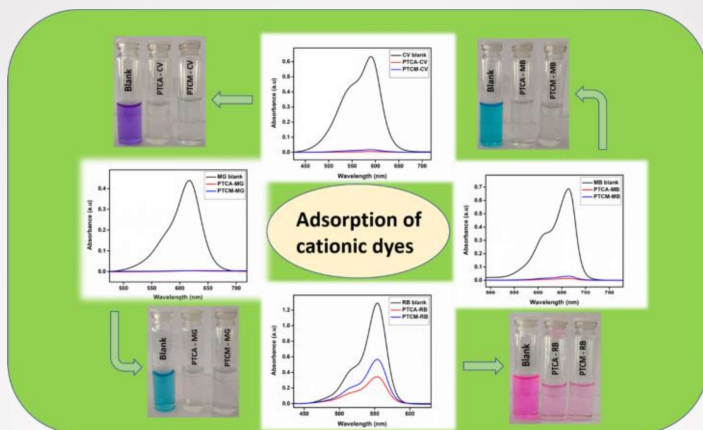
Received 9 November 2022; Received in revised form 31 December 2022; Accepted 7 January 2023

Available online 13 January 2023

0022-4596/© 2023 Elsevier Inc. All rights reserved.

Chapter 6

Thiophene containing bis-chalcone-based mesoporous polymers for the selective removal of cationic dyes



The polymers PTCA and PTCM show high removal efficiency towards cationic dyes compared to the anionic dyes. Since both of the polymers show the highest removal efficiency towards CV dye, it was chosen as a model cationic dye to study various factors affecting the adsorption process. The maximum adsorption capacity of CV obtained was 151.49 mg/g for PTCA and 142.28 mg/g for PTCM.

- 6.1. Introduction
- 6.2. Results and discussion
 - 6.2.1. Adsorption study
 - 6.2.2. Effect of adsorbent dosage
 - 6.2.3. Effect of pH
 - 6.2.4. Adsorption isotherms
 - 6.2.5. Adsorption kinetics
 - 6.2.6. Adsorption mechanism
 - 6.2.7. Selective adsorption
 - 6.2.8. Reusability studies
- 6.3. Conclusions

6.1. Introduction

Water pollution is a serious issue on a global scale and is caused by the enormous volume of effluents that industries discharge [1]. Among these effluents, organic dyes are one of the most considered contaminants due to their severe adverse effect on aquatic life and the environment [2]. Several industries such as food processing, cosmetics, paper, textile, leather, pharmaceutical, and printing sectors, employ a variety of dyes to colour their goods and release a large amount of dye-tainted water into nearby water bodies [3-7]. To protect public health, removing these harmful dyes from wastewater is crucial before releasing them into the environment [8]. Adsorption has drawn the most attention among various methods of dye removal because of its benefits, including high efficiency, high practicability, simple operational mode, and cost-effectiveness. The efficiency of the adsorption process depends on the nature of the adsorbent employed. Thus, in this study, we are focusing on two porous polymers having a great potential for dye removal. Since the cationic dyes cause more toxicity than the anionic dyes [9], it should be of utmost importance to get rid of these cationic dyes practically. The polymers used in this study are highly effective at removing cationic dyes like methylene blue, malachite green, and crystal violet. By using crystal violet as a model cationic dye in this study, various parameters that affect the adsorption of cationic dyes were thoroughly examined.

6.2. Results and discussion

6.2.1. Adsorption performance test

The UV–Vis spectra and the removal efficiency of a single dye solution (MB, MG, CV, RhB, MO, MR, and CR) before and after the adsorption are displayed in Fig. 1 and Fig. 2 respectively. The polymers were found to remove cationic dyes MB, MG, CV, and RhB more efficiently than anionic dyes, with removal efficiencies of 95.6%, 97.7%, 99.2%, and 73.3% for PTCA and 92.7%, 96.3%, 97.3%, and 56.0% for PTCM, respectively. It indicates the predominant effect of electrostatic interaction on the adsorption process, meanwhile, chemical interactions may play a minor role in the adsorption process [10].

Additionally, we compared the efficiency of the polymers towards different cationic dyes in a multi-cationic dye system. Fig. 3 and Fig. 4 display the UV–Vis spectra of the MB/MG/CV mixture solution during the adsorption by the polymers. The percentage removal of MB, MG, and CV by the polymer PTCA was found to be 95%, 92%, and 96% respectively, and by the polymer PTCM was found to be 75.6%, 69.0%, and 77.6% respectively. Hence, we conclude that the removal efficiency of cationic dyes in the MB/MG/CV mixture solution is lower than that of a single dye system, which may be the result of competing adsorption between the cationic dyes. Both polymers exhibit a higher removal efficiency for CV than the other two dyes, which may be due to the improved interaction of the polymers with CV dye molecules. So, in this study, we have chosen CV as the model cationic dye to explore various factors affecting the removal efficiency of the polymers [10].

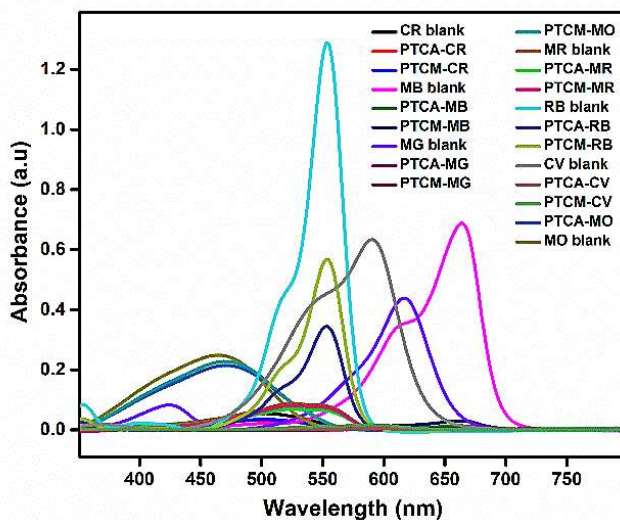


Fig. 1. The UV–Vis spectra of single dye (MB, MG, CV, RB, MO, MR, and CR) solution before and after adsorption by the polymers PTCA and PTCM.

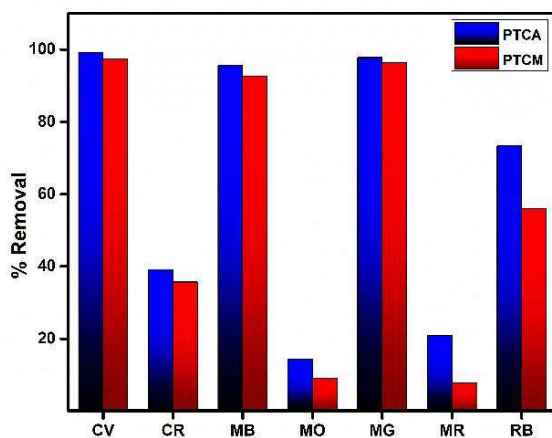


Fig. 2. The % removal efficiency of the dyes by the polymers PTCA and PTCM ($C_0 = 4$ ppm, adsorbent dosage = 1.6 mg, volume of solution = 50 mL, $t = 24$ h).

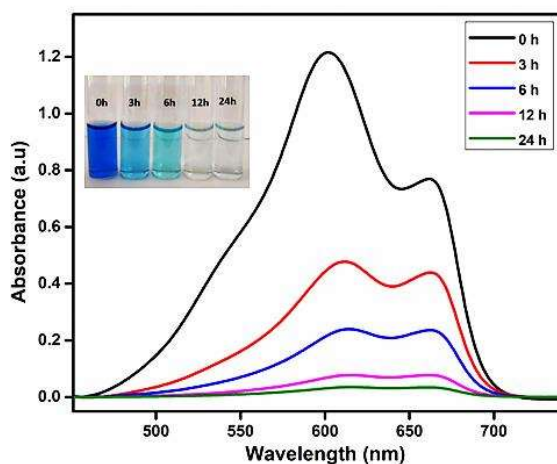


Fig. 3. The UV–Vis spectra of MB/MG/CV mixture solution during the adsorption by the polymers PTCA. The inset images show the color change of the mixed dye solution during the adsorption.

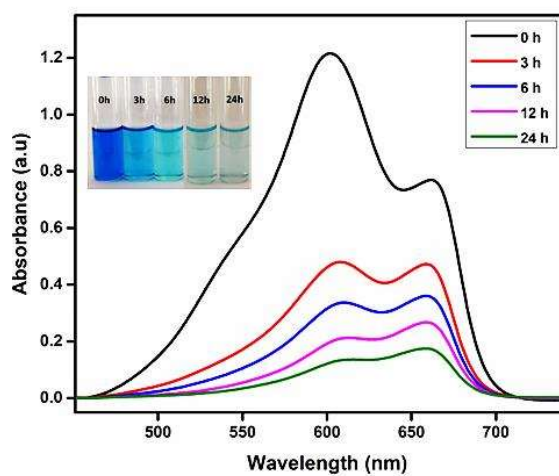


Fig. 4. The UV–Vis spectra of MB/MG/CV mixture solution during the adsorption by the polymer PTCM. The inset images show the color change of the mixed dye solution during the adsorption.

6.2.2. Effect of adsorbent dosage

The effect of the adsorbent amount on the removal of CV was assessed by adding different quantities of polymers to a fixed volume and concentration of dye solution at natural pH. Fig. 5a demonstrates that when the amount of polymer increases, the CV removal efficiency initially rises, reaches a maximum, and then nearly stays constant. The greater number of adsorption sites made available by the increased volume of adsorbents may have contributed to the initial improvement in removal efficiency [11]. Even in the presence of a large number of adsorption sites, the removal efficiency remains constant at greater concentrations of adsorbent, possibly because of the increased surface area and the quick formation of adsorption equilibrium. The maximum CV adsorption efficiency was observed with 1.6 mg of polymers for a 4-ppm dye solution. As a result, 1.6 mg of polymers were chosen for more studies.

6.2.3. Effect of pH

The CV adsorption effectiveness of PTCA ranged from 83.37% to 95.4% and that of PTCM ranged from 97.05% to 99.19% when the initial solution pH range was altered between 2 and 12 (Fig. 5b). It suggests that the material is usable in a wide pH range because the initial pH had little to no influence on CV adsorption by the polymer PTCA and nearly no effect on CV adsorption by the polymer PTCM [12]. Significantly, the pH of the final solution was in the range of 4.65 to 6.01, showing that the addition of the polymers significantly changed the pH of the solution. The acidic pH of the final solution may be due to the release of doped H⁺ ions during the adsorption process. For both the

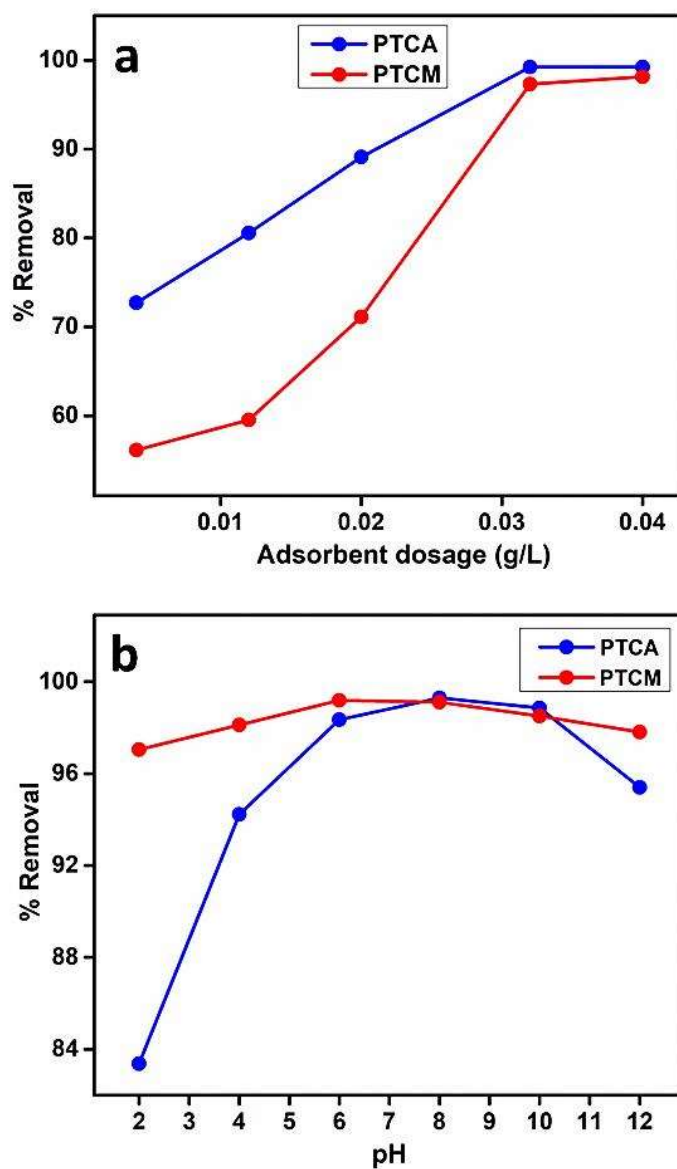


Fig. 5. (a) The effect of adsorbent dosage on the removal of CV ($C_0 = 4$ ppm, volume of solution = 50 mL, $t = 24$ h, pH = natural pH); (b) The effect of pH on the removal of CV ($C_0 = 4$ ppm, adsorbent dosage = 1.6 mg, volume of solution = 50 mL, $t = 24$ h).

polymers, the CV removal efficiency is found to be maximum around a neutral pH level. At lower pH values, the electron-rich heteroatoms of the polymer may involve in interaction with the competitive H^+ ions making them less available to interact with the dye molecules and leading to reduced adsorption efficiencies. The competing action of H^+ ions is lessened as pH rises, and more dye molecules can bind to these adsorption sites, thereby increasing the removal efficiency. However, due to the presence of competing adsorption of Na^+ ions produced by the addition of alkaline media, the removal efficiency marginally reduces in the higher pH range [10].

6.2.4. Effect of initial concentration and adsorption isotherms

The equilibrium uptake of the dye at different initial concentrations was examined as explained in the experimental section. As shown in Fig. 6a the adsorption capacity of both polymers was found to be increased with an increase in the initial concentration of the dye, reached a maximum value, and then practically remained constant. The maximum adsorption capacity obtained for PTCA and PTCM is 151.49 mg/g and 142.28 mg/g respectively. Also found that the % removal efficiency decreases as the initial dye concentration increases (Fig. 6b). At higher dye concentrations there is a greater chance of mass transfer due to the concentration variance between the bulk of the solution and the interface of the adsorbent [13].

The Freundlich adsorption isotherm and the Langmuir adsorption isotherm were used to fit the adsorption data to further examine the adsorption process of CV onto the polymers (Fig. 7). Table 1 displays

the calculated parameters for these two models. The parameter Q_m (mg/g) obtained from the Langmuir equation is the measure of monolayer adsorption capacity and K_L is a constant associated with the energy of adsorption. The bond energies and bond strengths between the dye molecule and the adsorbent are represented, respectively, by the parameters K_F and n derived from the Freundlich equation. The R^2 values are viewed as a gauge of how well the experimental data fit the isotherm models [11]. Since R^2 related to the Langmuir model is greater

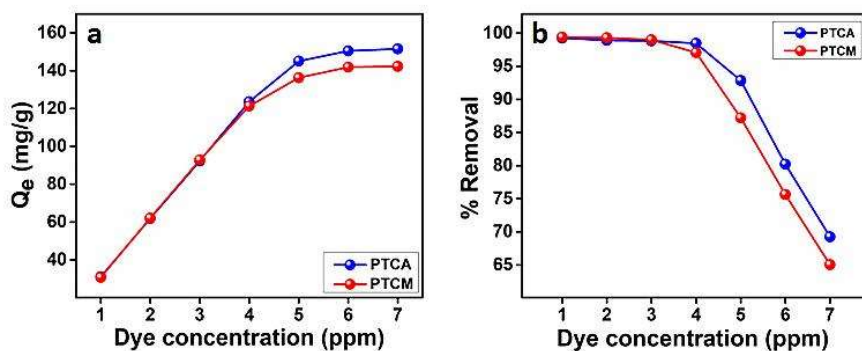


Fig. 6. (a,b) The effect of initial dye concentration on the removal of CV (Adsorbent dosage = 1.6 mg, volume of solution = 50 mL, $t = 24$ h, pH = natural pH).

than 0.999 which is very close to one for both the polymers, we conclude that the adsorption process follows the Langmuir adsorption isotherm. Thus, it is anticipated that chemical adsorption is the major process involved in the adsorption of dye molecules. The value of Q_m was reliable with the experimentally attained values, which confirms the monolayer adsorption. Meanwhile, the R^2 value related to the Freundlich adsorption isotherm model is only in the range of 0.83-0.86, which rules

out the likelihood of a larger contribution of the physisorption process in the adsorption of dye molecules.

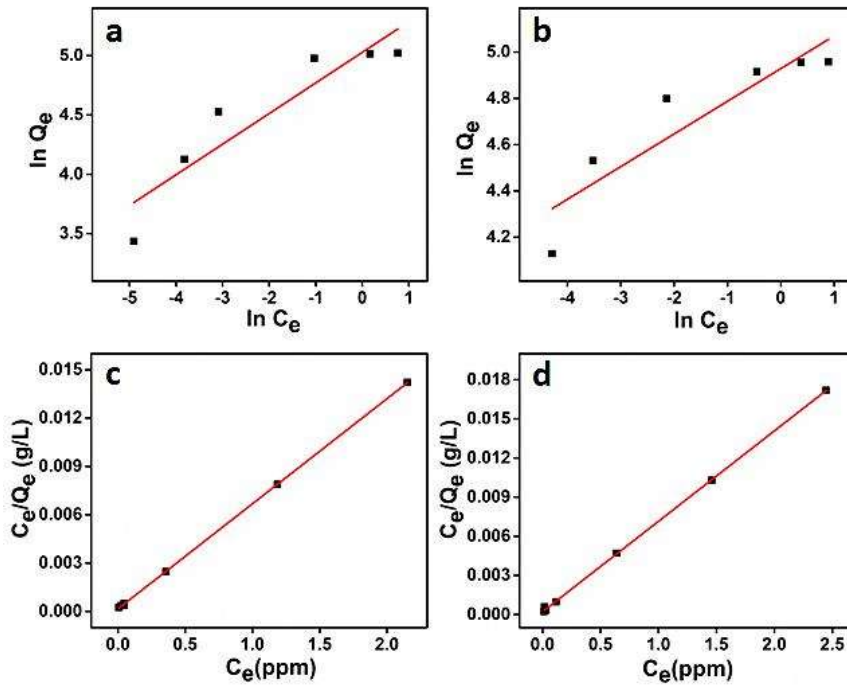


Fig. 7. (a,b) The Freundlich adsorption isotherms of CV adsorption on the polymer PTCA and PTCM respectively; (c,d) The Langmuir adsorption isotherms of CV adsorption on the polymer PTCA and PTCM respectively.

The Langmuir isotherm model also provides a parameter called separation factor R_L which is used to determine the suitability and shape of the isotherm and also helps to predict whether an adsorption system is favorable or not. R_L is given by equation 6.1

$$R_L = \frac{1}{1 + K_L C_0} \quad (\text{Equation 6.1})$$

where C_0 (mg/L) is the concentration of CV solution before adsorption, and K_L (L/mg) is the Langmuir adsorption equilibrium constant. $R_L = 0$, $0 < R_L < 1$, $R_L = 1$, and $R_L > 1$ represent irreversible adsorption, favorable adsorption, linear adsorption, and unfavorable adsorption respectively [10]. The R_L values obtained for both polymers lie in the range of 0 to 1 for all initial dye concentrations between 1-7 ppm (Table 1), signifying that the dyes exhibit favorable adsorption on both of the polymers.

Table 1. The parameters obtained from Freundlich and Langmuir adsorption isotherms.

Sorption Studies							
Adsorbate	Langmuir				Freundlich		
	Q_m (mg/g)	K_L (L/mg)	R^2	R_L	K_F (L/mg)	n	R^2
PTCA	153.85	32.5	0.9999	0.004 to 0.030	152.56	3.86	0.8569
PTCM	144.93	34.5	0.9997	0.004 to 0.028	138.21	7.08	0.8335

6.2.5. Effect of contact time and adsorption kinetics

The UV-Vis spectra and images of the CV dye solution at different time intervals are shown in Fig. 8 and Fig. 9. Meanwhile, Fig. 10a and Fig. 10b represent the percentage removal of the dye and the adsorption. The results of the analysis of the adsorption data using the pseudo-first-order, pseudo-second-order, and intraparticle diffusion model kinetics are

shown in Fig. 11 and Table 2. The first-order rate equation of Lagergren is one of the most widely used equations for the adsorption of a solute from the liquid solution. The pseudo-second-order considers that rate of occupation of adsorption sites is proportional to the number of unoccupied sites [11]. The highest value of the correlation coefficient is obtained for the pseudo-second-order kinetic model ($R^2 = 0.9989$ for PTCA and $R^2 = 0.9908$ for PTCM) compared to the pseudo-first-order kinetic model ($R^2 = 0.9862$ for PTCA and $R^2 = 0.9660$ for PTCM), hence this result reveals that the pseudo-second-order kinetic model is better suited to describe the adsorption behavior of CV onto the polymers, with chemisorption as the primary process.

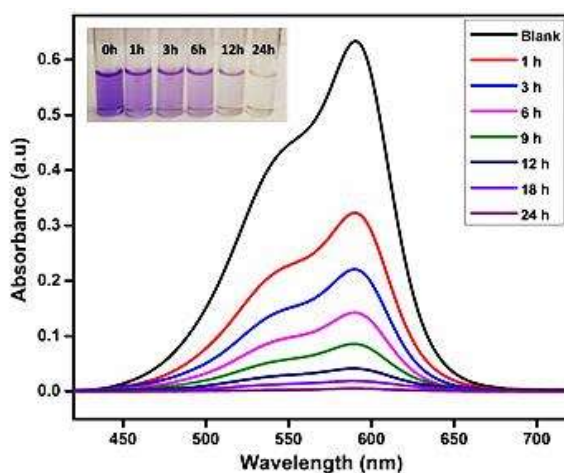


Fig. 8. UV-vis spectra of CV dye solution at different stages of adsorption (a) by the polymer PTCA ($C_0 = 4$ ppm, Adsorbent dosage = 1.6 mg, volume of solution = 50 mL, pH = natural pH). The inset images show the color change of the CV dye solution during the adsorption.

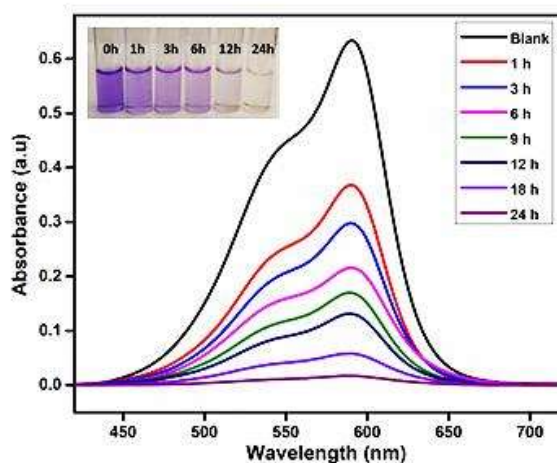


Fig. 9. UV-vis spectra of CV dye solution at different stages of adsorption (a) by the polymer PTCM ($C_0 = 4$ ppm, Adsorbent dosage = 1.6 mg, volume of solution = 50 mL, pH = natural pH). The inset images show the color change of the CV dye solution during the adsorption.

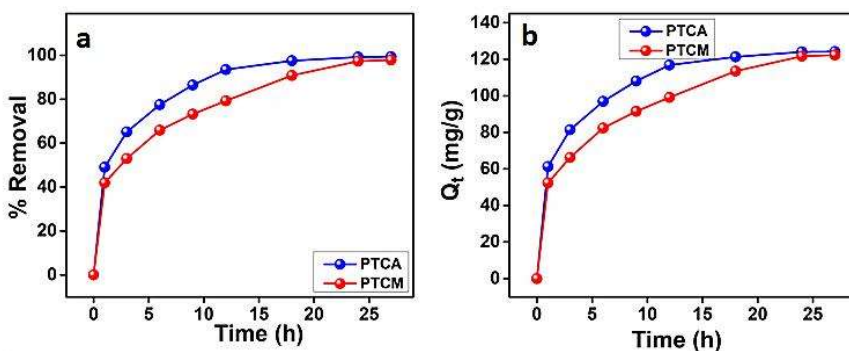


Fig. 10. (a) Percentage removal of the dye by the polymers PTCA and PTCM; (b) adsorption capacity of the polymers PTCA and PTCM. ($C_0 = 4$ ppm, Adsorbent dosage = 1.6 mg, Volume of solution = 50 mL, pH = natural pH).

6.2.6. Adsorption mechanism

Multiple successive mass transfer steps are anticipated to be involved in the kinetic mechanism of the adsorption process. First, the adsorbate flows from the bulk of the solution to the boundary layer (film) on the outer surface of the adsorbent, then the adsorbate diffuses from the adsorbent surface into the internal pores of the adsorbent. Finally, the dye molecules are adsorbed into the active sites inside the adsorbent particles, which entails a comparatively extensive contact time [14, 15].

The kinetic study reveals that intra-particle diffusion also occurs during the adsorption process. The curve of Q_t versus $t^{1/2}$ should be linear if the intra-particle diffusion mechanism is involved in the adsorption. If it plays a major role in the rate-determining step of adsorption, the straight line should pass through the origin. However, an intra-particle diffusion process exhibiting multilinear plots indicates more than one simultaneous process during adsorption. Fig. 11e and Fig. 11f show two linear zones on the plot of Q_t versus $t^{1/2}$, which is an indication of multiple simultaneous processes taking place during the adsorption of CV onto the polymers. The steeply sloping linear region on the plot is connected to the diffusion of dye molecules through the aqueous solution to the boundary layer or film of the polymer. The second phase is related to the internal diffusion towards the interior of the adsorbent through the pores and particles of the adsorbent. Moreover, none of the plots passing through the origin shows the presence of a second adsorption mechanism operating in addition to the intra-particle diffusion process [11]. This conclusion is further supported by the increased value of intercept (C), which shows the thickness of the

boundary layer. So, we conclude that the high removal efficiency of the polymers towards the CV dye is due to the combined effect of surface adsorption along with the intra-particle diffusion process [16].

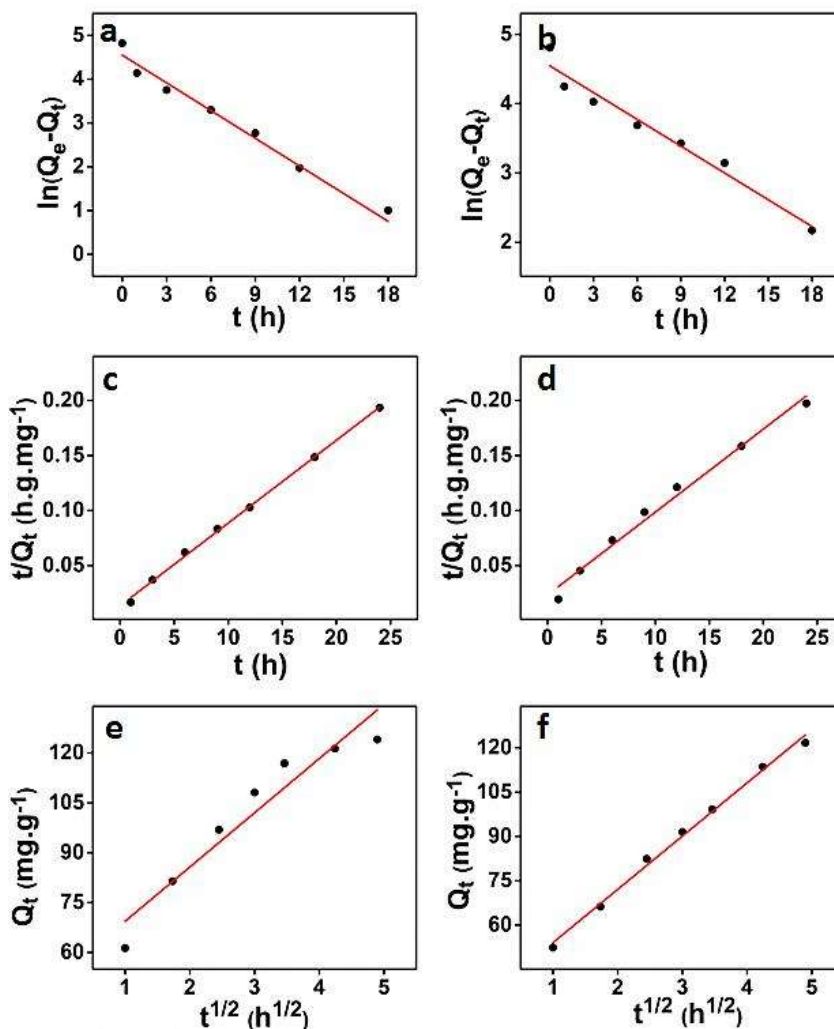


Fig. 11. (a,b) Pseudo-first-order, (c,d) pseudo-second-order, and (e,f) intraparticle diffusion model plots for the adsorption of CV on the polymers PTCA and PTCM respectively.

Table 2. Kinetic parameters for the adsorption of CV on the polymers PTCA and PTCM.

Kinetic Studies									
Adsorbate	pseudo-first order			pseudo-second order			Intraparticle diffusion		
	Q _e (mg/g)	k ₁ (h ⁻¹)	R ²	Q _e (mg/g)	k ₂ (g/mg h)	R ²	k _{int} (mg g ⁻¹ h ^{-1/2})	C (mg/g)	R ²
PTCA	94.53	0.21	0.9862	131.58	0.0044	0.9989	22.38	40.78	0.9944
							4.38	102.12	0.9653
PTCM	94.27	0.13	0.9660	135.13	0.0023	0.9908	19.26	33.47	0.9967
							13.76	52.92	0.9616

The FTIR spectra of the polymers were taken before and after the adsorption of CV dye to further understand the adsorption mechanism (Fig. 12 and Fig. 13).

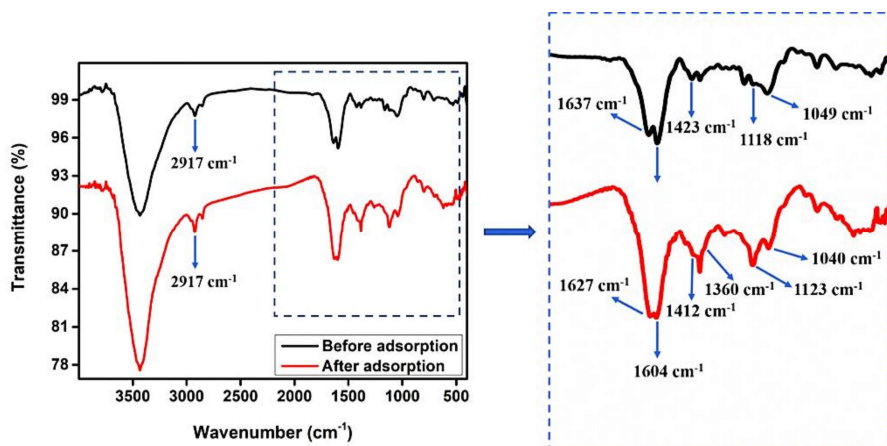


Fig. 12. FT-IR spectra of the polymer PTCA before and after the adsorption of CV dye.

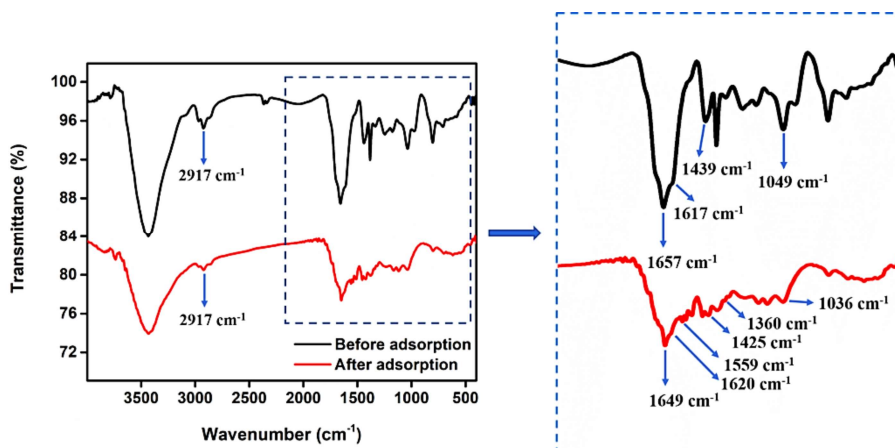
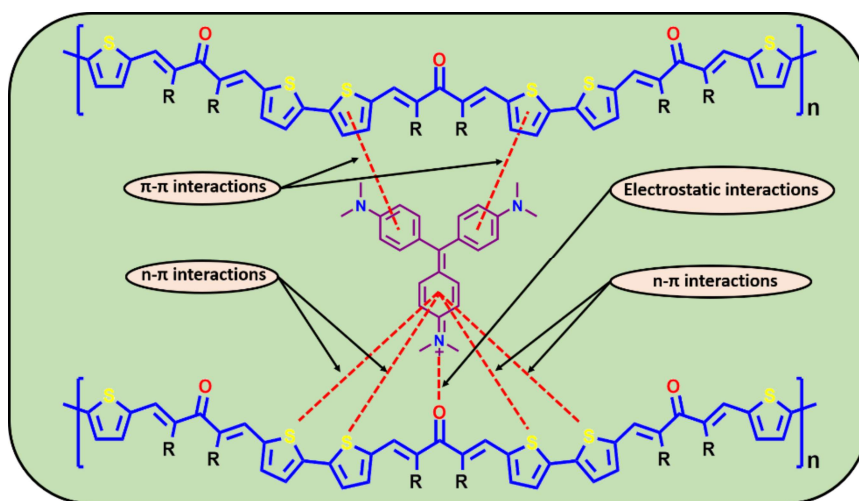


Fig. 13. FT-IR spectra of the polymer PTM before and after the adsorption of CV dye.

Upon adsorption, the spectra of adsorbents showed distinctive peaks corresponding to the characteristic frequencies of dye molecules. The peak at 2917 cm^{-1} and 1360 cm^{-1} corresponds to C-H stretching of the -CH_3 group and C-N stretching of aromatic tertiary amine respectively, while a small shoulder peak around 1559 cm^{-1} corresponds to C=C stretching of the aromatic ring. Successful adsorption of CV onto the polymer is also indicated by changes in the position and intensity of the characteristic peaks of the polymers [17]. The peaks correspond to C=C stretching of α,β -unsaturated ketone displays a shift from 1597 cm^{-1} to 1604 cm^{-1} and 1617 cm^{-1} to 1620 cm^{-1} for PTCA and PTCM respectively. Also, the peaks corresponding to C=C stretching of thiophene moiety show a shift from 1423 cm^{-1} to 1412 cm^{-1} and 1439 cm^{-1} to 1425 cm^{-1} for PTCA and PTCM respectively. These shifts point to the probable π - π interaction between the extended π conjugative system of the adsorbent and the aromatic rings of the dye molecules. Similarly, the peak at 1118 cm^{-1} and 1049 cm^{-1} corresponds to the C-S-C stretching vibration of the polymer PTCA and the thiophene skeletal vibration of the polymer PTCM was found to be shifted to 1123 cm^{-1} and 1036 cm^{-1} respectively, indicating the involvement of thiophene group in the adsorption process through n- π interaction or π - π interaction. A large shift (1637 cm^{-1} to 1627 cm^{-1} for PTCA and 1657 cm^{-1} to 1649 cm^{-1} for PTCM) exhibited by the characteristic peak attributed to the C=O group of the polymer indicates a strong electrostatic interaction between the tertiary amine group of the CV dye and the carbonyl group of the polymers. This possible potential interaction between the dye and the polymer is confirmed by the absence of a peak at 1178 cm^{-1} in the dye-adsorbed polymers, which is attributed

to the C-N stretching vibration of the tertiary amine of the dye molecules [17]. Therefore, we conclude that the remarkable adsorption performance of the adsorbents towards the CV dye results from the comprehensive combination of electrostatic interaction, $n-\pi$ interactions, and $\pi-\pi$ stacking interactions. The expected mechanism is shown in Scheme 1.



Scheme 1. Possible interactions involved in the adsorption of CV onto the polymers.

6.2.7. Selective adsorption experiments

A mixture of CV (cationic) and MO (anionic) dye solution was used to conduct the selective adsorption experiment. Fig. 14 and Fig. 15 display the UV-Vis spectra and photos of the combined dye solution during the adsorption. The UV-Vis spectra demonstrate that as adsorption proceeds, the intensity of the distinctive peak of the CV/MO mixture solution at 590 nm (corresponding to CV) weakens and almost

disappears, whereas the intensity of MO characteristic peak at 465 nm undergoes only a slight change in the intensity. This can be seen from how the color of the CV/MO mixed solution gradually changes from purple grape to yellowish orange (the color of MO) (inset of Fig. 14 and Fig. 15). These findings demonstrate that the polymers are capable of selectively removing and adsorbing cationic dye (CV) from the mixed

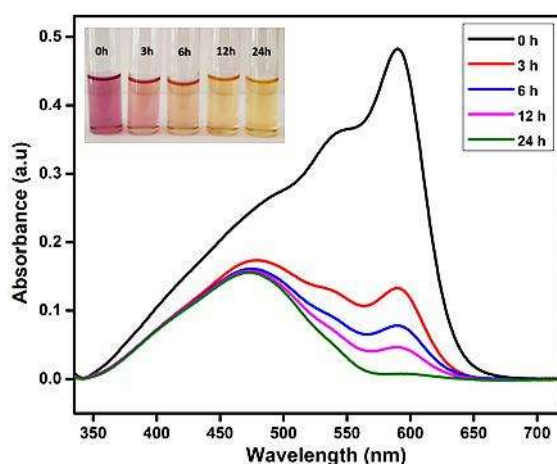


Fig. 14. UV-vis spectra of CV/MO mixed dye solution at different stages of adsorption by the polymer PTCA ($C_0 = 4$ ppm, Adsorbent dosage = 3.2 mg, Volume of solution = 50 mL, $t = 24$ h, pH = natural pH). The inset images show the color change of the mixed dye solution during the adsorption.

cationic/anionic dye solution. The carbonyl group of the polymers and the tertiary amine group of the CV dye molecules may interact chemically to cause preferential adsorption. The electrostatic interaction

between the anionic dyes and the polymers may be the cause of the negligible adsorption of anionic dyes [18].

6.2.8. Desorption and reusability studies

The reusable, high-regenerative adsorbent can only be used in industrial settings. The adsorbed dyes must be desorbed from the polymer surfaces to free up the active sites for the next adsorption cycle. We employed

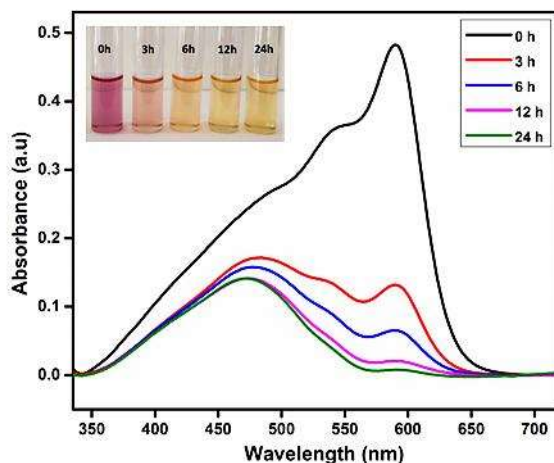


Fig. 15. UV-vis spectra of CV/MO mixed dye solution at different stages of adsorption by the polymer PTCM ($C_0 = 4$ ppm, Adsorbent dosage = 3.2 mg, Volume of solution = 50 mL, $t = 24$ h, pH = natural pH). The inset images show the color change of the mixed dye solution during the adsorption.

ethanol as the desorbing agent in this study. The addition of ethanol decreases the extent of interaction between polymer and CV molecules, as a result, CV molecules get desorbed from the surface of the adsorbent.

The desorption efficiency obtained for PTCA and PTCM is 99.04% and 93.78% respectively. To check the reusability of the polymers the adsorption-desorption cycles were carried out five times and the outcomes are presented in Fig. 16. According to the results, the removal efficiency of PTCA falls from 99.17% to 96.42% and PTCM falls from 97.99% to 92.46%. Also, after five cycles, it was revealed that the desorption efficiency for PTCA and PTCM declined from 99.04% to 92.08% and 93.78% to 87.43%, respectively. The occlusion of some active sites by dye molecules, which are challenging to desorb due to their strong chemical interactions with the polymer surface, may be the source of the predicted drop in the removal efficiency after each cycle [17].

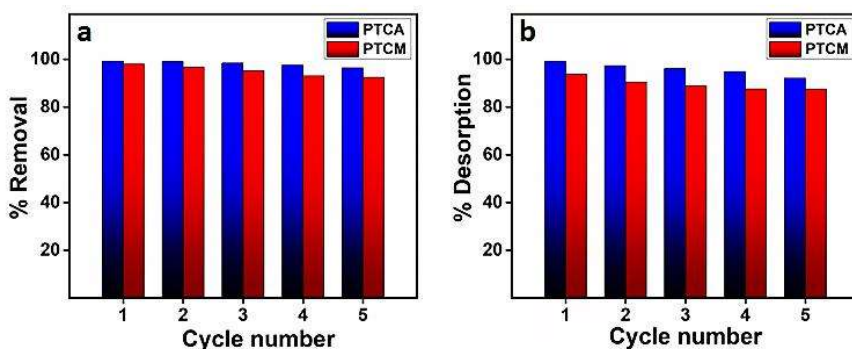


Fig. 16. (a) Percentage removal efficiency and (b) Percentage desorption efficiency of the polymers PTCA and PTCM during five adsorption-desorption cycles.

6.3. Conclusions

This study investigates the dye adsorption efficiency of two polymers PTCA and PTCM. Both the polymers exhibited high removal efficiency

towards cationic dyes. The study conducted using single dye solutions and mixed cationic dye solutions revealed that both of the polymers show the highest removal efficiency towards CV, hence it was selected as a model cationic dye to explore various factors influencing the adsorption process. The effect of adsorbent dosage, pH, initial dye concentration, and contact time were studied in detail. The maximum adsorption capacity obtained was 151.49 mg/g and 142.28 mg/g for the polymer PTCA and PTCM respectively. The Langmuir adsorption isotherm was satisfactorily used to describe the adsorption process. The kinetic studies demonstrate that the adsorption process adheres to pseudo-second-order kinetics, revealing chemisorption as the primary mechanism involved in the adsorption. Two linear plots observed in the intra-particle diffusion model confirmed the involvement of surface adsorption and intra-particle diffusion process in dye removal progression. FT-IR analysis pointed to the conclusion that a complex interplay of electrostatic interaction, n- π interactions, and π - π stacking interactions is responsible for the outstanding adsorption ability of the adsorbents. The polymers PTCA and PTCM retained 96.42% and 92.46% of removal efficiency even after five adsorption-desorption cycles, which shows exceptional reusability of the utilized polymers. Therefore, this study offers two polymers that could be employed as promising adsorbents for the selective removal of cationic dye molecules.

References

- [1] F.N. Chaudhry, M. Malik, Factors affecting water pollution: a review, *J Ecosyst Ecography*, 7(2017) 225-31.
- [2] M. Ismail, K. Akhtar, M. Khan, T. Kamal, M.A. Khan, A. M Asiri, et al., Pollution, toxicity and carcinogenicity of organic dyes and their catalytic bio-remediation, *Current pharmaceutical design*, 25(2019) 3645-63.
- [3] G. Ozdemir, I. Yasa, B. Pazarbasi, E. Ersoy, I. Karaboz, B. Basaran, et al., Decolorization of the leather industry dyes by newly isolated bacterial strains, *World Journal of Microbiology and Biotechnology*, 20(2006) 545-50.
- [4] L.C. Oliveira, C.V.Z. Coura, I.R. Guimarães, M. Gonçalves, Removal of organic dyes using Cr-containing activated carbon prepared from leather waste, *Journal of hazardous materials*, 192(2011) 1094-9.
- [5] H.A. Hamad, S. Abdelhafez, M. Elsenety, M.K. Sorour, N. Amin, O. Abdelwahab, et al., Fabrication and characterization of functionalized lignin-based adsorbent prepared from black liquor in the paper industry for superior removal of toxic dye, *Fuel*, 323(2022) 124288.
- [6] A. Gürses, M. Açıkyıldız, K. Güneş, M.S. Gürses, A. Gürses, M. Açıkyıldız, et al., Dyes and pigments: their structure and properties, *Dyes and Pigments*, (2016) 13-29.
- [7] N.P. Raval, S. Mukherjee, N.K. Shah, P. Gikas, M. Kumar, Hexametaphosphate cross-linked chitosan beads for the eco-efficient removal of organic dyes: Tackling water quality, *Journal of Environmental Management*, 280(2021) 111680.
- [8] M.M. Hasan, M. Shenashen, M.N. Hasan, H. Znad, M.S. Salman, M.R. Awual, Natural biodegradable polymeric bioadsorbents for efficient cationic dye encapsulation from wastewater, *Journal of Molecular Liquids*, 323(2021) 114587.
- [9] K.P. Singh, S. Gupta, A.K. Singh, S. Sinha, Optimizing adsorption of crystal violet dye from water by magnetic nanocomposite using response surface modeling approach, *Journal of hazardous materials*, 186(2011) 1462-73.
- [10] K. Li, J. Yan, Y. Zhou, B. Li, X. Li, β -cyclodextrin and magnetic graphene oxide modified porous composite hydrogel as a superabsorbent for adsorption cationic dyes: Adsorption performance, adsorption mechanism and hydrogel column process investigates, *Journal of Molecular Liquids*, 335(2021) 116291.

- [11] R. Ahmad, Studies on adsorption of crystal violet dye from aqueous solution onto coniferous pinus bark powder (CPBP), *Journal of Hazardous Materials*, 171(2009) 767-73.
- [12] Y. Yi, G. Tu, G. Ying, Z. Fang, E.P. Tsang, Magnetic biochar derived from rice straw and stainless steel pickling waste liquor for highly efficient adsorption of crystal violet, *Bioresource Technology*, 341(2021) 125743.
- [13] K.T. Kubra, M.S. Salman, H. Znad, M.N. Hasan, Efficient encapsulation of toxic dye from wastewater using biodegradable polymeric adsorbent, *Journal of Molecular Liquids*, 329(2021) 115541.
- [14] A. Pholosi, E.B. Naidoo, A.E. Ofomaja, Intraparticle diffusion of Cr(VI) through biomass and magnetite coated biomass: A comparative kinetic and diffusion study, *South African Journal of Chemical Engineering*, 32(2020) 39-55.
- [15] S. Chakraborty, S. Chowdhury, P. Das Saha, Adsorption of Crystal Violet from aqueous solution onto NaOH-modified rice husk, *Carbohydrate Polymers*, 86(2011) 1533-41.
- [16] Z. Mu, D. Liu, J. Lv, D.-F. Chai, L. Bai, Z. Zhang, et al., Insight into the highly efficient adsorption towards cationic methylene blue dye with a superabsorbent polymer modified by esterified starch, *Journal of Environmental Chemical Engineering*, 10(2022) 108425.
- [17] S. Sharma, G. Sharma, A. Kumar, T.S. AlGarni, M. Naushad, Z.A. Alothman, et al., Adsorption of cationic dyes onto carrageenan and itaconic acid-based superabsorbent hydrogel: Synthesis, characterization and isotherm analysis, *Journal of Hazardous Materials*, 421(2022) 126729.
- [18] L. Tian, S. Zhou, J. Zhao, Q. Xu, N. Li, D. Chen, et al., Sulfonate-modified calixarene-based porous organic polymers for electrostatic enhancement and efficient rapid removal of cationic dyes in water, *Journal of Hazardous Materials*, 441(2023) 129873.

Summary and Future Outlook

In this piece of work, we designed, synthesised and characterized two thiophene-bearing bis-chalcones; MTCA and MTCM. The chalcone MTCA acts as an excellent colorimetric probe for the rapid and selective detection of bisulfite/sulfite anions in aqueous solutions, as well as in real samples. This probe is based on the Michael addition reaction which is favoured in the presence of cationic micellar media CTAB. CTAB promoted Michael addition as an effective tool to determine SO₂ toxicity which is mainly expressed in terms of the collective concentration of bisulfite and sulfite anions. The probe showed high selectivity and sensitivity toward bisulfite and sulfite over other interfering anions, with a detection limit of 0.43 μ M and 0.23 μ M respectively.

Owing to the presence of terminal thiophene units, we attempted to use these monomers to develop a new class of polymers with a donor- π -acceptor- π -donor type of repeating units. To the best of our knowledge, we are the first to report this kind of synthesized polymers; PTCA and PTCM. By employing FeCl₃ mediated oxidative coupling reaction, we could achieve the template-free synthesis of mesoporous polymers which is not commonly known. The novelty of our work lies here. Moreover, FeCl₃-promoted oxidative coupling polymerization offers an added advantage of facile, low-cost, and large-scale syntheses.

The porous nature, presence of heteroatoms and electron-rich thiophene rings make the polymers excellent candidates for environmental applications such as iodine capture, heavy metal ion removal and organic dye adsorption. The maximum iodine capture capacity obtained

for PTCA and PTCM were 242 and 221 wt.% respectively. The maximum adsorption capacity of the polymer PTCA for Zn^{2+} and Pb^{2+} ions were obtained as 729.4 mg/g and 569.1 mg/g respectively, and the maximum adsorption capacity of the polymer PTCM for Zn^{2+} and Pb^{2+} was calculated as 652.7 mg/g and 545.1 mg/g respectively. Impressively, the maximum adsorption capacity of crystal violet obtained was 151.49 mg/g for PTCA and 142.28 mg/g for PTCM. These remarkable polymers can be recycled and reused without significant loss of efficiency towards various adsorbates, even after five cycles.



Scope for future work

The present study has resulted in the development of two novel and innovative thiophene-bearing bis-chalcone-based polymers, with exceptional potential for environmental applications. Our study opened up several promising avenues for future research including:

- Exploring the NLO properties of the synthesized polymers, and post-synthetic modification of the synthesized polymers.
- Design and synthesis of substituted monomers and the same kind of monomers with different aromatic rings (pyrrole, benzene, furan etc instead of thiophene) for sensing and NLO applications.
- Design and synthesis of substituted polymers and the same kind of polymers with different aromatic rings (pyrrole, benzene, furan etc instead of thiophene) for environmental and NLO applications.

List of Publications

	<p><i>A bis-chalcone based colorimetric probe for the selective detection of bisulfite/sulfite anions: exploring surfactant promoted Michael addition of anions to α, β -unsaturated ketones, P. Sowmya, S. Prakash, A. Joseph, RSC Advances, 13(2023) 2552-60.</i></p>
	<p><i>Design and synthesis of thiophene containing bis-chalcone-based mesoporous polymers for volatile iodine capture, P. Sowmya, S. Prakash, A. Joseph, Journal of Hazardous Materials Advances, 10(2023) 100272</i></p>
	<p><i>Adsorption of heavy metal ions by thiophene containing mesoporous polymers: An experimental and theoretical study, P. Sowmya, S. Prakash, A. Joseph, Journal of Solid State Chemistry, 320(2023) 123836</i></p>
	<p><i>Characterization and Temperature dependent DC conductivity study of bio templated nickel oxide nanoparticles (NiO) and their composites using polyaniline (PANI), L. Williams, A.R. Prasad, P. Sowmya, A. Joseph, Materials Chemistry and Physics, 242(2020) 122469</i></p>

	<p><i>Gamma-ray induced thermoluminescence emission of green synthesized zinc oxide nanophosphors</i>, A.R. Prasad, P. Sowmya, J. Garvasis, A. Joseph, Journal of the Indian Chemical Society, 98(2021) 100153</p>
	<p><i>Sensing of picric acid using an AIEE active “Turn Off” fluorescent probe derived from hydroxy naphthaldehyde and benzyloxy benzaldehyde</i>, M. Arshad, P. Sowmya, A. Paul, A. Joseph, Spectrochimica Acta Part A: Molecular and Biomolecular Spectroscopy, 305 (2024) 123465</p>

- Selective removal of cationic dyes using thiophene-based bis-chalcone polymers as an effective adsorbent – submitted to journal

Presentations

- **An experimental and theoretical study on heavy metal ion adsorption by a bischalcone-based mesoporous polymer,** National seminar on Emerging Frontiers in Chemical Sciences – EFCS, 19-20 January 2023, organized by Post Graduate and Research Department of Chemistry, Farook College.
- **Adsorption of Zn(II) and Pb(II) ions on thiophene containing porous polymer: An experimental and theoretical study,** National seminar on Frontiers in Chemical Sciences – FCS, 1-3 February 2023, organized by Department of Chemistry, University of Calicut.